Electric Power System Dynamics

Yao-nan Yu

Professor Emeritus
The University of British Columbia
Vancouver, British Columbia, Canada

1983

ACADEMIC PRESS
A Subsidiary of Harcourt Brace Jovanovich, Publishers

New York London
Paris San Diego San Francisco São Paulo Sydney Tokyo Toronto

ACADEMIC PRESS, INC.
111 Fifth Avenue, New York, New York 10003

United Kingdom Edition published by
ACADEMIC PRESS, INC. (LONDON) LTD.
24/28 Oval Road, London NW1 7DX

Library of Congress Cataloging in Publication Data

Yu, Yao-nan.
Electric power system dynamics.

Includes index.
1. Electric power system stability. 2. Transients (Electricity) I. Title.
TK1005.Y8 1983 621.319'1 83–2540
ISBN 0–12–774820–2

PRINTED IN THE UNITED STATES OF AMERICA

83 84 85 86 9 8 7 6 5 4 3 2 1

Contents

Preface

This book is intended for senior undergraduate and graduate students and practicing engineers who wish to familiarize themselves with electric power system dynamics. The objective of this book is to bridge a major gap in power system engineering between recent literature dealing with the dynamic performance of large electric power systems and classic books on power system stability before the inception of digital computers and modern control theory.

Since the development of large-scale electric power system interconnection, power system engineering has gone through great changes, and many new power system dynamic problems have emerged. Among them are low-frequency intersystem oscillations, torsional oscillations due to subsynchronous resonance of capacitor-compensated transmission lines, and the derivation of dynamic equivalents for large electric power system dynamic studies. Although most of these dynamic problems have been solved, the solutions can be improved with the aim of still better and more economical results.

This book deals with analysis and controller design aspects of these problems. Emphasis is placed on basic concepts and fundamental principles, not on ramifications. The book develops in such a way that only elementary matrix algebra and some knowledge of machines and power systems are required in reading the first few chapters. Control theory and computational techniques are developed along with the progress of the full text. The book is primarily an outgrowth of many years' teaching at both undergraduate and graduate levels at the University of British Columbia.

The book comprises seven chapters. An introduction to the modern electric power system and power system dynamic problems is given in

Chapter 1, and basic models for power system dynamic studies are included in Chapter 2. Subsequently, each chapter deals with a specific class of electric power system dynamic problems: low-frequency intersystem oscillations and supplementary control of the phase compensation type in Chapter 3; linear optimal control to stabilize one machine as well as multimachine, multimode systems in Chapter 4; control of torsional oscillations due to subsynchronous resonance of capacitor-compensated transmission lines in Chapter 5; derivation of dynamic equivalents of the external system for large electric power system dynamic studies in Chapter 6; and transient stability control of electric power systems in Chapter 7. Inasmuch as the subject material of the last two chapters is rapidly evolving, it is included as an introduction for beginners. For the readers' convenience, several computer programs and subprograms are included as an Appendix.

The author wishes to express his gratitude to the IEEE for permission to reprint a number of illustrations from their publications, to NSERC, Canada, for financial support, and to Academic Press. The subject material of this book is based on a large number of publications by many experts and acknowledgment of sources can therefore be made only through the lists of references. The author is especially indebted to Dr. Brian J. Cory who reviewed the manuscript and made many valuable suggestions, and to many pioneers and experts who have inspired and encouraged this endeavor. Among them are Mr. C. H. Chen of EPRI; Professor Guo Jing-De of China; Professor Shigeo Takata of Japan; Professor Fred Evans and Professor John Anderson of Australia; Mr. R. H. Park, Mr. C. Concordia, and Professor O. I. Elgerd of the United States; and Dr. H. Ellis, Dr. P. Kunder, Dr. A. M. El-Serafi, Dr. Eugene Hill and Dr. T. H. D. Lee of Canada. He also wishes to thank his colleagues at the University of British Columbia for their advice and suggestions, and his former students for their contributions. Finally, the manuscript preparation would not have been possible without the assistance of my son Dr. Yuan Yu and my wife Iris.

Chapter 1 Electric Power System and Dynamic Problems

With the advent of interconnection of large electric power systems, many new dynamic power system problems have emerged [1], which include the low-frequency oscillations of the interconnected large electric power systems [1–5], the subsynchronous torsional oscillations of turbines in a steam–electric power plant with capacitor-compensated transmission lines [6–9], and many others [10–22]. When engineers are confronted with a challenging problem, it is their responsibility to conceive new and improved analytical tools to solve the problem. On the other hand, once a new tool is available, they will use it to reexamine the problem to find still better and more economical solutions.

The large-scale power system interconnection was initiated at a time when digital computers and modern control theory began to develop. Although these events seemed to be coincidental, like the two wheels of a cart, they certainly have advanced together. In this regard, the recent development in analysis and control of electric power systems is but one application of modern computation and control techniques, among other notable applications such as space projects and economic systems.

The large-scale power system interconnection is intended to make electric energy generation and transmission more economical and reliable. The economic aspect is manifested through the drastic reduction of spinning reserve or the standby generating capacity for maintenance or emergency use, from 25% or more of the total capacity a few decades ago to much less in modern electric power systems. The reliability of the interconnected system is also enhanced by virtue of the capability of transferring power readily from one area to others within the system. But in the meantime, the multiple interconnections of multi-areas make the system much more

vulnerable to instability, not only because of the complexity of multi-area interconnections but also because of the drastic reduction of spinning reserves of individual areas.

New developments and new designs of power system components have also made their presence felt in the time of growing interconnection. For instance, the HVDC tie of the Pacific Northwest and Southwest Power Pools, the series capacitor compensation of long transmission lines, the fast excitation, and the larger per unit reactances and smaller inertia constants of the new synchronous generator designs have added complexities to an already complicated large interconnected electric power system.

The increasingly challenging dynamic electric power system problems, however, are not hopelessly unmanageable. On the contrary, while the electric power system continues to grow in size and complexity, engineering experience is also accumulated and control and computation techniques advanced. Thus a challenging new problem is always met by new ideas and new methods aimed at solving the problem.

The planning and operation of a power system involves many engineering phases [23–29], which include the load forecast, the energy source investigation, the design and construction of power plant and transmission lines, system protection, and the day-to-day and hour-to-hour energy dispatch. This book will address itself, however, to only one of the most important aspects, namely, electric power system dynamics or the dynamic behavior and control problems of electric power systems, which may be considered as the development of classical electric power system stability studies [30–34]. Modern electric power systems and dynamic problems are presented in this chapter, and the basic components of an electric power plant in the first section.

1-1 BASIC COMPONENTS OF AN ELECTRIC POWER PLANT

To understand the dynamic behavior of an electric power system and to design a control to improve its performance, it is necessary to be familiar with the basic components of an electric power plant, especially those that have significant effects on the dynamic behavior of electric power systems.

Mechanical–Electric Energy Conversion

Although the direct conversion to electric energy from other energy forms such as solar and fusion is being developed, the prime energy sources of

electric energy generation are still fossil fuels, hydropower and nuclear energy, and to a much lesser extent, tide and wind. These energies either are already in the form of mechanical energy as in the case of hydropower, tide, and wind or must first be converted into mechanical energy through steam turbines before the final process of mechanical–electric energy conversion, as with fossil fuel and fission material. Therefore, the important components basic to an electric power plant are the hydro and steam turbines, the electric generator, the governor control of the energy input to the turbines, and the exciter and voltage regulator control of the electric energy output of the generator. The major portion of the generated electric energy is transmitted to load centers through transmission lines, although some electric energy must be used for local supply, and some losses always occur in the generation and transmission process.

The basic components of an electric power plant may be schematically shown as in Fig. 1-1. In the figure, the turbine and governor with a speed feedback $\Delta\omega$ are shown on the left, the generator SG, exciter EX, and voltage regulator VR with a voltage feedback Δv_t are shown in the middle, and the transformer and transmission line are shown on the right.

The Steam Turbine

The steam–mechanical energy conversion is a thermodynamic process by which the steam is expanded through the high-, medium-, and low-pressure turbines, normally all on one shaft. High-pressure and high-temperature steam energy from a boiler is converted into mechanical energy through the turbine blades, and transmitted to the shaft. There are other important parts of the turbines: the control valves, which control the steam input; the intercept valves, which can be used to divert the steam from the high-pressure turbine directly to the steam condenser; the steam chamber in front of the high-pressure turbine, which causes a time delay of the steam

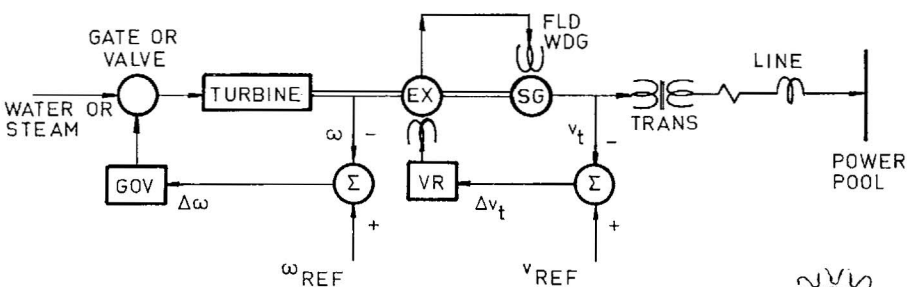

Fig. 1-1 Basic components of an electric power plant.

flow; the reheater between the high- and medium-pressure turbines, which causes another time delay; and the crossover connection between the medium- and low-pressure turbines, which causes still another time delay of the steam flow. Many other types of steam turbines are in use [35].

The Hydraulic Turbine

One of the oldest and most important prime movers, which has been serving mankind for thousands of years, is the water wheel. For large-scale electric energy generation, the water wheel has evolved into modern hydraulic turbines of power capacity as large as hundreds of megawatts. In most cases, the potential energy of water in a reservoir is converted into kinetic energy in the penstocks, and is then delivered to the turbine shaft.

There are many types of hydraulic turbines. The Kaplan turbine of the reaction type, with controllable wicket gates and adjustable runner blades, is efficient for very low and medium water heads. The Francis turbine, which is also of the reaction type, is efficient for medium and high water heads. The Pelton wheel, which is of the impulse type, is efficient for a very high water head. Transfer functions of hydraulic turbines can be found in reference [35].

The Governor

The function of a governor of an electric power plant is to maintain a constant speed, usually the synchronous speed of the turbine-generator set. A speed drop of the set due to an increase of electric power output will send the speed signal to the governor to increase the mechanical power input to the turbine(s), and a speed rise to decrease the mechanical input, maintaining a constant speed.

The governor of the major plant of a power area or subsystem is also given the function of power and frequency control of the area in a large interconnected electric power system. The governor responds not only to the scheduled electric power interchange among areas, but also to the change in system frequency due to local load variations. Another use of the governor is to implement a supplementary governor control to improve the stability of an electric power system.

There are two types of governors for both steam power and hydropower plants: the mechanical-hydraulic governor and the electric-hydraulic governor. More information can be found in reference [35]. One such system is shown in Fig. 1-2.

A Governor for a Hydroelectric Plant

Figure 1-2 shows a mechanical-hydraulic governor for a hydroelectric power plant [36]. The flyballs on top are held in position by springs during normal operation. Whenever a speed increase $\Delta\omega$ is sensed by the flyballs, the vertical rod a′ of the pilot valve will be lifted, and the fluid under pressure in the pilot valve will pass into the actuator servo to push a downward. In the meantime, the distribution valve with the vertical rod g′ also will be pushed downward; the fluid in the distribution valve will pass into the governor servo and push to the left so as to close the water gate to reduce the hydro energy input. The entire mechanism also works in the reverse direction, and a speed decrease will increase the hydro energy input. A dashpot in the middle of the figure is devised to stabilize the actuator itself. The transfer function of this governor and hydraulic power will be derived in Chapter 2.

The Synchronous Generator

The mechanical–electric energy conversion takes place in an electric generator, usually of the three-phase synchronous type, and is based on Faraday's induction law. The essential components are (1) an armature winding, (2) a magnetic field, and (3) a mechanical energy input, in the form of a force or a torque, which causes a relative motion of the armature winding with respect to the field.

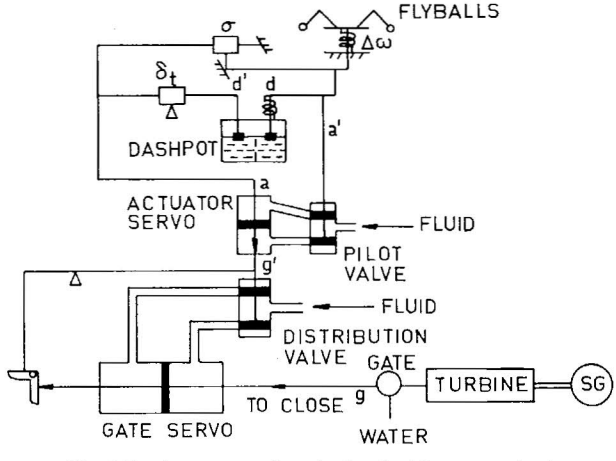

Fig. 1-2 A governor for a hydroelectric power plant.

One must note that whenever there is a voltage induced in the generator armature winding due to its relative motion with respect to the magnetic field, there is also an electric torque opposite to the mechanical torque of the prime mover when the generator has a load.

The three-phase synchronous generator used for large-scale electric energy generation has two synchronously rotating fields: one dc-excited field on the rotor with a field winding mechanically rotated normally at the synchronous speed and the other ac-excited on the stator with the three-phase armature winding, each phase winding 120° apart from the others electrically, and each phase current with a 120° time phase difference with respect to the others. The rotating field of the three-phase winding with three-phase excitation will be analyzed in Chapter 2. For the moment, the difference between the two fields should be noted. The speed of the three-phase ac field on the stator is completely dictated by the system frequency, and the field appears in and around the air gap of the machine instantly because of the nature of the electromagnetic field. On the other hand, the speed and hence the dc field of the rotor are affected by the inertia and damping of the rotating system. Only in the steady state, when the mechanical energy input and the electric energy output plus the system losses are in complete balance, will there be neither acceleration nor deceleration of the rotating system. In such a case, the two rotating fields, one dc and one ac, will be moving together synchronously, with the N poles of the ac field facing the S poles of the dc field, and the S poles of the ac field facing the N poles of the dc field across the air gap of the machine. However, when a disturbance occurs to the system and the input–output energy balance is upset, the N-to-S and S-to-N bonds will be shaken, causing a possible stability problem.

The Exciter and Voltage Regulator

For years the dc excitation of a synchronous machine field winding has been provided by the commutator-type rotating exciter. However, static exciters using thyristors and other devices are now available, which respond much more rapidly than the commutator type. Transfer functions and block diagrams of static exciters and voltage regulators for computer simulation can be found in reference [37].

A rotating exciter and voltage regulator system is shown in Fig. 1-3 [38]. The ac terminal voltage of the synchronous generator SG is sensed by a potential transformer PT, rectified and filtered, and then compared with a voltage reference v_{REF} to obtain the voltage deviation Δv_t. After being amplified by an amplifier AMPL, the signal is used to control the exciter

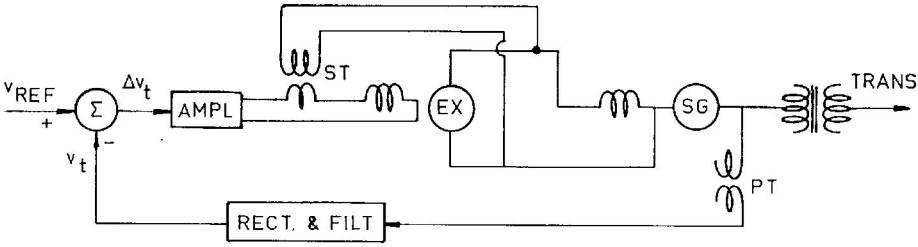

Fig. 1-3 A rotating exciter and voltage regulator system [38].

field, and the exciter output in turn to control the generator field excitation. The negative feedback works in such a way that the excitation will be increased whenever the terminal voltage drops below the voltage reference level and decreased whenever the terminal voltage rises above the voltage reference level. There is also a stabilizing transformer ST for the stabilization of the excitation system itself. The transfer functions and block diagrams of this excitation system will be derived in Chapter 2.

Although the original function of the exciter and voltage regulator system is to maintain a prescribed constant voltage at the synchronous generator terminal, the system also can be used to improve the dynamic and transient stabilities of a power system through supplementary excitation controls. These topics will be treated in subsequent chapters.

Summary of Section 1-1

In this section, an introduction has been given to the basic components of an electric power plant, which are important to power system dynamic studies: the hydraulic and steam turbines, which convert the hydraulic power or steam power to mechanical power; the governor, which controls the steam or hydraulic power of the turbine(s); the generator, wherein the mechanical–electric energy conversion takes place; and the exciter and voltage regulator, which control the electric power output. Although the governor has been used mainly to maintain a constant speed, and the excitation system to maintain a prescribed terminal voltage of the synchronous generator, they also can be used for power system stability control, which will be presented in later chapters. Details of modeling these system components—turbines, generators, governors, and excitation systems—will be presented in Chapter 2. Prior to that, an introduction to modern electric power systems will be given in the next section.

1-2 MODERN LARGE ELECTRIC POWER SYSTEMS

In the early stages of electric power system development, electric power plants burning oil or coal were built for local loads. With the development of hydroelectric power from the middle to the upper streams of rivers, electric power plants became more and more remote from local loads. High-voltage transmission lines were built, large and small electric power plants were interconnected for more economical and reliable generation and transmission of electric energy, and the electric power system began to take shape. As the trend continued, large and small electric power systems were also interconnected, which then grew to form national and international large electric power systems. Examples are as follows.

The North American Electric Power System

Almost all North American electric power systems of the United States and Canada are connected into one system, called NERC, the National Electric Reliability Council, which consists of nine regions as shown in Fig. 1-4 [39]. There are a few isolated power areas that are not connected to the system. There is only one weak link between the North American western system, which consists of only the WSCC region but has a vast espanse of geographic area, and the North American eastern system, which emcompasses all the NERC system except WSCC. The number of inter-regional connections are shown in the figure. The major transmission voltages are either 500 kV ac or ± 400 kV dc [39, 40].

The evolution of large-scale electric power system interconnections is interesting. British Columbia Hydro may be taken as an example. There were

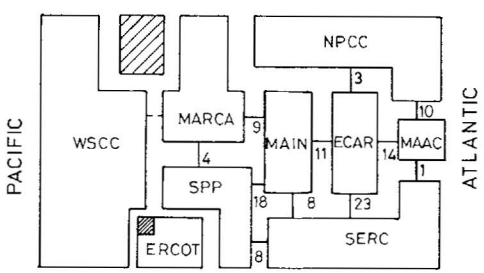

Fig. 1-4 The North American electric power system. (From [39], courtesy of IEEE, © 1977.) WSCC: Western Systems Coordinating Council; MARCA: Mid-Continent Area Reliability Coordinating Agreement; NPCC: Northeast Power Coordinating Council; ERCOT: Electric Reliability Council of Texas; SPP: Southeast Power Pool; MAIN: Mid-America Interpool Network; ECAR: East Central Area Reliability Coordinating Agreement; MAAC: Mid-Atlantic Area Council; SERC: Southeastern Electric Reliability Council.

many relatively small electric power companies in British Columbia, Canada, but gradually they were consolidated into two major "areas," the British Columbia Hydro and the West Kootenay, which in turn were joined by many other "areas" to form the Pacific Northwest Power Pool. The WSCC system was formed later by interconnecting the Pacific Northwest Power Pool and the Southwest Power Pool into one "region," extending from northern British Columbia, Canada, to the Mexican border, and from the Pacific coast to Colorado and other inland areas.

The British Super-Grid

After the original successful grid interconnection of all generating stations in Britain, a Super-Grid was completed and the transmission voltage raised from 275 kV to 400 kV [41]. According to a CEGB report [41], the British grid interconnects five regions: the Northwest, the Northeast, the Southwest, the Southeast, and the Midlands. The five regions and their headquarters are shown in Fig. 1-5. The Super-Grid is also connected to Scotland by 275-kV ac lines and to France across the Channel by ± 100-kV dc cables.

The Electric Power System in Western Europe

The electric power systems in western Europe are mainly interconnected by 400-kV ac lines, as shown in Fig. 1-6 [42]. There are also dc connections, for example, ± 250-kV dc between Denmark and Sweden, and ± 250-kV

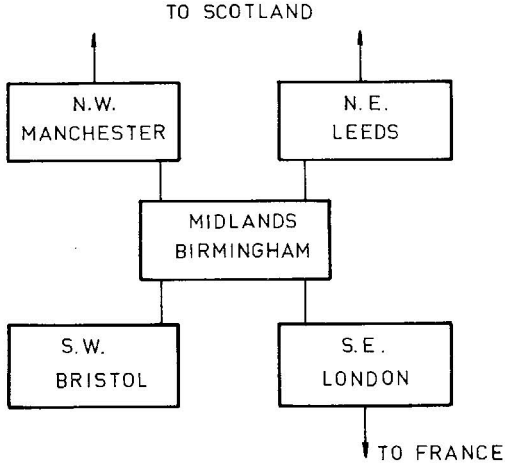

Fig. 1-5 The British Super-Grid.

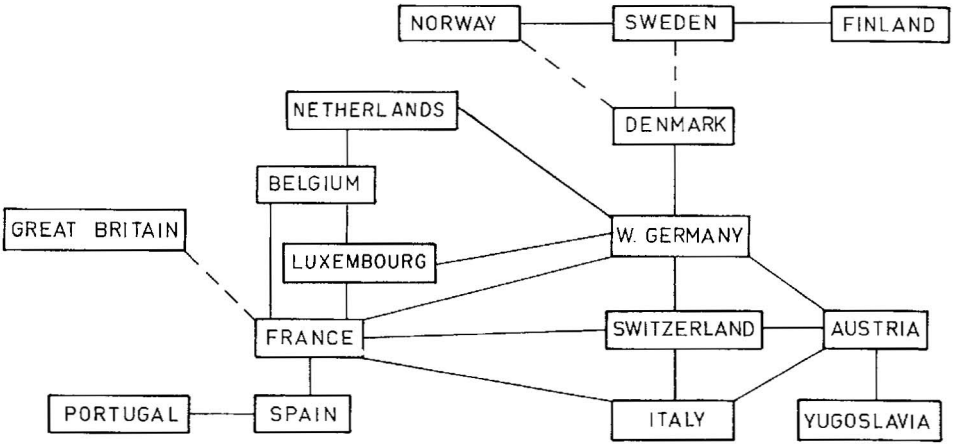

Fig. 1-6 The electric power system in Western Europe.

between Denmark and Norway. Finland, Austria, and Yugoslavia are also connected to eastern Europe. Belgium is connected either to West Germany through the Netherlands or to France, but not simultaneously.

The Electric Power System in Japan

There are nine regions of the electric power system in Japan, as shown in Fig. 1-7 [43], with Kyushu Electric Power in the southwest and Hokaido Electric Power in the Northeast. The major transmission voltage of the Japan electric power system is 500-kV ac, except for 275-kV dc between Tohoku (northeast) and Hokaido (Northern Sea district). Note that while the Japan Northeast electric power system is of 50 Hz, the Japan Southwest is of 60 Hz, and they are linked together by two 300-MW frequency converter

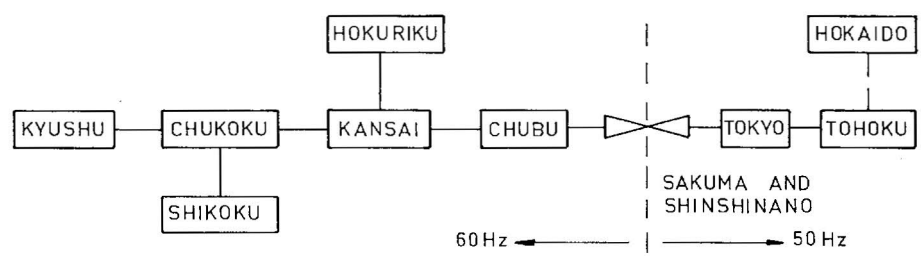

Fig. 1-7 The Japan electric power system.

stations at Sakuma and Shinshinano, which are capable of converting electric energy from one frequency to the other readily.

Comments

This section gives some notable examples of national and international large interconnected electric power systems. It must be noted that the interconnections, capacities, and voltage levels of these systems are constantly increasing.

Among the aforementioned systems, the North American electric power system is probably the most complicated. Since there are so many interconnections among regions, a major fault in any one region will normally affect the dynamic behavior of all neighboring regions and propagate beyond. Careful planning and effective protection are therefore necessary.

The transmission capacity of the British power grid is almost twice that of its generation capacity [44]. Therefore, the system is little affected by the loss of a line. This transmission capacity, however, cannot be afforded by the North American electric power system because of the longer distances involved.

The Japan electric power system is rather lucky with its two-frequrncy composition of 50 Hz in the Northeast and 60 Hz in the Southwest. The interconnection of the two-frequency system using dc converters was considered a great inconvenience, but its asynchronous ties improve the stability of the entire system.

Summary of Section 1-2

In this section, some national and international large electric power systems have been presented. The intention of large-scale electric power system interconnection is to achieve economical and reliable electric energy generation and transmission. Although it is understood that each participant in a power pool should have sufficient generating-capacity reserve or spinning reserve to meet sudden load increases or system maintenance requirements, some participants may not have enough reserves and rely heavily on interconnections. Such a practice makes system operation increasingly difficult.

One of the most important features of an electric power system is that there is practically no energy storage in the system. The electromagnetic and electrostatic energy storage associated with transmission is negligibly small as compared to the huge amount of electric energy transmitted. Therefore, the mechanical energy input to the system and the electric energy output

of the system plus energy losses of generation and transmission must be kept in balance everywhere in the system at all times. Despite accumulated valuable engineering experience and constant technical innovations, power system failures still occur. There are many increasingly challenging power system dynamic problems confronting power engineers, which will be introduced in the next section.

1-3 PROBLEMS OF ELECTRIC POWER SYSTEM DYNAMICS

In this section, problems associated with the dynamic behavior of electric power systems will be discussed. The analysis and solution of these problems will be treated in later chapters.

The term "dynamics" used here has a broader meaning than that associated with the term "stability" in the classical literature on electric power systems. It not only includes the stability analysis of electric power systems, but also deals with such topics as dynamic equivalents, torsional oscillations, and control. On the other hand, a line must be drawn to exclude some problem areas for various reasons. Examples include power and frequency control, which has been thoroughly treated in other books [26, 27]; the asynchronous operation of synchronous generators [21, 22], which is not a general practice; and the dual-axis excited synchronous generator [19, 20], which is generally considered uneconomical.

Before addressing these power system dynamic problems, we shall first present some stability definitions.

Stability Definitions

The power system stability definitions in the literature have been changing and the well-accepted definitions are two: the transient stability due to large disturbances, and the steady-state stability due to small disturbances. However, whether a disturbance is large or small is sometimes hard to define, as it may well depend on the capability of stability control.

Consider the two swing curves in Fig. 1-8 for a system with the same initial load P_{e0} and the same disturbance ΔP_e. Curve A corresponds to the system with an effective stability control and curve B without.

For the system without an effective stability control (curve B), the system will lose its stability at the first swing. The disturbance will be considered as large, and it will be a "transient stability" problem. For the system with an effective stability control (curve A), however, the system is not only

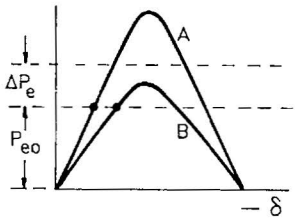

Fig. 1-8 A power system with and without stability control.

stable but also linearly stable. The disturbance will be considered small, and it will be a "steady-state stability" problem. Therefore, whether a disturbance should be categorized as large or small depends very much on the effectiveness of the stability control, and there are cases that cannot be adequately classified as either the steady-state stability or the transient stability.

There is another term often used in the literature, namely, "dynamic stability," which can be used properly to describe the case of curve A of Fig. 1-8. Therefore, the following stability definitions will be adopted in this book.

Steady-state stability refers to the stability of a power system subject to small and gradual changes in load, and the system remains stable with conventional excitation and governor controls.

Dynamic stability refers to the stability of a power system subject to a relatively small and "sudden" disturbance; the system can be described by linear differential equations, and the system can be stabilized by a linear and continuous supplementary stability control. Typical examples are the low-frequency oscillations of the interconnected large electric power systems and the torsional oscillations of a steam–electric power plant due to the subsynchronous resonance of the capacitor compensated transmission line.

Transient stability refers to the stability of a power system subject to a sudden and severe disturbance beyond the capability of the linear and continuous supplementary stability control, and the system may lose its stability at the first swing unless a more effective countermeasure is taken, usually of the discrete type, such as dynamic resistance braking or fast valving for the electric energy surplus area, or load shedding for the electric energy deficient area. For transient stability analysis and control design, the power system must be described by nonlinear differential equations.

Nonlinear stability is a mathematical term that refers to a general class of stability problem treated in all systems engineering, not just power system engineering. Here the system again must be described by nonlinear equations, but not necessarily nonlinear differential equations. Both the steady-state stability analysis using the equal-area criterion [33] and the transient

stability analysis by Lyapunov's direct method [18] are good examples of nonlinear stability studies.

Low-Frequency Oscillations of Large Electric Power Systems

One of the most important stability problems arising from large-scale electric power system interconnections is the low-frequency oscillations of interconnected systems [2–5]. The frequency is of the order of a fraction of 1 Hz to a few Hz. Examples include oscillations of the Saskatchewan–Manitoba–West Ontario system [3], the WSCC system [4], and the Southern Scotland electric power system connected to the British grid [46]. The oscillations may be sustained for minutes and grow to cause system separation if no adequate damping at the system oscillating frequency is available.

The low-frequency oscillations are attributed to the oscillations of the mechanical mode of the system and can be approximately analyzed with a linear "one-machine infinite-bus" model as follows [5]. Since the torque and speed may be treated as phasors during the periodic oscillations, a linearized torque equation can therefore be written

$$M\,\Delta\dot{\omega} + D\,\Delta\omega = \Delta T_m - \Delta T_e \tag{1-1}$$

where $M\,\Delta\dot{\omega}$ represents the accelerating torque, $D\,\Delta\omega$ the mechanical damping torque, ΔT_m the mechanical torque input, and ΔT_e the electric torque output, all in per unit of value. Other quantities are as follows: the speed ω in per unit of value, the inertia constant M in seconds, and the mechanical damping coefficient D in per unit of value.

When the synchronous speed $2\pi f$ rad/s is chosen as the base speed and denoted by ω_b, where f is the system frequency, the per-unit (pu) rotor speed can be expressed in terms of the base speed and the torque angle δ in electrical radians as follows:

$$\omega = \frac{1}{\omega_b}\frac{d\delta}{dt}, \qquad \Delta\omega = \frac{1}{\omega_b}\frac{d\,\Delta\delta}{dt} \quad \text{pu} \tag{1-2}$$

Next, since the mechanical damping of a machine in a large power system is negligibly small as compared with the damping required to attenuate the system oscillations, the $D\,\Delta\omega$ term of (1-1) may be neglected. Assuming also that the speed governor is not fast enough to affect the mechanical torque $\Delta T_m \simeq 0$, and that the electric torque ΔT_e has only a synchronizing component that may be denoted by $K_1\,\Delta\delta$, Eq. (1-1) may be written in the frequency domain as

$$(Ms^2 + K_1\omega_b)\,\Delta\delta = 0, \qquad \Delta\omega = s\,\Delta\delta/\omega_b \tag{1-3}$$

The solution of the undamped natural mechanical mode frequency becomes

$$s = \pm j\omega_n, \qquad \omega_n = \sqrt{K_1\omega_b/M} \tag{1-4}$$

Note that although $\Delta\omega$ of (1-1) is in per unit of value, ω_n of (1-4) is in radians per second, since M is in seconds and ω_b is in radians per second. Since K_1 is in the range of 0.5 to 1 and M in the range of 5 to 10, ω_n is of the order of $\sqrt{0.2\pi f}$ rad/s and the oscillating frequency f_n of the order of $\omega_n/2\pi$ Hz.

The techniques of stabilizing the low-frequency oscillations will be presented in Chapter 3.

Dynamic Stability and Linear Optimal Control

The low-frequency oscillations of large interconnected electric power systems, characterized by the mechanical mode oscillations, is not the only electric power system dynamic problem that can be analyzed by linear differential equations. There is a general class of electric power system dynamic problems that may involve several oscillating modes or several machines, and the oscillating frequencies are not necessarily very low. One example is the torsional oscillation of a steam–electric generating unit caused by the subsynchronous resonance of a capacitor compensated transmission system. It sometimes manifests multiple torsional mode oscillations. In such cases proper damping must be provided to all oscillating modes. Another example is multimachine system stabilization. Individual machines may have different requirements of damping torque and synchronizing torque, and multimachine multimode power system stabilization techniques must be sought.

The linear optimal control (LOC) developed in modern control theory provides just the right answer [10, 11]. It minimizes oscillations of all modes and optimizes the control effort at the same time. The first part implies that it will provide not only adequate damping but also proper synchronizing torques to all machines when the LOC is applied to a multimachine electric power system, and these damping and synchronizing torques are properly coordinated.

The principle of linear optimal control (LOC) and the application of LOC to electric power systems will be presented in Chapter 4.

Subsynchronous Resonance and Torsional Oscillations

Subsynchronous resonance (SSR) may occur in a steam–electric power plant connected to a capacitor compensated transmission system [6–9]. The

torsional oscillations of a steam–electric generating plant with high- medium- and low-pressure turbines, generator, and rotating exciter, all on one shaft, usually fall within the range of the system frequency or at subsynchronous frequencies. When a resonant frequency of the transmission system is complementary to any one of the torsional oscillating frequencies of the turbine-generator mass-spring system (i.e., when the two frequencies add up to the system frequency), the SSR will develop. The electric resonance of the transmission system and the torsional oscillations of the mass-spring system of the turbine-generator set will be mutually excited, and the torsional oscillations may grow to the extent that the shaft becomes seriously damaged.

Transmission of bulk electric energy over a long distance by capacitor-compensated transmission lines is far more economical than building more parallel transmission lines without the capacitor compensation. Generating electricity at the coal mine is much better than generating electricity near the load center in a thermal plant close to populated areas. For these reasons, the coal mine electricity generation and capacitor-compensated line transmission are very attractive.

The analysis of SSR and countermeasures will be presented in Chapter 5.

Dynamic Equivalencing of Large Electric Power Systems

As the interconnection of large electric power systems continues to grow, the system becomes larger and larger, covering an immense geographic area and including a huge number of electric machines [12–14]. For instance, the WSCC system has about 300 major generating units and covers about 50% of the area of North America. It is very difficult, if not impossible, to include all these machines in the dynamic studies for all conceivable contingencies, anywhere and everywhere in the system, even with a very large and fast computer. Indeed, we would be dealing with machines with reliable data and with significant effect, and machines without reliable data or significant effect, without discrimination. Furthermore, data acquisition and transmission present a very difficult problem even for off-line dynamic studies, not mentioning the possible need of on-line stability control.

One sensible approach is to draw a boundary line for a "study system" that includes a small number of machines of great concern, and separate them from the "external system," which may have a very large number of machines but of secondary concern. The "external system" will then be replaced by a small number of "dynamic equivalents" [12–14]. Our attention will not be focused on the dynamic behavior of the external system itself, but on the dynamic interacting effect of the external system on the study system.

The derivation of dynamic equivalents of large electric power systems will be presented in Chapter 6.

Nonlinear Stability Analysis and Transient Stability Controls

When a very large disturbance occurs suddenly to a power system because of a serious fault, more effective countermeasures than the linear continuous supplementary stability control must be taken immediately to balance the mechanical power input and the electric power output and to maintain the system stability. In the worst case, the faulted area must be isolated and the system separated, resulting in "island" operation.

There are also many effective measures, usually of the discrete type, which may be used to counter a serious fault [15, 16]. These measures include, for instance, dynamic resistance braking for a temporary electric energy surplus area, generator tripping for a permanent electric energy surplus area, and load shedding for a permanent electric energy deficiency area. For convenience, these countermeasures to control the transient stability of a power system due to a serious fault will be classified into two categories, the plant controls and the system controls. These topics will be introduced in Chapter 7.

There are also many nonlinear stability analysis techniques. One technique that has been fascinating power engineers for years, Lyapunov's direct method [17, 18], will also be introduced in Chapter 7.

Basic Models for Power System Dynamic Studies

For any power system dynamic study, a proper and adequate power system model must be chosen to include all significant components relevant to the problem in the model, and to exclude insignificant components irrelevant to the problem from the model. For example, for the study of low-frequency oscillations of a large electric power system as a one-machine infinite-bus system, a simple mechanical model with only one inertia constant, a simple synchronous generator model with only one field circuit differential equation, and an excitation system is sufficient. On the other hand, for the study of torsional oscillations of a steam turbine–generator plant due to the subsynchronous resonance of a capacitor-compensated transmission system to which the plant is connected, the simple model for the low-frequency study is neither proper nor adequate. For that study, the turbines and generator set must be considered as a multiple mass-spring system, and all generator windings, transmission lines, and the capacitor compensation must be described by differential equations.

Although there are many power system dynamic problems, the number of basic component models needed to describe any power system dynamic problem is rather limited. The basic models include the high- and low-order synchronous machines, the exciter and voltage regulator systems, and the turbines and governors.

The basic component models for power system dynamic studies will be presented in Chapter 2.

Summary of Section 1-3

In this section, an introduction has been given to the electric power system dynamic problems: the low-frequency oscillations of large electric power systems, the dynamic stability and the linear optimal control, the subsynchronous resonance and torsional oscillations, the dynamic equivalents of large electric power systems, nonlinear stability analysis and transient stability controls, and the basic component models for power system dynamic studies. More details will be presented in subsequent chapters.

1-4 SUMMARY

In the first section of this chapter, an introduction to the basic components of electric power plants for dynamic studies was given: the hydraulic and steam turbines, which provide the mechanical energy input; the synchronous generator, which converts mechanical energy into electric energy; the governor, which controls mechanical power input; and the excitation system, which controls electric power output. In the second section, examples of some notable national and international electric power systems are presented. In the last section, important electric power system dynamic problems are introduced. Since a proper and adequate model must be chosen for any power system dynamic studies, the basic component models of electric power systems will be presented next in Chapter 2.

Problems

1-1 An electric power system tends to develop low-frequency oscillations. Find the undamped mechanical mode frequencies in Hz for

(a) $K_1 = 0.8$ pu, $M = 5, 6, 7, 8, 9$ s,
(b) $M = 0.7$ s, $K_1 = 0.5, 0.6, 0.7, 0.8, 0.9$ pu,

if the system can be modeled as a one-machine infinite-bus system and the system frequency is 60 Hz.

1-2 Repeat Problem 1-1 for a system frequency of 50 Hz.

1-3 An electric power system has a low-frequency oscillation of 1 Hz. What will be the equivalent inertia M of the system if $K_1 = 0.7$ pu and the system can be modeled as a one-machine infinite-bus system? Assume that there is no system damping and the system frequency is

(a) 60 Hz,
(b) 50 Hz.

1-4 (a) Draw a connecting diagram for the electric power system in your area including major power plants, transmission lines, interconnections with the neighboring areas, and other components important to power system dynamic studies.

(b) Are there stability and other dynamic problems of the system?

(c) What stabilizing and control means are used or are being considered to solve those problems?

References

[1] R. T. Byerly and E. W. Kimbark, eds., "Stability of Large Electric Power Systems." IEEE Press Book, IEEE, New York, 1974.

[2] H. M. Ellis, J. E. Hardy, A. L. Blythe, and J. W. Skooglund, Dynamic stability of the Peace River transmission system. *IEEE Trans. Power Appar. Syst.* 586–600, June (1966).

[3] O. W. Hanson, C. J. Goodwin, and P. L. Dandeno, Influence of excitation and speed control parameters in stabilizing intersystem oscillations. *IEEE Trans. Power Appar. Syst.* 1306–1313, May (1968).

[4] F. R. Schleif, H. D. Hunkins, G. E. Martin, and E. E. Hattan, Excitation control to improve power system stability. *IEEE Trans. Power Appar. Syst.* 1426–1434, June (1968).

[5] F. P. deMello and C. Concordia, Concepts of synchronous machine stability as affected by excitation control. *IEEE Trans. Power Appar. Syst.* 316–329, April (1969).

[6] C. E. J. Bowler, D. N. Ewart, and C. Concordia, Self excited torsional frequency oscillations with series capacitors. *IEEE Trans. Power Appar. Syst.* 1688–1695, Sept./Oct. (1973).

[7] R. G. Farmer, A. L. Schwalb, and E. Katz, Navajo project report on subsynchronous resonance—analysis and solutions. *IEEE Trans. Power Appar. Syst.* 1226–1232, July/Aug. (1977).

[8] L. A. Kilgore, D. G. Ramey, and M. C. Hall, Simplified transmission and generation system analysis procedures for subsynchronous resonance problems. *IEEE Trans. Power Appar. Syst.* 1840–1846, Nov./Dec. (1977).

[9] Yao-nan Yu, M. D. Wvong, and K. K. Tse, Multi-mode wide-range subsynchronous stabilization. *IEEE PES Summ. Meet.* IEEE PES Paper A 78 554-8 (1978).

[10] Yao-nan Yu, K. Vongsuriya, and L. N. Wedman, Application of an optimal control theory to a power system. *IEEE Trans. Power Appar. Syst.* 55–62, Jan. (1970).

[11] J. H. Anderson, The control of a synchronous machine using optimal control theory. *Proc. IEEE* **90,** 25–35 (1971).

[12] J. M. Undrill, J. A. Casazza, E. M. Gulachenski, and L. K. Kirchmayer, Electromechanical equivalents for use in power system stability studies. *IEEE Trans. Power Appar. Syst.* 2060–2071, Sept./Oct. (1971).

[13] R. Podmore and A. Germond, Development of dynamic equivalents for transient stability studies. *Spec. Rep.—Electr. Power Res. Inst.* **EPRI EL-456** (*Palo Alto, Calif.*) (1977).

[14] W. W. Price, D. N. Ewart, G. M. Gulachemsli, and R. F. Silva, Dynamic equivalents from on-line measurements. *IEEE Trans. Power Appar. Syst.* 1349–1357, July/Aug. (1975).

[15] R. H. Park, Improved reliability of bulk power supply by fast load control. *Proc. Am. Power Conf.* **30,** 1128–1141 (1968).

[16] IEEE Committee, A description of discrete supplementary controls for stability. *IEEE Trans. Power Appar. Syst.* 149–165, Jan./Frb. (1978).

[17] A. H. El-Abiad and K. Nagappan, Transient stability regions of multi-machine power systems. *IEEE Trans. Power Appar. Syst.* 169–179, Feb. (1966).

[18] Yao-nan Yu and K. Vongsuriya, Nonlinear power system stability study by Liapunov function and Zubov's method. *IEEE Trans. Power Appar. Syst.* 1480–1485, Dec. (1967).

[19] S. C. Kapoor, S. S. Kalsi, and B. Adkins, Improvement of alternator stability by controlled quadrature excitation. *Proc. Inst. Electr. Eng.* **116,** 771–780 (1969).

[20] S. Takada, E. Ohta, and Y. Nagamura, Suppression of hunting in two-axis synchronous machine by control of field winding. *Electr. Eng. Jpn.* pp. 28–37 (1968).

[21] M. M. Botvinnik, "Asynchronized Synchronous Machine." Pergamon, Oxford, 1964.

[22] O. P. Malik and B. J. Cory, Study of asynchronous operation and resynchronization of synchronous machines. *Proc. Inst. Electr. Eng.* **113,** 1977 1990 (1966).

[23] "Electrical Transmission and Distribution," Westinghouse Reference Book, Chapter 13, Westinghouse, East Pittsburgh, 1964.

[24] I. Hano, "Operating Characteristics of Electric Power Systems." Denki Shoin, Tokyo, 1967.

[25] V. A. Venikov, "Transient Phenomena in Electrical Power Systems," 1958, Abridged English edition. Pergamon, Oxford, 1964.

[26] L. K. Kirchmayer, "Economic Control of Interconnected Systems." Wiley, New York, 1959.

[27] N. Cohn, "Control of Generation and Power Flow on Interconnected Systems." Wiley, New York, 1966.

[28] G. W. Stagg and A. H. El-Abiad, "Computer Methods in Power System Analysis." McGraw-Hill, New York, 1968.

[29] O. I. Elgerd, "Electric Energy System Theory." McGraw-Hill, New York, 1971.

[30] S. B. Crary, "Power System Stability," Vols. I and II. Wiley, New York, 1945, 1947.

[31] E. W. Kimbark, "Power System Stability," Vols. I, II, and III. Wiley, New York, 1948, 1950, 1956.

[32] J. R. Mortlock and M. W. Humphrey Davies, "Power System Analysis." Chapman & Hall, London, 1962.

[33] W. D. Stevenson, "Elements of Power System Analysis," 2nd ed. McGraw-Hill, New York, 1962

[34] P. M. Anderson and A. A. Fouad, "Power System Control and Stability." Iowa State Univ. Press, Ames, Iowa, 1977.

[35] IEEE Committee, Dynamic models for steam and hydro turbines in power system studies. *IEEE Trans. Power Appar. Syst.* 1904–1915, Nov./Dec. (1973).

[36] L. M. Hovey and L. A. Bateman, Speed regulation tests on a hydro station supplying an isolated load. *Trans. Am. Inst. Electr. Eng., Part 3* **81,** 364–371 (1962).

[37] IEEE Committee, Computer representation of excitation systems. *IEEE Trans. Power Appar. Syst.* 1460–1464, June (1968).

[38] H. F. Messerly and R. H. Bruck, Steady state stability of synchronous generators as affected by regulators and governors. *Proc. Inst. Electr. Eng., Part C* **102,** 24–34 (1955).
[39] IEEE Committee, "Symposium on Reliability Criteria for Power System Dynamic Performance," Publ. 77CH1221-1-PWR. IEEE, New York, 1977.
[40] IEEE Committee, Dynamic performance characteristics of North American HVDC systems for transient and dynamic stability evaluations. *IEEE Trans. Power Appar. Syst.* 3356–3364, July (1981).
[41] Central Electricity Generating Board, "CEGB Annual Report," Vol. 2, CEGB, London, 1972–1973.
[42] I. Hano, chief ed., "Power Engineering Desk Book." Denki Shoin, Tokyo, 1970; communication with Dr. M. Dommelen of Belgium, 1980.
[43] Official Report, "Electric Power Industry in Japan." Overseas Electrical Industry Survey Institute, Tokyo, 1978.
[44] G. Shackshaft, private communication, Central Electricity Generating Board, June 1974.
[45] Kyushu Electric Power Co., Japan, private communication with power engineers, Oct., 1977.
[46] T. R. Foord, Glasgow University, Scotland, private communication, June 1974.

Chapter 2 Basic Models for Power System Dynamic Studies

For any electric power system dynamic study, a proper mathematical model must be chosen. Yet the selection of a power system model cannot be dissociated from the problem itself, nor from the computational facilities and control techniques available. It is neither adequate nor practical to devise a "universal model" for all power system dynamic problems.

When the power system stability problem was investigated years ago using an ac calculating board, the model of voltage behind reactance with a second-order torque equation was the best choice; the system was relatively small, and there were no other computational facilities available. With modern digital computers, however, there is a tendency to overrepresent an electric power system.

There are various kinds of power system dynamic problems: high- or low-frequency oscillations, large or small system disturbances, and large or small electric power systems. However, there are only a limited number of system components important to the dynamic study: the hydraulic and steam turbines, the synchronous generator, the governor, and the excitation system. For each of them, several basic models are recommended by the professional societies, and can be adapted for the studies of specific problems. Among the basic models, those of the synchronous generator are probably the most important and complicated. Therefore, the fundamental equations of synchronous machines will be presented first in this chapter.

2-1 FUNDAMENTAL EQUATIONS OF SYNCHRONOUS MACHINES

The power system dynamic problems are mainly those of the synchronous machines in a power system. For instance, the low-frequency oscillations

of a large electric power system are due to the mechanical mode oscillations of the machines in the system, and the torsional oscillations of a steam–electric plant at the subsynchronous frequencies are due to the mechanical oscillations of the steam turbines, the synchronous generator, and the exciter interacting with the electrical resonance of a capacitor-compensated transmission system.

Fundamental equations of synchronous machines were derived by Park and others years ago [1–7]. Park's equations have the simplest form and are most well known. His voltage equations are described by a coordinate system consisting of a d axis or direct axis fixed on the field winding axis or pole axis, and a q axis or quadrature axis fixed in quadrature with respect to the d axis. In this section, Park's equations are rederived from the concepts of two-phase equivalent and commutator coordinates. For the original derivation, see references [1, 2].

Park's Voltage Equations of Synchronous Generators

Park's synchronous machine may be schematically shown as Fig. 2-1. There are three armature phase windings a, b, and c on the stator of the machine, which have been replaced by two equivalent armature phase windings, a d winding on the d axis and a q winding on the q axis. There are two damper windings on the rotor, D on the d axis and Q on the q axis, which are permanently short-circuited. There is also a field winding F on the d axis, which is dc-excited.

Since there is no static coupling between any d-axis winding and any q-axis winding, Park's voltage equations for a synchronous machine have the simplest form. The equations may be written as follows [1–7],

$$\begin{aligned} V_d &= R_a(-I_d) + p\lambda_d - \lambda_q p\theta \\ V_q &= R_a(-I_q) + p\lambda_q + \lambda_d p\theta \\ V_F &= R_F I_F + p\lambda_F \\ 0 &= R_D I_D + p\lambda_D \\ 0 &= R_Q I_Q + p\lambda_Q \end{aligned} \tag{2-1}$$

In (2-1), V denotes a voltage in volts, I a current in amperes, R a resistance in ohms, λ a flux linkage in webers, and $p\theta$ a speed in electrical radians per second. Subscripts d, q, F, D, and Q signify the windings. Both d and q windings have the same resistance; it is denoted by R_a. Negative signs are given to I_d and I_q since the armature winding of a generator is an "active" network that converts mechanical energy into electric energy.

In engineering analysis, the International System of Units (Système International d'Unités, SI) is recommended, which consists mainly of the MKS units, such as meter (m), newton-meter (N-m), weber (Wb), and so on.

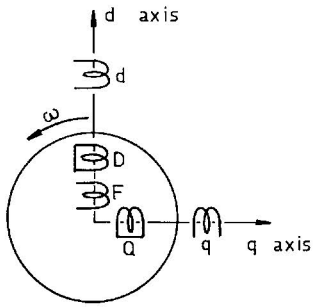

Fig. 2-1 Park's synchronous machine.

In modern electric power system analysis, however, equations are preferably written in per unit of value. Therefore, we must first be familiar with the basic per-unit relations, especially those for electric power system dynamic studies.

Per-Unit Relations

Let a power system frequency be f(Hz), a machine angle be θ(rad), and the corresponding speed be $p\theta$ or ω_e(rad/s) where p denotes the differential operator d/dt(1/s). Let the system speed $2\pi f$(rad/s) be chosen as the base speed ω_b(rad/s). The per unit machine speed ω(pu) becomes

$$\omega(\text{pu}) = \omega_e(\text{rad/s})/\omega_b(\text{rad/s}) \tag{2-2a}$$

where

$$\omega_e = p\theta, \qquad \omega_b = 2\pi f \tag{2-2b}$$

In Eq. (2-2a), the unit of a variable is explicitly expressed and included in parentheses following the variable. We may write a parameter with its unit in the same way. Thus we may write a base voltage as V_b(V), a base current as I_b(A), a base resistance as $R_b(\Omega)$, and a base flux linkage as λ_b(Wb), where the subscript b signifies a base value. Then we have

$$V_b(\text{V}) = R_b(\Omega)I_b(\text{A})$$

and (2-3)

$$V_b(\text{V}) = \omega_b(\text{rad/s})\lambda_b(\text{Wb})$$

Dividing through various terms of the first equation of (2-1) by a base voltage of the proper form, we shall have

$$v_d(\text{pu}) = -r_a(\text{pu})i_d(\text{pu}) + \dot{\psi}_d(\text{pu/s})/\omega_b(\text{rad/s}) - \omega(\text{pu})\psi_q(\text{pu}) \tag{2-4a}$$

Therefore, Eqs. (2-1) can be written in per unit of value, similarly to (2-4a), resulting in the following:

$$\begin{aligned} v_d &= r_a(-i_d) + \dot{\psi}_d/\omega_b - \omega\psi_q \\ v_q &= r_a(-i_q) + \dot{\psi}_q/\omega_b + \omega\psi_d \\ v_F &= r_F i_F + \dot{\psi}_F/\omega_b \\ 0 &= r_D i_D + \dot{\psi}_D/\omega_b \\ 0 &= r_Q i_Q + \dot{\psi}_Q/\omega_b \end{aligned} \tag{2-4b}$$

In Eqs. (2-4b), v, i, r, ψ, and ω, respectively, denote the voltage, current, resistance, flux linkage, and speed, all in per unit of value, and the subscripts d, q, F, D, and Q signify the respective windings. The time derivative of ψ is $\dot{\psi}$ and $2\pi f$ radian per second is chosen as the base speed ω_b. But ω_b will become unity if one radian per second is chosen as the base speed.

Other important per-unit relations for power system dynamic studies are as follows. First

$$X(\Omega) = \omega_e(\text{rad/s})L(\text{H}), \qquad X_b(\Omega) = \omega_b(\text{rad/s})L(\text{H})$$

therefore we have

$$x(\text{pu}) = \omega L(\text{pu}) \qquad \text{and} \qquad x(\text{pu}) \simeq L(\text{pu}) \tag{2-5a}$$

at the system frequency. Since

$$\lambda(\text{Wb}) = L(\text{H})I(\text{A}) \qquad \text{and} \qquad \lambda_b(\text{Wb}) = L_b(\text{H})I_b(\text{A})$$

we have

$$\psi(\text{pu}) = L(\text{pu})i(\text{pu}) = x(\text{pu})i(\text{pu}) \tag{2-5b}$$

although we still can distinguish a per-unit reactance x from a per-unit inductance L by writing

$$\psi(\text{pu}) = \frac{1}{\omega_0} x(\text{pu})i(\text{pu}), \qquad \omega_0 = 1 \tag{2-5c}$$

Finally, since

$$\begin{aligned} T_e(\text{N-m}) &= P_e(\text{W})/\omega_m(\text{mech. rad/s}) \\ T_b(\text{N-m}) &= P_b(\text{W})/\omega_{mb}(\text{mech. rad/s}) \end{aligned}$$

where ω_m is the mechanical speed, ω_{mb} the base mechanical speed, and N-m is the abbreviation of newton-meter, we also have

$$T_e(\text{pu}) = P_e(\text{pu})/\omega(\text{pu}), \qquad \omega \simeq 1 \tag{2-5d}$$

Note that the electrical per-unit speed and the mechanical per-unit speed are equal since an electrical speed including the base speed is $p/2$ times the corresponding mechanical speed, where $p/2$ is the number of pole pairs.

The time constant of a machine winding circuit will be expressed in seconds in this book. For instance, the field winding circuit time constant

$$T'_{d0}(\text{s}) = \frac{L_F(\text{H})}{R_F(\Omega)} = \frac{1}{2\pi f\,(\text{rad/s})} \frac{X_F(\Omega)}{R_F(\Omega)} = \frac{1}{\omega_b(\text{rad/s})} \frac{x_F(\text{pu})}{r_F(\text{pu})} \tag{2-5e}$$

the base ohm being the same for resistance and reactance.

The Mechanical–Electric Energy Conversion Torque

To apply Park's equations for power system dynamic analysis, the mechanical–electric energy conversion torque, or simply the electric torque, is calculated as follows. Since the mechanical–electric energy conversion is taking place only in the armature windings through their speed voltages, the electric torque

$$T_e = P_e/\omega = [i_d(-\omega\psi_q) + i_q(\omega\psi_d)]/\omega \doteq i_q\psi_d - i_d\psi_q \tag{2-6}$$

Note that an armature winding is always considered to be moving with respect to the field, which is deemed stationary.

Two-Phase Equivalent of the Three-Phase Winding

The derivation of the two-phase equivalent of Fig. 2-1 for a three-phase armature winding of a synchronous machine can be achieved as follows: first, replacing the three-phase winding by a two-phase winding with the same exciting effect at any point around the machine air gap between the stator and the rotor; and second, observing the two-phase equivalent from a commutator coordinate system with two sets of fictitious brushes on the d and q axes [8].

The time variation of magnetomotive forces (mmfs) and their space distribution around the air gap of the three-phase windings a, b, and c can be expressed by

$$\begin{aligned} A_a &= A_m \sin \omega_e t \cdot \cos\theta \\ A_b &= A_m \sin(\omega_e t - 2\pi/3) \cdot \cos(\theta - 2\pi/3) \\ A_c &= A_m \sin(\omega_e t - 4\pi/3) \cdot \cos(\theta - 4\pi/3) \end{aligned} \tag{2-7}$$

where the time variation of mmfs stemming from the currents are represented by the sine functions, $\omega_e t$ is a time angle, ω_e equals $2\pi f$, f is the system

frequency, and time zero is chosen when the a-phase current is zero and increasing. The space distributions of the mmfs are represented by the cosine functions, θ is a space angle, and the space origin is chosen at the a-winding axis; see Figs. 2-2 and 2-3a.

In Eqs. (2-7), a symmetrical three-phase winding with a balanced three-phase current has been assumed, and the maximum mmf per phase may be calculated from

$$A_m = \frac{4}{\pi} \frac{K_d K_p N}{p} \sqrt{2} I \tag{2-7a}$$

The first factor $4/\pi$ stems from the Fourier series analysis; the second consists of the winding distribution factor K_d, the winding pitch factor K_p, the number of turns in series per phase N, and the number of poles p; and the last is the maximum value of the rms phase current I. For a symmetrical three-phase winding with unbalanced three-phase currents, the currents should be resolved into three symmetrical components, and the positive sequence current can be resolved into the d and q components.

Equations (2-7) represent three "alternating mmfs" with the time variation and the space distribution explicitly expressed by two separate functions.

Figure 2-2 shows the space distributions of the a-phase mmf at two instants. As in the case of a typical alternating mmf, the nodal points of the mmf distribution are fixed but the magnitude varies with time.

The picture changes completely when the three-phase mmfs of Eq. (2-7) are combined, resulting in

$$A_a + A_b + A_c = \tfrac{3}{2} A_m \sin(\omega_e t - \theta) \tag{2-8}$$

The resulting mmf is an explicit function of both time and space. In other words, the space varies with time. It is no longer an "alternating mmf" with fixed nodes and time-varying amplitude, but a "revolving mmf" with a constant wave front.

To find the speed of the resulting mmf of Eq. (2-8), let us imagine that we are sitting somewhere on the wave front, as if we were aboard a moving ship. Since we do not detect any change in our position with respect to the ship's

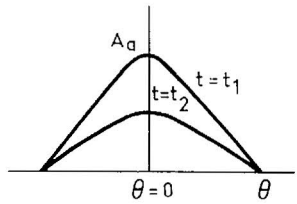

Fig. 2-2 a-phase mmf.

deck although the ship itself is moving, it suggests that

$$\frac{d}{dt}\left[\tfrac{3}{2}A_{\mathrm{m}}\sin(\omega_{\mathrm{e}}t-\theta)\right]=0 \tag{2-8a}$$

Therefore we have

$$\dot{\theta}=\omega_{\mathrm{e}}=2\pi f=f(2\pi) \tag{2-8b}$$

That is a speed of $2\pi f$ electrical rad/s, 2π rad, or one "pole-pair" (one N and one S) per cycle, or the "synchronous speed." Therefore, three symmetrical phase windings with three balanced phase currents always give rise to a single revolving field at synchronous speed.

The three-phase winding with balanced currents is not the only configuration that gives rise to a revolving field. So does a two-phase or semi-quarter-phase winding with balanced currents. Let the two-phase winding mmfs be

$$\begin{aligned}A_{\alpha}&=\tfrac{3}{2}A_{\mathrm{m}}\sin\omega_{\mathrm{e}}t\cdot\cos\theta\\ A_{\beta}&=\tfrac{3}{2}A_{\mathrm{m}}\sin(\omega_{\mathrm{e}}t-\tfrac{1}{2}\pi)\cdot\cos(\theta-\tfrac{1}{2}\pi)\end{aligned} \tag{2-9}$$

In other words, for an α-winding coaxial with winding a, an α-phase current in phase with the a-phase current, a β winding in quadrature with α or a, a β-phase current lagging behind the α-phase current by $\pi/2$, and each mmf magnitude of α and β being $\frac{3}{2}$ times that of the three phases, it can be shown that the three-phase winding and the two-phase winding will have exactly the same resulting mmf with the same exciting effect at any point around the machine air gap between the stator and the rotor. These two sets of windings are shown in Fig. 2-3a and b. The damper windings are omitted for clarity.

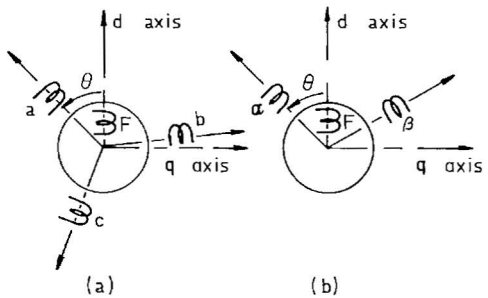

Fig. 2-3 A three-phase winding and its two-phase equivalent.

The d and q Commutator Coordinates

Since the armature windings are moving relatively with respect to the field, the mutual inductance of a and F in Fig. 2-3a and that of α and F in Fig. 2-3b, for instance, are functions of the space angle θ. Consequently, the voltage equations of the two-phase equivalents are not much simpler than those of the original three-phase windings. However, the results would be much simpler if the phenomena of the two-phase equivalents were observed from two sets of fictitious commutator brushes on the d axis and q axis, as in Fig. 2-4, like dc commutator windings. This is essentially the basic concept leading to the simplicity of Park's equations. While the two commutator phase windings can be identified as d and q, the α and β windings may be deemed as the slip-ring windings.

The conversion of Fig. 2-3b into Fig. 2-4 makes the configuration of windings much simpler, since d and q are in quadrature or orthogonal and there is no static coupling of any winding on the d axis with any winding on the q axis. Therefore, Eqs. (2-1) can be readily written except for the speed voltage terms.

The Speed Voltages

The speed voltages of Eqs. (2-1) can be derived from a general inductance formula for rotating electric machines [7], and a general speed voltage sign rule for the cross-field commutator armature windings [8].

Consider two typical windings of an electric machine, an induced voltage winding m and an excitation winding n, as shown in Fig. 2-5. The two windings may be both moving, both stationary, or one moving while the other is stationary. The induced voltage can be expressed in either of the two forms

$$e_m = -\frac{d}{dt}(N_m \phi_m) \tag{2-10a}$$

$$e_m = -\frac{d}{dt}(L_{mn} i_n) \tag{2-10b}$$

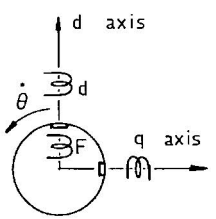

Fig. 2-4 The d and q commutator coordinates.

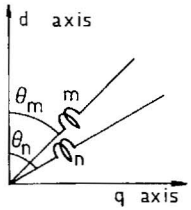

Fig. 2-5 Two typical windings of an electric machine.

where L_{mn} is the mutual inductance of windings m and n, N_m the effective number of turns per phase of winding m, N_n that of winding n, $N_n i_n$ the mmf, and ϕ_n the flux due to $N_n i_n$. In the linear case, we shall have

$$L_{mn} = N_m \phi_n / i_n = N_m (N_n i_n P)/i_n = N_m N_n P \tag{2-10c}$$

where P is the average permeance per pole. In other words, the inductance of an electric machine can be calculated from the flux linkage per unit exciting current.

For a salient-pole machine, the effective permeance of the d axis and that of the q axis are different. Therefore, the d and q components of the inductance must be calculated separately. Assume that both the mmf of the n winding and linkage of the m winding can be resolved into the d and q components, and the d axis is chosen as the reference; the component mmfs, fluxes, and flux linkages are shown in the accompanying tabulation, where P_d and P_q

	d component	q component
Mmf of n	$N_n i_n \cos\theta_n$	$N_n i_n \sin\theta_n$
Flux due to $N_n i_n$	$N_n i_n \cos\theta_n \cdot P_d$	$N_n i_n \sin\theta_n \cdot P_q$
Flux linkage with m	$N_n i_n \cos\theta_n \cdot P_d \cdot N_m \cos\theta_m$	$N_n I_n \sin\theta_n \cdot P_q \cdot N_m \sin\theta_m$

are the average permeances per pole of the respective axes. Therefore, the mutual inductance L_{mn} of windings m and n becomes

$$L_{mn} = L_{mn(d)} \cos\theta_m \cos\theta_n + L_{mn(q)} \sin\theta_m \sin\theta_n \tag{2-11}$$

$$L_{mn(d)} \triangleq N_m N_n P_d, \qquad L_{mn(q)} \triangleq N_m N_n P_q \tag{2-11a}$$

where L_{mn} is a function of both θ_m and θ_n. Since "n" could be "m" itself, the general mutual inductance formula L_{mn} also includes self-inductance as a special case. Equation (2-11) also applies to a cylindrical-rotor machine. In that case, P_d equals P_q and hence L_d equals L_q.

In the derivation of L_{mn}, the leakage inductance l_m was not included. Therefore, the complete voltage equation of winding m should be written [8]

$$v_m = (r_m + l_m p) i_m + p L_{mn}(\theta_m, \theta_n) i_n \tag{2-12}$$

The first term of the RHS of Eq. (2-12) represents the leakage impedance voltage of winding m. The second term may be expanded into three terms,

$$p[L_{mn}(\theta_m, \theta_n)i_n] = L_{mn}pi_n + \dot{\theta}_m \frac{\partial L_{mn}}{\partial \theta_m} i_n + \frac{\partial L_{mn}}{\partial \theta_n} \dot{\theta}_n i_n \tag{2-13}$$

There are two speed voltages on the RHS of Eq. (2-13). The first one is due to the speed $\dot{\theta}_m$ of the induced voltage winding, which is relevant to the mechanical–electric energy conversion process. The second one is due to the speed $\dot{\theta}_n$ of the excitation winding, which is irrelevant to the energy conversion process. Furthermore, a commutator winding as an excitation winding with stationary brushes always appears to be stationary. Therefore,

$$\dot{\theta}_n = 0 \tag{2-14}$$

and Eq. (2-13) becomes

$$v_m = [r_m + (l_m + L_{mn})p]i_n + \dot{\theta}_m \frac{\partial L_{mn}}{\partial \theta_m} i_n \tag{2-15}$$

Note that both Eqs. (2-13) and (2-15) are written in a general form applicable to machines with any number of windings. In such a case, v_m and i_n are column matrices and r_m, l_m, θ_m, and θ_n become diagonal matrices.

Our present concern is to find the speed voltages of the synchronous machine in Park's coordinates. From Eq. (2-11), we have

$$\frac{\partial L_{mn}}{\partial \theta_m} = -L_{mn(d)} \sin \theta_m \cos \theta_n + L_{mn(q)} \cos \theta_m \sin \theta_n \tag{2-16}$$

For all combinations of a d- or q-axis commutator armature winding with a cross-field excitation, either 90° leading or lagging in the direction of rotation of the armature winding, we have

θ_m	0°	90°	180°	270°	0°	90°	180°	270°
θ_n	90°	180°	270°	0°	−90°	0°	90°	180°
Speed voltage sign	+	+	+	+	−	−	−	−

A general rule emerges:

The speed voltage of a commutator winding is always *positive* if the cross-field excitation is *leading* in the direction of rotation of the armature winding, and *negative* if the cross-field excitation is *lagging* in the direction of rotation of the armature winding.

Therefore, according to Fig. 2-1, the speed voltage of d winding in Eq. (2-1) is negative, and that of q winding positive.

Discussion of Equation (2-1)

For synchronous motors, the negative signs of i_d and i_q in Eq. (2-1) will be removed since the armature winding of a motor is a "passive" electric network that converts electric energy into mechanical energy.

For a synchronous generator that has a second damper winding S on the q axis of the rotor, a voltage equation similar to the Q winding may be added. Similarly, for a dual-axis excited synchronous generator that has a second field winding G on the q axis of the rotor, a voltage equation similar to the F winding must be added.

Saturation of the synchronous machines may be considered. It is the magnetic circuit, not the winding, that is saturated. Therefore, the total excitation of the magnetic circuit, not just the field current, should be used to find the saturation factor.

Summary of Section 2-1

In this section, Park's voltage equations of synchronous generators are derived from the concepts of a two-phase equivalent of a three-phase winding and commutator coordinates with fictitious brushes. A general rule to determine the speed voltage signs of the d and q windings is presented. A discussion of equations for synchronous motors, generators with more than one rotor winding, and saturation is also included.

2-2 FLUX LINKAGES, REACTANCES, AND TIME CONSTANTS

To develop the high- and low-order synchronous machine models from Park's equations for various power system dynamic studies, it is necessary to have clear definitions of the flux linkages, the reactances, and the time constants of the machine. During the development of synchronous machine theory, many reactances and time constants have been defined. They include the synchronous reactances for steady-state analysis; the transient reactances, which include the field winding effect for electric transient analysis and certain dynamic studies; the subtransient reactances, which further include the damper effect for the fastest electric transient analysis and other dynamic

studies; and the transient and subtransient time constants associated with the reactances.

The d- and q-Axis Flux Linkages and Equivalent Circuits

Consider the flux linkages of the d- and q-axis windings of Fig. 2-1. Assuming only one common mutual reactance for all windings per axis, the flux linkages may be expressed as follows. Including ω_0 of Eq. (2-5c) to distinguish a per-unit reactance from a per-unit inductance, we shall have

$$\begin{bmatrix} \psi_d \\ \psi_F \\ \psi_D \end{bmatrix} = \frac{1}{\omega_0} \begin{bmatrix} x_d & x_{md} & x_{md} \\ x_{md} & x_F & x_{md} \\ x_{md} & x_{md} & x_D \end{bmatrix} \begin{bmatrix} -i_d \\ i_F \\ i_D \end{bmatrix} \tag{2-17}$$

$$\begin{bmatrix} \psi_q \\ \psi_Q \end{bmatrix} = \frac{1}{\omega_0} \begin{bmatrix} x_q & x_{mq} \\ x_{mq} & x_Q \end{bmatrix} \begin{bmatrix} -i_q \\ i_Q \end{bmatrix} \tag{2-18}$$

In Eqs. (2-17) and (2-18), the total reactances of the respective windings are denoted by x_d, x_F, x_D, x_q, and x_Q, and the mutual reactances of the respective axes by x_{md} and x_{mq}. All flux linkages, speed, reactances, and currents are in per unit of value. The speed ω_0, although one per unit, is used in these equations to convert a per-unit reactance into a per-unit inductance. For the flux linkages to have the simple form of Eqs. (2-17) and (2-18), certain relations exist [10], which will be discussed in a later part of this section.

Based on Eqs. (2-17) and (2-18), the d- and q-axis equivalent circuit for the synchronous machine, similar to those of the three-winding transformer and the two-winding transformer, may be drawn as in Fig. 2-6. In the figure, r_a, r_F, r_D, and r_Q, respectively, denote the individual resistances of the d and q windings, the field winding, the D-damper winding, and the Q-damper winding, and x_l, x_{lF}, x_{lD}, and x_{lQ} the respective leakage reactances.

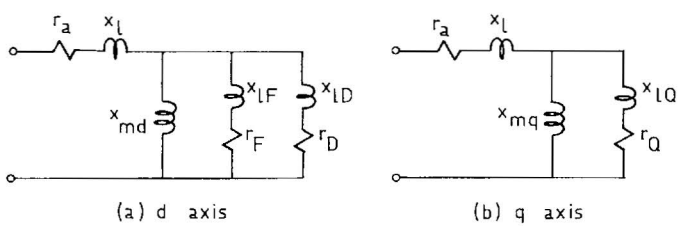

Fig. 2-6 The d- and q-axis equivalent circuits of the synchronous machine.

Reactances and Time Constants

Based on Fig. 2-6, the following reactances can be defined:

Synchronous reactances

$$x_d \triangleq x_l + x_{md}, \qquad x_q \triangleq x_l + x_{mq} \tag{2-19}$$

Field and damper total reactances

$$x_F \triangleq x_{lF} + x_{md}, \qquad x_D \triangleq x_{lD} + x_{md}, \qquad x_Q \triangleq x_{lQ} + x_{mq} \tag{2-20}$$

Transient reactances

$$x'_d \triangleq x_l + \frac{x_{lF}x_{md}}{x_{lF} + x_{md}}, \qquad x_q \triangleq x_l + x_{mq} \tag{2-21}$$

Subtransient reactances

$$x''_d \triangleq x_l + \frac{x_{lF}x_{lD}x_{md}}{x_{lF}x_{lD} + x_{lF}x_{md} + x_{lD}x_{md}}, \qquad x''_q \triangleq x_l + \frac{x_{lQ}x_{mq}}{x_{lQ} + x_{md}} \tag{2-22}$$

Note that all synchronous, transient, and subtransient reactances are defined from the series–parallel reactances of Fig. 2-6 as seen from the armature terminals. All resistances, being relatively small as compared with the respective reactances, are neglected.

Again based on Fig. 2-6, the following time constants in seconds can be defined. According to Eq. (2-5e), we shall have

Transient time constants

$$T'_{do} \triangleq \frac{1}{\omega_b r_F}(x_{lF} + x_{md}) \tag{2-23a}$$

$$T'_d \triangleq \frac{1}{\omega_b r_F}\left(x_{lF} + \frac{1}{(1/x_l) + (1/x_{md})}\right) \tag{2-23b}$$

Subtransient time constants

$$\begin{aligned}
T''_{do} &\triangleq \frac{1}{\omega_b r_D}\left(x_{lD} + \frac{1}{(1/x_{lF}) + (1/x_{md})}\right) \\
T''_d &\triangleq \frac{1}{\omega_b r_D}\left(x_{lD} + \frac{1}{(1/x_l) + (1/x_{lF}) + (1/x_{md})}\right) \\
T''_{qo} &\triangleq \frac{1}{\omega_b r_Q}(x_{lQ} + x_{mq}) \\
T''_q &\triangleq \frac{1}{\omega_b r_Q}\left(x_{lQ} + \frac{1}{(1/x_l) + (1/x_{mq})}\right)
\end{aligned} \tag{2-24}$$

Note also that all time constants are defined by the ratio of the series–parallel reactances as seen from an individual winding over the resistance of that winding. All other winding resistances, being small as compared with the respective reactances, are neglected. Two kinds of time constants are defined: one with the armature winding circuit opened, and the other with the armature winding short-circuited. The open-circuited time constants are identified with an additional subscript o.

These reactances and time constants were originally used in electric transient analysis. At the very beginning of a transient state, or in the subtransient state, there will be sudden changes in armature currents and mmfs due to a fault or switching. Changes also occur in field as well as damper currents and mmfs due to the transformer action between the stator and rotor windings. Therefore, the subtransient reactances and time constants will be used for the subtransient state analysis.

During the subtransient state, the damper winding effect will rapidly disappear due to the small time constants of the damper windings. After the subtransient state, the field winding effect still exists due to the large time constant of the field winding. Therefore, transient reactances and time constants will be used for the transient state analysis.

It should be noted that the subtransient, transient, and steady states are not discrete phenomena. They actually constitute a continuous process. For details, see reference [9].

The synchronous, transient, and subtransient reactances and time constants are also used in power system dynamic studies. Both field winding effect and damper winding effect are felt whenever there are rotor oscillations with respect to the synchronously rotating field on the stator.

Example 2-1. Show that there are two identities relating reactance and time constant definitions,

$$\frac{T'_d}{T'_{do}} = \frac{x'_d}{x_d}, \qquad \frac{T''_d}{T''_{do}} = \frac{x''_d}{x'_d} \tag{2-25}$$

Solution: From the definitions, we have

$$\frac{T'_d}{T'_{do}} = \frac{x_{lF} + x_l x_{md}/(x_l + x_{md})}{x_{lF} + x_{md}} = \frac{1}{x_l + x_{md}}\left(x_l + \frac{x_{lF}x_{md}}{x_{lF} + x_{md}}\right) = \frac{x'_d}{x_d}$$

and

$$\frac{T''_d}{T''_{do}} = \frac{x_{lD} + x_l x_{lF} x_{md}/(x_l x_{lF} + x_{lF}x_{md} + x_{md}x_l)}{x_{lD} + x_{lF}x_{md}/(x_{lF} + x_{md})}$$

$$= \frac{(x_{lF} + x_{md})}{(x_l x_{lF} + x_{lF}x_{md} + x_{md}x_l)}$$

(equation continues)

$$= \frac{x_l(x_{lD}x_{lF} + x_{lD}x_{md} + x_{lF}x_{md}) + x_{lD}x_{lF}x_{md}}{x_{lD}(x_{lF} + x_{md}) + x_{lF}x_{md}}$$

$$= \frac{x_l + x_{lD}x_{lF}x_{md}/(x_{lD}x_{lF} + x_{lD}x_{md} + x_{lF}x_{md})}{x_l + x_{lF}x_{md}/(x_{lF} + x_{md})} = \frac{x''_d}{x'_d}$$

Reactance Matrices and Mutual Reactances

Let the two-axis flux linkage equations be written in SI units as

$$\begin{bmatrix} \lambda_d \\ \lambda_F \\ \lambda_D \end{bmatrix} = \begin{bmatrix} L_d & L_{aF} & L_{aD} & -I_d \\ \frac{3}{2}L_{Fa} & L_F & L_{FD} & I_F \\ \frac{3}{2}L_{Da} & L_{DF} & L_D & I_D \end{bmatrix} = \frac{1}{\omega_e}\begin{bmatrix} X_d & X_{aF} & X_{aD} \\ \frac{3}{2}X_{Fa} & X_F & X_{FD} \\ \frac{3}{2}X_{Da} & X_{DF} & X_D \end{bmatrix}\begin{bmatrix} -I_d \\ I_F \\ I_D \end{bmatrix} \quad (2\text{-}26)$$

$$\begin{bmatrix} \lambda_q \\ \lambda_Q \end{bmatrix}\begin{bmatrix} L_q & L_{aQ} \\ \frac{3}{2}L_{Qa} & L_Q \end{bmatrix}\begin{bmatrix} -I_q \\ I_Q \end{bmatrix} = \frac{1}{\omega_e}\begin{bmatrix} X_q & X_{aQ} \\ \frac{3}{2}X_{Qa} & X_Q \end{bmatrix}\begin{bmatrix} -I_q \\ I_Q \end{bmatrix} \quad (2\text{-}27)$$

where the flux linkages λ are in webers, currents I in amperes, inductances L in henrys, reactances X in ohms, the speed $\omega_e = 2\pi f$ rad/s, and

$$\begin{aligned} L_{Fa} &= L_{aF}, & L_{Da} &= L_{aD}, & L_{DF} &= L_{FD}, & L_{Qa} &= L_{aQ} \\ X_{Fa} &= X_{aF}, & X_{Da} &= X_{aD}, & X_{DF} &= X_{FD}, & X_{Qa} &= X_{aQ} \end{aligned} \quad (2\text{-}28)$$

Previous analysis has shown that for the two-phase equivalent to have the same exciting effect as the three-phase winding at any point around the air gap of the synchronous machine, both the mmf of d and that of q windings of Fig. 2-4 must be increased to 3/2 times that of each of the three phase windings of Fig. 2-3a. This numerical factor has been used to modify L_{Fa}, X_{Fa}, etc., of the first columns of the inductance and reactance matrices of Eqs. (2-26) and (2-27), but is implicitly included in the total inductances L_d and L_q and the total reactances X_d and X_q of the two equations. Also included in other diagonal elements of these matrices are the leakage inductances and reactances, and X_F, X_D, etc., are the total reactances of the respective windings.

It is noted that the L and X mattices of Eqs. (2-26) and (2-27) are not symmetrical. To make them symmetrical and to convert them into per-unit values, certain conditions must be met. Since our primary concern is the reactance matrices, let all reactances of these two equations be divided by the base reactances, each of which equals the base voltage divided by the base current of the respective windings. We shall have the per-unit reactances

as follows:

$$x_d = X_D \frac{I_B}{V_B}, \qquad x_{dF} = X_{aF} \frac{I_{FB}}{V_B}, \qquad x_{dD} = X_{aD} \frac{I_{DB}}{V_B}$$

$$x_{Fd} = (\tfrac{3}{2}X_{Fa}) \frac{I_B}{V_{FB}}, \qquad x_F = X_F \frac{I_{FB}}{V_{FB}}, \qquad x_{FD} = X_{FD} \frac{I_{DB}}{V_{FB}} \tag{2-29}$$

$$x_{Dd} = (\tfrac{3}{2}X_{Da}) \frac{I_B}{V_{DB}}, \qquad x_{DF} = X_{DF} \frac{I_{FB}}{V_{DB}}, \qquad x_D = X_D \frac{I_{DB}}{V_{DB}}$$

and

$$x_q = X_q \frac{I_B}{V_B}, \qquad x_{qQ} = X_{qQ} \frac{I_{QB}}{V_B}$$

$$x_{Qq} = X_{Qa} \frac{I_B}{V_{QB}}, \qquad x_Q = X_Q \frac{I_{QB}}{V_{QB}} \tag{2-30}$$

In these equations, the subscript B is used to identify the base values; V_B and I_B are the base voltage and the base current for the d and q windings, V_{FB} and I_{FB} those for the field winding, etc.

Altlough the original reactance matrices of Eq. (2-26) and (2-27) are not symmetrical, the per-unit reactance matrices will be symmetrical if the following conditions are met:

$$\tfrac{3}{2}V_B I_B = V_{FB} I_{FB} = V_{DB} I_{DB} = V_{QB} I_{QB} \tag{2-31}$$

Moreover, one may have the same per-unit mutual reactance per axis, x_{md} for all d-axis windings and x_{mq} for all qu-axis windings if the following conditions are further observed:

$$x_{dF} = x_{dD} = x_{FD} = x_{md}, \qquad x_{qQ} = x_{mq} \tag{2-32}$$

The voltages and currents are also converted into per unit. The per-unit reactance matrices were included in (2-17) and (2-18). For details, see reference [10].

Determination of Synchronous Machine Parameters from Test

According to the IEEE test procedures for synchronous machines [9], eight Park's d-axis parameters, r_a, x_d, x'_d, x''_d, T'_d, T'_{do}, T''_d and T''_{do} can be determined from test. However, by virtue of the two identities of (2-25), only six of the eight Park's parameters can be used for the calculation of the seven circuit parameters r_a, r_F, r_D, r_1, x_{lF}, x_{lD}, and x_{md} of Fig. 2-6a. Therefore, one

additional test is required to find all circuit parameters from Park's parameters. Three alternative tests are proposed in reference [10].

One of them is to define a new damper time constant with the field winding open,

$$T_D \triangleq \frac{x_D}{\omega_b r_D}, \qquad x_D \triangleq x_{lD} + x_{md} \tag{2-33}$$

and determine it from a varying-slip test. Another is to determine T_D from a current decaying test by short-circuiting an armature winding on the d axis, being excited by dc, while the field winding is left open. Still another is to define a new reactance x'_{do}, similar to x'_d, but with the field winding open, and determine it from a modified Dalton and Cameron test. Therefore, all equivalent circuit parameters can be calculated from the test results of IEEE testing procedures in conjunction with either one of the methods just described. Details of the additional texting and calculation of the circuit parameters from the test results are given in reference [10].

There is a renewed interest in testing synchronous machine parameters due to the requirement for more accurate synchronous machine models for modern large electric power system dynamic studies. More references are given at the end of this chapter [11–17]. Some tests are performed on-line.

Summary of Section 2-2

In this section, synchronous machine reactances and time constants are defined, and concepts of transient and subtransient presented. Because of the two-phase-equivalent excitation of the three-phase winding on the stator, and the single-phase excitation of windings on the rotor, the mutual inductance between a stator and a rotor winding in SI units is not reciprocal; a factor $\frac{3}{2}$ is involved in Eqs. (2-26) and (2-27). These asymmetrical reactance matrices in SI units, however, can be made symmetrical in per unit of value and with a common mutual reactance for all windings per axis when certain conditions are met. It is also pointed out that one more test, in addition to the IEEE testing procedures, is required to determine all equivalent circuit parameters of the synchronous machine.

There is also renewed interest in testing synchronous machine parameters for more accurate modeling. References are given at the end of this chapter [11–17].

2-3 LOW-ORDER SYNCHRONOUS GENERATOR MODELS

As stated at the beginning of this chapter, the selection of synchronous generator models for power system dynamic studies depends not only on

the nature of the problems themselves, but also on the computational facilities and control techniques available.

Many synchronous machine models have been developed for dynamic studies. A second-order model and a third-order model will be presented in this section. The former was used with an ac calculating board, and the latter is being used with the digital computer. Both models are still used to describe some synchronous machines in large electric power systems.

The Second-Order Synchronous Generator Model

For the second-order synchronous generator model [18], only the torque relation is described by differential equations, the rest being algebraic. The complete model includes the following equations:

$$\begin{aligned} \dot{\omega} &= \frac{1}{M}(T_m - T_e - T_D) \quad \text{per unit/s} \\ \dot{\delta} &= \omega_b(\omega - 1) \quad \text{elec rad/s} \end{aligned} \tag{2-34}$$

where

$$\begin{aligned} T_e \simeq P_e &\simeq \frac{e'v_t}{x'_d}\sin\delta \quad \text{per unit} \\ e' &= v_t + jx'_d i \quad \text{per unit} \end{aligned} \tag{2-35}$$

Equation (2-34) corresponds to the original nonlinear version of (1-1), but is written in the state variable form in two first-order differential equations, which is required for modern analysis and digital integration. In Eq. (2-34), $M\dot{\omega}$ is the accelerating torque, T_m the mechanical input torque, T_e the electric output torque, and T_D the mechanical damping torque, all in per unit of value. Note that while the torque angle δ in electrical radians is in Park's coordinates, $(\omega - 1)$ is the per-unit relative speed of the coordinates with respect to the system synchronous speed $(2\pi f)$, which is chosen as ω_b.

Equation (2-35) may be considered as the auxiliary equation of (2-34). T_e equals P_e divided by the speed ω, and ω is very close to one per unit. The e' of the second equation of (2-35) is known as the voltage behind the transient reactance. Therefore, the electric power P_e may be calculated as follows. According to Fig. 2-7,

$$x'_d i\cos\theta = e'\sin\delta \tag{2-35a}$$

Therefore

$$P_e = v_t i\cos\theta = \frac{e'v_t}{x'_d}\sin\delta \tag{2-35b}$$

Note that the resistance voltage $r_a i$ has been neglected in Fig. 2-7.

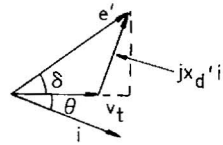

Fig. 2-7 A voltage behind reactance.

The torque equation of a generating unit may be written in SI units, which consist mainly of the MKS units as follows,

$$J\frac{d\omega_m(\text{MKS})}{dt} = T_m(\text{MKS}) - T_e(\text{MKS}) - T_D(\text{MKS}) \tag{2-36}$$

where J is the moment of inertia of the rotating system of the generating unit, ω_m the mechanical speed, T_m the input mechanical torque, T_e the output electric torque, and T_D the mechanical damping torque, all in MKS. Let a base torque be

$$T_b(\text{MKS}) \triangleq P_b(\text{MKS})/\omega_{mb}(\text{MKS}) \tag{2-37}$$

where P_b is the base power and ω_{mb} the base mechanical speed corresponding to the rpm on the nameplate. Also, two inertia constants may be defined,

$$M \triangleq 2H, \qquad H \triangleq \tfrac{1}{2}J\omega_{mb}^2(\text{MKS})/P_b(\text{MKS}) \tag{2-38}$$

where $\frac{1}{2}J\omega_{mb}^2$ is the kinetic energy of the rotating system at the base speed and P_b the base power. In other words, H represents MJ per MW rating of the generating unit, and has a unit of seconds. Dividing (2-36) by (2-37) gives

$$\frac{J\omega_{mb}^2}{P_b}\frac{d}{dt}\frac{\omega_m}{\omega_{mb}} = \frac{T_m(\text{MKS})}{T_b(\text{MKS})} - \frac{T_e(\text{MKS})}{T_b(\text{MKS})} - \frac{T_D(\text{MKS})}{T_b(\text{MKS})} \tag{2-39}$$

or

$$M\dot{\omega}(\text{pu}) = T_m(\text{pu}) - T_e(\text{pu}) - T_D(\text{pu}) \tag{2-40}$$

which will be written hereafter simply as

$$M\dot{\omega} = T_m - T_e - T_D \quad \text{per unit} \tag{2-41}$$

Since the MKS electrical speed is $p/2$ times the MKS mechanical speed,

and it is also true for the base speeds, we shall have

$$\omega(\text{pu}) = \frac{\omega_e(\text{MKS})}{\omega_{eb}(\text{MKS})} = \frac{\omega_m(\text{MKS})}{\omega_{mb}(\text{MKS})} \tag{2-42}$$

Conventionally, the unit "electrical radian" is chosen for the torque angle δ, and ω_e or $(2\pi f)$ radian per second for the base speed ω_b. Therefore,

$$\dot{\delta} = \omega_b(\omega - 1) \quad \text{rad/s} \tag{2-43}$$

where

$$\omega_b = 2\pi f \quad \text{rad/s} \tag{2-44}$$

Finally, the torque equation in the state variable form becomes

$$\begin{aligned} \dot{\omega} &= \frac{1}{M}(T_m - T_e - T_D) \quad \text{per unit/s} \\ \dot{\delta} &= \omega_b(\omega - 1) \quad \text{elec. rad/s} \end{aligned} \tag{2-34}$$

These two first-order differential equations and the algebraic equations of (2-35) constitute the second-order model of the synchronous machine.

There are alternative forms of Eq. (2-34). For instance, if δ is in radians and ω and ω_b in radians per second, se shall have

$$\begin{aligned} \dot{\omega} &= \frac{\pi f}{H}(T_m - T_e - T_D) \quad rad/s^2 \\ \dot{\delta} &= \omega - \omega_b \quad \text{rad/s} \end{aligned} \tag{2-34a}$$

and if δ is in electrical degrees and ω and ω_b in degrees per second, we shall have

$$\begin{aligned} \dot{\omega} &= \frac{180f}{H}(T_m - T_e - T_D) \quad \text{deg/s}^2 \\ \dot{\delta} &= \omega - \omega_b \quad \text{deg/s} \end{aligned} \tag{2-34b}$$

Note that T_m, T_e, and T_D are still in per unit of value in these equations.

The Third-Order Synchronous Generator Model

For certain power system dynamic studies, the change in flux linkage of the field winding cannot be neglected, although the changes in flux linkages of other windings are still negligible. Therefore, there is one more state equation for the third-order synchronous machine model [19, 20].

The state equations of the third-order model may be written

$$\begin{aligned}\dot{\omega} &= \frac{1}{M}(T_m - T_e - T_D)\\ \dot{\delta} &= \omega_b(\omega - 1)\\ \dot{e}'_q &= \frac{1}{T'_{do}}[E_{FD} - e'_q - (x_d - x'_d)i_d]\end{aligned} \tag{2-45}$$

and the auxiliary equations

$$\begin{aligned}T_e \simeq P_e \simeq \frac{e'_q v_t}{x'_d}\sin\delta + \frac{v_t^2(x'_d - x_q)}{2x'_d x_q}\sin 2\delta\\ e'_q = v_t + jx'_d i_d + jx_q(ji_q)\end{aligned} \tag{2-46}$$

Consider the third equation of (2-4). It can be written as

$$\dot{\psi}_F/\omega_b = v_F - r_F i_F \tag{2-47}$$

Although Eq. (2-47) is already in the state variable form, traditionally, the field flux linkage is replaced by a voltage, and the flux linkage equation is converted into a voltage equation.

Let some new voltages be defined as follows,

$$e'_q \triangleq \frac{x_{md}}{x_F}\omega_0\psi_F, \qquad E \triangleq x_{md}i_F, \qquad E_{FD} \triangleq \frac{x_{md}v_F}{r_F} \tag{2-48}$$

where e'_q, E, and E_{FD} are all internal voltages of the armature, v_F is the voltage applied to the field winding, i_F the field current, x_{md} the per-unit mutual reactance of the d axis, and r_F the resistance of the entire field circuit. E_{FD} may be interpreted also as the field voltage as seen from the armature. E_{FD} equals E only in the steady state, since a field voltage variation does not produce a field current variation immediately in the transient state due to the field time constant.

Multiplying both sides of Eq. (2-47) by x_{md}/r_F and utilizing the definitions of Eq. (2-48) and the field time constant

$$T'_{do} \triangleq \frac{x_F}{\omega_b r_F} \tag{2-23a}$$

we shall have

$$T'_{do}\dot{e}'_q = E_{FD} - E \tag{2-49}$$

To complete the derivation, let the armature voltage and current in d

and q components be

$$v_t = v_d + jv_q, \qquad i = i_d + ji_q \tag{2-50}$$

Let ω of the first two equations of (2-4) be approximated by the synchronous speed ω_0, and ψ_d, ψ_q, and r_a be neglected. We shall have two equations for the armature windings

$$\begin{aligned} v_d &= -\omega_0 \psi_q = x_q i_q \\ v_q &= \omega_0 \psi_d = x_{md} i_F - x_d i_d = E - x_d i_d \end{aligned} \tag{2-51}$$

For the last part of this derivation, the relations of Eq. (2-17) and (2-18) are utilized.

A phasor diagram for a low-order synchronous generator in steady state and transient state may therefore be drawn as Fig. 2-8. Note that while E of Eq. (2-51) represents only the voltage magnitude, E in Fig. 2-8 is a phasor in phase with ji_q. The voltage phasors e' of the second-order model and e'_q of the third-order model are

$$\begin{aligned} e' &= v_t + jx'_d i \\ e'_q &= v_t + jx'_d i_d + ix_q(ji_q) \end{aligned} \tag{2-52a}$$

They are different not only in phase, but also in magnitude. Another phasor relation

$$E_q = v_t + jx_q i \tag{2-52b}$$

is useful for the measurement of the phase difference δ between E_q and v_t.

Let us continue the derivation of the third equation of (2-45). Since

$$e'_q = E - (x_d - x'_d) i_d \tag{2-53}$$

in magnitude according to Fig. 2-8, which also can be derived directly from

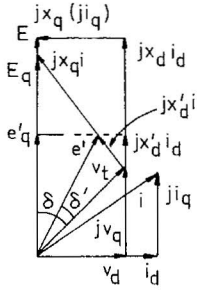

Fig. 2-8 A phasor diagram for low-order synchronous generators.

e'_q of (2-48) and ψ_F of (2-17), then

$$\omega_0 \psi_F = x_F i_F - x_{md} i_d, \quad i_D = 0 \tag{2-17a}$$

and

$$\begin{aligned} e'_q &= (x_{md}/x_F)\omega_0 \psi_F = E - (x_{md}^2/x_F) i_d \\ &= E - (x_d - x'_d) i_d \end{aligned} \tag{2-53a}$$

In the last part of this derivation, the identity

$$x_{md}^2/x_F = x_d - x'_d \tag{2-54}$$

has been applied, which can be proved from the reactance definitions of Eqs. (2-19) and (2-21). Finally, substituting E from (2-53) into (2-49) gives

$$\dot{e}'_q = \frac{1}{T'_{do}} [E_{FD} - e'_q - (x_d - x'_d) i_d] \tag{2-45a}$$

which is the last equation of (2-45).

The electric torque T_e of Eq. (2-45) can be derived from the electric power P_e as follows. Since, in per unit of value,

$$\begin{aligned} T_e &= P_e/\omega, \qquad \omega \simeq 1 \\ P_e &= \mathrm{Re}[(i_d + j i_q)^*(v_d + j v_q)] = i_d v_d + i_q v_q \end{aligned} \tag{2-55a}$$

and the voltage and current component magnitudes can be found from Fig. 2-8,

$$\begin{aligned} v_d &= v_t \sin \delta, \qquad v_q = v_t \cos \delta \\ i_d &= (e'_q - v_t \cos \delta)/x'_d, \qquad i_q = v_t \sin \delta / x_q \end{aligned} \tag{2-55b}$$

substituting (2-55b) into (2-55a) results in T_e of (2-46).

Summary of Section 2-3

In this section, the second-order and the third-order synchronous generator models are derived. The former has been used since the advent of the ac calculating board, and the latter since the development of the digital computer. The main difference is the inclusion of the field winding differential equation in the third-order model. There is some difference between e'_q and e' according to the phasor diagram of Fig. 2-8, but there will be only a small difference between $\Delta e'_q$ and $\Delta e'$ in their linearized form.

2-4 HIGH-ORDER SYNCHRONOUS GENERATOR MODELS

For certain power system dynamic studies, more elaborate synchronous generator models than the third order are required. Not only the field winding voltage relation, but also the armature and damper winding voltage relations must be described by differential equations.

Basic ψ Model of Synchronous Generators

For the high-order modeling, flux linkages themselves in (2-4) can be chosen as state variables. Including (2-34), the complete set of state equations for the synchronous generator may be written

$$\begin{aligned}
\dot{\omega} &= \frac{1}{M}(T_m - T_e - T_D) \\
\dot{\delta} &= \omega_b(\omega - 1) \\
\dot{\psi}_d/\omega_b &= v_d + r_a i_d + \omega\psi_q \\
\dot{\psi}_q/\omega_b &= v_q + r_a i_q - \omega\psi_d \\
\dot{\psi}_F/\omega_b &= v_F - r_F i_F \\
\dot{\psi}_D/\omega_b &= -r_D i_D \\
\dot{\psi}_Q/\omega_b &= -r_Q i_Q
\end{aligned} \tag{2-56}$$

where

$$T_e = i_q\psi_d - i_d\psi_q \tag{2-6}$$

Indeed, these equations have the simplest form. There are concerns that these flux linkages are not directly measurable. However, they can be expressed in terms of power, reactive power, voltages, and currents in most cases.

Equations (2-56) and (2-6) form the basic ψ model for synchronous machines. They are nonlinear because of the variable products $i_q\psi_d$, $i_d\psi_q$, $\omega\psi_d$, $\omega\psi_q$, and the possible inclusion of the saturation effect in ψ_d and ψ_q. Equations (2-56) and (2-6) will be linearized when they are applied to solve dynamic problems of a power system encountering relatively small disturbances.

High-Order E and ψ Models of Synchronous Machines

Conventionally, voltages instead of flux linkages have been chosen as the state variables, such as the use of e'_q of (2-45) instead of ψ_F of (2-47) for the

third-order synchronous machine model. Olive's seventh-order model [21] will be derived in this subsection. For the derivation, the following voltage definitions may be defined:

$$\begin{aligned} e'_q &\triangleq \frac{x_{md}}{x_F}\omega_0\psi_F, & e_{q1} &\triangleq x_{md}i_F \\ e''_q &\triangleq \frac{x_{md}}{x_D}\omega_0\psi_D, & e_{q2} &\triangleq x_{md}i_D \\ e''_d &\triangleq \frac{x_{mq}}{x_Q}\omega_0\psi_Q, & e_{d2} &\triangleq x_{mq}i_Q \\ e'_d &\triangleq \frac{x_{mq}}{x_S}\omega_0\omega_S, & e_{d1} &\triangleq x_{mq}i_S \end{aligned} \tag{2-57}$$

The last two definitions are required only when there is a second damper winding S on the q axis. The notation is a compromise of various notations used by many authors. Note that, in (2-57), a voltage is always denoted by e, a flux linkage by ψ, a current by i, etc., and the speed ω_0, although being unity for the base speed we have chosen, is always kept in the equation to avoid confusing a voltage with a flux linkage. For convenience, Olive's notations of reference [21] and ours are compared as follows:

Olive's	λ	V_F	e'_q	e''_q	e''_d	e_{q1}	e_{q2}	$-e_d$	X's
Ours	ψ	E_{FD}	e'_q	e''_q	e''_d	e_{q1}	e_{q2}	e_{d2}	x's

To derive Olive's high-order synchronous machine model with only one damper winding on the q axis, the following identities are useful,

$$\begin{aligned} x_d - x'_d &= x_{md}^2/x_F \\ x_q - x''_q &= x_{mq}^2/x_Q \\ x_d - x''_d &= \frac{x_{md}^2(x_F + x_D - 2x_{md})}{(x_F x_D - x_{md}^2)} \\ x'_d - x''_d &= \frac{x_{md}^2(x_F - x_{md})^2}{x_F(x_F x_D - x_{md}^2)} \\ \frac{x_d - x''_d}{x'_d - x''_d} &= \frac{(x_F + x_D - 2x_{md})x_F}{(x_F - x_{md})^2} \end{aligned} \tag{2-58}$$

The first identity of (2-58) is the same as (2-54), the second is similar to the first since there is only one rotor winding on the q axis, and the third may be derived from the original reactance definitions of (2-19) and (2-22). The

fourth identity is the difference of the first and the third, and the last is the ratio of the third and the fourth.

The machine armature open-circuited time constants become

$$
\begin{aligned}
T'_{do} &\triangleq \frac{x_F}{\omega_b r_F} = \frac{1}{\omega_b r_F}\frac{x_{md}^2}{x_d - x'_d} \\
T''_{do} &\triangleq \frac{1}{\omega_b r_D}\left(x_{lD} + \frac{x_{lF}x_{md}}{x_F}\right) = \frac{1}{\omega_b r_D}\frac{x_F x_D - x_{md}^2}{x_F} \\
T''_{qo} &\triangleq \frac{x_Q}{\omega_b r_Q} = \frac{1}{\omega_b r_Q}\frac{x_{mq}}{x_q - x''_q}
\end{aligned}
\tag{2-59}
$$

and Olive's seventh-order synchronous machine model may be written as

$$
\begin{aligned}
\dot{\omega} &= \frac{1}{M}(T_m - T_e - T_D) \\
\dot{\delta} &= \omega_b(\omega - 1) \\
\dot{\psi}_d/\omega_b &= v_d + r_a i_d - (x_q i_q - e_{d2}) \\
\dot{\psi}_q/\omega_b &= v_q + r_a i_q + (x_d i_d - e_{q1} - e_{q2}) \\
\dot{e}'_q &= (E_{FD} - e_{q1})/T'_{do} \\
\dot{e}''_d &= -e_{d2}/T''_{qo} \\
\dot{e}''_q &= -\frac{(x'_d - x''_d)}{(x_d - x''_d)}\frac{e_{q2}}{T''_{do}}
\end{aligned}
\tag{2-60}
$$

Derivations of the third and fourth equations of (2-60) involve only the flux linkage equations of (2-17) and (2-18) and the voltage definitions of (2-57). The fifth state equation corresponds to (2-49) and the sixth is similar to the fifth except that the Q winding is permanently short-circuited.

To derive the last state equation of (2-60), let both sides of the sixth equation of (2-56) be multiplied by $\omega_b x_{md}/ x_D$. The LHS becomes $\dot{e}''_q$ according to (2-57), and the RHS

$$
-\frac{\omega_b r_D}{x_D} x_{md} i_D = -\frac{\omega_b r_D}{x_D} e_{q2} = -\frac{e_{q2}}{T''_{do}}\frac{x_F x_D - x_{md}^2}{x_F x_D} \tag{2-61}
$$

according to (2-59). In Olive's original derivation, however, the following assumption was tacitly made:

$$
x_D \simeq x_{md} \tag{2-62}
$$

and the last equation of (2-58) becomes

$$\frac{x_d - x''_d}{x'_d - x''_d} \simeq \frac{x_F}{x_F - x_{md}} \tag{2-63}$$

Therefore,

$$\dot{e}''_q = -\frac{(x'_d - x''_d)}{(x_d - x''_d)} \frac{e_{q2}}{T''_{do}} \tag{2-60a}$$

To solve Olive's differential equations, the following auxiliary equations are required:

$$\begin{aligned} e'_q &= -(x_d - x'_d) i_d + e_{q1} + \frac{x_d - x'_d}{x_d - x''_d} e_{q2} \\ e''_q &= -(x_d - x''_d) i_d - e_{q1} + e_{q2} \\ e''_d &= (x_q - x''_q) i_q - e_{d2} \\ T_e &= e''_q i_q + e''_d i_d - (x''_d - x''_q) i_d i_q \end{aligned} \tag{2-64}$$

Derivations of (2-64) involve voltage and flux linkage definitions and some identities of (2-58).

Other High-Order Synchronous Machine Models

Formulation similar to the ψ model of (2-56) can be found in reference [22], except for differences in notation. There are also other high-order E and ψ models. An example can be found in reference [23], which has two rotor windings per axis.

Summary of Section 2-4

In this section, two high-order models for synchronous generators have been presented, a seventh-order ψ model (2-56) and a seventh-order E and ψ model (2-60). Both are useful for power system dynamic studies, and they can be readily extended to include more field and damper windings on the rotor. There are many ways to model a synchronous generator and one must choose a proper model for a particular power system dynamic study.

Having gained sufficient knowledge of synchronous machine modeling, we shall turn our attention to other important power system component models

2-5 EXCITER AND VOLTAGE REGULATOR MODELS

Consider the excitation system first. The original function of the exciter and voltage regulator is to provide an adequate excitation to the synchronous machine field winding, an excitation increase for a voltage drop, and an excitation decrease for a voltage rise. Traditionally, a voltage error is defined by

$$\Delta v_t \triangleq v_{REF} - v_t \tag{2-65}$$

in power engineering, which is equivalent to

$$\Delta v_t = -(v_t - v_{REF}) \tag{2-66}$$

including an error and a negative feedback as emphatically advocated by control engineers. In these two equations, v_t represents the generator terminal voltage measured through a potential transformer, rectified and filtered, and v_{REF} a reference voltage.

The original function of the excitation system, however, has been constantly expanded. Supplementary excitation controls are designed not only to enhance the damping of the power system during low frequency oscillations, but also to improve the transient stability of a power system when seriously disturbed.

A Continuously Acting Excitation System

There are two IEEE committee reports on excitation system modeling [24, 25]. Figure 2-9 shows the most commonly used Type 1 continuously acting excitation system [24]. The first block from the left represents the transfer function of rectifier and filter of the measured terminal voltage v_t, which has a very small time constant. The voltage error Δv_t is obtained from

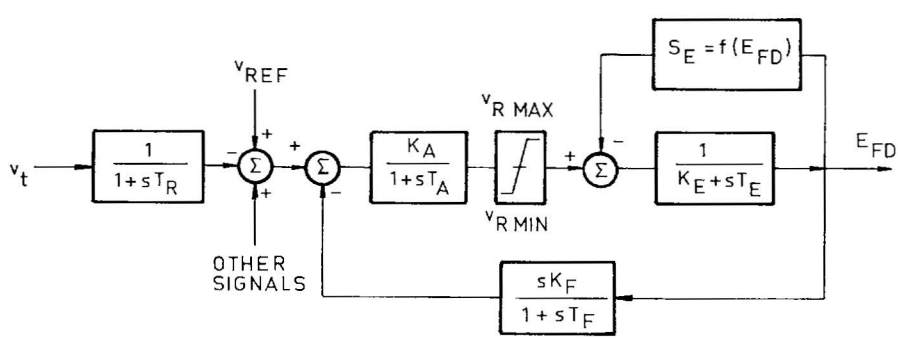

Fig. 2-9 IEEE Type 1 excitation system. (From [24], courtesy of IEEE, © 1968.)

a comparison of v_t with a reference voltage v_{REF} at the first summer. Other signals, such as supplementary excitation to improve the dynamic stability of a power system, can be also added to that summer.

The block after the second summer represents the transfer function of a voltage regulator that has a time constant T_A and a gain K_A. The linear proportionality and the ceiling voltages $v_{R\,MAX}$ and $v_{R\,MIN}$ are also shown in the next block.

The last block on the forward branch with a negative feedback S_E represents the transfer function of the exciter. It has an output voltage E_{FD} corresponding to the generator internal voltage E_{FD} of (2-48). There are two constant K_E and T_E of this block, but T_E is not itself a time constant because of the presence of the other constant K_E.

There are two negative feedback loops of the Type 1 excitation system. One of them has a factor S_E that represents the saturation effect of the exciter. The other includes a time constant T_F and a gain K_F of a stabilizer of the excitation system. Both of them require further explanation.

Typical data of the Type 1 excitation system are as follows [24]:

T_R	T_A	K_A	$v_{R\,MAX}$	$v_{R\,MIN}$	T_E	K_E	S_E	$S_{E.75}$	T_F	K_F
0–0.06	0.06–0.2	25–50	1.0	−1.0	0.5	−0.05	0.267	0.074	0.35–1	0.01–0.08

where S_E and $S_{E.75}$ are saturation factors corresponding to the maximum E_{FD} and 0.75 times the maximum, respectively.

Saturation Function and Schleif's Analysis

The saturation effect is generally a function of the total excitation of a magnetic circuit. The saturation function S_E or $f(E_{FD})$ of Fig. 2-9 is determined from Fig. 2-10 by

$$S_E = f(E_{FD}) \triangleq \frac{A - B}{B} \tag{2-67}$$

In Fig. 2-10 the no-load saturation curve NL and the constant resistance load saturation curve CR are determined directly from tests. The air gap line AG tangential to the lower part of NL is drawn to separate the excitation B for the air gap from the excitation (A − B) for the iron part of the magnetic circuit. The saturation factor S_E or (A − B)/B is a function of E_{FD}. To characterize the function, two specific values are recommended by the IEEE Committee, one at the maximum E_{FD} and the other at 0.75 times the maximum.

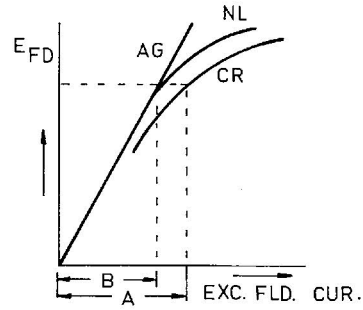

Fig. 2-10 Determination of the saturation factor S_E.

It is pointed out by Schleif that T_E of the exciter block in Fig. 2-9 is not itself a time constant, that $-K_E$ is the slope of the field rheostat line ($K_E < 0$) of the exciter, and that the transfer function shall be obtained as follows [24, 26].

Let the saturation block of Fig. 2-9 be redrawn as Fig. 2-11a with both saturation function S_E and constant K_E as negative feedbacks, and let both S_E and $-K_E$ versus E_{FD} be plotted as Fig. 2-11b. According to (a), the combined feedback equals $(S_E + K_E)$ or $S_E - (-K_e)$. Let a be the slope difference of S_E and $-K_e$, or $(S_E + K_E)$, at the intersection. Then we have

$$E_{FD} = \frac{1}{sT_E}[v_R - (S_E + K_E)E_{FD}] = \frac{1}{sT_E}(v_R - aE_{FD}) \tag{2-68}$$

Therefore

$$\frac{E_{FD}}{v_R} = \frac{1}{a + sT_E} = \frac{1/a}{1 + sT_E/a} \tag{2-69}$$

and that will be the transfer function of the exciter block of Fig. 2-9 [26].

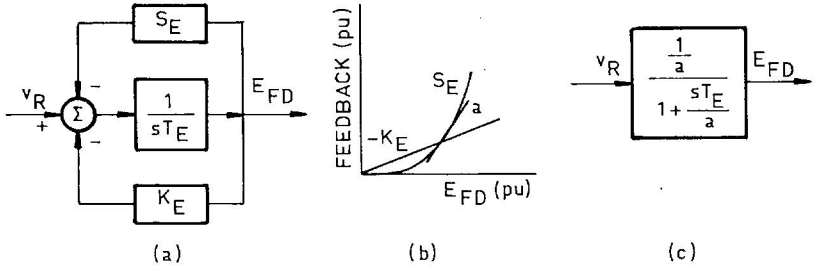

Fig. 2-11 Transfer function of the last block of Fig. 2-9. (From [26], courtesy of IEEE, © 1975.)

The Stabilizing Circuit

Reference [27] has shown that there are many ways to realize the stabilizing function $sK_F/(1 + sT_F)$ of Fig. 2-9. In Fig. 1-3 a series transformer ST was used [28]. Let a two-winding transformer with a high-impedance secondary circuit be used as shown in Fig. 2-12. Let the resistance, the leakage reactance, and the mutual reactance be denoted by R, L, and M, and the subscripts 1 and 2 be used to identify the primary and the secondary circuits of the transformer, respectively. Let us also define

$$K_F \triangleq M/R_1, \qquad T_F \triangleq L_1/R_1 \tag{2-70}$$

Since $i_2 \simeq 0$ because of the high-impedance circuit,

$$\begin{aligned} v_1 &= (R_1 + sL_1)i_1 + sMi_2 \simeq (R_1 + sL_i)i_1 \\ v_2 &= sMi_1 + (R_2 + sL_2)i_2 \simeq sMi_1 \end{aligned} \tag{2-71}$$

we will have

$$\frac{v_2}{v_1} = \frac{sM}{R_1 + sL_1} = \frac{sK_F}{1 + sT_F} \tag{2-72}$$

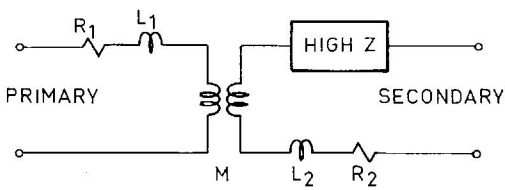

Fig. 2-12 A stabilizing transformer.

The stabilizing circuit of Fig. 2-9 is therefore a negative derivative feedback control, and its function is to improve the response of the excitation system. However, a stabilizing circuit good for this subsystem is not necessarily helpful for the overall performance of the entire electric power system.

Summary of Section 2-5

In this section, the most commonly used IEEE Type 1 excitation system [24] has been presented. Schleif's analysis of the saturation and field rheostat effect on the transfer function is also included. Finally, the realization of the stabilizing circuit using a series transformer is shown. There are a large variety of exciters and voltage regulators in use. Information can be found in power engineering practice.

2-6 HYDRAULIC POWER AND GOVERNOR MODELS

The original function of a governor is to maintain a constant speed of the prime mover by controlling the energy input using a speed deviation as the control feedback. The speed deviation is obtained by comparing the actual speed ω with a reference speed ω_{REF},

$$\Delta\omega = \omega_{REF} - \omega = -(\omega - \omega_{REF}) \tag{2-73}$$

which is a negative feedback. The governor is so designed that a speed drop of the prime mover below a reference level will bring about an energy increase, and a speed increase above the reference level will bring about an energy decrease.

The original governor function has also been expanded to include, for instance, the area power and frequency control, that is, maintenance of the electrical and mechanical energy balance at a constant frequency not only within an area of the system but also including the committed interchanges with the neighboring areas. This function is usually designated to the area's major generating plant being used as the spinning reserve. The power and frequency control presents a very important power system dynamic problem, but it has already been thoroughly treated elsewhere [26, 27, 29 of Chapter 1], and will not be addressed in this book.

Hovey's Hydraulic Power and Governor Model

The transfer function block diagram of Fig. 2-13, derived by Hovey [29], corresponds to the mechanical–hydraulic governor for a hydroelectric power plant as shown in Fig. 1-2. The first block from the left on the forward branch of Fig. 2-13 represents the transfer function of an actuator with an output signal a. The second block represents a gate servo with an output signal g, and the last block the hydraulic power of turbine and penstock with an output ΔT_m. In addition, there is also a dashpot feedback block with an

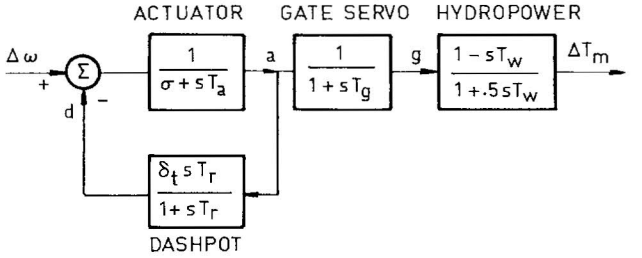

Fig. 2-13. Hovey's hydro and governor transfer functions.

output d. Not represented in the linear model of Fig. 2-13 are the servo speed and gate opening limits. There is a minor departure from the original presentation; the output of the last block was a water head h, but has been changed to ΔT_m in Fig. 2-13.

The transfer functions are derived as follows:

Hydropower. Consider the last block on the forward branch of Fig. 2-13 first. Let the water velocity be U, the gate opening be G, and the water head be H, all in MKS. We shall have

$$\begin{aligned} U &= K\sqrt{H}\cdot G \quad \text{MKS} \\ \Delta U &= \frac{KG}{\sqrt{H}}\frac{\Delta H}{2} + K\sqrt{H}\,\Delta G \quad \text{MKS} \end{aligned} \tag{2-74}$$

where K is a constant. Dividing both sides of the second equation of (2-74) by the base values, and approximating H by H_b and G by G_b gives

$$\frac{\Delta U}{U_b} = \frac{1}{2}\frac{\Delta H}{H_b} + \frac{\Delta G}{G_b} \quad \text{per unit} \tag{2-75}$$

or simply

$$u = 0.5h + g \quad \text{per unit} \tag{2-76}$$

The subscript b is used to signify the base values in (2-75) and equations to follow.

Next, since a gate closure decreasing the water flow will increase the water pressure, and a gate opening will decrease the water pressure, we will have

$$\rho L A\,\Delta\dot{U} = -G_c \rho A\,\Delta H \quad \text{MKS} \tag{2-77}$$

where G_c is the gravity constant, ρ the water density, L the effective length of the waterway including the penstock, and A its cross section, all in MKS. Furthermore, let a water time constant T_w be defined by

$$T_w \triangleq U_b L/(G_c H_b) \quad \text{s} \tag{2-78}$$

Dividing both sides of (2-77) by $G_c \rho A H_b$, we have

$$T_w\left(\frac{\Delta\dot{U}}{U_b}\right) = -\frac{\Delta H}{H_b} \quad \text{per unit} \tag{2-79}$$

or

$$sT_w u = -h \quad \text{per unit} \tag{2-80}$$

Substituting (2-76) into (2-80), we have

$$h = \frac{-sT_w}{1 + 0.5sT_w} g \quad \text{per unit} \tag{2-81}$$

Finally, according to Paynter and Vaughan's discussion of [29], a mechanical power or torque variation ΔT_m may be approximated by

$$\Delta T_m \simeq g + 1.5h \quad \text{per unit} \tag{2-82}$$

if the turbine and load self-regulation can be neglected. Therefore, we will have

$$\Delta T_m \simeq \frac{1 - sT_w}{1 + 0.5sT_w} g \quad \text{per unit} \tag{2-83}$$

which is the transfer function of the last block of Fig. 2-13.

Gate Servo. There is a time lag of the gate servo of Fig. 1-2. Letting the gate servo time constant be T_g, the gate equation may be written

$$\dot{g} = g'/T_g \qquad \text{or} \qquad g' = sT_g g \tag{2-84}$$

But g' is moving in the same direction as a and in the opposite direction to g, according to Fig. 1-2, so

$$g' = a - g \tag{2-85}$$

Substituting g' of (2-84) into (2-85) and solving for g gives

$$g = \frac{1}{1 + sT_g} a \tag{2-86}$$

which is the transfer function of the second forward block of Fig. 2-13.

Actuator Servo. There is also a time lag of the actuator servo of Fig. 1-2. Let it be T_a. Since a and a' are moving in opposite directions due to the actuator servo, we have

$$\dot{a} = -a'/T_a \qquad \text{or} \qquad a' = -sT_a a \tag{2-87}$$

But a' is also affected by the mechanical linkages. It will be lifted by a speed increase $-\Delta\omega$, an uplift of a dashpot rod d, and a pulling down of a through a pivoted linkage with an adjustable arm-length ratio σ. Therefore, we also have

$$a' = -\Delta\omega + d + \sigma a \tag{2-88}$$

Substituting a' of (2-88) into (2-87) and solving for a gives

$$a = \frac{1}{\sigma + sT_a}(\Delta\omega - d) \tag{2-89}$$

which corresponds to the first forward block of Fig. 2-13.

The adjustable arm-length ratio σ is called the permanent droop of a governor, and is usually set at a value of 0.04 to 0.05 per-unit speed variation to one per-unit load or "full load" variation.

Similar to Schleif's observation of the IEEE Type 1 exciter [24, 26], it is noted that T_a itself is not a time constant and $1/\sigma$ is the governor's overall gain.

Dashpot. The dashpot of Fig. 1-2 contains oil and is partitioned by a separator with tiny holes. The oil can be squeezed from one side to another slowly through those tiny holes. There is also a spring attached to the dashpot to support d but not d'.

Let the spring constant be K and the dashpot oil constant be B, and let a dashpot relaxation time constant be defined by B/K. Since the two vertical rods d and d' of the dashpot are moving in opposite directions, we will have

$$(K + sB)d = -sBd' \tag{2-90}$$

or

$$(1 + sT_R)d = -sT_r d' \tag{2-91}$$

where

$$T_r \triangleq B/K \tag{2-91a}$$

But d' is also connected to a by a mechanical linkage through an adjustable arm-length ratio δ_t. Since d' and a are moving in opposite directions,

$$d' = -\delta_t a \tag{2-92}$$

Substituting d' of (2-92) into (2-91) and solving for d gives

$$d = \frac{sT_r\delta_t}{1 + sT_r}a \tag{2-93}$$

which corresponds to the beedback block of Fig. 2-13.

The adjustable arm-length ratio δ_t is called the transient droop or temporary droop of a governor, and is usually set at a value of 0.3 to 0.4 per unit. The optimum settings according to reference [29] are

$$T_r = 5T_w, \qquad \delta_t = 2.5T_w/(2H) \tag{2-94}$$

IEEE's Mechanical-Hydraulic Governor for Hydroturbines

In an IEEE committee report [30], the block diagram shown in Fig. 2-14 is recommended for the representation of the mechanical-hydraulic governor for hydroturbines. The speed reference SR of Fig. 2-14 corresponds to our ω_{REF}, the controlled valve or gate position C_V to g, the time constant T_p to T_a, T_G to T_g, and the transient droop δ to δ_t. Note that the transient droop and permanent droop compensation blocks are now connected across the pilot valve (actuator) and gate servos in Fig. 2-14. Typical data are given as follows:

Parameters	$T_R(T_r)$	$T_p(T_a)$	$T_G(T_g)$	σ	$\delta(\delta_t)$
Typical value	5.0	0.04	0.2	0.05	0.3
Range	2.5–25	0.03–0.05	0.2–0.4	0.03–0.06	0.2–1

Electrical-Hydraulic Governors for Hydroturbines

There are also electrical-hydraulic governors for hydroturbines, by which the mechanical part of the governor is replaced by electrical circuits. It not only improves the linearity of the dynamic response of the governor, but also provides a variety of choices of proportional, integral, derivative and combined controls. For details, see references [30–32].

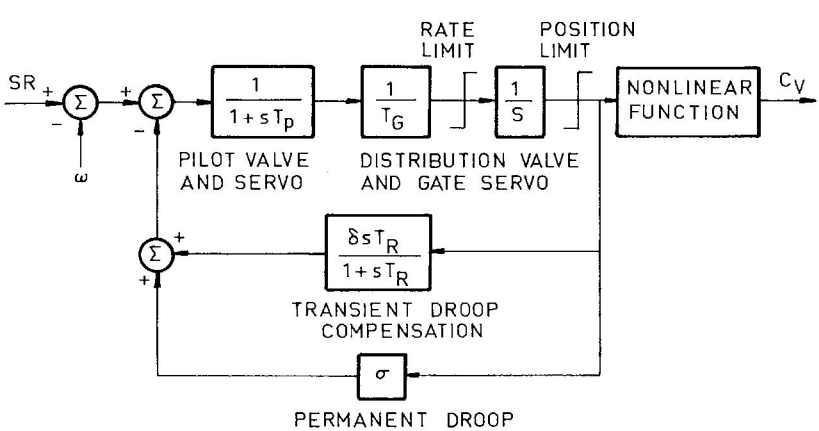

Fig. 2-14 IEEE's mechanical-hydraulic governor for hydroturbines. (From [30], courtesy of IEEE, © 1973.)

Summary of Section 2-6

In this section, governors for hydroturbines are presented. Hovey's derivation of the transfer functions of hydraulic power and governor is given. Although the original function of a governor is to maintain a constant speed of a generating unit, the governor of a major generating unit in a power area is also used for the area power and frequency control.

2-7 STEAM TURBINE AND GOVERNOR MODELS

There are also mechanical-hydraulic governors and electro-hydraulic governors for steam turbines. Although the steam governors are designed mainly to maintain a constant speed by controlling the steam energy input to the turbines, the steam control valves and intercept valves also can be used to improve power system stability.

Steam Turbine Models

Six steam turbine models are included in an IEEE Committee report [30]:

Type A: Nonreheat
Type B: Tandem compound, single reheat
Type C: Tandem compound, double reheat
Type D: Cross compound, single reheat
Type E: Same as D, but with different shaft arrangement
Type F: Cross compound, double reheat

Figure 2-15 shows a functional diagram of the Type B steam turbine. There are four turbines of Type B: the high-pressure turbine HP, the medium-pressure turbine IP, and the two low-pressure turbines LPA and LPB, all on one shaft. Each turbine and shaft constitutes a torsional mass-spring

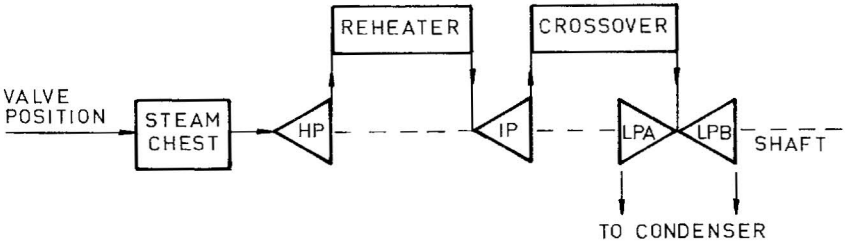

Fig. 2-15 Functional diagram of tandem-compound single-reheat steam turbines. (From [30], courtesy of IEEE, © 1973.)

system. There are a steam chest in front of HP, a reheater between HP and IP, and a steam crossover connection between IP and LPs, and each of them causes a time lag of steam flow. After the steam–mechanical energy conversion in the turbines, the steam is discharged into a water-cooled steam condenser and then reenters the working cycle.

Figure 2-16 shows the transfer functions of the Type B steam turbine. The time constants of the steam chest, the reheater, and the crossover connection, respectively, are denoted by T_{CH}, T_{RH}, and T_{CO}, and the fractions of torques contributed by respective turbines are F_{HP}, F_{IP}, F_{LPA}, and L_{LPB}. The control valves CV and the intercept valves IV are also included. In case of a severe system fault, CV can be used to shut off the steam power completely and IV can be used to divert the steam power directly to the steam condenser to rapidly reduce the steam energy input to the turbines to maintain power system stability. This part of the discussion will be presented in Chapter 7.

In Fig. 2-16, the governor-controlled steam power input is denoted by P_{GV} and the turbine mechanical power output by P_m. The fractions F_{HP}, F_{IP}, F_{LPA} and F_{LPB} are proportional constants, and

$$F_{HP} + F_{IP} + F_{LPA} + F_{LPB} = 1 \tag{2-95}$$

Mechanical–Hydraulic Governors for Steam Turbines

Figure 2-17 shows a nonlinear mathematical model of mechanical-hydraulic governors for steam turbines, recommended by IEEE [30]. The linear model is similar to the nonlinear one except that CAM and VALVE are omitted.

The speed reference SR as shown in the figure can be set a priori or automatically adjusted according to the area power and frequency control requirement. The valve position C_V corresponds to the steam power input

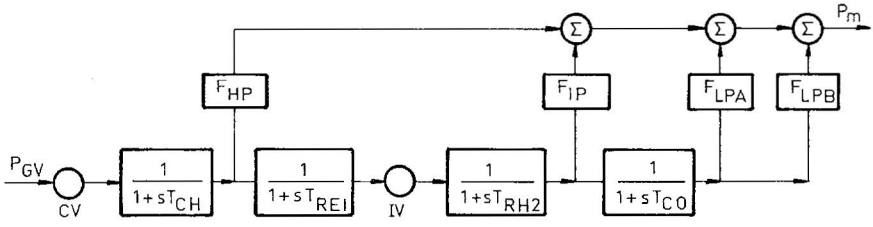

Fig. 2-16 Transfer functions of tandem-compound single-reheat steam turbines. (From [30], courtesy of IEEE, © 1973.)

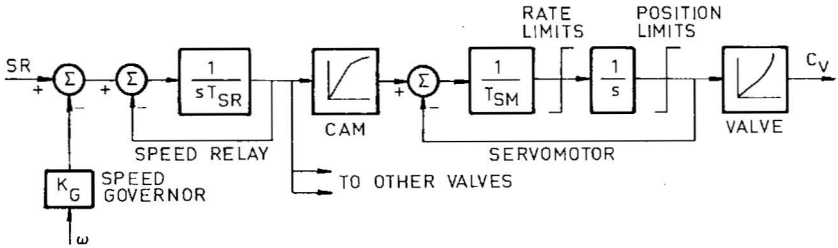

Fig. 2-17. Mechanical-hydraulic governors for steam turbines. (From [30], courtesy of IEEE, © 1973.)

to the steam turbine. Typical data are

Parameters	K_G	T_{SR}	T_{SM}	$\dot{C}_{V\,OPEN}$	$\dot{C}_{V\,CLOSE}$
Values	20	0.1	0.2–0.3	0.1 pu/s/value	1.0 pu/s/value

K_G is a gain, corresponding to the reciprocal value of σ, the permanent droop of the hydroturbine governor, T_{SR} the time constant of the speed relay, and T_{SM} that of the servomotor. $\dot{C}_V$ is the servo speed.

Electrical–Hydraulic Governors for Steam Turbines

In the same IEEE committee report [30], the electrical-hydraulic governor models for steam turbines are also included. Figure 2-18 shows General Electric EHC governor model and Fig. 2-19 Westinghouse EH governor model for steam turbines. In both models, $\dot{m}_{HP}$ denotes the high-pressure turbine steam flow, and K_p of Fig. 2-18 or K_{PR} of Fig. 2-19 is a feedback gain associated with the steam flow. The $\dot{m}_{HP}$ signal is used to improve the linearity of governor response.

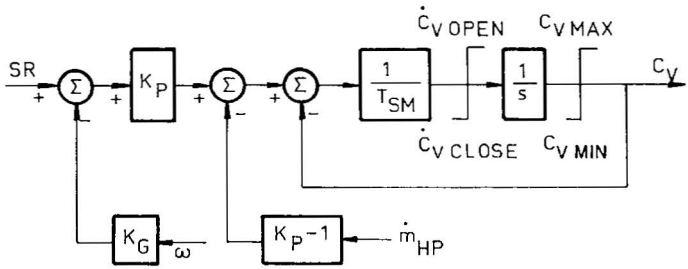

Fig. 2-18 General Electric EHC governor model for steam turbines. (From [30], courtesy of IEEE, © 1973.)

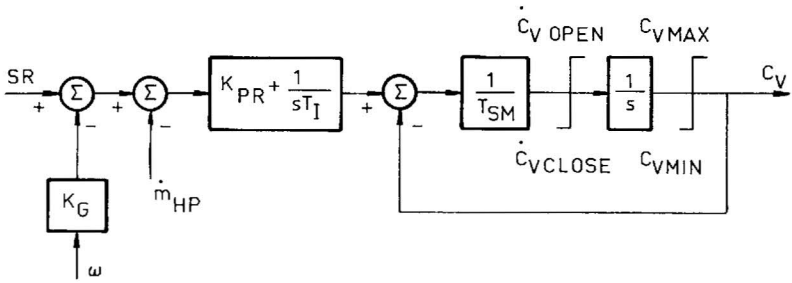

Fig. 2-19 Westinghouse EH governor model for steam turbines. (From [30], courtesy of IEEE, © 1973.)

Typical parameter values are

Parameters	K_G	T_{SM}	$\dot{C}_{V\,OPEN}$	$\dot{C}_{V\,CLOSE}$
Values	20	0.1	0.1 pu/s/valve	0.1 pu/s/valve

K_P of Fig. 2-18 equals 3.0 for governors with high-pressure turbine steam feedback and 1.0 for those without. For Fig. 2-19, $K_{PR} = 1$, and T_I of the same model = 1–2 s. For details, see reference [30].

Summary of Section 2-7

In this section, mathematical models of steam turbines and governors are presented. Transfer functions of the tandem-compound single-reheat turbines are described in detail. The control valves and intercept valves shown in Fig. 2-16 may be used to improve the transient stability of a power system. Other mechanical-hydraulic and electrical-hydraulic governors for steam turbines are also included. For details, see references [30–32].

2-8 SUMMARY

In the first section of this chapter, the synchronous generator equations are derived from the concepts of two-phase equivalent and commutator coordinates. The per-unit relations are clearly explained. Section 2-2 defines the flux linkages, reactances, and time constants. The low-order synchronous generator models are derived in Section 2-3, and the high-order models in Section 2-4. Following that, models for computer simulation are presented in the subsequent sections: excitation systems in Section 2-5, hydraulic power and governors in Section 2-6, and steam turbines and governors in Section

2-7. Both mechanical-hydraulic governors and electrical-hydraulic governors are presented.

Other electric power system component models for power system dynamic studies are being developed; for instance, the model of HVDC power modulation and that of the dynamic load. Modeling is very important. A model more elaborate than necessary may cloud the issue and miss the point, and an oversimplified model may be totally inadequate for the required system representation.

Problems

2-1 Find the d-axis circuit parameters x_{md}, x_{lF}, x_{lD}, r_F, and r_D from the d-axis Park's parameters x_d, x'_d, x''_d, T'_{do} and T''_{do}, assuming that x_l and r_a of Fig. 2-6a have been determined.

2-2 Find the reactive power expressions similar to the power expressions of (2-35) and (2-46) for

(a) the second-order synchronous machine, and
(b) the third-order synchronous machine.

2-3 Some identities and auxiliary equations are very useful for the derivation of high-order synchronous machine models. Prove

(a) all equations of (2-58), and
(b) all equations of (2-63).

2-4 Figure 2-4P shows an excitation system for a synchronous generator. The generator field winding is excited by a main exciter that in turn is excited by a pilot exciter. The pilot exciter, the main exciter, and the generator field winding circuit, respectively, are identified by the subscripts 1, 2, and F; the resistance, inductance, voltage, and current, respectively, are denoted by r, L, v, and i; and the speed voltage of the pilot exciter is $k_1 i_{f1}$ and that of the

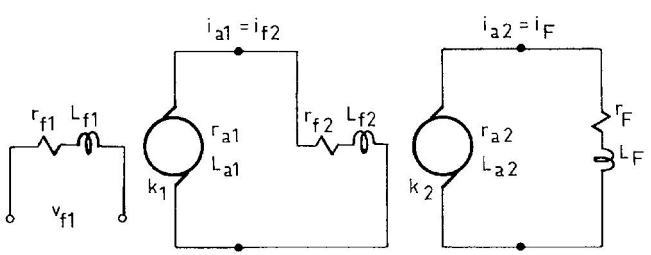

Fig. 2-4P A rotating excitation system.

main exciter $k_e i_{f2}$. Find the transfer function of the excitation system in terms of time constants and gains with v_{f1} of the pilot exciter as the input and i_F of the generator as the output.

References

[1] R. H. Park, Two-reaction theory of synchronous machines. *Trans. Am. Inst. Electr. Eng., Part 1*, 716–730, July (1929); *Part 2*, 352–355, June (1933).

[2] C. Concordia, "Synchronous Machines." Wiley, New York, 1951.

[3] W. A. Lewis, "The Principles of Synchronous Machines." IIT Press, Chicago, Illinois, 1949.

[4] E. W. Kimbark, "Power System Stability," Vol. III. Wiley, New York, 1956.

[5] B. Adkins and R. G. Harley, "The General Theory of Alternating Current Machines." Chapman & Hall, London, 1975.

[6] G. Kron, "Application of Tensors to the Analysis of Rotating Electrical Machinery," G.E. Review. General Electric, Schenectady, 1942.

[7] Yao-nan Yu, The torque tensor of the general machine. *IEEE Trans. Power Appar. Syst.* 623–629, Feb. (1963).

[8] Yao-nan Yu, "Power System Dynamics," Lecture Notes. University of British Columbia, Vancouver, B.C., Canada, 1970–1976.

[9] "Test Procedures for Synchronous Machines," IEEE Publ. No. 115. IEEE, New York, 1965.

[10] Yao-nan Yu and H. A. M. Moussa, Experimental determination of exact equivalent circuit parameters of synchronous machines. *IEEE Trans. Power Appar. Syst.* 2555–2560, Nov./Dec. (1971).

[11] Y. Takeda and B. Adkins, Determination of synchronous machine parameters allowing for unequal mutual inductances. *Proc. Inst. Electr. Eng.* **121**, 1501–1515 (1974).

[12] F. P. deMello and J. R. Ribeiro, Derivation of synchronous machine parameters from tests. *IEEE Trans. Power Appar. Syst.* 1211–1218, July/Aug. (1977).

[13] J. D. Hurley and H. R. Schwenk, Standstill frequency response modeling and evaluation by field tests on a 645 MVA turbine generator. *IEEE Trans. Power Appar. Syst.* 828–836, Feb. (1981).

[14] P. L. Dandeno, P. Kundur, A. T. Poray, and H. M. Zein El-Din, Adaptation and validation of turbogenerator model parameters through on-line frequency response measurements. *IEEE Trans. Power Appar. Syst.* 1656–1664, April (1981).

[15] F. P. deMello and L. H. Hannett, Validation of synchronous machine models and derivation of model parameters from tests. *IEEE Trans. Power Appar. Syst.* 662–672, Feb. (1981).

[16] M. Namba, J. Hosoda, S. Doi, and M. Udo, Development for measurement of operating parameters of synchronous generator and control systems. *IEEE Trans. Power Appar. Syst.* 618–628, Feb. (1981).

[17] T. Sugiyama, T. Nishiwaki, S. Takeda, and S. Abe, Measurement of synchronous machine parameters under operating condition. *IEEE Trans. Power Appar. Syst.* 895–904, April (1981).

[18] E. W. Kimbark, "Power System Stability," Vol. I. Wiley, New York, 1948.

[19] F. P. deMello and C. Concordia, Concepts of synchronous machine stability as affected by excitation control. *IEEE Trans. Power Appar. Syst.* 316–329, April (1969).

[20] W. G. Heffron and R. A. Philips, Effect of modern amplidyne voltage regulators on under-excited operation of large turbine generators. *AIEE Trans. Power Appar. Syst.* 692–697, Aug. (1952).

[21] D. W. Olive, Digital simulation of synchronous machine transients. *IEEE Trans. Power Appar. Syst.* 1669–1675, Aug. (1968).

[22] G. Manchur, D. C. Lee, M. E. Coultes, J. D. A. Griffin, and W. Watson, Generator models established by frequency response tests on a 555 MVA machine. *IEEE Trans. Power Appar. Syst.* 2077–2084, Sept./Oct. (1972).

[23] R. P. Schulz, "Synchronous Machine Modelling," IEEE Publ. 75 CH0970-4-PWR, pp. 24–28. IEEE, New York, 1975.

[24] IEEE Committee, Computer representation of excitation system. *IEEE Trans. Power Appar. Syst.* 1460–1464, June (1968).

[25] IEEE Committee, Excitation system models for power system stability studies. *IEEE Trans. Power Appar. Syst.* 494–509, Feb. (1981).

[26] F. R. Schleif, "Excitation System Modelling," IEEE Publ. 75 CH0970-4-PWR, pp. 29–32. IEEE, New York, 1975.

[27] IEEE Committee, Excitation system dynamic characteristics. *IEEE Trans. Power Appar. Syst.* 64–75, Jan./Feb. (1973).

[28] H. F. Messerly and R. W. Bruck, Steady state stability of synchronous generators as affected by regulators and governors. *Proc. Inst. Electr. Eng., Part C* **102,** 24–34 (1955).

[29] L. M. Hovey and L. A. Bateman, Speed regulation tests on hydro station supplying an isolated load. *IEEE Trans. Power Appar. Syst.* 364–371, Oct. (1962).

[30] IEEE Committee, Dynamic models for steam and hydro turbines in power system studies. *IEEE Trans. Power Appar. Syst.* 1904–1915, Nov./Dec. (1973).

[31] M. E. Leum, The development and field experience of a transistor electric governor for hydro turbines. *IEEE Trans. Power Appar. Syst.* 393–402, April (1966).

[32] D. G. Ramey and J. W. Skooglund, Detailed hydrogovernor representation for system stability studies. *IEEE Trans. Power Appar. Syst.* 106–112, Jan. (1970).

Chapter 3 Low-Frequency Oscillations and Supplementary Controls

Since the development of interconnection of large electric power systems, there have been spontaneous system oscillations at very low frequencies in the order of several cycles per minute [1–7]. Once started, they would continue for a while and then disappear, or continue to grow, causing system separation.

The first example of intersystem low-frequency oscillations was observed during a trial interconnection of the Northwest Power Pool and the Southwest Power Pool before the existence of the WSCC (Western Systems Coordinating Council) [2]. The interconnected system operated satisfactorily for a while, but low-frequency oscillations at about 6 cycles per minute developed. The interconnection was then tripped off, leaving the Northwest Power Pool oscillating at about 3 cycles per minute and the Southwest Power Pool oscillating at about 11 cycles per minute. It was noted that the Northwest Power Pool had predominantly hydroelectric power plants and the Southwest Power Pool predominantly steam–electric power plants.

With more experience accumulated from interconnected electric power system operation, power system engineers are now convinced that the low-frequency oscillations are due to the lack of damping of the mechanical mode of the interconnected system, and the desired additional damping can be provided by supplementary excitation control.

To date, most major electric power plants in North America are equipped with supplementary excitation control, commonly referred to as the power system stabilizer (PSS). However, low-frequency oscillations still occur. Note that so far the PSSs have been designed primarily from a one-machine infinite-bus model. In recent years, progress has been made in coordinated

application of PSS to a multimachine system [8], and coordination of PSSs already installed in power systems [9, 10].

3-1 A POWER SYSTEM MODEL FOR LOW-FREQUENCY OSCILLATION STUDIES

During low-frequency oscillations, the current induced in a damper winding is still negligibly small; hence the damper windings can be completely ignored in system modeling. As for the d and q armature windings of a synchronous machine, their natural oscillating frequency is extremely high, their eigenmodes will not affect the low-frequency oscillations, and hence they can be described simply by algebraic equations. What is left is the field winding circuit of the machine, which must be described by a differential equation, not only because of its low eigenmode frequency, but also because it is connected directly to the excitation system to which the supplementary excitation control is applied. Of course, the excitation system itself must be described by differential equations. Finally, the torque differential equation of the synchronous machine must be included in the model.

Transfer Functions for Low-Frequency Oscillation Studies

With these considerations, a complete system model for low-frequency oscillation studies can be derived, and a block diagram may be drawn as Fig. 3-1 [11–13].

There are two major loops in Fig. 3-1, the mechanical loop on top and the electrical loop at the bottom. The mechanical loop is based on Eqs. (2-34) but linearized, with ΔT_D being replaced by $D\,\Delta\omega$. The linearized equations are used because we are dealing with periodic small oscillations. The incremental torque $(\Delta T_m - \Delta T_e)$ is considered as the input and the torque angle $\Delta\delta$ as the output. The mechanical loop has two transfer function blocks from left to right. The first block is based on the equation of torque equilibrium, and the second block shows the relation of the angle and speed for the units chosen. In these blocks, M is the inertia constant, D the mechanical damping coefficient, and $2\pi f$ the synchronous speed.

The electrical loop of Fig. 3-1 has a supplementary control u_E minus the incremental terminal voltage Δv_t as the input and the incremental internal voltage $\Delta e'_q$ as the output, which is multiplied by K_2 to become part of the electric torque ΔT_e of the system. It has two transfer function blocks from right to left. The first block represents an exciter and voltage regulator system of the fast-response type with a time constant T_A and an overall

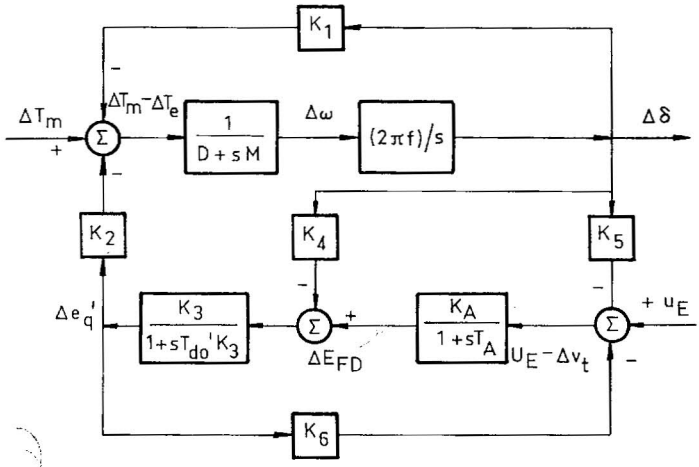

Fig. 3-1 Transfer function block diagram for low-frequency oscillation studies. (From [11–13], courtesy of IEEE. © 1969, 1952, 1971.)

gain K_A. This block should be expanded when the system has rotating exciter and voltage regulator. The second block represents the transfer function of the field circuit as affected by the armature reaction, with an effective time constant $T'_{do}K_3$ and a gain K_3.

Finally, Δv_t consists of two components, $K_5\,\Delta\delta$ due to the torque angle variation $\Delta\delta$ and $K_6\,\Delta e'_q$ due to the internal voltage variation $\Delta e'_q$. Here Δv_t means $(v_t - v_{REF})$, and a negative sign is given to Δv_t because of the negative feedback.

The d and q Components of the Armature Current

For the calculation of constants $K_1, K_2, \ldots, K_6$ of Fig. 3-1, the armature current components i_d and i_q must be known. Figure 3-2 shows the one-machine infinite-bus model of a power system with a synchronous generator

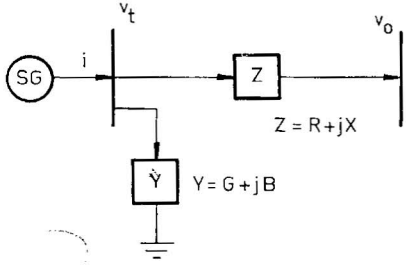

Fig. 3-2 A one-machine infinite-bus power system.

SG, an armature current i, a terminal voltage v_t, an infinite-bus voltage v_o, a series transmission impedance Z, and a shunt load admittance Y.

Let the current and voltage phasors be drawn as shown in Fig. 3-3, and a torque angle δ be defined as the angle between the infinite-bus voltage v_o and the internal voltage e'_q.

Let

$$i \triangleq i_d + ji_q, \qquad v_t \triangleq v_d + jv_q \tag{3-1}$$

$$[\text{phasor } v_o] \triangleq v_o(\sin\delta + j\cos\delta)$$

where

$$\delta \triangleq \angle(e'_q, v_o) \tag{3-2}$$

For convenience, the following constants and parameters are introduced:

$$\begin{gathered} 1 + ZY \triangleq C_1 + jC_2 \\ R_1 \triangleq R - C_2 x'_d, \qquad X_1 \triangleq X + C_1 x_q \\ X_2 \triangleq X + C_1 x'_d, \qquad R_2 \triangleq R - C_2 x_q \\ Z_e^2 \triangleq R_1 R_2 + X_1 X_2 \\ Y_d \triangleq (C_1 X_1 - C_2 R_2)/Z_e^2, \qquad Y_q \triangleq (C_1 R_1 + C_2 X_2)/Z_e^2 \end{gathered} \tag{3-3}$$

From Fig. 3-2, we shall have

$$i = Yv_t + Z^{-1}(v_t - v_o) \qquad \text{or} \qquad Zi = (1 + ZY)v_t - v_o \tag{3-4}$$

Separating the last equation into real and imaginary parts, the results can be written in matrix form in real numbers as follows,

$$\begin{bmatrix} R & -X \\ X & R \end{bmatrix} \begin{bmatrix} i_d \\ i_q \end{bmatrix} = \begin{bmatrix} C_1 & -C_2 \\ C_2 & C_1 \end{bmatrix} \begin{bmatrix} v_d \\ v_q \end{bmatrix} - v_o \begin{bmatrix} \sin\delta \\ \cos\delta \end{bmatrix} \tag{3-5}$$

where

$$C_1 \triangleq 1 + RG - XB, \qquad C_2 \triangleq XG + RB \tag{3-5a}$$

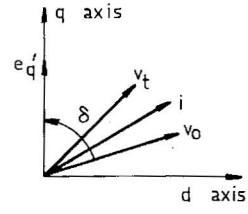

Fig. 3-3 Current and voltage phasors.

But according to Fig. 2-8, the magnitudes of v_d and v_q are

$$\begin{bmatrix} v_d \\ v_q \end{bmatrix} = \begin{bmatrix} 0 \\ 1 \end{bmatrix} e'_q - \begin{bmatrix} 0 & -x_q \\ x'_d & 0 \end{bmatrix} \begin{bmatrix} i_d \\ i_q \end{bmatrix} \tag{3-6}$$

Substituting (3-6) into (3-5) and solving for i_d and i_q gives

$$\begin{bmatrix} i_d \\ i_q \end{bmatrix} = \begin{bmatrix} Y_d \\ Y_q \end{bmatrix} e'_q - \frac{v_o}{z_e^2} \begin{bmatrix} R_2 & X_1 \\ -X_2 & R_1 \end{bmatrix} \begin{bmatrix} \sin \delta \\ \cos \delta \end{bmatrix} \tag{3-7}$$

Linearization of (3-7) results in

$$\begin{bmatrix} \Delta i_d \\ \Delta i_q \end{bmatrix} = \begin{bmatrix} Y_d \\ Y_q \end{bmatrix} \Delta e'_q + \begin{bmatrix} F_d \\ F_q \end{bmatrix} \Delta\delta \tag{3-8}$$

where Y_d and Y_q are given in (3-3),

$$\begin{bmatrix} F_d \\ F_q \end{bmatrix} = \frac{v_o}{Z_e^2} \begin{bmatrix} -R_2 & X_1 \\ X_2 & R_1 \end{bmatrix} \begin{bmatrix} \cos \delta_o \\ \sin \delta_o \end{bmatrix} \tag{3-9}$$

and δ_o is the initial angle.

Constants $K_1, K_2, \ldots, K_6$

K_1 and K_2 from Electric Torque. The electric torque of a synchronous machine near the synchronous speed can be approximated by

$$T_e \simeq P_e = i_d v_d + i_q v_q \quad \text{per unit} \tag{3-10}$$

Substituting v_d and v_q from (3-6) into (3-10) yields

$$T_e = i_q e'_q + (x_q - x'_d) i_d i_q \tag{3-11}$$

Substituting Δi_d and Δi_q of (3-8) into the linearized results of (3-11) gives

$$\Delta T_e = K_1 \Delta\delta + K_2 \Delta e'_q \tag{3-12}$$

where

$$\begin{bmatrix} K_1 \\ K_2 \end{bmatrix} = \begin{bmatrix} 0 \\ i_{q0} \end{bmatrix} + \begin{bmatrix} F_d & F_q \\ Y_d & Y_q \end{bmatrix} \begin{bmatrix} (x_q - x'_d) i_{q0} \\ e'_{q0} + (x_q - x'_d) i_{d0} \end{bmatrix} \tag{3-13}$$

K_3 and K_4 from the Field Voltage Equation. The field winding circuit voltage equation of (2-45) may be linearized and written

$$(1 + sT'_{do}) \Delta e'_q = \Delta E_{FD} - (x_d - x'_d) \Delta i_d \tag{3-14}$$

Substituting Δi_d of (3-8) into (3-14) results in

$$(1 + sT'_{do}K_3)\Delta e'_q = K_3[\Delta E_{FD} - K_4\,\Delta\delta] \tag{3-15}$$

where

$$\begin{aligned} K_3 &= 1/[1 + (x_d - x'_d)Y_d] \\ K_4 &= (x_d - x'_d)F_d \end{aligned} \tag{3-16}$$

K_5 and K_6 from the Terminal Voltage Magnitude. The magnitude of the generator terminal voltage can be expressed in terms of its d and q components as

$$v_t^2 = v_d^2 + v_q^2 \tag{3-17a}$$

and the deviation as

$$\Delta v_t = (v_{do}/v_{to})\Delta v_d + (v_{qo}/v_{to})\Delta v_q \tag{3-17b}$$

Substituting (3-8) into the linearized results of (3-6) and Δv_d and Δv_q thus obtained into (3-17b) gives

$$\Delta v_t = K_5\,\Delta\delta + K_6\,\Delta e'_q \tag{3-18}$$

where

$$\begin{bmatrix} K_5 \\ K_6 \end{bmatrix} = \begin{bmatrix} 0 \\ v_{q0}/v_{t0} \end{bmatrix} + \begin{bmatrix} F_d & F_q \\ Y_d & Y_q \end{bmatrix} \begin{bmatrix} -x'_d v_{q0}/v_{t0} \\ x_q v_{d0}/v_{t0} \end{bmatrix} \tag{3-19}$$

In (3-19), F_d and F_q are given in (3-9) and Y_d and Y_q in (3-3).

In this section the initial values of currents, voltages, and their components are all identified by subscript 0, e.g., i_{d0}.

Summary of Section 3-1

In this section the transfer function block diagram of Fig. 3-1 for low-frequency oscillation studies is derived. It is based on a one-machine, infinite-bus power system model with a local load [13]. Constants K_1 and K_2 are derived from the electric torque expression, K_3 and K_4 from the field winding circuit equation, and K_5 and K_6 from the generator terminal voltage mag-

nitude. For the calculation of these constants, the initial currents, voltages, and torque angle of the system in the steady state must be known.

3-2 INITIAL CURRENTS, VOLTAGES, AND TORQUE ANGLE

The initial currents, voltages, and torque angles in steady state are usually found from a load flow study for a multimachine system. For a one-machine infinite-bus system, two cases are conceivable:

1. The electric power P_{e0}, the reactive power Q_{e0}, and the machine terminal voltage $|v_{t0}|$ are given;
2. The electric power P_{e0}, the machine terminal voltage $|v_{t0}|$, and the infinite-bus voltage $|v_o|$ are given.

Example 3-1. Find the initial steady-state value of the d and q component currents, voltages and the torque angle of the one-machine, infinite-bus system as shown in Fig. 3-2 for given P_{e0}, Q_{e0} and v_{t0} [14].

Solution: The second subscript 0 to identify the initial values will be omitted in this section for conciseness, but the first subscript o in v_o will be kept to signify the infinite-bus voltage. The power and reactive power of a synchronous machine can be calculated from

$$P_e + jQ_e = (i_d + ji_q)^*(v_d + jv_q) \tag{3-20}$$

The magnitude of v_d and that of v_q can be calculated from (3-6), and the machine terminal voltage v_t can be expressed in terms of v_d and v_q. There are five independent equations

$$\begin{aligned} P_e &= i_d v_d + i_q v_q, & Q_e &= i_d v_q - i_q v_d \\ v_d &= x_q i_q, & v_q &= e'_q - x'_d i_d \\ v_t^2 &= v_d^2 + v_q^2 \end{aligned} \tag{3-21}$$

for the five unknowns i_d, i_q, v_d, v_q, and e'_q.

If i_d is eliminated from the first two equations of (3-21), we have

$$P_e v_q - Q_e v_d = i_q v_t^2 \tag{3-22}$$

Solving i_q and v_q respectively, from the third and the last equation of (3-21), and substituting the results into (3-22) gives

$$P_e(v_t^2 - v_d^2)^{1/2} - Q_e v_d = v_d(v_t^2/x_q) \tag{3-23}$$

Therefore, v_d can be found first, which leads to the following:

$$\begin{aligned} v_d &= P_e v_t [P_e^2 + (Q_e^2 + v_t^2/x_q)^2]^{-1/2} \\ v_q &= (v_t^2 - v_d^2)^{1/2} \\ i_q &= v_d/x_q \\ i_d &= (P_e - i_q v_q)/v_d \qquad \text{or} \qquad (Q_e + i_q v_d)/v_q \\ e'_q &= v_q + x'_d i_d \end{aligned} \tag{3-24}$$

The initial values of v_o and δ remain to be determined. From the torque angle definition of Fig. 3-3 and Eq. (3-5), we have

$$\begin{aligned} v_{od} &= v_o \sin\delta = C_1 v_d - C_2 v_d - R i_d + X i_q \\ v_{oq} &= v_o \cos\delta = C_2 v_d + C_1 v_q - X i_d - R i_q \end{aligned} \tag{3-25}$$

Consequently,

$$\delta = \tan^{-1}(v_{od}/v_{oq}), \qquad v_o = (v_{od}^2 + v_{oq}^2)^{1/2} \tag{3-26}$$

Example 3-2. Find the initial steady-state values of the d and q component currents, voltages, and the torque angle of the one-machine, infinite-bus system as shown in Fig. 3-2 for given P_{eo}, $|v_{to}|$, and $|v_o|$.

Solution: Again the second subscript o to identify the initial values will be omitted for conciseness, but the subscript o of v_o will remain.

Let the transmission line impedance angle be defined by

$$\alpha \triangleq \tan^{-1}(X/R) \tag{3-27}$$

and other angles as shown in Fig. 3-4 be defined by

$$\beta \triangleq \angle(e'_q, v_t), \qquad \gamma \triangleq \angle(v_t, v_o), \qquad \phi \triangleq \angle(v_t, i) \tag{3-28}$$

Then, the angle β can be calculated from the partly dotted right-angled triangle in Fig. 3-5 as follows:

$$\beta = \tan^{-1} \frac{x_q |i| \cos\phi}{|v_t| + x_q |i| \sin\phi} \tag{3-29}$$

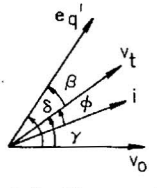

Fig. 3-4 Phase angles.

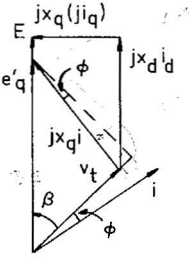

Fig. 3-5 Calculation of β.

For the calculation of γ, v_o may be chosen as the reference phasor. According to Figs. 3-2 and 3-4,

$$i = |v_t|e^{j\gamma}\left[(G + jB) + \frac{1}{R + jX}\right] - \frac{v_o}{R + jX} \tag{3-30}$$

Since $(P_e + jQ_e)$ is defined by i^*v_t,

$$P_e - jQ_e = iv_t^* = |v_t|^2(G + R/|Z|^2) + j(B - X/|Z|^2)] - \frac{v_o|v_t|}{|Z|}e^{-j(\alpha+\gamma)} \tag{3-31}$$

or

$$\begin{aligned} P_e &= |v_t|^2\left(G + \frac{R}{|Z|^2}\right) - \frac{v_o|v_t|}{|Z|}\cos(\alpha + \gamma) \\ Q_e &= |v_t|^2\left(-B + \frac{X}{|Z|^2}\right) + \frac{v_o|v_t|}{|Z|}\sin(\alpha + \gamma) \end{aligned} \tag{3-32}$$

Therefore γ can be found from either P_e or Q_e of (3-32). From P_e we have

$$\gamma = \cos^{-1}\frac{|v_t|^2(G + R/|Z|^2) - P_e}{v_o|v_t|/|Z|} - \alpha \tag{3-33}$$

Having found β and γ, the torque angle, the currents, and the voltages can be calculated as follows:

$$\begin{aligned} &\delta = \beta + \gamma \\ &v_d = |v_t|\sin\beta, \qquad v_q = |v_t|\cos\beta \\ &i_d = |i|\sin(\beta + \gamma), \qquad i_q = |i|\cos(\beta + \gamma) \\ &e'_q = v_q + x'_d i_d \end{aligned} \tag{3-34}$$

Summary of Section 3-2

In this section two examples of calculating the initial steady-state values of currents, voltages, and torque angle of a one-machine, infinite-bus system are shown: one for given electric power, reactive power, and machine terminal voltage, and the other for given electric power, machine terminal voltage, and infinite-bus voltage. The results are useful for calculating constants $K_1, K_2, \ldots, K_6$ of Fig. 3-1. For a multimachine system, these initial values can be found from a load flow study.

3-3 IMPROVING SYSTEM DAMPING WITH SUPPLEMENTARY EXCITATION

A power system may lose its stability due to the lack of damping or inadequate synchronizing torque as shown in Fig. 3-6a and b, respectively. The sustained low-frequency oscillations of a large electric power system are due to the lack of damping of the system mechanical mode. A synchronous machine may have mechanical damping adequate for the machine itself, but not sufficient for the machine operating in a large electric power system. Therefore, supplementary damping must be sought.

Desired Damping to Attenuate Low-Frequency Oscillations

Because of the periodical variations of angle, speed, and torque in a large electric power system during the low-frequency oscillations, like current and voltage, these physical quantities can be treated as phasors as well. Figure 3-7 shows an electric torque ΔT_e and a mechanical torque ΔT_m on the $\Delta\delta$–$\Delta\omega$ phase plane at the oscillating frequency.

Consider the torque equation (2-41). Since we are dealing with small oscillations, the equation can be linearized, resulting in

$$M\,\Delta\dot{\omega} = \Delta T_m - \Delta T_e - \Delta T_D \tag{3-35}$$

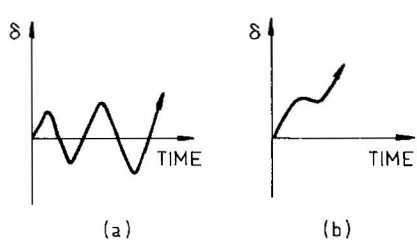

Fig. 3-6 Unstable electric power system.

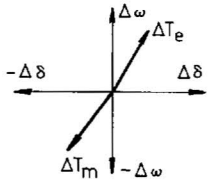

Fig. 3-7 Torque phasors on the $\Delta\delta$–$\Delta\omega$ phase plane.

To derive an extra damping ΔT_E through supplementary excitation, ΔT_e must be in phase with $\Delta\omega$ according to (3-35) and Fig. 3-7. Similarly, an extra damping through the governor control must be in phase with $-\Delta\omega$.

Consider a general case of supplementary excitation and governor control of low-frequency oscillations. Let the extra electric damping ΔT_E be included in ΔT_e and the extra mechanical damping ΔT_M be included in ΔT_m, and let

$$\Delta T_M = -D_M \Delta\omega, \qquad \Delta T_E = D_E \Delta\omega \tag{3-36a}$$

Assume that the original ΔT_m from regular governor control is still negligible, and let the original ΔT_e from voltage regulator control be $K_1 \Delta\delta$. We have

$$\begin{aligned} \Delta T_m &\simeq \Delta T_M = -D_M \Delta\omega \\ \Delta T_e &= K_1 \Delta\delta + D_E \Delta\omega \\ \Delta T_D &= D \Delta\omega \end{aligned} \tag{3-36b}$$

and

$$[Ms^2 + (D_M + D_E + D)s + \omega_b K_1] \Delta\delta = 0 \tag{3-37}$$

since

$$\Delta\delta = (\omega_b \Delta\omega)/s, \qquad \omega_b = 2\pi f \tag{3-38}$$

Normalization of (3-37) yields

$$(s^2 + 2\zeta_n \omega_n s + \omega_n^2) \Delta\delta = 0 \tag{3-39}$$

Therefore

$$s = (-\zeta_n \pm j\sqrt{1 - \zeta_n^2})\omega_n \tag{3-40}$$

where

$$\omega_n = \sqrt{\omega_b K_1 / M}, \qquad \zeta_n = (D_M + D_E + D)/(2\omega_b M) \tag{3-40a}$$

and ω_n is the undamped mechanical mode oscillating frequency in radians per second for $\zeta_n = 0$, and ζ_n is the damping coefficient in per unit. The

characteristic equation is normalized because only in this form can we have a clear idea of the magnitude and degree of damping.

Supplementary Excitation Control Design

The supplementary excitation control of the low-frequency oscillations is currently known as the power system stabilizer (PSS). The idea of supplementary excitation is to apply a signal through the excitation system to increase the damping torque of the generator in a power system. For the one-machine, infinite-bus model of Fig. 3-1, the supplementary control u_E is applied through the T_A, T'_{do}, and K_2 blocks to obtain the extra damping ΔT_E. Since Fig. 3-1 is a linearized model, the superposition principle applies.

Because of the phase lags of $(1 + sT_A)$ and $(1 + sT'_{do}K_3)$ for $s = j\omega_n$, a phase lead compensation must be included in the supplementary excitation design, so as to have a damping torque ΔT_E in phase with $\Delta\omega$ at the oscillating frequency. The compensation also must have a gain in order to have an adequate magnitude of damping.

Various input signals can be used for the supplementary excitation design: the speed deviation $\Delta\omega$, the accelerating power ΔP_a, or the system frequency Δf. The PSS may be designed from the undamped natural mechanical mode frequency $j\omega_n$, or from the complex frequency $\sigma + j\omega$ of the mechanical mode obtained from system eigenvalue analysis.

Consider the $j\omega_n$ design first. Let $\Delta\omega$ be the control input. A general design procedure may be outlined as follows.

a. Find ω_n from the Mechanical Loop Alone First. Directly from Fig. 3-1 but neglecting the damping, or from (3-37) but neglecting all dampings, the characteristic equation of the mechanical loop may be written

$$Ms^2 + \omega_b K_1 = 0 \tag{3-41}$$

and the solutions are

$$s = \pm j\omega_n, \qquad \omega_n = \sqrt{\omega_b K_1 / M} \tag{3-42}$$

where ω_n is the undamped natural frequency of the mechanical mode, ω_b or $2\pi f$ is the system frequency, both in radians per second, K_1 is a constant for given system parameters and operating conditions, and M is the inertia constant in seconds.

b. Find the Phase Lag $\angle G_E$ between u_E and e'_q of the Electrical Loop. The transfer function between u_E and e'_q of Fig. 3-1, including the feedback

effect of K_6, is

$$G_E = \frac{K_A K_3}{(1 + sT_A)(1 + sT'_{do}K_3) + K_A K_3 K_6} \tag{3-43}$$

and the phase lag may be calculated from

$$\text{phase lag of } G_E = \angle G_E|_{s=j\omega_n} \tag{3-44}$$

c. Design a Phase Lead Compensation $\angle G_C$ for the Phase Lag $\angle G_E$. When $\Delta\omega$ is chosen as the supplementary excitation input, we shall have

$$\angle G_C + \angle G_E = 0, \qquad \angle G_E < 0 \tag{3-45}$$

The phase lead compensation may be realized by operational amplifiers, and the simplest transfer function may be chosen in the form of

$$G_C = \left(\frac{1 + sT_1}{1 + sT_2}\right)^k, \qquad k = 1 \text{ or } 2, \quad T_1 > T_2 \tag{3-46}$$

There is a phase angle limit that a compensation block can provide, and T_2 cannot be too small. For a T_2 chosen as 0.2 s and T_1 as $10T_2$, the phase lead provided by each compensation block is about 34° for $s = j2\pi$ rad/s corresponding to 1 Hz.

d. Design a Gain K_C for the Supplementary Excitation. For this excitation control design, D_M and D of (3-40) are neglected. A reasonable choice for the damping coefficient ζ_n of the normalized characteristic equation (3-39) is about 0.1 to 0.3 per unit. From (3-40), neglecting D_M and D, we have

$$D_E \simeq 2\zeta_n \omega_n M \tag{3-47}$$

But according to Fig. 3-1 and including the supplementary excitation, we also have

$$D_E = K_C K_2 |G_C|_{s=j\omega_n} |G_E|_{s=j\omega_n} \tag{3-48}$$

Therefore

$$K_C = \frac{2\zeta_n \omega_n M}{K_2 |G_C(j\omega_n)| |G_E(j\omega_n)|} \tag{3-49}$$

e. Design a Reset Block for u_E. The supplementary excitation control should be activated only when the low-frequency oscillation begins to develop, and it should be automatically terminated when the system oscillation ceases. It should not interfere with the regular function of excitation

during steady-state operation at the system frequency. A reset block is therefore necessary, which may have the form of

$$G_{\text{RESET}} = \frac{sT}{1 + sT} \tag{3-50}$$

Since the reset block should not have any effect on phase shift or gain at the oscillating frequency, it can be achieved by choosing a large T value, so that sT is much larger than unity and

$$G_{\text{RESET}}|_{s=j\omega_n} \simeq 1 \tag{3-50a}$$

Figure 3-8 shows the block diagram of a supplementary excitation control with one compensation block and one reset block. The supplementary excitation will not have any effect on the steady state of the system, since in steady state

$$s\,\Delta\omega = 0 \tag{3-51}$$

f. Eigenvalue Analysis of the System with and without u_E. Although this step was not performed in the early development of PSS, it is very useful to find how much damping the various modes of a system have at the oscillating frequencies. For a typical eigenvalue $(\sigma + j\omega)$, the oscillating frequency is ω rad/s or $\omega/(2\pi)$ Hz, and the damping coefficient ζ is found from the real part of the normalized eigenvalue, namely,

$$\zeta = \sigma/\sqrt{\sigma^2 + \omega^2} \quad \text{per unit} \tag{3-52}$$

State Equations of the One-Machine Infinite-Bus System

To find the eigenvalues of a system, the system equations must be written in the standard state variable form in the first-order differential equations, with all derivatives as a column matrix on the LHS of the equations, and the rest on the RHS of the equations. For a system without control, the state equations may be simply written as

$$\dot{x} = Ax, \qquad u_E = 0 \tag{3-53}$$

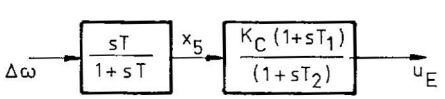

Fig. 3-8 A supplementary excitation control.

where x is the state variable vector and A the system matrix. The state equations of the one-machine, infinite-bus system may be derived from Fig. 3-1 as follows:

$$\begin{aligned} Ms\,\Delta\omega &= -\Delta T_e = -(K_1\,\Delta\delta + K_2\,\Delta e'_q) \\ s\,\Delta\delta &= \omega_b\,\Delta\omega \\ (1 + sT'_{do}K_3)\,\Delta e'_q &= K_3(-K_4\,\Delta\delta + \Delta E_{FD}) \\ (1 + sT_A)\,\Delta E_{FD} &= K_A(u_E - \Delta v_t) = K_A(u_E - K_5\,\Delta\delta - K_6\,\Delta e'_q) \end{aligned} \tag{3-54}$$

Since $s\,\Delta\omega$, $s\,\Delta\delta$, $s\,\Delta e'_q$, and $s\,\Delta E_{FD}$ correspond to $\Delta\dot{\omega}$, $\Delta\dot{\delta}$, $\Delta\dot{e}'_q$, and $\Delta\dot{E}_{FD}$, respectively, the state variable vector becomes

$$x = [\Delta\omega, \Delta\delta, \Delta e'_q, \Delta E_{FD}]^T \tag{3-55}$$

and the system matrix elements can be found according to the relation

$$\begin{bmatrix} \Delta\dot{\omega} \\ \Delta\dot{\delta} \\ \Delta\dot{e}'_q \\ \Delta\dot{E}_{FD} \end{bmatrix} = \begin{bmatrix} & & A & \\ & & & \\ & & & \\ & & & \end{bmatrix} \begin{bmatrix} \Delta\omega \\ \Delta\delta \\ \Delta e'_q \\ \Delta E_{FD} \end{bmatrix} \tag{3-56}$$

Therefore, we have

$$[A] = \begin{bmatrix} 0 & -K_1/M & -K_2/M & 0 \\ \omega_b & 0 & 0 & 0 \\ 0 & -K_4/T'_{do} & -1/(T'_{do}K_3) & 1/T'_{do} \\ 0 & -K_AK_5/T_A & -K_AK_6/T_A & -1/T_A \end{bmatrix} \tag{3-56a}$$

For the system with the supplementary excitation control u_E, the system equations may be written

$$\dot{x} = Ax + Bu_E = A_c x \tag{3-57}$$

where B is the control matrix, u_E the supplementary excitation, and A_c the controlled system matrix. If the supplementary control has the form of Fig. 3-8, the additional equations are

$$\begin{aligned} (1 + sT)x_5 &= sT\,\Delta\omega \\ (1 + sT_2)u_E &= K_C(1 + sT_1)x_5 \end{aligned} \tag{3-58}$$

The new state variable vector becomes

$$x = [\Delta\omega, \Delta\delta, \Delta e'_q, \Delta E_{FD}, x_5, u_E]^T \tag{3-59}$$

and the controlled system matrix becomes

$$[A_c] = \left[\begin{array}{cccc|cc} & & [A] & & 0 & 0 \\ & & & & 0 & 0 \\ & & & & 0 & 0 \\ & & & & 0 & K_A/T_A \\ \hline 0 & -K_1/M & -K_2/M & 0 & -1/T & 0 \\ 0 & -\dfrac{K_C K_1 T_1}{MT_2} & -\dfrac{K_C K_2 T_1}{MT_2} & 0 & \dfrac{K_C}{T_2}\left(1-\dfrac{T_1}{T_2}\right) & -\dfrac{1}{T_2} \end{array}\right] \quad (3\text{-}60)$$

For the derivation of (3-60), $s\,\Delta\omega$, and sx_5 of (3-58) must be successively substituted by algebraic relations from earlier derivations.

Example 3-3. Design a supplementary excitation u_E for a one-machine, infinite-bus system using $\Delta\omega$ as the control input and ω_n for the design. The system is similar to Fig. 3-1 and all data are given in per unit of value, except that M and time constants are in seconds.

Generator $M = 9.26 \quad T'_{do} = 7.76 \quad D \simeq 0$

$x_d = 0.973 \quad x'_d = 0.190 \quad x_q = 0.550$

Excitation $K_A = 50 \quad T_A = 0.05$

Line and load $R = -0.034 \quad X = 0.997 \quad G = 0.249 \quad B = 0.262$

Initial state $P_{e0} = 1.0 \quad Q_{e0} = 0.015 \quad v_{t0} = 1.05,$

Note that the negative R stems from deriving the one-machine, infinite-bus model for a multimachine system by equivalencing smaller generators by equivalent impedances with negative resistances. Design the supplementary excitation and compare the eigenvalues of the system with and without the supplementary control. It is a 60-Hz system.

Solution: The initial d and q current and voltage components and torque angle of the initial steady state are found from (3-24) and (3-26) as follows:

$$v_{d0} = 0.4659 \quad v_{q0} = 0.9410 \quad i_{d0} = 0.4354 \quad i_{q0} = 0.8471$$

$$e'_{q0} = 1.024 \quad v_o = 1.051 \quad \delta_o = 68.01^\circ$$

The K constants from (3-13), (3-16, and (3-19) are

$$K_1 = 0.5441 \quad K_2 = 1.2067 \quad K_3 = 0.6584 \quad K_4 = 0.6981$$

$$K_5 = -0.0955 \quad K_6 = 0.8159$$

For the supplementary excitation design, it is found that one compensation block is sufficient. The following values are chosen

$$\zeta_n = 0.3 \quad T_2 = 0.1 \quad T = 3.0$$

The results are

$$\omega_n = 4.707 \text{ rad/s} \quad \angle G_E = -47.57^\circ \quad |G_E| = 1.001$$

$$T_1 = 0.6851\ s \qquad K_C = 7.09$$

Therefore, the control including the reset block becomes

$$u_E = \left(\frac{1 + 0.685\ s}{1 + 0.1\ s}\right)\left(\frac{7.091(3\ s)}{1 + 3\ s}\right)\Delta\omega$$

The system matrix A of (3-56) for the system without control and the controlled system matrix A_c of (3-60) are then constructed. Double precision is used to find the system eigenvalues, and the results are

System mode	Without u_E	With u_E
Mechanical	$0.195 \pm j4.96$	$-1.127 \pm j4.33$
Electrical	$-10.393 \pm j3.284$	$-4.618 \pm j7.483$
Control	—	$-0.3439, -15.726$

Since an eigenvalue with a positive real part corresponds to an eigenmode with a negative damping, the unstable system without the supplementary excitation u_E is stabilized by the supplementary excitation, and the new mechanical mode damping becomes

$$\zeta_n = 1.127/\sqrt{1.127^2 + 4.33^2} = 0.252$$

which is close to what is designed for.

The various eigenmodes are identified one at a time. It may begin with the mechanical loop alone, which is a second-order system, and the undamped natural mechanical mode frequency ω_n is found to be 4.707 rad/s. The next step is an eigenvalue analysis of the fourth-order system of Fig. 3-1 without u_E. Two pairs of eigenvalues are found, as shown in the table. Because of the dynamic interaction between the electrical and mechanical loops, there is a change in the mechanical mode eigenvalues, from $\pm j4.707$ to $0.295 \pm j4.96$. But the frequency change is relatively small. The other pair, which has a different frequency, belongs to the electrical mode. The final step is the eigenvalue analysis of the entire system, including the supplementary excitation u_E, which is of the sixth order, and hence has two more eigenvalues. The frequencies of the electrical and mechanical modes have

some changes between the fourth-order and the sixth-order eigenvalue analysis. Therefore, the two new eigenvalues belong to the mode of control.

Summary of Section 3-3

In this section the principle and procedure of supplementary excitation design of one-machine, infinite-bus system are presented, and a numerical example of design is given. The basic idea is to provide extra damping to the machine through the excitation system, in phase with the speed deviation $\Delta\omega$ at the oscillating frequency. The phase lag of the excitation loop must be compensated, an adequate damping magnitude must be chosen, and a reset block provided. The reset block is used to activate the control only when the low-frequency oscillations begin to develop, and the control action is automatically terminated after the system ceases to oscillate so that the control will not interfere with the regular function of the excitation system.

The effect of the supplementary excitation control is significant, and the designed damping is close to the value chosen.

From eigenvalue analysis, various eigenmodes of the one-machine, infinite-bus system can be identified: the mechanical mode from the second-order system, the electrical mode from the fourth-order system, and the control mode from the sixth-order system. Should there be two mode frequencies that are very close, for instance, the electrical and the mechanical, they can still be distinguished from each other by artificially varying one of the parameters, for instance, the electrical loop gain K_A. This technique can be developed to identify various modes of very high order electric power systems.

3-4 THE DEVELOPMENT OF SUPPLEMENTARY EXCITATION CONTROL

In this section some historical developments of supplementary excitation control will be reviewed, and current development trends will be introduced. More references can be found in Byerly and Kimbark [15].

Peace River Project of British Columbia Hydro

When the Peace River Project of British Columbia Hydro was developed, dynamic resistance braking was used to improve the transient stability, and supplementary excitation was used to enhance the damping of the low-frequency system oscillations [1]. The generation at Portage Mountain was

modeled as "one-machine" with fixed-shaft power input, and the Bonneville Power Administration System as an "infinite bus" for the supplementary excitation design. Many signals were examined and $\Delta\omega$ was found to give particularly good results, which was further confirmed in a field test [16]. In the final application, the incremental accelerating power ΔP_a was used as the supplementary excitation input. Jones and Luini pointed out in their discussion in Shier and Blythe [16] that when

$$\Delta P_m \ll \Delta P_e \tag{3-61}$$

the incremental kinetic energy of the rotating system can be expressed by

$$\Delta \text{KE} = \int \Delta P_a \, dt \simeq -\int \Delta P_e \, dt \tag{3-62}$$

Hence

$$\Delta\omega = -k \int \Delta P_e \, dt, \qquad \text{KE} = \tfrac{1}{2} J \omega_m^2 \tag{3-63}$$

In other words, the integral of the incremental accelerating power is proportional to the incremental speed $\Delta\omega$.

Moose River Project of Ontario Hydro

During the development of the Moose River Project of Ontario Hydro [17], it was found that the damping effect of the amortisseur windings was quite small, that the speed governor could not contribute significant damping to the low-frequency system oscillations due to the water inertia, and that a rotating exciter was not as good as a fast-response rectifier exciter. The fast-response exciter was chosen and a supplementary excitation was designed. A toothed steel wheel was mounted below the generator guide bearing, and several shaft positions were sensed by magnetic pickups, which were processed to produce the speed deviation signal for the supplementary excitation input. Field tests showed that both dynamic and transient stabilities were improved by the supplementary excitation control. In the discussion in Dandeno *et al.* [17], Schleif and Hunkins reported that the damping effect of the amortisseur windings was rather appreciable toward the higher end of the low-frequency band of oscillations.

First Interconnection of Pacific Power Systems at Glenn Canyon

When the Pacific Northwest and Southwest Power Pools were first interconnected at Glenn Canyon [18], the generators with rotating exciters and

voltage regulators were modeled on an analog computer as a one-machine, infinite-bus system. The generator terminal frequency Δf was used as the supplementary excitation input. Two phase compensation blocks were used to improve the system damping over a wide frequency range of low-frequency oscillations. A reset block was designed with a chosen time constant of 10 s to avoid the phase shift effect toward the lower-frequency end of oscillations. The results of analog studies were further verified in field tests. In a discussion in Schleif *et al.* [18] by Krahn, it is confirmed from digital simulation that the low-order generator model without damper windings could be used for the low-frequency oscillation study, which was used in the analog study.

deMello and Concordia's Analysis

Most of the analytical results of deMello and Concordia [11] have been introduced in the earlier part of this chapter. Considerations were given to the design of a universally applicable stabilizing function under a wide range of conceivable inertia, impedance, load values, and oscillating frequencies, from 0.5 to 2 Hz with 0.1-Hz and 4-Hz extremities. The universal function has the following form:

$$\frac{\Delta v_{\text{t REF}}}{\Delta \omega} = \frac{60s(1 + s/8)^2}{(1 + 3s)(1 + s/20)^2} \tag{3-64}$$

In their discussion of system dynamics it was pointed out that although K_1 of the mechanical loop was positive in most cases, it could be negative for a very long transmission line with a heavy load. In such a case, $K_1 \Delta\delta$ would represent a negative synchronizing torque and the system might lose stability at the first swing.

In investigating the voltage regulator effect, it was pointed out that while a considerable large voltage-regulator gain was desirable for steady-state operation, a much smaller gain was more appropriate in transient state. The voltage-regulator gain could be reduced during the transient by a compensating block $(1 + sT_a)/(1 + sT_b)|_{s\to\infty}$, where $T_a < T_b$, resulting in T_a/T_b only.

Complex Frequency Design of Supplementary Excitation

Since the electrical loop of Fig. 3-1 interacts with the mechanical loop, the supplementary excitation control should probably be designed from the mechanical mode complex frequency based on eigenvalue analysis of the entire system, not just from $j\omega_n$ of the mechanical loop alone [19]. A pro-

cedure for complex-frequency supplementary-excitation design may be outlined as follows.

a. Find the Mechanical Mode Complex Frequency $\sigma + j\omega$. It can be found from an eigenvalue analysis of the entire system without u_E.

b. Find the Phase Lag of $G_E(\sigma + j\omega)$ Let the phase lag be

$$\angle G_E(\sigma + j\omega) \triangleq \gamma, \qquad \gamma < 0 \tag{3-65}$$

c. Design a Phase Lead Compensation for $\angle G_E(\sigma + j\omega)$. If $\Delta\omega$ is chosen as the control input and if one compensation block is sufficient,

$$G_C = \frac{1 + sT_1}{1 + sT_2} \tag{3-46a}$$

we shall have

$$\angle \frac{1 + sT_1}{1 + sT_2} + \gamma = 0 \tag{3-66}$$

or

$$\angle(1 + sT_1) = \angle(1 + sT_2) - \gamma \tag{3-67}$$

Let

$$\phi \triangleq \tan^{-1}[(\omega T_2)/(1 + \sigma T_2)] \tag{3-68}$$

we shall have

$$\tan^{-1} \frac{\omega T_1}{1 + \sigma T_1} = \phi - \gamma \tag{3-69}$$

therefore

$$T_1 = \frac{\tan(\phi - \gamma)}{\omega - \sigma \tan(\phi - \gamma)} \tag{3-70}$$

The formulation can be modified for multiple-block phase compensation. For instance, if two identical blocks are used for the design, $\angle G_E(\sigma + j\omega)$ may be defined as

$$\angle G_E(\sigma + j\omega) \triangleq 2\gamma, \qquad \gamma < 0 \tag{3-65a}$$

and there will be no changes in other equations.

The formulation also includes the $j\omega_n$ supplementary excitation design as a special case. By then, σ equals zero and ω becomes ω_n in these equations.

d. Design an Adequate Damping Magnitude for the Mechanical Mode. Equation (3-47) is still valid. But Eqs. (2-48) and (2-49) must be modified as

follows:

$$D_E = K_C K_2 |G_C|_{s=\sigma+j\omega} |G_E|_{s=\sigma+j\omega} \tag{3-48a}$$

and

$$K_E = \frac{2\zeta_n \omega_n M}{K_2 |G_C|_{s=\sigma+j\omega} |G_E|_{s=\sigma+j\omega}} \tag{3-49a}$$

For the supplementary excitation design, an adequate ζ_n must be chosen. As stated earlier, only when the characteristic equation is in the normalized form can we have a clear idea of the magnitude and degree of damping. Because when the second-order system

$$[Ms^2 + D_E s + \omega_b K_1] \Delta\delta = 0 \tag{3-37a}$$

is normalized, it becomes

$$(s^2 + 2\zeta_n \omega_n s + \omega_n^2) \Delta\delta = 0 \tag{3-39}$$

the solutions of the characteristic equation are

$$s = (-\zeta_n \pm j\sqrt{1 - \zeta_n^2})\omega_n \tag{3-71}$$

which corresponds to

$$s = \sigma \pm j\omega \tag{3-72}$$

Therefore

$$\omega_n = \sqrt{\sigma^2 + \omega^2} \qquad |\zeta_n| = \sigma/\sqrt{\sigma^2 + \omega^2} \tag{3-73}$$

Note that

$$|-\zeta_n \pm j\sqrt{1 - \zeta_n^2}| = 1 \tag{3-74}$$

In other words, the increase of positive damping or the negative real part of an eigenvalue will not change ω_n but will rotate the eigenvalue locus counterclockwise as shown in Fig. 3-9 according to (3-71). Again the ζ_n value may be chosen as 0.1–0.3 per unit for this design.

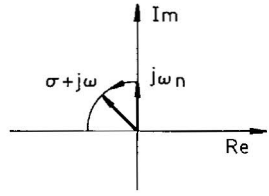

Fig. 3-9 Shift $(\sigma + j\omega)$ counterclockwise.

e. Design a Reset Block for u_E. Same as (3-50).

f. Find the Eigenvalues of the System with and without u_E. An example of the complex-frequency supplementary-excitation design is given in Moussa and Yu [19], although the paper mainly deals with the dynamic interaction between machines and loops. The mechanical mode eigenvalues of machine 1 of $(\sigma + j\omega)$ design and of $j\omega_n$ design are as follows:

Machine 1	Without u_E	Desired shift	$(\sigma \pm j\omega)$ design	$j\omega_n$ design
Mechanical loop	$0.336 \pm j5.13$	$-2.56 \pm j4.42$	$-2.56 \pm j4.42$	$-1.87 \pm j5.13$

While the $(\sigma + j\omega)$ design gives exactly the desired damping, the $j\omega_n$ design does not.

Damping and Synchronizing Torques of the System of Fig. 3-1

Since the damping torque and synchronizing torque are both important to power system stability, they will be accurately calculated. In small oscillations, the synchronizing torque is in phase with $\Delta\delta$ or $-j\,\Delta\omega$, and the damping torque in phase with $\Delta\omega$ or $j\,\Delta\delta$. Therefore, they can be calculated as follows.

Example 3-4. Find the damping torque and synchronizing torque of Fig. 3-1 for the system with supplementary excitation control.

Solution: Being a linear system, the superposition principle applies. There are four components of ΔT_e of Fig. 3-1:

$$\Delta T_e|_{K_1} = K_1\,\Delta\delta$$

$$\Delta T_e|_{K_4} = \frac{K_2K_3K_4(1 + sT_A)}{K_3K_6K_A + (1 + sT'_{do}K_3)(1 + sT_A)}\Delta\delta \tag{3-75a}$$

$$\Delta T_e|_{K_5} = \frac{K_2K_3K_5K_A}{K_3K_6K_A + (1 + sT'_{do}K_3)(1 + sT_A)}\Delta\delta \tag{3-75b}$$

$$\Delta T_e|_{u_E} = \frac{sT}{1 + sT}\,\frac{K_C(1 + sT_1)}{(1 + sT_2)}\,\frac{K_2K_3K_A}{K_3K_6K_A + (1 + sT'_{do}K_3)(1 + sT_A)}\Delta\omega$$

To calculate $\Delta T_e|_{K_4}$, both K_6 and K_A blocks may be considered as the negative feedback; to $\Delta T_e|_{K_5}$, only K_6; and to $\Delta T_e|_{u_E}$, the reset and compensation blocks are in series with the transfer function of $\Delta T_e|_{K_5}$. Let

$$\Delta T_e = \Delta T_e|_{K_1} + \Delta T_e|_{K_4} + \Delta T_e|_{K_5} + \Delta T_e|_{u_E} \tag{3-76a}$$

We now have the synchronizing torque component ΔT_S and the damping torque component ΔT_D as follows:

$$\Delta T_S = \Delta T_e|_{\text{component in phase with } \Delta\delta}$$
$$\Delta T_D = \Delta T_e|_{\text{component in phase with } \Delta\omega} \tag{3-76b}$$

For the calculation, the mechanical mode eigenvalue $\sigma + j\omega$ must be used for s.

Coordination of Power System Stabilizers

To date, the supplementary excitation or PSS design has been based on the one-machine, infinite-bus model. After the installation of PSSs on most machines of a large electric power system, low-frequency oscillations may still occure becuase of the lack of coordination of these stabilizers designed from the one-machine, infinite-bus model. In recent years, progress has been made in coordinated application of power system stabilizers [8] and coordination of power system stabilizers already installed in power systems [9, 10].

In deMello *et al.* [8], a ten-machine system is investigated. Each machine is modeled as a second-order system and an eigenvalue and eigenvector technique is used to find where in the system the power system stabilizers are most needed. For each eigenvalue, there is an eigenvector that has ten components, and the machine corresponding to the largest eigenvector component will need the PSS most. The search begins with the eigenvector corresponding to the eigenvalue with the lowest frequency. The results are in full agreement when each machine is modeled as a fourth-order system [20].

Progress also has been made in coordinating the existing power system stabilizers of multimachine systems [9, 10]. In Gooi *et al.* [10], the stabilizers for a thermal unit, a nuclear unit, and a hydro unit of an operating system are coordinated to optimize their performance by adjusting the PSS parameters using a multimachine power system model and an iterative procedure. The multimachine model is an extension of Fig. 3-1; each of $K_1, K_2, \ldots, K_6$ parameters becomes K_{1ij}, K_{2ij}, etc. Derivation of the multimachine model will be given in Chapter 6.

The ultimate solution of the stabilization of low-frequency oscillations of a multimachine system should be a multimode stabilizer design based on the multimachine model.

Summary of Section 3-4

This section has reviewed some important historical developments of PSS design including the Peace River Project of B.C. Hydro, the Moose River

Project of Ontario Hydro, the first interconnection of the Pacific Power system at Glenn Canyon, and a systematic analysis by deMello and Concordia. A complex frequency design procedure of the supplementary excitation was then proposed, and damping and synchronizing torque calculation procedure given. Finally, the coordinated application of stabilizers to a multimachine system and the coordination of existing stabilizers of power systems were introduced. Since the PSS design so far is based on a one-machine, infinite-bus model, a procedure for multimachine PSS design should be developed in the future.

3-5 IMPROVING SYSTEM DAMPING WITH GOVERNOR CONTROL

This section will introduce a supplementary governor control to enhance the damping of low-frequency oscillations. It was tried [21] but discontinued since the development of supplementary excitation control. As in the case of fast valving, which was developed 50 years ago [23] and has gained renewed interest in recent years, we shall not entirely rule out the possibility of redevelopment of supplementary governor control in the future.

First Try at Grand Coulee

When an interconnection of the Northwest and Southwest Power Pools of North America was tried at Grand Coulee, a supplementary governor control was designed for a large hydrogenerating unit to damp the low-frequency oscillations of the entire system [21]. The unit was situated at a strategic point, the control was effective, but the hard-working governor oil pumps developed serious overheating problems due to prolonged operation. An interesting point that should be noted was that the dashpot transfer function was removed from the supplementary governor control design. Unaware of the earlier development [21], another supplementary governor control was designed later, independently, in Moussa and Yu [22].

The Effect of a Governor of a Hydroplant on System Damping

Consider again the transfer functions of Hovey's hydrogovenor of Fig. 2-13. For typical data of hydropower plants given in Ramey and Skooglund [32] of Chapter 2, the $\Delta T_m(j\omega_n)$ locus of Hovey's system with a dashpot is shown in Fig. 3-10a, and without the dashpot in Fig. 3-10b [22]. Since a supplementary mechanical damping torque ΔT_m will be in phase with $-\Delta\omega$, a governor without dashpot should be used for the control design.

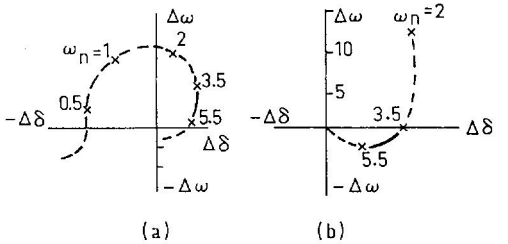

Fig. 3-10 $\Delta T_m(j\omega_m)$ loci of a hydroplant with and without dashpot.

A Supplementary Governor Control Design

Our purpose is to design a supplementary mechanical damping in phase with $-\Delta\omega$ according to Fig. 3-7 and the first equation of (3-36a),

$$\Delta T_M = -D_M \Delta\omega \tag{3-36a}$$

Let the hydraulic power transfer function be examined first. Since the water time constant T_w is in the order of seconds and the mechanical oscillating frequency is in the order of radians per second, the last block of Fig. 2-13 becomes

$$\frac{\Delta T_m}{g} = \left.\frac{1 - sT_w}{1 + 0.5sT_w}\right|_{s=j\omega n} \simeq -2 \tag{3-77}$$

The minus sign is exactly what is desired for the supplementary governor control design.

With the dashpot transfer function removed from Fig. 2-13, the design procedure is very simple; we shall have one compensation block for the governor servo, another for the actuator servo, an adequate stabilizer gain, and a reset block. Therefore, a general form of the supplementary governor control for a hydro plant may be approximated by

$$u_G = K_M \frac{sT}{1 + sT} \frac{1 + sT_a/\sigma}{1 + sT_2} \frac{1 + sT_g}{1 + sT_2} \Delta\omega \tag{3-78}$$

A numerical example is given in Moussa and Yu [22],

$$u_G = \frac{2.2s}{1 + 3s} \frac{1 + 0.4s}{1 + 0.05s} \frac{1 + 0.5s}{1 + 0.05s} \Delta\omega$$

The $\Delta T_M(j\omega_n)$ locus of the system with the supplementary governor control is shown as Fig. 3-11.

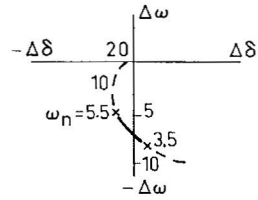

Fig. 3-11 $\Delta T_m(j\omega_m)$ locus of system with supplementary governor control.

The mechanical mode eigenvalues of the system for different electric power outputs are

P_{e0}(pu)	0.30	1.0	1.2
With u_G	$-0.536 \pm j5.19$	$-2.23 \pm j4.54$	$-3.85 \pm j4.10$
Without	$-0.049 \pm j5.14$	$0.238 \pm j4.60$	$0.590 \pm j3.57$

For details, see Moussa and Yu [22].

Summary of Section 5-3

In this brief section the supplementary governor control of low-frequency oscillations of a hydroelectric power system and a simple design procedure are presented. Although it is currently not the practice, we should not rule out the possible development of such a control scheme in the future, especially for long-term dynamics studies.

3-6 SUMMARY

In the first two sections of this chapter, a one-machine, infinite-bus electric power system for supplementary excitation control design is derived, and methods to find the initial currents, voltages, and torque angles are given. The model is derived for the low-frequency oscillation studies. Following that, the principle, procedure, and example of supplementary excitation control design are presented in Section 3-3, and some important historical developments are reviewed and current developments introduced in Section 3-4. Finally, a supplementary governor control to improve the damping of a hydroelectric power system is presented in Section 3-5.

The main concern of this chapter is to increase the damping of the mechanical mode low-frequency oscillations of a one-machine, infinite-bus system, and the basic concept of the supplementary excitation or governor

control design is the phase compensation of the control signal input. There are, however, a general class of power system dynamic problems that involves many oscillating modes and many machines; and both the damping and the synchronizing torque are of great concern. These problems and control design techniques will be presented in the subsequent chapters.

Problems

3-1 Find the initial steady-state current and voltage in d and q components and the torque angle of a synchronous generator in a one-machine, infinite-bus system with generator terminal voltage $v_t = 1.02$ pu, power output $P_e = 0.9$ pu, and infinite-bus voltage $v_o = 1.06$ pu. The system parameters corresponding to Fig. 3-2 are $x_d = 1.0$, $x_q = 0.6$, $x'_d = 0.2$, $Z = 0.2 + j1.0$, $Y = 0$ pu.

3-2 (a) Find the $K_1, K_2, \ldots, K_6$ constants of Fig. 3-1 for the system of Problem 3-1;

(b) Find the eigenvalues of the system without a supplementary control. Assume that $T'_{do} = 7.76$ s, $K_A = 50$, $T_A = 0.05$ s.

3-3 (a) Design a supplementary excitation control for the aforementioned system using $\Delta\omega$ as the control input and ω_n for the design, and assuming one compensation block with $T_2 = 0.1$ s, one reset block with $T = 5$ s, and a damping coefficient $\zeta_n = 0.3$ pu;

(b) Find eigenvalues of the system with the supplementary control;

(c) Find the damping and synchronizing torque of the system with and without the control.

3-4 If a governor transfer function as shown in Fig. 3-4P is included in the low-order system model, what will become Fig. 3-1 and the state equation (2-56)? P_m approximately equals T_m when ω is per unit.

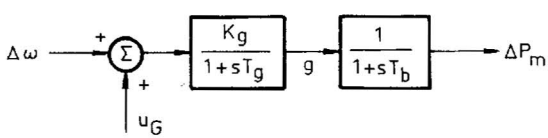

Fig. 3-4P A two-time constant governor.

References

[1] H. M. Ellis, J. E. Hardy, A. L. Blythe, and J. W. Skooglund, Dynamic stability of the Peace River transmission system. *IEEE Trans. Power Appar. Syst.* 586–600, June (1966).

[2] F. R. Schleif and J. H. White, Damping for the northwest-southwest tieline oscillations—an analog study. *IEEE Trans. Power Appar. Syst.* 1239–1247, Dec. (1966).

[3] C. W. Hanson, C. J. Goodwin, and P. L. Dandeno, Influence of excitation and speed control parameters in stabilizing intersystem oscillations. *IEEE Trans. Power Appar. Syst.* 1306–1313, May (1968).

[4] T. R. Foord, Glasgow University Scotland, private communication, June, 1974.

[5] V. Arcidiacono, E. Ferrari, R. Marconato, T. Brikic, M. Niksic, and M. Kajari, Studies and experimental results on electromechanical oscillation damping in Yugoslav power system. *PES Summ. Meet., 1975* IEEE Pap. A 75 420-0 (1975).

[6] A. Arciciacono, E. Ferrari, and F. Saccomanno, Studies on damping of electromechanical oscillations in multimachine system with longitudinal structure. *IEEE Trans. Power Appar. Syst.* 450–460, March/Apr. (1976).

[7] Kyushu Electric Power Co., Japan, private communication with power engineers, Oct. 1977.

[8] F. P. deMello, P. J. Nolan, T. F. Laskowski, and J. M. Undrill, Coordinated application of stabilizers in multimachine power systems. *IEEE Trans. Power Appar. Syst.* 892–901 May/June (1980).

[9] R. J. Fleming, M. A. Mohan, and K. Parvatisam, Selection of parameters of stabilizers in multimachine power systems. *IEEE Trans. Power Appar. Syst.* 2329–2333, May (1981).

[10] H. B. Gooi, E. F. Hill, M. A. Mobarak, D. H. Thorne, and T. H. Lee, Coordinated multi-machine stabilizer settings without eigenvalue drift. *IEEE Trans. Power Appar. Syst.* 3879–3887, Aug. (1981).

[11] F. P. deMello and C. Concordia, Concepts of synchronous machine stability as affected by excitation control. *IEEE Trans. Power Appar. Syst.* 316–329, April (1969).

[12] W. G. Heffron and R. A. Phillips, Effect of modern amplidyne voltage regulator on underexcited operation of large turbine generators. *Trans. Am. Inst. Electr. Eng., Part 3* **71,** 692–697 (1952).

[13] Yao-nan Yu and C. Siggers, Stabilization and optimal control signals for a power system. *IEEE Trans. Power Appar. Syst.* 1469–1481, July/Aug. (1971).

[14] Yao-nan Yu and K. Vongsuriya, Steady-state stability limits of a regulated synchronous machine connected to an infinite system. *IEEE Trans. Power Appar. Syst.* 759–767, July (1966).

[15] R. T. Byerly and E. W. Kimbark, eds., "Stability of Large Electric Power Systems." IEEE Press Book, IEEE, New York, 1974.

[16] R. M. Schier and A. L. Blythe, Field tests of dynamic stability using a stabilizing signal and computer program verification. *IEEE Trans. Power Appar. Syst.* 315–322, Feb. (1968).

[17] P. L. Dandeno, A. N. Karas, K. R. McClymont, and W. Watson, Effect of high-speed rectifier excitation systems on generator stability limits. *IEEE Trans. Power Appar. Syst.* 190–201, Jan. (1968).

[18] F. R. Schleif, H. D. Hunkins, G. E. Martin, and E. E. Hattan, Excitation control to improve powerline stability. *IEEE Trans. Power Appar. Syst.* 1426–1434, June (1968).

[19] H. A. M. Moussa and Yao-nan Yu, Dynamic interaction of multi-machine system and excitation control. *IEEE Trans. Power Appar. Syst.* 1150–1158, July/Aug. (1974).

[20] Z. Weng, Selection of optimum sites in large electric power systems for PSS installation using eigenvector analysis. *J. Electr. Eng. (China)* (1982).

[21] F. R. Schleif, G. E. Martin, and R. R. Angell, Damping of system oscillations with hydrogenerator unit. *IEEE Trans. Power Appar. Syst.* 438–442, April (1967).

[22] H. A. M. Moussa and Yao-nan Yu. Improving power system damping through supplementary governor control. *PES Summ. Meet., 1972* IEEE Pap. C 72 470-3 (1972).

[23] R. H. Park, Fast turbine valving. *IEEE Trans. Power Appar. Syst.* 1065–1073, May/June (1973).

Chapter 4 Linear Optimal Stabilization of Electric Power Systems

This chapter will develop a general linear stabilizing technique for electric power systems, which is not only applicable to the one-machine, low-frequency, mechanical-mode oscillations, but also applicable to multimachine, multimode high- and low-frequency oscillations. One example is the optimal stabilization of the low-frequency oscillations of a multimachine system, and the other is the effective stabilization of the subsynchronous torsional oscillations of several possible modes of the steam turbines, generator, and exciter mass-spring system.

The stabilizing technique aforementioned was originally developed by control engineers and is known as linear optimal control. The system to be controlled is described by linear state equations and the control is designed by minimizing a function of both state deviations and control effort. When the technique is applied to electric power systems, however, further developments are necessary, which will be presented in this chapter. For conciseness, some abbreviations will be adopted: LOC for linear optimal control and LOS for linear optimal stabilization.

4-1 PRINCIPLE OF LINEAR OPTIMAL CONTROL (LOC)

The LOC of electric power systems presented in this chapter is derived from the minimization of the state variable deviations and control effort at the same time. The system state equations, or the state variable equations, must be sought first. A performance index of the system is then chosen, which shall be a function of both the state deviations and the control effort. Finally, the state equations are appended to the performance index by a co-state

variable vector to find the linear optimal control (LOC). The co-state variable vector in modern control theory corresponds to the Lagrange multipliers in classic mechanics.

The System State Equations

Since modern control theory and computation technique are all developed with the state equations, a proper model should always be chosen and the state equations for a system formulated before an optimization technique is applied to find the optimal control.

After a proper model is chosen, the model for the system without control is first described by a set of nonlinear differential equations written in the form of

$$\dot{x} = f(x) \tag{4-1}$$

where x is the state variable vector. For instance, the state variable vector of (2-56) is

$$x = [\omega, \delta, \psi_d, \psi_F, \psi_D, \psi_Q]^T \tag{4-2}$$

For the LOC design, the nonlinear state equation of the system without control must be linearized with respect to an initial steady state represented by ω_0, δ_0, etc. Including control, the linearized system state equation becomes

$$\Delta\dot{x} = A\,\Delta x + Bu \tag{4-3}$$

For a power system with both excitation and governor control, the control vector becomes

$$u = [u_E, u_G]^T \tag{4-4}$$

For conciseness, however, Eq. (4-3) will be written hereafter simply as

$$\dot{x} = Ax + Bu \tag{4-5}$$

In (4-5), x is called the state vector, u the control vector, A the system matrix, and B the control matrix. Although A is always a square matrix, B is usually a rectangular matrix and the number of columns of the B matrix depends on how many feedback loops are used for the design.

There are generally two types of linear differential equations: equations with time-varying coefficients such as the sine and cosine functions associated with inductances when synchronous machines are described in a-b-c phase coordinates; and equations with time-invariant coefficients or constant coefficients such as the inductances when the synchronous machines are

described in Park's d-q coordinates. Since Park's equations are used for most power system dynamic studies, our main concern is with the linear differential equations with constant coefficients.

The Performance Index

For the LOC design of an electric power system, a performance index of the quadratic form is usually chosen:

$$J = \frac{1}{2}\int_0^\infty [x^T Q x + u^T R u]\, dt \tag{4-6}$$

where Q is the weighting matrix of the state variable deviations and R that of the control effort. In most cases, both Q and R are chosen as diagonal matrices. Therefore, all terms in the brackets have the form of energy. For instance, $\frac{1}{2}q_{\Delta\omega}\cdot\Delta\omega^2$ is the kinetic energy of the rotating system, $\frac{1}{2}q_{\Delta\delta}\cdot\Delta\delta^2$ the potential energy of the system, and so on. In classical mechanics, they are called the generalized energy functions [1, 2].

The performance index is also called the performance function, the cost function, or the cost index by different authors, and the choice of Q elements, as found from power system dynamic studies, depends on many factors, for instance, on the units chosen for the individual state variables. Whether the unit of the speed $\Delta\omega$ is in rad per second or in per unit of value certainly makes the values of $\Delta\omega$, and hence the choice of $q_{\Delta\omega}$, quite different.

The Linear Optimal Control (LOC)

The LOC is derived from the minimization of the performance index as described by Eq. (4-6) in conjunction with the state equation (4-5). Some theories are involved that can be found in control literature [3–5]. The major step of the minimization is to append (4-5) to (4-6) to form a Hamiltonian generalized-energy function,

$$H \triangleq \tfrac{1}{2}[x^T Q x + u^T R u] + p^T[Ax + Bu] \tag{4-7}$$

The unknown vector p corresponds to the Lagrange multipliers in classical mechanics and is called the co-state vector in modern control theory. Note that the Hamiltonian energy function is a scalar, and there will be no effect on results whether or not the RHS of (4-7) is transposed for differentiation.

To find the LOC, the following condition must be satisfied.

$$\partial H/\partial u = 0 \tag{4-8}$$

Carrying out the differentiation, we shall have

$$Ru + B^{\mathrm{T}}p = 0 \tag{4-9a}$$

and the control law

$$u = -R^{-1}B^{\mathrm{T}}p \tag{4-9b}$$

Note that the term $\frac{1}{2}u^{\mathrm{T}}Ru$ must be differentiated twice, once as it is and the second time as its transpose. Note also that the term $p^{\mathrm{T}}Bu$ must be transposed before it is differentiated with respect to u. The co-state vector p remains to be found.

State and Co-state Equations

In classic mechanics, the Hamiltonian H is generally related to the Lagrangian L as follows

$$H(p, x, t) = \dot{x}^{\mathrm{T}}p - L(x, \dot{x}, t) \tag{4-10}$$

where H and L are both functions of time.

Let us find the derivatives of both sides of (4-10) separately. From the LHS of (4-10), we have

$$dH = dp^{\mathrm{T}}\frac{\partial H}{\partial p} + dx^{\mathrm{T}}\frac{\partial H}{\partial x} + dt\frac{\partial H}{\partial t} \tag{4-11}$$

From the RHS, we have

$$dH = (d\dot{x}^{\mathrm{T}}p + dp^{\mathrm{T}}\dot{x}) - \left(dx^{\mathrm{T}}\frac{\partial L}{\partial x} + d\dot{x}^{\mathrm{T}}\frac{\partial L}{\partial \dot{x}} + dt\frac{\partial L}{\partial t}\right) \tag{4-12}$$

Comparison of the last term of both equations gives

$$\frac{\partial H}{\partial t} = -\frac{\partial L}{\partial t} \tag{4-13}$$

which is not required in our studies as we are dealing with the time-invariant power system state equations.

To continue the derivation, the Lagrange–Euler equation of the conservative system in classic mechanics [1, 2] may be applied,

$$\frac{\partial L}{dx} = \frac{d}{dt}\left(\frac{\partial L}{\partial \dot{x}}\right) \tag{4-14}$$

Since in forming the Hamiltonian H of (4-7) we have introduced a new un-

known p, we may also make a new assumption that

$$p \triangleq \frac{\partial L}{\partial \dot{x}} \tag{4-15}$$

resulting in the cancellation of the first and the fourth terms of the RHS of (4-12). Differentiation of p and application of the Lagrange–Euler equations yields

$$\dot{p} = \frac{d}{dt}\left(\frac{\partial L}{\partial \dot{x}}\right) = \frac{\partial L}{\partial x} \tag{4-16}$$

Comparison of the dx^{T} terms on the RHS of both (4-11) and (4-12) gives

$$\dot{p} = -\frac{\partial H}{\partial x} \tag{4-17a}$$

Finally, direct comparison of the dp^{T} terms of both equations results in

$$\dot{x} = \frac{\partial H}{\partial p} \tag{4-17b}$$

Equations (4-17b) and (4-17a) constitute the state and co-state equations of the system.

We shall apply these results to (4-7). For conciseness, let

$$S \triangleq BR^{-1}B^{\mathrm{T}} \tag{4-18}$$

From (4-9) and (4-18), the control term of Eq. (4-5) becomes

$$Bu = -BR^{-1}B^{\mathrm{T}}p = -Sp \tag{4-19}$$

Partial differentiation of H of Eq. (4-7) with respect to x and p, respectively, gives

$$\begin{aligned} \dot{x} &= \frac{\partial H}{\partial p} = Ax + Bu = Ax - Sp \\ \dot{p} &= -\frac{\partial H}{\partial x} = -(Qx + A^{\mathrm{T}}p) \end{aligned} \tag{4-20}$$

There is no surprise that we have obtained the same state equations (4-5) in (4-20) from the new formulation, but we also have obtained the co-state equation in (4-20), and they may be written together as

$$\begin{bmatrix} \dot{x} \\ \dot{p} \end{bmatrix} = \begin{bmatrix} A & -S \\ -Q & -A^{\mathrm{T}} \end{bmatrix} \begin{bmatrix} x \\ p \end{bmatrix} \tag{4-21}$$

The last equations are very useful in LOC design.

Summary of Section 4-1

In this section, the principle of linear optimal control is presented and the control law derived. It is based on the concept of minimization of the state variable variations and the control effort at the same time. To find the control, a performance index of the quadratic form is chosen, to which the state equations are appended to form a Hamiltonian by Lagrange multipliers or a co-state vector, and the Hamiltonian is minimized. The state equations are then rederived and the co-state equations are found from the Hamiltonian. Finally, the state and co-state equations are written together for LOC design.

4-2 SOLUTION OF THE RICCATI MATRIX EQUATION

To find the LOC, it is necessary to find the solution of the co-state variable vector p. Since we are dealing with the linear state space, the co-state variable vector p can be related to the state variable vector x linearly by

$$p = Kx \tag{4-22}$$

where K is called the Riccati matrix, which is a square matrix. Therefore, the solution of p can be found if K is found.

The Riccati Matrix Equation

Consider the general case that K is also a function of time. The time derivative of p of (4-22) becomes

$$\dot{p} = \dot{K}x + K\dot{x} \tag{4-23}$$

Note that each term of (4-23) is a column matrix, and the results from the differentiation also must be written as such. Substitution of $\dot{x}$ and $\dot{p}$ of (4-21) into (4-23) and replacing p by Kx gives

$$-(Q + A^{\mathrm{T}}K)x = \dot{K}x + (KA - KSK)x$$

or

$$KA + A^{\mathrm{T}}K - KSK + Q = -\dot{K} \tag{4-24}$$

which is the Riccati matrix equation [3, 4]. Since the transpose of the entire Riccati matrix equation results in

$$A^{\mathrm{T}}K^{\mathrm{T}} + K^{\mathrm{T}}A - K^{\mathrm{T}}SK^{\mathrm{T}} + Q = -\dot{K}^{\mathrm{T}} \tag{4-25}$$

In other words, K^T also satisfies Eq. (4-24), K is a symmetric matrix, and

$$K^T = K \tag{4-26}$$

Note that Q and R are symmetric matrices. So is S, since

$$S^T = (BR^{-1}B^T)^T = BR^{-1}B^T = S \tag{4-27}$$

When synchronous machines of a power system are described in Park's d-q coordinates, the coefficients of the system equations are all time invariant. Therefore, we have a time-invariant system, and hence

$$KA + A^TK - KSK + Q = 0, \qquad K = \text{const} \tag{4-28}$$

Iterative Solution of *K*

Two methods of solving the Riccati matrix equation (4-28) for K will be presented in this book. Consider an iterative solution first. Let (4-28) be written

$$K(A - SK) + (A - SK)^TK + (Q + KSK) = 0$$

or

$$KA_c + A_c^TK + Q' = 0 \tag{4-29}$$

where

$$A_c \triangleq A - SK, \qquad Q' = Q + KSK \tag{4-29a}$$

Note that A_c represents the controlled system matrix, since

$$\dot{x} = Ax + Bu = Ax - Sp = (A - SK)x \tag{4-29b}$$

according to (4-20) and (4-22).

The form of (4-29) lends itself to an iterative solution,

$$K^{(j)}A_c^{(j)} + A_c^{T(j)}K^{(j)} + Q'^{(j)} = 0$$

where

$$A_c^{(j)} = A - SK^{(j-1)}, \qquad Q'^{(j)} = Q + K^{(j-1)}SK^{(j-1)} \tag{4-30}$$

But the system corresponding to $A_c^{(1)}$ must be already stable according to Puri and Gruver [6]. In other words, all eigenvalues of $A_c^{(1)}$ must already be on the LHS of the complex variable plane. Wedman [7] developed an eigenvalue shift technique using the sensitivities of system eigenvalues with respect to the K elements to obtain an $A_c^{(1)}$. Siggers [8] came up with a still simpler method by assuming an artificial large mechanical damping to start the computation, but gradually removing it when the convergence was underway.

Closed Form Solution of K

The Riccati matrix K also can be calculated from the eigenvectors of the state and co-state system matrix. Let the matrix of (4-21) be

$$[M] \triangleq \begin{bmatrix} A & -S \\ -Q & -A^{\mathrm{T}} \end{bmatrix} \tag{4-31}$$

which is a $2n$ by $2n$ matrix for an nth-order system. The eigenvalues of this matrix on the complex variable plane are so distributed that they are symmetrical not only with respect to the real axis but also to the imaginary axis [9]. Let the $2n$ eigenvalues be written as a diagonal matrix

$$[\Lambda] \triangleq \begin{bmatrix} \Lambda_- & \\ & \Lambda_+ \end{bmatrix}, \qquad [\Lambda_-] = -[\Lambda_+] \tag{4-32}$$

where $[\Lambda_-]$ represents the eigenvalues on the LHS and $[\Lambda_+]$ those on the RHS of the complex variable plane, respectively.

Since for each eigenvalue, a corresponding eigenvector can be found from

$$[M][x_i] = [x_i]\lambda_i, \qquad i = 1, \ldots, 2n \tag{4-33}$$

where x_i is a column matrix and λ_i a scalar, the $2n$ eigenvector equations may be written in matrix form [10] as

$$[M][X] = [X][\Lambda] \tag{4-34}$$

Here $[\Lambda]$ is a diagonal eigenvalue matrix with $2n$ elements, and $[X]$ is a $2n$ column eigenvector matrix with $2n$ elements per column.

Let the eigenvector matrix be partitioned into four n by n matrices such that

$$[X] = \begin{bmatrix} X_{\mathrm{I}} & X_{\mathrm{III}} \\ X_{\mathrm{II}} & X_{\mathrm{IV}} \end{bmatrix} \tag{4-35}$$

where the first column partitioned matrices corresponds to $[\Lambda_-]$ and the second column to $[\Lambda_+]$. It can be shown that $[X_{\mathrm{II}}][X_{\mathrm{I}}]^{-1}$ satisfies the Riccati matrix equation (4-28).

Example 4-1. Show that $[X_{\mathrm{II}}][X_{\mathrm{I}}]^{-1}$ satisfies the Riccati matrix equation (4-28).

Solution: Let Eq. (4-34) be written in the partitioned matrix form according to (4-35) and (4-32). We shall have

$$\begin{bmatrix} A & -S \\ -Q & -A^{\mathrm{T}} \end{bmatrix} \begin{bmatrix} X_{\mathrm{I}} & X_{\mathrm{III}} \\ X_{\mathrm{II}} & X_{\mathrm{IV}} \end{bmatrix} = \begin{bmatrix} X_{\mathrm{I}} & X_{\mathrm{III}} \\ X_{\mathrm{II}} & X_{\mathrm{IV}} \end{bmatrix} \begin{bmatrix} \Lambda_- & \\ & \Lambda_+ \end{bmatrix} \tag{4-36}$$

Equation (4-36) can be expanded into four matrix equations. Considering these associated with $[\Lambda_-]$ alone, we shall have

$$AX_{\mathrm{I}} - SX_{\mathrm{II}} = X_{\mathrm{I}}\Lambda_- \tag{4-37a}$$

$$-QX_{\mathrm{I}} - A^{\mathrm{T}}X_{\mathrm{II}} = X_{\mathrm{II}}\Lambda_- \tag{4-37b}$$

Solving for Λ_- from (4-37a), substituting the result into (4-37b), and post-multiplying both sides by X_{I}^{-1} gives

$$-Q - A^{\mathrm{T}}(X_{\mathrm{II}}X_{\mathrm{I}}^{-1}) = X_{\mathrm{II}}[X_{\mathrm{I}}^{-1}(AX_{\mathrm{I}} - SX_{\mathrm{II}})]X_{\mathrm{I}}^{-1}$$

or

$$(X_{\mathrm{II}}X_{\mathrm{I}}^{-1})A + A^{\mathrm{T}}(X_{\mathrm{II}}X_{\mathrm{I}}^{-1}) - (X_{\mathrm{II}}X_{\mathrm{I}}^{-1})S(X_{\mathrm{II}}X_{\mathrm{I}}^{-1}) + Q = 0 \tag{4-38}$$

Since $(X_{\mathrm{II}}X_{\mathrm{I}}^{-1})$ satisfies the Riccati matrix equation (4-28), it is the solution of the Riccati matrix K of Eq. (4-28):

$$K = X_{\mathrm{II}}X_{\mathrm{I}}^{-1} \tag{4-39}$$

The linear optimal control now becomes

$$Bu = -Sp = -SKx = -S(X_{\mathrm{II}}X_{\mathrm{I}}^{-1})x \tag{4-40}$$

Note that for an nth-order electric power system, K, S, X_{II}, and X_{I} are all n by n matrices.

Summary of Section 4-2

In this section the Riccati matrix equation is derived, and two methods of solving the matrix equation are given: the iterative solution, which was used in the early development of linear optimal stabilizer design for power systems, and the closed-form solution in terms of eigenvectors, which has been used ever since [11, 12].

There are still some problems of the LOC design that must be addressed, for instance, the selection of the weighting matrices Q and R, the design of an LOC over a wide range of power system operating conditions, and so on. Before applying the LOC design technique to high-order electric power systems, let us employ a simple numerical example to demonstrate the effectiveness of LOC in the next section.

4-3 LOC DESIGN OF A SECOND-ORDER SYSTEM

For the LOC design of an electric power system, an adequate model for synchronous generator and control loop(s) must be chosen, which is usually

of a high order and invariably involves digital computation. To demonstrate the effectiveness of LOC, we shall briefly present a second-order system LOC design.

Example 4.2. Consider the mechanical loop of Fig. 3-1 alone and design an LOC for the system using the mechanical torque signal as the control input as shown in Fig. 4-1. The system data are $M = 10$ s, $D = 0$, $K_1 = 0.5$, $f = 60$ Hz.

(a) Find the eigenvalues of the system without control.

(b) Design an LOC for the system and find the eigenvalues of the system with control.

Solution: (a) The state equations of the system without control may be written

$$\begin{bmatrix} \Delta\dot{\delta} \\ \Delta\dot{\omega} \end{bmatrix} = \begin{bmatrix} 0 & 377 \\ -K_1/M & D/M \end{bmatrix} \begin{bmatrix} \Delta\delta \\ \Delta\omega \end{bmatrix}$$

For the data given, the characteristic equation of the system becomes

$$\begin{vmatrix} -\lambda & 377 \\ -0.05 & -\lambda \end{vmatrix} = 0, \qquad \lambda^2 + 18.85 = 0$$

and the eigenvalues are

$$\lambda = \pm j4.342 \quad \text{elec. rad/s}$$

which represents an oscillatory system since there is no damping.

(b) The system with control may be written

$$\begin{bmatrix} \Delta\dot{\delta} \\ \Delta\dot{\omega} \end{bmatrix} = \begin{bmatrix} 0 & 377 \\ -K_1/M & D/M \end{bmatrix} \begin{bmatrix} \Delta\delta \\ \Delta\omega \end{bmatrix} + \begin{bmatrix} 0 \\ 1/M \end{bmatrix} u_T$$

For the data given,

$$\begin{bmatrix} \Delta\dot{\delta} \\ \Delta\dot{\omega} \end{bmatrix} = \begin{bmatrix} 0 & 377 \\ -0.05 & 0 \end{bmatrix} \begin{bmatrix} \Delta\delta \\ \Delta\omega \end{bmatrix} + \begin{bmatrix} 0 \\ 0.1 \end{bmatrix} u_T$$

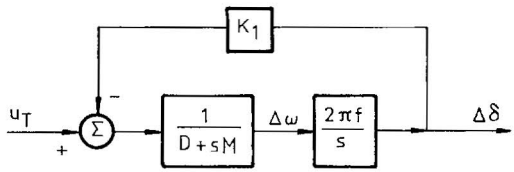

Fig. 4-1 A second-order electric power system.

and the system and control matrices become

$$A = \begin{bmatrix} 0 & 377 \\ -0.05 & 0 \end{bmatrix}, \qquad B = \begin{bmatrix} 0 \\ 0.1 \end{bmatrix}$$

For the LOC design, let

$$Q = \begin{bmatrix} 0.25 & 0 \\ 0 & 1 \end{bmatrix}, \qquad R = 1$$

which means that, in selecting the Q matrix, the speed deviation is weighted four times that of the angle deviation. There is a good reason for that, as it is the acceleration that causes the speed deviation, which in turn causes the angle deviation.

Having decided B and R, R being unity, we shall have

$$S = BR^{-1}B^{\mathrm{T}} = \begin{bmatrix} 0 \\ 0.1 \end{bmatrix}[0 \quad 0.1] = \begin{bmatrix} 0 & 0 \\ 0 & 0.01 \end{bmatrix}$$

Since K is a symmetric matrix, we may write

$$SK = \begin{bmatrix} 0 & 0 \\ 0 & 0.01 \end{bmatrix}\begin{bmatrix} k_1 & k_2 \\ k_2 & k_3 \end{bmatrix} = \begin{bmatrix} 0 & 0 \\ 0.01k_2 & 0.01k_3 \end{bmatrix}$$

and we found that only k_2 and k_3, the second row of K elements, are required for the LOC design. Applying (4-28), we have

$$\begin{bmatrix} k_1 & k_2 \\ k_2 & k_3 \end{bmatrix}\begin{bmatrix} 0 & 377 \\ -0.05 & 0 \end{bmatrix} + \begin{bmatrix} 0 & -0.05 \\ 377 & 0 \end{bmatrix}\begin{bmatrix} k_1 & k_2 \\ k_2 & k_3 \end{bmatrix} - \begin{bmatrix} k_1 & k_2 \\ k_2 & k_3 \end{bmatrix}\begin{bmatrix} 0 & 0 \\ 0 & 0.01 \end{bmatrix}\begin{bmatrix} k_1 & k_2 \\ k_2 & k_3 \end{bmatrix} + \begin{bmatrix} 0.25 & 0 \\ 0 & 1 \end{bmatrix} = 0$$

From the first column and the first row we have

$$k_2^2 + 10k_2 - 25 = 0, \qquad k_2 = 2.071 \text{ or } -12.07$$

and from the second column and the second row we have

$$0.01k_3^2 + 754k_2 + 1 = 0, \qquad k_3 = \pm\sqrt{1 + 754k_2}$$

Since the state variables and the co-state variables are co-related by the Riccati matrix K linearly in the state space, K elements must be real. Therefore, k_2 equals -12.07 must be rejected because it leads to an imaginary k_3. Next, the negative k_3 solution also must be rejected because it leads to an unstable system. The final solutions of k_2 and k_3 are

$$k_2 = 2.071, \qquad k_3 = 395.3$$

and the LOC becomes

$$Bu_T = -SKx = \begin{bmatrix} 0 & 0 \\ 0.02071 & 3.953 \end{bmatrix} \begin{bmatrix} \Delta\delta \\ \Delta\omega \end{bmatrix}$$

The eigenvalues of the controlled system are generally found from

$$|[A - SK] - I| = 0$$

where I is an identity matrix. Therefore we have

$$\begin{vmatrix} -\lambda & 377 \\ -0.707 & -\lambda - 3.953 \end{vmatrix} = 0$$

or

$$\lambda^2 + 3.953\lambda + 26.65 = 0$$

The eigenvalues of the controlled system are

$$\lambda = -1.9765 \pm j4.769$$

and the damping factor

$$\zeta_n = \text{Re}\,\lambda/|\lambda| = -0.383$$

which characterizes a fairly stable system.

Summary of Section 4-3

To demonstrate the effectiveness of LOC, a second-order electric power system is chosen for the control design. The initially oscillatory system is well stabilized by the LOC. Although the power system in the example is simplified, the effectiveness of LOC is convincingly demonstrated.

4-4 EARLY EXPERIENCE WITH LOC DESIGN

When the principle of LOC was first applied to a power system, the main difficulties in design were the solution of Riccati matrix K and the selection of the weighting matrices Q and R. The iterative process of solving K was improved [7, 8] and the eigenvector solution developed (Example 4-1 and [9]). At that time, no example of high-order LOC design could be found in control literature, and unit matrices were chosen for Q and R.

The first application of LOC to power systems was to design a stabilizer for a hydroelectric power plant [13].

Modeling a Hydroelectric Power System

For the linear optimal stabilizer (LOS) design, the system was modeled as a one-machine, infinite-bus system, with only one major generating plant left and all other plants being replaced by equivalent impedances with negative resistances. The synchronous generator was modeled as a third-order system, the exciter and voltage regulator as a second-order system, and the governor and hydraulic power as a third-order system, and the transmission system was described by algebraic equations. It was readily found that although the dashpot of a governor was useful to improve the governor performance itself, it has a tendency to prolong system oscillations following a disturbance; it was removed from the governor model for the design.

The Selection of the Weighting Matrix Q

Figure 4-2 shows the swing curve of the hydroelectric power system without any supplementary control. It was assumed that there was a large angular swing but other state deviations were zero. This could happen after a severe fault occurred to a system. The system was very oscillatory and would take a long time to reach the steady state.

To design an LOC to improve the stability of the system, two Q matrices were chosen: one as a diagonal matrix with all unit elements

$$Q = \text{DIAG}[1, 1, 1, 1, 1, 1, 1, 1]$$

and the other also as a diagonal matrix but with $q_{\Delta\omega}$ and $q_{\Delta\delta}$ weighted ten times larger than the other state variables

$$Q = \text{DIAG}[10, 10, 1, 1, 1, 1, 1, 1]$$

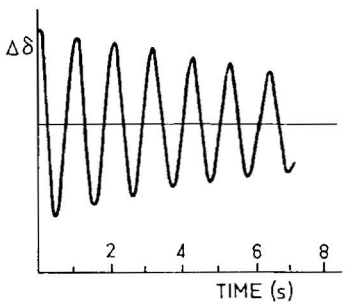

Fig. 4-2 Swing curve of the system without any supplementary control.

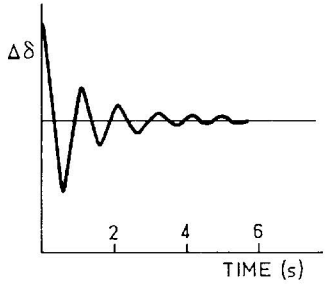

Fig. 4-3 Swing curve of the system with LOC $Q = \text{DIAG}[1, 1, 1, 1, 1, 1, 1, 1]$.

Nonlinear Simulation Test

With the LOC designed, the system was given a nonlinear simulation test, by which the system was described in detail by high-order nonlinear differential equations. Many nonlinearities could be included, but the most important ones were the ceiling voltage of the excitation system and the speed and opening limits of the governor. Other nonlinearities are the product of variables such as the torque components $i_d\psi_q$ and $i_q\psi_d$ and the speed voltages $\omega\psi_d$ and $\omega\psi_q$. The saturation of the magnetic circuit was not considered in this study.

Only the nonlinear simulation test results of the $\Delta\delta$ swing curves for the system with LOC are recorded here as Figs. 4-3 and 4-4 for comparison. The oscillations in Fig. 4-2 are stabilized as shown in Figs. 4-3 and 4-4, and the effect of LOC is noticeable. It is also noted that the choices of Q make the results quite different.

Differences in LOC and Conventional PSS Designs

Whereas the objective of the conventional PSS design as presented in Chapter 3 is to improve the system mechanical mode damping alone, that of the LOC design is to minimize the system state variation in conjunction with the control effort. The minimization of state variation does imply that

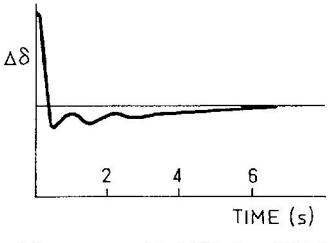

Fig. 4-4 Swing curve of the system with LOC $Q = \text{DIAG}[10, 10, 1, 1, 1, 1, 1, 1]$.

not only the system damping but also the synchronizing torque are being improved. The other difference is in the realization of control schemes. Whereas the conventional PSS has been designed with a single signal input using phase compensation and for a narrow band of oscillating frequencies, the LOC synthesizes the control input from many state variable signals that themselves have different phases, has no need of compensation blocks, and is good over a wide band of frequencies. Still another and probably the most significant difference is that the conventional PSS design is based on a one-machine infinite-bus model, whereas the LOC design can be readily applied to multimachine electric power systems.

Summary of Section 4-4

In this section, the first application of LOC to stabilize an electric power system is briefly recapitulated. The hydroelectric power plant is modeled as an eighth-order system, a third-order for the synchronous machine, a second-order for the excitation, and a third-order for the governor and hydraulic power. Two performance indices with different weighting matrices were chosen, and two LOCs were designed. From the nonlinear simulation tests it was found that the LOC of electric power systems is very effective and that the selection of the weighting matrix Q is very important to the LOC design. Toward the end of the section, the differences in LOC and conventional PSS designs are discussed.

4-5 LOC DESIGN WITH DOMINANT EIGENVALUE SHIFT

Since the selection of the weighting matrix Q is very important to the LOC design, the selection must be done systematically. One idea is to link the selection with the left-shift of the dominant eigenvalues of an electric power system as much as possible within the exciter and governor's capability, which will be developed and applied for the LOC design in this section [11, 12].

The dominant eigenvalues are the eigenvalue pair closest to the imaginary axis if they are already on the LHS of the complex plane; there will be no system eigenvalues on the RHS of the complex plane as long as there is an LOC.

General Procedure of LOC Design

Before presenting an algorithm for the selection of the weighting matrix Q with dominant eigenvalue shift for the LOC design, the general procedure

of LOC design may be recapitulated as follows:

(a) Select a proper linear model for the electric power system and obtain the state equations in the form

$$\dot{x} = Ax + Bu \tag{4-5}$$

(b) Select the weighting matrices Q and R of the performance index

$$J = \frac{1}{2}\int_0^\infty [x^T Q x + u^T R u]\, dt \tag{4-6}$$

(c) Construct the state and co-state system matrix M

$$M = \begin{bmatrix} A & -S \\ -Q & -A^T \end{bmatrix} \tag{4-31}$$

where

$$S \triangleq BR^{-1}B^T \tag{4-18}$$

and compute the eigenvalues

$$\Lambda = \begin{bmatrix} \Lambda_- & \\ & \Lambda_+ \end{bmatrix} \tag{4-32}$$

and eigenvectors

$$X = \begin{bmatrix} X_{\mathrm{I}} & X_{\mathrm{III}} \\ X_{\mathrm{II}} & X_{\mathrm{IV}} \end{bmatrix} \tag{4-35}$$

(d) Calculate the Riccati matrix K and the control Bu:

$$K = X_{\mathrm{II}} X_{\mathrm{I}}^{-1}, \qquad Bu = -SK \tag{4-39), (4-40}$$

(e) Find the eigenvalues of the system with LOC

$$\dot{x} = Ax + Bu = (A - SK)x \tag{4-29a}$$

(f) Using a nonlinear model for the system, including especially the controller's limits such as the excitation ceiling voltage, find the dynamic response of the system to a given disturbance.

An Algorithm of LOC Design with Dominant Eigenvalue Shift

Figure 4-5 shows an algorithm of LOC design [11] by selecting the weighting matrix Q with the dominant eigenvalue shift:

(a) Begin with an initial weighting matrix Q, say, a unit matrix.

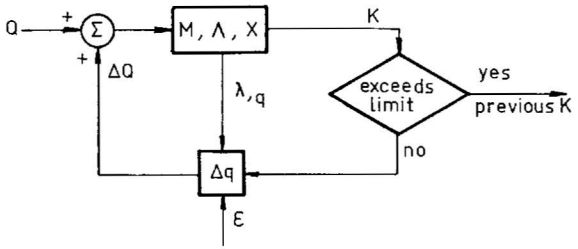

Fig. 4-5 An algorithm of LOC design with dominant eigenvalue shift.

(b) Find the state and co-state system matrix M, the eigenvalues Λ, the eigenvector matrix X, and the Riccati matrix K.

(c) Determine whether the controller has exceeded the exciter voltage limit and/or the governor limit. If not, proceed with the dominant eigenvalue shift. If yes, stop and print K of previous results.

(d) For the shift

$$\lambda = \lambda + \Delta\lambda, \qquad \Delta\lambda < 0 \text{ (real)} \tag{4-41}$$

each weighting matrix element is changed by small amounts and calculated from the eigenvalue sensitivity $\lambda_{,q}$,

$$\Delta q = \Delta\lambda/\lambda_{,q}, \qquad \Delta q < \varepsilon \tag{4-42}$$

where $\lambda_{,q}$ is the sensitivity of the dominant eigenvalue with respect to a Q element

$$\lambda_{,q} \triangleq (\partial\lambda)/\partial q \tag{4-43}$$

(e) Update Q and reenter the interative loop.

(f) Reorder the eigenvalues for the next shift.

After a dominant eigenvalue shift, the eigenvalues of the system will move with respect to each other, and they can be redivided into three groups: the most dominant eigenvalue pair; the less dominant eigenvalues, some of which may have negative real parts five to ten times the dominant ones; and the rest. Only the dominant ones need be left-shifted, the movement of the less dominant ones to the right will be prohibited, and the movement of the rest eigenvalues shall be free. For details, see Moussa and Yu [11].

The calculation of eigenvalue sensitivity with respect to a Q element is shown in Example 4-3.

Example 4-3. Find the sensitivity of eigenvalue λ_i of the system with LOC with respect to q or the element of the weighting matrix Q.

Solution: The eigenvector x_i of the state and co-state matrix M is calculated from

$$Mx_i = \lambda_i x_i \tag{4-44}$$

and the eigenvector v_i of M^T from

$$M^T v_i = \lambda_i v_i \tag{4-45}$$

Note that M and M^T have the same set of eigenvalues but different eigenvectors.

Partial differentiation of (4-44) with respect to the weighting matrix element q gives

$$M_{,q}x_i + Mx_{i,q} = \lambda_{i,q}x_i + \lambda_i x_{i,q} \tag{4-46}$$

Note that each term of the preceding equation is a column matrix. Premultiplying each term of the last equation by v_i^T and applying (4-45) yields

$$\lambda_{i,q} = v_i^T M_{,q} x_i / C_i \tag{4-47}$$

where

$$v_i^T x_i = C_i \tag{4-48}$$

which is a scalar. Since the eigenvector matrices may be written

$$X = \begin{bmatrix} X_{\mathrm{I}} & X_{\mathrm{III}} \\ X_{\mathrm{II}} & X_{\mathrm{IV}} \end{bmatrix}, \qquad V = \begin{bmatrix} X_{\mathrm{IV}} & -X_{\mathrm{II}} \\ -X_{\mathrm{III}} & X_{\mathrm{I}} \end{bmatrix} \tag{4-49}$$

For the ith row of $[X_{\mathrm{IV}}^T, -X_{\mathrm{III}}^T]$ and the ith column of $[X_{\mathrm{I}}, X_{\mathrm{II}}]^T$

$$C_i = \sum_{j=1}^{n} [X_{\mathrm{IV}i}(j)X_{\mathrm{I}i}(j) - X_{\mathrm{III}i}(j)X_{\mathrm{II}i}(j)] \tag{4-50}$$

where $j = 1, \ldots, i, \ldots, n$. Finally

$$\Delta M = \begin{bmatrix} 0 & 0 \\ -\Delta Q & 0 \end{bmatrix}, \qquad M_{,q} = \begin{bmatrix} 0 & 0 \\ -I & 0 \end{bmatrix} \tag{4-51}$$

where I is an identity matrix. Therefore

$$\lambda_{i,q} = \frac{1}{C_i}[X_{\mathrm{IV}i}^T(j), -X_{\mathrm{III}i}^T(j)] \begin{bmatrix} 0 & 0 \\ -I & 0 \end{bmatrix} \begin{bmatrix} X_{\mathrm{I}i}(j) \\ X_{\mathrm{II}i}(j) \end{bmatrix}$$

$$= \frac{1}{C_i} X_{\mathrm{III}i}^T(j) X_{\mathrm{I}i}(j) \tag{4-52}$$

Generally, there are n elements of Q. Therefore

$$\lambda_{i,q} = [\lambda_{i,q1}, \lambda_{i,q2}, \ldots, \lambda_{i,qj}, \ldots, \lambda_{i,qn}]^T \tag{4-53}$$

Linear Optimal Stabilization of a One-Machine, Infinite-Bus System

The dominant eigenvalue shift technique of LOC design was applied to the linear optimal stabilization of a one-machine, infinite-bus system [11]. Six cases were investigated, including the system without supplementary control and the system with a phase-compensation supplementary excitation control. For comparison, they are identified as follows:

1. system without any supplementary control, $u = 0$;
2. system with a phase-compensation excitation control, u_{EC};
3. system with a linear optimal excitation control, u_E;
4. system with a linear optimal governor control, u_G;
5. same as case 4 but without dashpot, $u_{G'}$;
6. system with linear optimal excitation and governor control, u_E plus $u_{G'}$.

For the studies, the following models are used:

$$x = [\Delta\psi_F, \Delta v_F, \Delta\delta, \Delta\omega)^T$$

$$x = [\Delta\psi_F, \Delta v_F, \Delta\delta, \Delta\omega, a, a_f, g, h]^T$$

$$x = [\Delta\psi_F, \Delta v_F, \Delta\delta, \Delta\omega, g, h]^T$$

The first model is used for $u = 0$, u_{EC}, and u_E studies, which is essentially the same as Fig. 3-1; the second model for u_G study, which also includes a governor with dashpot; and the third model for $u_{G'}$ and u_E plus $u_{G'}$ studies, which also includes a governor but without dashpot. In the second model, Hovey's original governor transfer functions are used, of which a_f corresponds to the dashpot feedback d of Fig. 2-13, and h, the waterhead, can be replaced by the mechanical torque output T_m as shown in (2-81) and (2-83) of Chapter 2. In the third model, the actuator time constant is neglected but not the permanent droop.

Applying the dominant eigenvalue shift technique presented in this section, four LOCs corresponding to u_E, u_G, $u_{G'}$, and u_E plus $u_{G'}$ are designed. Typical Q matrices from the dominant eigenvalue shift LOC design are

$$Q_{uE} = \text{DIAG}[2524, 0, \underline{914}, \underline{23856}]$$

$$Q_{uE,uG'} = \text{DIAG}[1.42, 0, \underline{0.0859}, \underline{25.8}, 82.28, 0.025]$$

Although it is very difficult to find a general rule for the choice of all weighting matrix elements since most state variables are different physical quantities, like speed, flux linkage, governor opening, and so on, one result clearly emerges that $q_{\Delta\omega}$ is always much larger than $q_{\Delta\delta}$. There may be two reasons: one is that it is the $\Delta\omega$ change that causes the $\Delta\delta$ change; and the other is

that while $\Delta\delta$ is in radians, $\Delta\omega$ is per unit, or $(2\pi f)$ rad/s, which is a much larger unit but is a time derivative.

A set of swing curves from the nonlinear simulation test results chosen from Moussa and Yu [11] is shown here as Fig. 4-6. For all tests, a three-phase fault for five cycles was assumed on one of the double-circuit transmission lines followed by the faulted line removal, fault clearing, and the system restoration at the end of 30 cycles. The system without any supplementary control is unstable (curve 1). Although the system with conventional PSS or the phase-compensation supplementary excitation (curve 2) is stable, it has not quite settled down at the end of 3 s. It is interesting to note that the system with all LOCs is stabilized within 3 s, the most effective one is the linear optimal excitation and governor control without dashpot (u_E plus $u_{G'}$), and almost equally effective but having much simpler design and instrumentation is the linear optimal excitation control (u_E).

Linear Optimal Stabilization of a Multimachine System

Since the state equation

$$\dot{x} = Ax + Bu \tag{4-5}$$

is in the general form, it is applicable to any number of machines. So is the

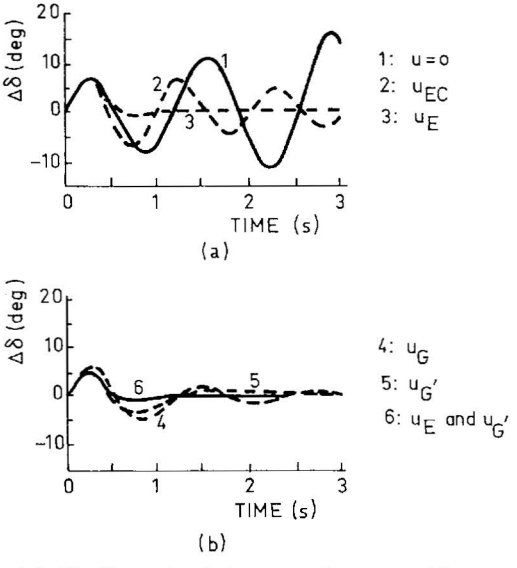

Fig. 4-6 Nonlinear simulation tests of a one-machine system.

dominant eigenvalue shift technique developed for the LOC design. A three-machine, infinite-bus system was also investigated [12]. The system matrix was partitioned as follows:

$$\begin{bmatrix} \dot{x}_1 \\ \dot{x}_2 \\ \dot{x}_3 \end{bmatrix} = \begin{bmatrix} A_{11} & A_{12} & A_{13} \\ A_{21} & A_{22} & A_{23} \\ A_{31} & A_{32} & A_{33} \end{bmatrix} \begin{bmatrix} x_1 \\ x_2 \\ x_3 \end{bmatrix} + [B] \begin{bmatrix} u_1 \\ u_2 \\ u_3 \end{bmatrix} \tag{4-54}$$

where x_1, x_2, and x_3, respectively, are the state variable vectors of machines 1, 2, and 3; u_1, u_2, and u_3 are the controls; B is the control matrix; A_{11}, A_{22}, and A_{33} are the local system matrices of the individual machines; and the off-diagonal matrices A_{12}, A_{23}, and so on, represent the paths of dynamic interaction between machines. Note that (4-54) can be expanded to any number of machines using high- or low-order machine and control models.

For the multimachine stability study, the individual machine coordinates d_k-q_k may be related to common system coordinates D-Q as in Fig. 4-7, where δ_k is the phase angle difference of the d_k axis with respect to the D axis or the q_k axis with respect to the Q axis. δ_k can be positive or negative.

Although the machines are usually described in common or individual rotating coordinates, the transmission network is static. Let the current vector $[i]$, the voltage vector $[v]$, the transmission admittance matrix $[Y]$, and the transmission impedance matrix $[Z]$ in the static coordinates be identified by an extra subscript N, and those in the rotating coordinates by an extra subscript m. It is assumed that the load damping is negligibly small and all load buses can be eliminated after a load flow study. Otherwise, the load should be properly modeled and included in the system model. Then we have the machine bus current vector in the static coordinates,

$$[i_N] = [Y_N][v_N] \tag{4-55}$$

and the current vector in the common rotating coordinates,

$$[i_N]e^{j\omega_e t} = [Y_N][v_N]e^{j\omega_e t} \tag{4-55a}$$

where $e^{j\omega_e t}$ is a synchronously rotating phasor.

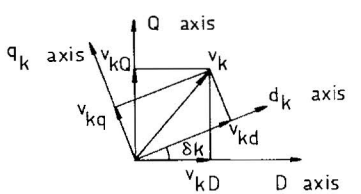

Fig. 4-7 Individual machine and common system coordinates.

Therefore, the current and voltage of the kth machine in the individual coordinates become

$$\begin{aligned} v_{kN}e^{j\omega_c t} &= v_{km}e^{j(\omega_c t+\delta_k)} \\ i_{kN}e^{j\omega_c t} &= i_{km}e^{j(\omega_c t+\delta_k)} \end{aligned} \tag{4-56}$$

or

$$v_{kN} = v_{km}e^{j\delta_k}, \qquad i_{kN} = i_{km}e^{j\delta_k} \tag{4-56a}$$

For n machines, it must be written,

$$\begin{aligned} [v_N] &= (e^{j\delta_i}][v_m], \qquad i = 1, \ldots k, \ldots n; \\ [i_N] &= [e^{j\delta_j}][i_m], \qquad j = 1, \ldots k, \ldots n \end{aligned} \tag{4-57}$$

Since all voltage and current vectors are column matrices, $[e^{j\delta_i}]$ and $[e^{j\delta_j}]$ are diagonal matrices. Substituting (4-57) into (4-55) gives

$$[v_m] = [Z_m][i_m]$$

where (4-58)

$$[Z_m] = [e^{-j\delta_i}][Y_N]^{-1}[e^{j\delta_j}]$$

Thus we have found a relation between the machine terminal voltages and currents in terms of the transmission admittances, and the highest-order matrix inversion is $[Y_N]^{-1}$ for an n-machine system.

The dominant eigenvalue shift technique is then applied to the linear optimal excitation control (LOEC) design of a three-machine system described by (4-56), of which machine 1 is a thermal plant of 360 MW, machine 2 a hydroplant of 503 MW, and machine 3 also a hydroplant, but of 1673 MW. Four LOECs were designed:

1. a u_{EM} design by which u_1, u_2, and u_3 are designed simultaneously for the entire system;
2. a u_{EI} design by which u_1 and u_2 are omitted from (4-54) and u_3 is designed for the entire system;
3. a u_E design by which not only u_1 and u_2, but also $\dot{x}_1$ and $\dot{x}_2$, are omitted from (4-54), and only u_3 is designed for the entire system;
4. completely ignoring the dynamic interaction between machines, u_1, u_2, and u_3 are designed separately from local system dynamics,

$$\dot{x}_1 = A_{11}x_1 + B_1u_1, \quad \dot{x}_1 = A_{22}x_2 + B_2u_2, \quad \dot{x}_3 = A_{33}x_3 + B_3u_3 \tag{4-54a}$$

Full state variable feedbacks are used for u_{EM} and u_{EI} LOEC designs. For

u_E design, the partitioned matrix equation

$$\left[\begin{array}{c} 0 \\ 0 \\ \hline \dot{x}_3 \end{array}\right] = \left[\begin{array}{cc|c} A_{11} & A_{12} & A_{13} \\ A_{21} & A_{22} & A_{23} \\ \hline A_{31} & A_{32} & A_{33} \end{array}\right] \left[\begin{array}{c} x_1 \\ x_2 \\ \hline x_3 \end{array}\right] \tag{4-54b}$$

is used for the elimination of x_1 and x_2 leaving only the x_3 state variables for the feedback.

Typical results of the nonlinear simulation tests are shown in Fig. 4-8. The LOEC designs of case 4 do not work in harmony, leading only to system instability, which is rather as expected. Among the other three LOEC designs, u_{EM} of case 1 gives the best result but requires the full state feedback. u_{EI} of case 2 is also effective, but also requires full state feedback. Therefore, the best choice is U_E of case 3, one LOEC of the largest machine in the system for the entire system, which requires the least instrumentation, but is almost equally effective as u_{EM}.

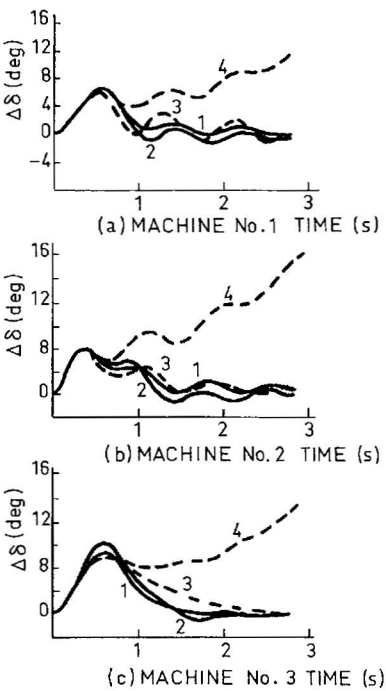

Fig. 4-8 Nonlinear simulation tests of a three-machine system: 1, u_{EM}; 2, u_{EI}; 3, u_E; 4, separate designs.

Summary of Section 4-5

In this section the dominant eigenvalue shift technique for LOC design is presented, and the weighting matrix q is decided from the dominant eigenvalue shift. The technique is then applied to various LOC designs of a one-machine, infinite-bus system: the linear optimal excitation control u_E, the linear optimal governor control u_G, the linear optimal governor control without dashpot $u_{G'}$, and the linear optimal excitation and governor control without dashpot u_E plus $u_{G'}$. Nonlinear computer simulation results as shown in Fig. 4-6 indicate that (1) the system without control ($u = 0$) is unstable, (2) the system with a conventional PSS is stable, but not quite stabilized at the end of 3 s, (3) the system with an LOEC u_E gives the best result and the system is stabilized in less than 2 s, (4) the system with a linear optimal governor control u_G also works, (5) the system with a linear optimal governor control without dashpot $u_{G'}$ gives even better results, but still not as good as the system with u_E control, and (6) the system with linear optimal excitation and governor control without dashpot is equally effective as the u_E control, but requires more instrumentation. Therefore, the LOEC u_E is the best of all.

The dominant eigenvalue shift technique for LOC design is also applied to a multimachine system. Four types of LOEC are designed: three LOECs for three machines designed simultaneously (u_{EM}), one LOEC for the entire system using full system state variable for the feedback (u_{EI}), also one LOEC for the entire system but using only the state variables of the local machine for the feedback (u_E), and three LOECs designed separately by considering the local machine dynamics alone and completely neglecting the dynamic interaction between machines. The last design does not work at all as found from the computer simulation test (curve 4, Fig. 4-8), which is rather as expected. Among the other three, it is noted that one LOEC of the largest power plant of the system can be designed for the stabilization of the entire system using the state variables of the local machine alone as the feedback (curve 3).

4-6 LOC DESIGN WITH EIGENVALUE ASSIGNMENT

Since a single variable nth-order ordinary differential equation can be transformed into n first-order multivariable state equations, and vice versa, and since the eigenvalues of systems of linear transformation are identical, the LOC can be designed for a system with its state matrix equation in a canonical form, and a simple eigenvalue assignment technique can be developed, which will be presented in this section [14].

Three Sets of State Equations

For the design, three sets of state equations are involved. The first is a matrix state equation of which some state variables are not directly measurable. For instance,

$$\dot{x} = Ax + Bu \tag{4-5}$$

where

$$x = [\Delta\delta, \Delta\omega, \Delta\psi_F, \Delta\psi_D, \Delta\psi_Q, \Delta E_{FD}]^T \tag{4-59}$$

which corresponds to the ψ model of (2-56) with the omission of $\dot{\psi}_d$ and $\dot{\psi}_q$ and the addition of the excitation voltage ΔE_{FD}. The three flux linkages of (4-59), however, are not directly measurable, but they can be expressed in terms of Δv_t, ΔP_e, and Δi_F, which are measurable.

Let the second matrix state equation be

$$\dot{z} = Fz + Gu \tag{4-60}$$

where

$$z = [\Delta\delta, \Delta\omega, \Delta v_t, \Delta P_e, \Delta i_F, \Delta E_{FD}]^T \tag{4-60a}$$

and let the two sets of state variables be related by

$$z = Cx \tag{4-61}$$

where C is a transformation matrix that is a square matrix in this particular case. Differentiating (4-61) and substituting (4-60) and (4-5) into the result gives

$$\dot{z} = C\dot{x} = CAC^{-1}z + CBu = Fz + Gu \tag{4-60b}$$

where

$$F \triangleq CAC^{-1}, \qquad G \triangleq CB \tag{4-60c}$$

To change (4-60) into a canonical form, another transformation is required. Let the third matrix state equation in canonical form be

$$\dot{y} = F_o y + G_o u \tag{4-62}$$

where

$$\dot{y}_1 = y_2, \qquad \dot{y}_2 = y_3, \qquad \ldots, \qquad \dot{y}_{n-1} = y_n \tag{4-62a}$$

and

$$F_o = \begin{bmatrix} 0 & 1 & 0 & \cdots & 0 \\ 0 & 0 & 1 & \cdots & 0 \\ 0 & 0 & 0 & \cdots & 0 \\ \vdots & \vdots & \vdots & \vdots & \vdots \\ 0 & 0 & 0 & \cdots & 1 \\ -\alpha_1 & -\alpha_2 & -\alpha_3 & \cdots & -\alpha_n \end{bmatrix} \tag{4-62b}$$

The first $(n-1)$ rows of F_o are simply a restatement of the relation of (4-62a) and the last row corresponds to

$$\dot{y}_n = -\alpha_n y_n - \alpha_{n-1} y_{n-1} - \cdots - \alpha_2 y_2 - \alpha_1 y_1$$

or

$$\frac{d^n y_1}{dt^n} + \alpha_n \frac{d^{n-1} y_1}{dt^{n-1}} + \alpha_{n-1} \frac{d^{n-2} y_1}{dt^{n-2}} + \cdots + \alpha_2 \frac{dy_1}{dt} + \alpha_1 y_1 = 0 \tag{4-62c}$$

To find the relation of the y and z state variables, let

$$z = Ty \tag{4-63}$$

Then we have

$$\dot{y} = T^{-1}\dot{z} = T^{-1}FTy + T^{-1}Gu = F_o y + G_o u \tag{4-62d}$$

where

$$F_o \triangleq T^{-1}FT, \qquad G_o \triangleq T^{-1}G \tag{4-62e}$$

The transformation matrix T can be found from a comparison of the eigenvalues of the two system matrices F of (4-60) and F_o of (4-62). Since the determinants of the two corresponding characteristic equations may be written

$$|\lambda I - F| = (\lambda - \lambda_1)(\lambda - \lambda_2)\cdots(\lambda - \lambda_n) \tag{4-64}$$

$$|\lambda I - F_o| = \lambda^n + \alpha_n \lambda^{n-1} + \alpha_{n-1}\lambda^{n-2} + \cdots + \alpha_1 \tag{4-65}$$

and since the eigenvalues of the two equations are equal, we shall have

$$\begin{aligned}
\alpha_n &= -\sum_{i=1}^{n} \lambda_i, \qquad i = 1, 2, \ldots, n \\
\alpha_{n-1} &= \lambda_1\lambda_2 + \lambda_1\lambda_3 + \cdots + \lambda_{n-1}\lambda_n \\
\alpha_{n-2} &= -(\lambda_1\lambda_2\lambda_3 + \lambda_1\lambda_2\lambda_4 + \cdots + \lambda_{n-2}\lambda_{n-1}\lambda_n) \\
&\vdots \\
\alpha_1 &= (-1)^n \sum_{i=1}^{n} \lambda_i
\end{aligned} \tag{4-66}$$

F_o can thus be decided, and the transformation matrix T can be determined from

$$TF_o = FT \tag{4-67}$$

For details, see Habibullah and Yu [14].

Equations for the Eigenvalue Assignment

For the LOC design, a performance index for the system represented by the y state equations may be chosen as

$$J = \frac{1}{2}\int_0^\infty [y^T Q y + u^T R u]\, dt \tag{4-68}$$

Because of the canonical form, the weighting matrices now become

$$Q = qI_n, \qquad R = rI_r \tag{4-69}$$

where q and r are scalars, and I_n and I_r are identity matrices of different orders.

With the system state equations in the canonical form, the state and co-state matrix equation (4-21) becomes

$$\begin{bmatrix} \dot{y} \\ \dot{p}_o \end{bmatrix} = \begin{bmatrix} F_o & -(1/r)G_oG_o^T \\ -qI_n & -F_o^T \end{bmatrix} \begin{bmatrix} y \\ p_o \end{bmatrix} \tag{4-70}$$

where p_o is the co-state variable vector corresponding to the y state variable vector, and the characteristic equation becomes

$$|(\lambda I_n - F_o)(\lambda I_n + F_o^T) - (q/r)G_oG_o^T| = 0 \tag{4-71}$$

Let a linear optimal excitation control (LOEC) be designed for the y system with matrix state equation in the canonical form. Since there is only

one control loop and ΔE_{FD} is the last state variable, we shall have

$$G_o = [0, 0, 0, 0, 1]^T \tag{4-72}$$

Therefore, the characteristic equation becomes

$$|\lambda I_n - F_o||\lambda I_n + F_o^T| + q/r = 0 \tag{4-73}$$

or

$$(\lambda^n + \alpha_n\lambda^{n-1} + \cdots + \alpha_1)[\lambda^n - \alpha_n\lambda^{n-1} + \cdots + (-1)^n\alpha_1] + (-1)^n q/r = 0 \tag{4-74}$$

The last two equations indicate that the eigenvalues of the state and co-state system are function of the scalar ratio q/r. One can find the eigenvalue loci by varying q/r, and also left-shift the dominant eigenvalue from the loci with an optimal control. Note that the αs and hence F_o are known from eigenvalues of the system matrix F.

LOEC Design with Eigenvalue Assignment

The first step is to find the eigenvalue loci of the state and co-state system by varying the q/r ratio. Since the eigenvalues of this system are symmetrical with respect not only to the real axis but also to the imaginary axis of the complex plane, we should only be interested in the eigenvalue loci mainly on the LHS of the plane, which corresponds to the state equations of the system with control.

The second step is to select a set of eigenvalues from the loci for a q/r ratio, shift the dominant eigenvalues close to the imaginary axis to the left to a desired position, and design the LOC. Since the characteristic equation of the system without control

$$\begin{aligned} |\lambda I_n - F_o| &= |\lambda I_n - F| \\ &= (\lambda - \lambda_1)(\lambda - \lambda_2)\cdots(\lambda - \lambda_n) \\ &= \lambda^n + \alpha_n\lambda^{n-1} + \cdots + \alpha_1 \end{aligned} \tag{4-75}$$

and that with control

$$\begin{aligned} |\lambda I_n - (F_o - G_oS_o)| &= (\lambda - \hat{\lambda}_1)(\lambda - \hat{\lambda}_2)\cdots(\lambda - \hat{\lambda}_n) \\ &= \lambda^n + \hat{\alpha}_n\lambda^{n-1} + \cdots + \hat{\alpha}_1 \end{aligned} \tag{4-76}$$

where $\hat{\lambda}_i$, $i = 1, \ldots, n$, are the desired new eigenvalues of the controlled system, the differences

$$\beta_i = \hat{\alpha}_i - \alpha_i, \qquad i = 1, 2, \ldots, n \tag{4-77}$$

are due to the control of the system. Let the state equation of the system with control be

$$\dot{y} = F_0 y + G_0 u = (F_0 - G_0 S_0) y \tag{4-78}$$

the control becomes

$$u = -S_0 y = -S_0 T^{-1} z \tag{4-79}$$

where

$$S_0 = \text{DIAG}[\beta_1, \beta_2, \ldots, \beta_n] \tag{4-80}$$

Note that each term of (4-78) is a column matrix.

It is interesting to note that although the matrix state and co-state equation is still required for the LOC design by this method, there is no longer any need to solve the Riccati matrix equation.

Wide Power Range System Stabilization

The eigenvalue assignment technique developed in this section for LOC design is applied to a one-machine, infinite-bus system to design a controller that can effectively stabilize the system over a wide-range operating condition [14]. Having obtained a power system model for a given operating condition, the x-state equations are transformed into the z-state and y-state equations for the LOC design. The first step is to find the eigenvalue loci in the y state by varying q/r. The second step is to choose a set of eigenvalues on the loci for a given q/r, left-shift the dominant eigenvalue to a desired position, and design an LOC. The third step is to design several LOCs by choosing several q/r ratios, find the best LOC that can stabilize the system over a wide power range of $P_e = 0.3$ to 1.25 per unit, and test the control on the corresponding nonlinear model.

Results of Habibullah and Yu [14] are summarized as follows. The system state variables are given as (4-59), the eigenvalues of the system without control are $0.203 \pm j4.99$, $-8.465 \pm j5.26$, -13.2, -27.3 and the system is unstable.

Following the first step eigenvalue assignment LOC design using the canonical form, the eigenvalue loci for various q/r ratios are plotted as Fig. 4-9. Similar to the system without control, there are two conjugate eigenvalue pairs and two real eigenvalues of the system with LOC. All eigenvalues are moving to the left with the increase of q/r. Not shown in the figure are λ_2 and λ_4, which are conjugate with λ_1 and λ_3, respectively. Note that λ_1 is on the RHS of the complex plane when q/r equals zero or the system is without control.

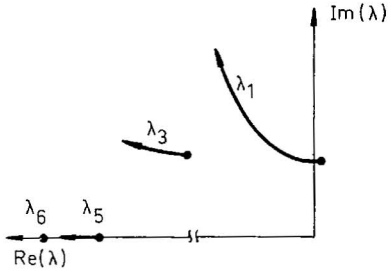

Fig. 4-9 Eigenvalue loci of a power system as the function of q/r.

Examination of Fig. 4-9 shows that only λ_1 and λ_2 need a left shift. Since it can be started from any point set of λ_1 and λ_2, three point sets are chosen, and three different controllers, I, II, and III, are designed. The eigenvalue loci for the system with different controllers and that without control are plotted in Fig. 4-10 where points 1, 2, 3, ..., 7 correspond to

$$P_{e0} = 1.25, 1.20, 1.15, 0.952, 0.70, 0.50, 0.30$$

per unit, respectively. Among the controllers, only III can effectively stabilize the system over a wide power range of P_e from 0.3 to 1.25 per unit.

Stabilizer III is further given a nonlinear computer simulation test for a P_e of 1.23, 0.95, and 0.3 per unit. The results are shown in Fig. 4-11 as curves 1, 2, and 3, respectively. The system remains stable under all power conditions. But the results suggest that probably one should use $P_{e0} = 1.25$ per-unit overload condition, instead of the full load condition, for a power system stabilizer design.

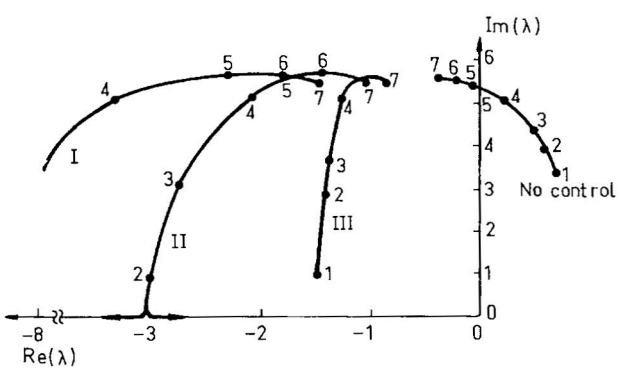

Fig. 4-10 Eigenvalue loci of the system with different controllers.

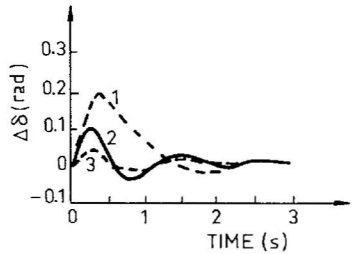

Fig. 4-11 Nonlinear simulation test of stabilizer III.

Summary of Section 4-6

In this section an eigenvalue assignment technique for LOC design is developed and applied to a one-machine, infinite-bus system. Three sets of state equations are involved: one conventional, the other with all measurable state variables, and the third in canonical form.

In canonical form, the characteristic equation of the state and co-state system matrix becomes a function of a single scalar ratio q/r. The eigenvalue assignment LOC design may proceed in two steps: (1) find the eigenvalue loci in the y state by varying q/r; and (2) choose a set of eigenvalues of the loci for a given q/r, left-shift the dominant eigenvalue to a desired position, and design an LOC. For wide-power range stabilization, however, another step is required; design several LOCs by choosing several q/r ratios, find the best LOC that can effectively stabilize the system over a wide power range of operating conditions, and give the control a nonlinear computer simulation test. It is found that it is the overload, not the underload, that one should pay more attention to in the stabilizer design.

The LOC design technique using the canonical form has been extended to output feedback using minimum measurements [15, 16], and can be further extended for the stabilization of a multimachine system.

4-7 OTHER DEVELOPMENTS OF LOC DESIGN AND TESTING

There are many other significant contributions to the LOC design for the stabilization of electric power systems, and to micromachine testing in the laboratory. A number of references are given at the end of this chapter [17–36], and there are many others. Some references are summarized in this section.

A Micromachine Model and LOC Testing

When the principle of LOC was first applied to the stabilization of a power system [13], the phase compensation PSS had already been well developed by the power industry. Following the first wave of development of design techniques of LOC [11–14, 17–32], people began to turn their attention to the microalternator test in research laboratories. One laboratory setup and test results are summarized in this subsection.

Figure 4-12 schematically shows a dynamic power system model for LOC and other stability control tests [34]. A student laboratory dc-motor, synchronous-generator set was adapted to simulate a megawatt hydraulic or steam turbine generator plant with various kinds of stability controls utilizing electronic circuits and power amplifiers. A large turbine generator set was simulated on the micromachine on a per unit basis.

For the given small motor-generator set without the facility of changing the rotors, there are only a limited number of large machine parameters that can be exactly simulated on the small machine set. Sensitivity analysis [33] indicates that the dynamic response of a simulated power system is most sensitive to the errors of the q-axis synchronous reactance x_q, the inertia constant M, and the field circuit time constant T'_{d0}. Both x_q and M can be exactly simulated with proper choices of the base voltage and base power for the small machine, and T'_{d0}, which is about 0.24 s for the small machine, can be increased to 6–7 s for large machines by inserting into the field winding circuit an active electronic circuit which will produce a negative resistance effect ($-$R).

The general layout of the dynamic power system model is schematically shown in Fig. 4-12: the turbine and governor and valving controls are on

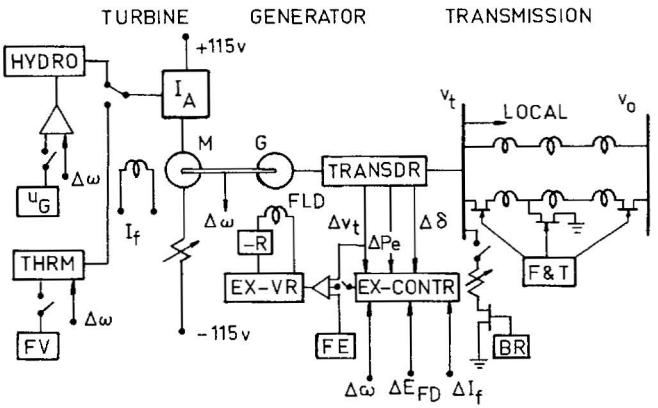

Fig. 4-12 A dynamic power system model for control test.

the left, the generator and excitation controls are at the center, and the transmission and fault simulation and braking resistance control are on the right.

At the top left of Fig. 4-12 are the hydraulic power output HYDRO, which affects the dc motor power input by controlling its armature current, and a governor that has a conventional negative feedback $\Delta\omega$ in addition to an optional phase-compensation supplementary governor control u_G. At the bottom left are the steam turbine power output THRM and a governor that also has a conventional negative feedback $\Delta\omega$ in addition to an optional fast valving control FV. The dc motor M in the figure, representing the hydraulic or steam turbines, is given a constant field excitation I_f. It has a starting rheostat, and its armature current I_A is controlled by either HYDRO or THRM to simulate the controlled turbine(s).

The time constant T'_{d0} of the synchronous generator G is adjustable by varying the $-R$ effect. The field winding is connected to the exciter and voltage regulator EX-VR, which has a conventional negative feedback of Δv_t in addition to two optionals: a linear optimal control EX-CONTR with various input signals and a forced excitation control FE.

At the top right of Fig. 4-12 a transmission system is shown. It constitutes three-phase, three-section, double-circuit transmission lines connected to an infinite bus with a voltage v_o. Each section is simulated by a π circuit with inductor and capacitor, and one circuit is installed with fault simulation and timing devices F & T. A three-phase fault can be simulated on the line including grounding, faulted-line opening, fault clearing, and cleared-line restoration by relays and circuit breakers. The time and sequence of operation can be set a priori by decade counters from 0.00 to 9.99 s, and the entire process will be automatically executed with a single pushbutton. At the bottom right of Fig. 4-12 is a braking resistance BR.

There are also the synchronizing and various protection devices, including an emergency shutdown pushbutton, which are not shown. Most devices, except the machine and transmission, are simulated by analogs and power amplifiers, and the fast valving FV, the fast excitation FE, and the dynamic resistance braking BR are provided with control logics.

Figure 4-13 shows one set of test results on the micromachine. The system that was unstable due to the lack of damping is shown on top. The same system becomes stabilized in a few seconds with an LOC, and the result is shown at the bottom. The large swings were clipped in recording. This micromachine test further shows the effectiveness of LOC.

Linear Optimal Excitation and Steam Valving Control

Comprehensive microalternator test results of linear optimal excitation and steam valving control of a power system are reported in Lu *et al.* [37].

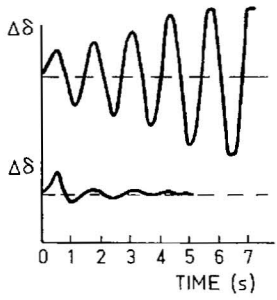

Fig. 4-13 Micromachine test of LOC.

A 600-MW turbogenerator connected to an infinite bus through a long transmission line is simulated on a dynamic power system model. The system is described by the following state equation:

$$\dot{x} = Ax + Bu \tag{4-5}$$

where

$$x = [\Delta P_e, \Delta\omega, \Delta v_t, \Delta P_m, \Delta\mu]^T \tag{4-81}$$

and ΔP_m and $\Delta\mu$ respectively represent the mechanical power input and the regulated steam valve opening.

A linear optimal excitation and steam valving control of the system is designed, and both the mechanical power input and the electric power output of the turbine-generator are controlled upon a system disturbance. Comparisons are made between the following three cases:

1. the system without any supplementary control;
2. the system with a phase compensation PSS;
3. the system with linear optimal excitation and steam valving.

For a relatively small three-phase disturbance, the system without any supplementary control takes a longer time and more swings to reach the steady state, the system with the phase-compensation PSS takes less time and fewer swings, and the system with the LOC still less. The stability limits are

	Control	δ_{max} (deg)	$P_{e\,max}$ (pu)
1	No supplementary	98	0.93
2	Conventional PSS	113	1.05
3	Linear optimal	120	1.14

For relatively large disturbances, the stability limits of the system from the microalternator test are

	Control	δ_{max} (deg)			$P_{e\,max}$ (pu)		
1	No supplementary	70	73	75	0.51	0.60	0.62
2	Conventional PSS	72	75	77	0.55	0.65	0.70
3	Linear optimal	87	93	100	0.83	0.92	1.00
	(type of fault)	3ϕ	2ϕ	1ϕ	3ϕ	2ϕ	1ϕ

Swing curves 1, 2, and 3 of the three cases are recorded in Fig. 4-14. There is a three-phase fault on one of the double-circuit transmission line for 0.15 s, the fault is then cleared, and the line is restored at 0.75 s. The results not only indicate that the LOC is more effective in stabilizing the system than conventional PSS, but also clearly demonstrate the coordinated effort of the steam valving control of the mechanical power input and the excitation control of the electric power output.

When a three-phase fault occurs in the system, the electric power output P_e drops immediately and the excitation rises rapidly to its ceiling value (Fig. 4-14). In the meantime, the steam valves close as fast as possible to reduce the mechanical power input P_m. When the faulted line is tripped off at 0.15 s, the speed begins to drop, the excitation rapidly falls to zero, and

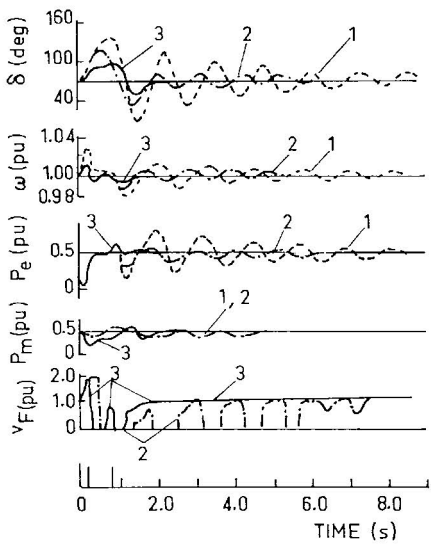

Fig. 4-14 Excitation and steam valving control of a power system.

the steam valves begin to increase the opening to prevent an excessive downswing of the speed. At about 0.6 s, there is a tendency for both δ and ω to increase and the excitation v_F rapidly rises. There is another excitation drop after the line is restored at 0.75 s and a rise to steady state after that. The system is completely stabilized within 2.5 s (curve 3), which presents a striking contrast to the system with a conventional PSS (curve 2) or the system without any supplementary control (curve 1).

Note also that although the system equations for LOC design are linear, the control signals v_F, etc., are by no means small. The coordinated effort of several large input signals makes the LOC far more effective than other types of linear controls.

A Parallel ac–dc System Model for LOC Design

Figure 4-15 shows a one-machine infinite-bus system with parallel ac–dc transmission lines. The generator has a terminal voltage v_t and the infinite bus a voltage v_o. The dc line, which is in parallel with the ac line, has a rectifier at the sending end and an inverter at the receiving end, although the rectifier and inverter functions are interchangeable for a dc line in a large electric power system. At the generator terminal bus, there is a local load R_L, a capacitor bank C to supply the reactive power required by the dc system, and several harmonic filters to improve the wave form of ac voltage and current.

To derive a reasonable low-order model for such a system for dynamic studies [29], let us start with a full high-order model and find the eigenvalues of the system for order reduction. The generator G may be described by seven state equations, five for the windings and two for the torque equilibrium; the excitation system by one; the dc line may be represented by a π equivalent and described by three equations; and the ac line also may be be represented by a π equivalent but requires six equations in d and q components.

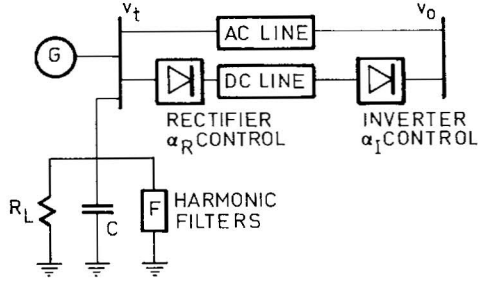

Fig. 4-15 A parallel ac–dc electric power system.

In addition, there will be two equations for the rectifier and inverter currents, and two for the firing angle functions $\cos \alpha_R$ and $\cos \alpha_I$.

So far we have 21 state equations. But there are two more for the capacitor for the reactive power supply, and four each for the 5th-, 7th-, 11th-, and 13th-order filters in d and q components. Therefore, we have altogether 39 state differential equations.

The number of eigenvalues of a system matrix is equal to the number of state variables of the system, and each eigenvalue or eigenvalue pair can be associated with a system component although the dynamic interacting effect among system components is included. Although it is not easy to identify an eigenvalue or eigenvalue pair with the corresponding system component, the task can be done carefully. It may begin with the lowest order of the system, say, the machine torque equation alone, and neglect the other system components. There will be only one eigenvalue pair. Then the field winding and the excitation system equations may be added, like the 4th-order system model of Fig. 3-1. Another eigenvalue pair may be obtained, and there will be some change in the mechanical mode eigenvalues of the torque equation. In case the two pairs of eigenvalue frequencies are very close, an artificially large change in excitation system parameter(s) may be assumed. There will be a substantial change in the electrical mode frequency, but not the mechanical mode. Thus the original electrical mode can be identified. After that, the state equations of other windings of the machine, the ac transmission line, the dc line, the capacitor, and the filters can be added in steps to build up the entire system and to identify the corresponding system components of the eigenmodes one by one.

The identification will be easier with more experience. For instance, we know that the frequency of the mechanical mode is always low, that of the stator windings always high, that of the dampers always real and negative.

The eigenvalues of the ac–dc system as shown in Fig. 4-15 for a given operating condition are:

Harmonic filters (16)	$-8.95 \pm j1490$,	$-9.50 \pm j2245$,	$-18.0 \pm j2191$,
	$-23.7 \pm j2947$,	$-55.0 \pm j4358$,	$-73.0 \pm j5118$,
	$-92.0 \pm j3568$,	$-123 \pm j4335$	
ac line (6)	$-2620 \pm j4267$,	$-59.1 \pm j1216$,	$-50.0 \pm j376$
Stator windings (2)	$-847 \pm j1892$		
dc line (3)	$-185 \pm j761$,	$-20.5 \pm j1327$	
Shunt capacitor (2)	$-18250 \pm j59136$		
Damper windings (2)	-41.9,	-26.1	
dc currents (2)	-360,	-360	
$\overline{\cos \alpha_R}$, $\overline{\cos \alpha_I}$ (2)	-362,	-35156	
$\Delta\delta$, $\Delta\omega$, $\Delta\psi_F$, Δv_R (4)	$-0.052 \pm j7.10$,	$-0.336 \pm j1.11$	

These eigenvalues are not listed in the original sequence as they are found, but listed for the convenience of order reduction of the model. Note that listed with the dc line are two eigenvalue pairs instead of three eigenvalues, due to the coupling of one of the dc line eigenvalues with one of the firing-angle function eigenvalues in a reduced-order model analysis.

For power system dynamic analysis, which involves mainly the low frequencies, any eigenmode with a frequency higher than the synchronous frequency can be ignored, although it would be different for the electric transient analysis, which always involves the high frequencies. Also the eigenmodes with fast decay or those with largest negative real values can be ignored except for those modes associated with the control loops. Therefore, a reduced 6th-order model can be developed for the ac–dc system for dynamic analysis by retaining only the state variables corresponding to the last two rows of the foregoing listed eigenvalues, resulting in

$$x = [\Delta\delta, \Delta\omega, \Delta\psi_F, \Delta v_R, \Delta\overline{\cos\alpha_R}, \Delta\overline{\cos\alpha_I}]^T \tag{4-82}$$

Although most state variable derivatives of the original 39th-order ac–dc system can be ignored, the algebraic equations of transmission lines, capacitor current for the reactive power supply, generator stator windings, etc., which represent the interaction between components, cannot. To arrive at the reduced 6th-order model from the original 39th-order model of the ac–dc system, the following matrix equation reduction process may be followed. Let the original system equation be

$$\begin{bmatrix} \dot{x}_1 \\ \dot{x}_2 \end{bmatrix} = \left[\begin{array}{c|c} A_{11} & A_{12} \\ \hline A_{21} & A_{22} \end{array}\right] \begin{bmatrix} x_1 \\ x_2 \end{bmatrix} \tag{4-83}$$

Let x_1 be the six state variables to be retained, (4-82), and let x_2 be the state variables that will be eliminated. In other words,

$$[\dot{x}_2] = 0 \tag{4-83a}$$

Eliminating x_2 from (4-83) gives

$$[\dot{x}_1] = [A_{11} - A_{12}A_{22}^{-1}A_{21}][x_1] \tag{4-84}$$

which corresponds to the reduced 6th-order of the ac–dc system.

Figure 4-16 compares the swing curves of the reduced-order model (curve 2) with the original 39th-order system (curve 1), both with the same fault. Also shown in the figure is curve 3, which is based on the nonlinear full model computer simulation test for the same fault but with an LOC designed from the reduced 6th-order linear model. The results show that the dynamic responses of the reduced 6th-order model and the original 39th-order system for the same fault are very close, and the LOC designed from the reduced order are extremely effective in stabilizing the ac–dc system.

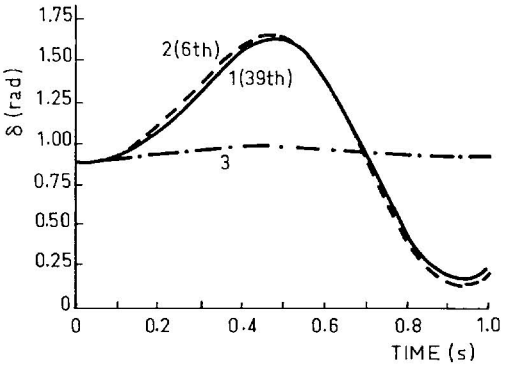

Fig. 4-16 Comparison of the 6th- order and the 39th-order system.

Summary of Section 4-7

In this section, additional developments of LOC design and system modeling are presented. A dynamic power system model usually known as the micromachine or microalternator model is described, and test results for the machine-simulated power system with and without an LOC are shown. The LOC is very effective in stabilizing the system. Test results of another dynamic power system model of linear optimal excitation and steam valving control by a different group are also shown. The simultaneous control of the mechanical power input by fast valving and the electric power output by excitation is far more effective in stabilizing a faulted power system than the phase compensation PSS. The coordinated effort of the fast valving and excitation by LOC is also manifested.

Toward the end of this section, a reduced 6th-order model of an ac–dc system is derived from an original 39th-order system, and the technique of order reduction is shown. Computer simulation test results show that the low-order model is fairly accurate, which can be used for LOC design to stabilize an ac–dc system.

4-8 SUMMARY

In Sections 4-1 and 4-2 the principle of linear optimal control and the derivation and solution of the Riccati matrix equation for the LOC design are presented. To demonstrate the effectiveness of LOC, a second-order numerical example is shown in Section 4-3. The first application of LOC to power system stabilization is summarized in Section 4-4 and the main

finding is that in LOC design it is very important to select a proper weighting matrix for the state variables.

Two systematic methods of selecting the weighting matrices are then developed. In Section 4-5 the weighting matrix Q is decided simultaneously with the dominant eigenvalue shift to the left as much as actual controllers permit. The technique is applied to the LOC design of a one-machine infinite-bus system as well as a multimachine system. The main findings of this study are: (1) $q_{\Delta\omega}$ is much larger than $q_{\Delta\delta}$ because of the units chosen and also the cause–effect relation; (2) an LOC is more effective than a phase-compensation PSS, a linear optimal governor control with dashpot is not as good as that without, and a linear optimal excitation control (LOEC) is almost as good as the linear optimal excitation and governor control without dashpot, which is the best; and (3) the LOECs for individual machines in a multimachine system cannot be designed separately and must be designed together, although one LOEC can be designed for the largest machine in the system for the stabilization of the entire system.

An eigenvalue assignment technique for the LOC design is developed in Section 4-6. The system matrix state equation is ultimately transformed in a canonical form, and the characteristic equation of the system state and co-state equations becomes a simple function of a single scalar ratio q/r of the system weighting matrices qI_n and rI_r where I_n and I_r are identity matrices. The system state eigenvalue loci are plotted for various q/rs, several sets of eigenvalues on the loci corresponding to different q/rs are chosen and the dominant eigenvalues are shifted to the left, and the LOCs thus designed for a given operating condition are then tested for the electric power output P_e from 0.3 to 1.25 per unit to find the best LOC that can effectively stabilize a system over the wide power range operating condition. The design technique has been applied to a one-machine infinite-bus system, and is being extended to multimachine systems.

In the last section of the chapter, Section 4-7, other developments of LOC of electric power systems are briefly presented. Some details of the layout of a dynamic power system model are presented first, along with some test results of LOC to show its effectiveness. Following that, micromachine test results of linear optimal excitation and steam valving control by another group are presented. The simultaneous control of the mechanical power input by steam valving and the electric power output by excitation is extremely effective. The coordinated effort of controls is manifested. Finally, a technique of reducing a 39th-order ac–dc system model to a reasonably low-order model of the 6th order for the LOC design are presented. Once again the effectiveness of LOC is demonstrated.

With the design technique greatly improved, and the effectiveness clearly shown, the LOC certainly provides a better means than a conventional PSS

in the coordinated stabilization of modern large multimachine electric power systems.

Problems

4-1 Derive the co-state equation of (4-20) from (4-7) and (4-17a).

4-2 Design two different LOCs for the system of Example 3-3 by selecting

(a) $q_{\Delta\omega} = 1, q_{\Delta\delta} = 1, q_{\Delta e'_q} = 1, q_{\Delta E_{FD}} = 1$

(b) $q_{\Delta\omega} = 50, q_{\Delta\delta} = 10, q_{\Delta e'_q} = 1, q_{\Delta E_{FD}} = 1$

and find the eigenvalues of the system with and without LOC.

4-3 Find the matrix state equation of $\dot{x}_3$ of (4-54b) after eliminating x_1 and x_2.

4-4 Find the linear transformation relation between $[\Delta\psi_F, \Delta\psi_D, \Delta\psi_Q]^T$ of (4-59) and $(\Delta v_t, \Delta P_e, \Delta i_F]^T$ of (4-60a) of the 6th order system. It is suggested that (2-17) and (2-18) may be utilized for the derivation,

$$\begin{bmatrix} \Delta\psi_d \\ \Delta\psi_q \\ \Delta v_t \\ \Delta P_e \\ \Delta i_F \end{bmatrix} = \begin{bmatrix} & & ? & & \end{bmatrix} \begin{bmatrix} -\Delta i_d \\ \Delta i_F \\ \Delta i_D \\ -\Delta i_q \\ \Delta i_Q \end{bmatrix} \tag{4-4P}$$

that (4-4P) be found first, and that the following assumptions be made: $\dot{\psi}_d = 0, \dot{\psi}_q = 0, \omega \simeq 1$.

References

[1] H. Goldstein, "Classic Mechanics." Addison-Wesley, Reading, Massachusetts, 1950.

[2] D. C. White and H. H. Woodson, "Electromethanical Energy Conversion." Wiley, New York, 1959.

[3] A. P. Sage, "Optimal System Control." Prentice-Hall, Englewood Cliffs, New Jersey, 1968.

[4] M. Athans and P. L. Falb, "Optimal Control." McGraw-Hill, New York, 1966.

[5] S. S. L. Chang, "Synthesis of Optimal Control Systems." McGraw-Hill, 1961.

[6] N. N. Puri and W. A. Gruver, Optimal control design via successive approximations. *Proc. Jt. Autom. Control Conf., 1967*, 335–343, June (1967).

[7] L. N. Wedman and Yao-nan Yu, Computation techniques for the stabilization and optimization of high order power systems. *IEEE Power Ind. Comput. Appl.* (PICA) *Proc. 1969*, 324–343, May (1969).

[8] Y-N Yu and C. Siggers, Stabilization and optimal control signals for a power system. *IEEE Trans. Power Appar. Syst.* 1469–1481, July/Aug. (1971).
[9] T. F. Potter, Matrix quadratic solutions. *SIAM J. Appl. Math.* **14** (3), 496–506 (1966).
[10] C. Lanczos, "Applied Analysis." Prentice-Hall, Englewood Cliffs, New Jersey, 1961.
[11] H. A. M. Moussa and Yao-nan Yu, Optimal power system stabilization through excitation and/or governor control. *IEEE Trans. Power Appar. Syst.* 1166–1174. May/June (1972).
[12] Yao-nan Yu and H. A. M. Moussa, Optimal stabilization of multi-machine system. *IEEE Trans. Power Appar. Syst.* 1174–1182, May/June (1972).
[13] Yao-nan Yu, K. Vongsuriya, and L. N. Wedman, "Application of an optimal control theory to a power system." *IEEE Trans. Power Appar. Syst.* 55–62, Jan. (1970).
[14] B. Habibullah and Yao-nan Yu, Physically realizable wide power range optimal controllers for power systems. *IEEE Trans. Power Appar. Syst.* 1498–1506, Sept./Oct. (1974).
[15] C. M. Lim and B. S. Habibullah, Design of optimal controller for linear single-input system. *Electron. Lett.* **15** (20), 660–661 (1979).
[16] C. M. Lim and Y.-N. Yu, Output feedback optimal controller for linear single-input system. *Electron. Lett.* **18**(1), 36–38 (1982).
[17] O. I. Elgerd and C. E. Fosha, Jr., Optimum megawatt-frequency control of multi-area electric energy systems. *IEEE Trans. Power Appar. Syst.* 556–563, April (1970).
[18] C. E. Fosha, Jr. and O. I. Elgerd, The megawatt-frequency control problem: A new approach via optimal control theory. *IEEE Trans. Power Appar. Syst.* 563–577, April (1970).
[19] J. H. Anderson, The control of synchronous machine using optimal control theory. *Proc. IEEE* **90,** 25–35 (1971).
[20] E. J. Davison and N. S. Rau, The optimal output feedback control of a synchronous machine. *IEEE Trans. Power Appar. Syst.* 2123–2134, Sept./Oct. (1971).
[21] S. Narayana Iyer and B. J. Cory, Optimal control of a turbo-generator including an exciter and governor. *IEEE Trans. Power Appar. Syst.* 2142–2149, Sept./Oct. (1971).
[22] S. Elangovan and A. Kuppurajulu, Suboptimal control of power system using simplified models. *IEEE Trans. Power Appar. Syst.* 911–919, May/June (1972).
[23] J. Meisel, R. D. Barnard, and R. S. Elliott, Dynamic control of multi-machine systems based on two-step optimization over admissible trajectories. *IEEE Trans. Power Appar. Syst.* 920–927 May/June (1972).
[24] H. A. M. Moussa and Yao-nan Yu, Optimum stabilization of a power system over wide range operating conditions. *PES Summ. Meet. 1972* IEEE Pap. C72 459-6.
[25] F. L. Stromotich and R. J. Fleming, Generator damping enchancement using suboptimal control method, *PES Summ. Meet., 1972* IEEE Pap. C72 472-9 (1972).
[26] A. K. De Sarkar and N. D. Rau, Stabilization of a synchronous machine through output feedback control. *IEEE Trans. Power Appar. Syst.* 159–166, Jan./Feb. (1973).
[27] P. Subramaniam and O. P. Malik, Closed loop optimization of power systems with two-axis excitation control. *IEEE Trans. Power Appar. Syst.* 167–176, Jan./Feb. (1973).
[28] M. S. Calovic, An output feedback proportional-plus-integral regulator for automatic generation control. *PES Summ. Meet., 1973* IEEE Pap. C73 489-2 (1973).
[29] A. A. Metwally, Modelling of parallel HVDC-AC power system for dynamic studies and optimal stabilization. Ph.D. Thesis, Dept. of Electrical Engineering, University of British Columbia (1973).
[30] P. K. Dash, B. Puthal, O. P. Malik, and G. S. Hope, Transient stability and optimal control of parallel AC-DC power systems. *IEEE Trans. Power Appar. Syst.* 811–820, May/June (1976).
[31] V. H. Quintana, M. A. Hohdy, and J. H. Anderson, On the design of output feedback

excitation controllers of synchronous machines. *IEEE Trans. Power Appar. Syst.* 954–961, May/June (1976).

[32] N. A. Vovos and G. D. Galanos, Damping of power swings in AC tie lines using a parallel DC link operating at constant reactive power control. *IEEE Trans. Power Appar. Syst.* 416–425 (1979).

[33] G. E. Dawson, A dynamic test model for power system stability and control studies. Ph.D. Thesis, Dept. of Electrical Engineering, University of British Columbia (1969).

[34] Yao-nan Yu, J. H. Sawada, and M. D. Wvong, A dynamic power system model for teaching and research. *IEEE Trans. Power Appar. Syst.* 1507–1512, July/Aug. (1976).

[35] M. E. Newton and B. W. Hogg, Optimal control of a micro-alternator system. *IEEE Trans. Power Appar. Syst.* 1822–1833, Nov./Dec. (1976).

[36] J. H. Anderson, M. A. Hutchinson, W. J. Wilson, V. N. Raina, V. M. Okungwu, and V. H. Quintana, A practical application of optimal control using a micro-alternator. *IEEE Trans. Power Appar. Syst.* 729–740, May/June (1977).

[37] Q. Lu, Z.-H. Wang, and Y.T. Han, Integrated optimal control of large turbogenerator and tests on micro-alternator system. *J. Qinghua Univ.* (*China*) No. 2 (1981).

Chapter 5 Subsynchronous Resonance and Torsional Oscillations

In this chapter, a relatively new power system dynamic problem will be presented, namely, the subsynchronous torsional oscillations of the steam turbines and generator shaft. The oscillations are caused by the electrical resonance of the synchronous generator and the capacitor-compensated transmission lines. The phenomena are generally known as subsynchronous resonance or SSR [1]. Countermeasures will be presented; and one of them that is especially effective, the linear optimal excitation control, will be given in detail.

In recent years, many thermal–electric power plants are being built at coal mines far away from load centers. Bulk electric power is transmitted over long distance to the load centers by series capacitor-compensated transmission lines, eliminating the need for more parallel and uneconomical transmission lines.

A capacitor-compensated transmission line, however, is not without difficulty. When the degree of series capacitor compensation is increased, an electrical resonance of the generator, transformer, transmission line, and capacitor may develop, usually at the subsynchronous frequency. If the resonant frequency becomes complementary with that of the torsional oscillation of the mass springs of the mechanical system, they will be mutually excited, causing serious shaft and other damages.

Let us explain the SSR problem and some countermeasures first.

5-1 SUBSYNCHRONOUS RESONANCE (SSR) AND COUNTERMEASURES

Since the first two shaft failures due to SSR occurred at the Mohave station in 1970 and 1971 [2], causes of the shaft failures have been analyzed,

problems identified, and countermeasures suggested [3]. Some countermeasures are already in practice. Also reported are the methods of testing the mechanical mode natural oscillating frequencies [4, 5]. These and other important results will be highlighted in this section.

Induction Generator Mode of a Synchronous Machine

When an electrical resonance occurs in a capacitor-compensated transmission line that is connected in series with a synchronous generator, there will be a revolving field on the generator stator corresponding to the resonant frequency. When the resonant frequency f_e is below the system frequency f, or at the subsynchronous frequency, $f_e < f$, the revolving field due to the electric resonance is rotating at a subsynchronous speed. Since the generator rotor itself is mechanically rotating at the synchronous speed, the synchronous machine behaves like an induction generator with respect to the subsynchronously rotating field due to the electric resonance.

Figure 5-1 shows the well-known equivalent circuit of a three-phase induction generator, by which the per unit relative speed of the rotor with respect to the stator rotating field or the "slip" s is negative,

$$s \triangleq (f_e - f)/f_e < 0, \qquad f_e < f \tag{5-1}$$

An electrical resonance will occur when the total reactance of the capacitor-compensated line and synchronous machine becomes zero and the total resistance becomes negative.

Although Fig. 5-1 is helpful to illustrate the concept of induction generator mode of the synchronous generator, it is not sufficient for calculating the equivalent resistance and reactance of a synchronous machine. For more details, see Kilgore *et al.* [6].

Torsional Interaction

The high-, medium-, and low-pressure steam turbines, the generator, and the exciter are usually on the same shaft, constituting a linear mass-spring system. There are generally $m - 1$ modes of torsional oscillations for an m-mass-spring system, in addition to a zero mode by which the entire mass-

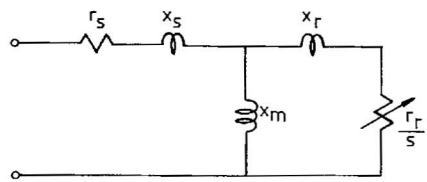

Fig. 5-1 Equivalent circuit of induction generator; $s < 0$.

spring system oscillates in unison. These oscillations usually occur at subsynchronous frequencies. They are also affected by the interaction with the electric torques of the generator and exciter.

When a torsional oscillation occurs to the turbines and generator rotating system at a subsynchronous frequency f_m, while the generator field winding itself on the rotor is rotating at an average speed corresponding to the system frequency f, there will be voltages and currents induced in the generator armature three-phase winding at frequencies $f \pm f_m$. Should the induced current of the subsynchronous frequency $f - f_m$ coincide or be very close to an electric resonance frequency f_e of the generator and transmission system,

$$f - f_m = f_e \tag{5-2}$$

the torsional oscillation and the electrical resonance will be mutually excited or reinforced resulting in SSR. In such a case, the electrical resonance acts as a negative damping to the torsional oscillation, and the torsional oscillation acts as a negative resistance to the electrical resonance, which can be proved by computer simulation test.

Natural Oscillating Frequencies

In Table 5-1 the electrical system natural frequencies f_e of a rather complicated system under certain operating conditions are listed in column 1 and frequencies of the corresponding torsionals $f - f_m$, not the torsional frequencies themselves f_m, in column 2. The five torsionals f_m are identified as modes 1, 2, 3, 4, and 5 [3]. There is also mode zero by which all mass springs oscillate in unison. Examination of Table 5-1 indicates that torsional mode 1 is most vulnerable to SSR, since the electrical natural frequency 44.5 Hz of column 1 and the corresponding torsional 44.2 Hz of column 2 are so close.

Scanning programs are written to find the electrical natural frequencies of complicated electrical system. Methods of testing the torsional natural frequencies have developed as:

(1) engaging and disengaging the turning gears of the turbines and generator repeatedly;

(2) synchronizing the generator to the system manually and deliberately with a small phase angle mismatch;

(3) varying the frequency of excitation of the generator to excite the torsionals one by one;

(4) inserting and bypassing some series capacitor modules repeatedly.

Table 5-1

Natural Oscillating Frequencies[a]

Electrical system natural frequencies f_e (Hz)	Corresponding torsionals $f - f_m$ (Hz)	Mode
44.5		
	44.2	1
43.5		
	38.8	2
	34.0	3
30.7		
28.3		
	26.7	4
25.5		
10.5		
10.0		
	6.8	5

[a] Courtesy of IEEE, © 1977, [3].

The third method is probably the best, giving the most accurate results. For details, see Walker *et al.* [4, 5].

Countermeasures of SSR

To prevent SSR and to protect the system, many countermeasures of SSR have been developed.

Poleface Amortisseurs. Poleface amortisseurs have the effect of decreasing induction generator equivalent rotor resistance.

Static Blocking Filters. To block the electric resonance current of the transmission system from entering the generator, which may interact with the torsional modes, high-Q parallel resonance filters are designed and tuned to the torsional mode natural frequencies, and inserted between the wye-connected high voltage winding of the step-up transformer and the ground as shown in Fig. 5-2.

When electrical resonance corresponding to any one torsional mode natural frequency begins to develop, the impedance of one of the mode filters will become extremely large to prevent further growth of the electric resonance current, but will be small at other frequencies. In Fig. 5-2, four mode filters are connected in series. There is little likelihood that mode 5 of Table 5-1, which corresponds to the highest frequency of f_m, will be excited by an

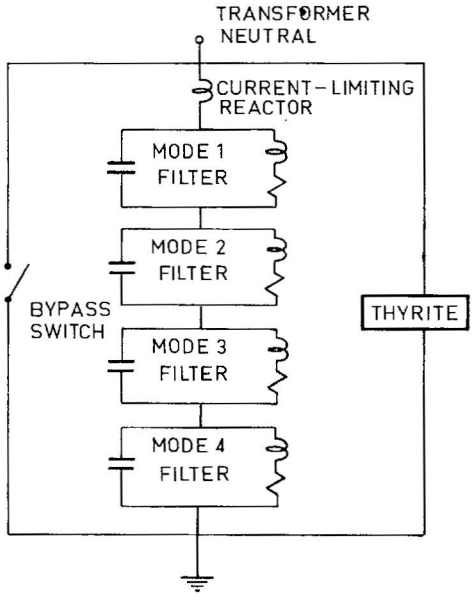

Fig. 5-2 Schematic of static blocking filters (From [3], courtesy of IEEE, © 1977.)

electrical resonance. There are also current limiter and overvoltage protection of the system as shown in Fig. 5-2 [3].

The main difficulty in the blocking filter design is to maintain constant filter parameter values in an environment of drastic changes in temperature between day and night. It is also very expensive because the filter units are designed for high voltage and large current, and the insulation level of the transformer must be increased.

Excitation Control. The excitation control of SSR, if workable, will be far less expensive than using static filters, since it is the low-energy side that is being controlled. There is great difficulty with the phase compensation PSS type of control, because several controls designed for individual torsional modes of different frequencies will interfere with each other. However, all torsional modes including mode 0 of a power system over a wide range of capacitor compensation can be stabilized if a linear optimal excitation control (LOEC) is designed. The LOEC design technique and test results will be presented in subsequent sections of this chapter.

Dual-Gap Flashing. To protect the generating unit itself from shaft damage due to SSR in a system with large capacitor compensation, a dual-gap flashing scheme of capacitors has been developed. Air gaps parallel to the capacitor will flash over at a lower current level of about 2.2 per unit

to reduce a transient torque impact to the generator shaft, and the current level will be reset each time after flashing to about 3.0–3.5 per unit to allow a current decay to the level for successful reinsertion of the series capacitor [3].

Other SSR Countermeasures. Many other SSR countermeasures have been developed: the dynamic filter [11], the reactive power control [12], the damping of SSR by an HVDC link [13], the thyristor control of the series capacitor [14], and many others. For details, see the references.

The Concept of Shaft Life

The life expectancy of a turbine-generator shaft depends on not only the magnitude of the transient torque but also the fatigue of the steel shaft [3]. Figure 5-3 shows the relation between the oscillating shaft torque and the loss of shaft life. Level A is the infinite-life level; any oscillating torque magnitude (one-half peak to peak) below this level for any length of time will not damage the shaft at all. Level B is the once-in-a-lifetime level; the entire shaft life will be lost immediately for any oscillating torque magnitude equal to or above this level. Between A and B, there will be a percentage life expenditure corresponding to the oscillating shaft torque each time; the effect is cumulative, and the life will be completely lost when the accumulation reaches 100%.

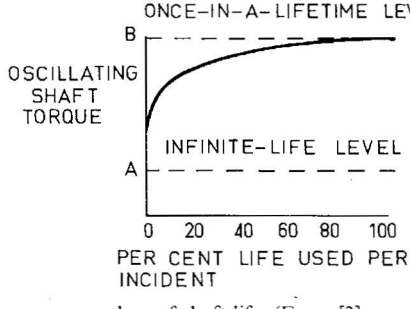

Fig. 5-3 Shaft torque versus loss of shaft life. (From [3], courtesy of IEEE, © 1977.)

Summary of Section 5-1

An introduction has been given to the SSR problem and countermeasures. It includes the induction generator concept of the synchronous generator during SSR, the torsional interaction of the electrical resonance and torsional

oscillations, the methods of testing torsional mode natural frequencies, and various countermeasures. Also included is the concept of shaft life.

SSR phenomena are relatively new and the countermeasures are still evolving. One of the most effective and also the least expensive countermeasures of SSR, namely, the linear optimal excitation control (LOEC) of SSR, will be presented in subsequent sections.

5-2 A UNIFIED ELECTRICAL AND MECHANICAL MODEL FOR SSR STUDIES

Although the induction generator and torsional interaction concepts lend a clear insight into SSR phenomena, it might not be sufficiently accurate for analysis. Since SSR constitutes the electrical resonance, the torsional oscillation, and the interaction between them, a single, unified, and complete electrical and mechanical system model for SSR study is very desirable. The SSR system model should include the mass-spring system of turbines, generator, and exciter, the turbine torques and governor, the capacitor-compensated transmission line, the synchronous generator, and the excitation system.

Basic Equations of the Mass-Spring System

Consider a steam turbine, generator, and exciter set. Let the tandem-compound, single-reheat steam turbines be chosen as an example. A schematic of the mass-spring system is shown in Fig. 5-4. In the figure there are six rotating masses; the high-pressure turbine (HP), the medium-pressure turbine (IP), the two low-pressure turbines (LPA and LPB), the generator (GEN), and the exciter (EX), all on one shaft. Also, sections of shaft behave like springs and together they constitute a linear six-mass-spring system.

Assume an inertia constant M for each rotating mass and a stiffness K for each shaft section. The torsional relation of the ith mass-spring system may be depicted as in Fig. 5-5. In the figure the shaft torque on the left and the external torque input T_i are in one direction; and the accelerating torque $M_i\dot{\omega}_i$, the damping torque $D_i\omega_i$ on the mass, and the shaft torque on the right are in the opposite direction. Therefore, the torque equilibrium of the ith-mass-spring system in linear form becomes

$$M_i\Delta\dot{\omega}_i = \Delta T_i - D_i\,\Delta\omega_i + K_{i-1,i}(\Delta\theta_{i-1} - \Delta\theta_i) - K_{i,i+1}(\Delta\theta_i - \Delta\theta_{i+1}) \quad (5\text{-}2)$$

Fig. 5-4 A linear six-mass-spring turbine-generator system.

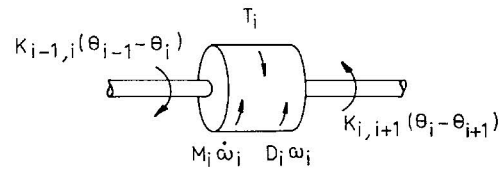

Fig. 5-5 The ith-mass-spring system.

where

$$K_{i-1,i}|_{i=1} = 0, \qquad K_{i,i+1}|_{i=m} = 0, \qquad i = 1, 2, \ldots, m \tag{5-2a}$$

Note that there is no torsional torque at the two extreme ends of the shaft, and T_i becomes negative if it is an electric torque output.

When Eq. (5-2) is applied to the linear six-mass-spring system of Fig. 5-4, the turbines, generator, and exciter from left to right are identified, respectively, by subscripts H, I, A, B, G, and X, and the shaft stiffness by K_{HI}, K_{IA}, etc., the state equations of the linear six-mass-spring system become

$$\begin{aligned}
\Delta\dot{\omega}_{\mathrm{H}} &= \frac{1}{M_{\mathrm{H}}}\left[\Delta T_{\mathrm{H}} - D_{\mathrm{H}}\,\Delta\omega_{\mathrm{H}} - K_{\mathrm{HI}}(\Delta\theta_{\mathrm{H}} - \Delta\theta_{\mathrm{I}})\right] \\
\Delta\dot{\theta}_{\mathrm{H}} &= \omega_{\mathrm{b}}\,\Delta\omega_{\mathrm{H}} \\
\Delta\dot{\omega}_{\mathrm{I}} &= \frac{1}{M_{\mathrm{I}}}\left[\Delta T_{\mathrm{I}} - D_{\mathrm{I}}\,\Delta\omega_{\mathrm{I}} + K_{\mathrm{HI}}(\Delta\theta_{\mathrm{H}} - \Delta\theta_{\mathrm{I}}) - K_{\mathrm{IA}}(\Delta\theta_{\mathrm{I}} - \Delta\theta_{\mathrm{A}})\right] \\
\Delta\dot{\theta}_{\mathrm{I}} &= \omega_{\mathrm{b}}\,\Delta\omega_{\mathrm{I}} \\
\Delta\dot{\omega}_{\mathrm{A}} &= \frac{1}{M_{\mathrm{A}}}\left[\Delta T_{\mathrm{A}} - D_{\mathrm{A}}\,\Delta\omega_{\mathrm{A}} + K_{\mathrm{IA}}(\Delta\theta_{\mathrm{I}} - \Delta\theta_{\mathrm{A}}) - K_{\mathrm{AB}}(\Delta\theta_{\mathrm{A}} - \Delta\theta_{\mathrm{B}})\right] \\
\Delta\dot{\theta}_{\mathrm{A}} &= \omega_{\mathrm{b}}\,\Delta\omega_{\mathrm{A}} \\
\Delta\dot{\omega}_{\mathrm{B}} &= \frac{1}{M_{\mathrm{B}}}\left[\Delta T_{\mathrm{B}} - D_{\mathrm{B}}\,\Delta\omega_{\mathrm{B}} + K_{\mathrm{AB}}(\Delta\theta_{\mathrm{A}} - \Delta\theta_{\mathrm{B}}) - K_{\mathrm{BG}}(\Delta\theta_{\mathrm{B}} - \Delta\delta)\right] \\
\Delta\dot{\theta}_{\mathrm{B}} &= \omega_{\mathrm{b}}\,\Delta\omega_{\mathrm{B}} \\
\Delta\dot{\omega} &= \frac{1}{M_{\mathrm{G}}}\left[-\Delta T_{\mathrm{e}} - D_{\mathrm{G}}\,\Delta\omega + K_{\mathrm{BG}}(\Delta\theta_{\mathrm{B}} - \Delta\delta) - K_{\mathrm{GX}}(\Delta\delta - \Delta\theta_{\mathrm{X}})\right] \\
\Delta\dot{\delta} &= \omega_{\mathrm{b}}\,\Delta\omega \\
\Delta\dot{\omega}_{\mathrm{X}} &= \frac{1}{M_{\mathrm{X}}}\left[-\Delta T_{\mathrm{ex}} - D_{\mathrm{X}}\,\Delta\omega_{\mathrm{X}} + K_{\mathrm{GX}}(\Delta\delta - \Delta\theta_{\mathrm{X}})\right] \\
\Delta\dot{\theta}_{\mathrm{X}} &= \omega_{\mathrm{b}}\,\Delta\omega_{\mathrm{X}}
\end{aligned} \tag{5-3}$$

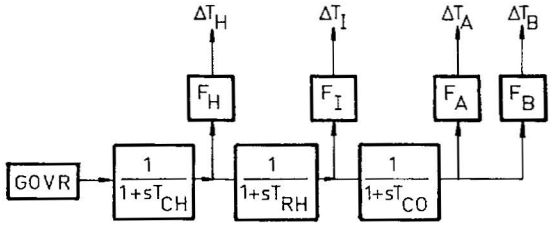

Fig. 5-6 Transfer functions of steam turbines.

where the ω's are the speeds in per unit value, ω_b is the base speed or $2\pi f$ rad/s, the θ's are the mechanical angles in mechanical radians, and δ is the electrical angle in electrical radians, with θ_G and δ being equal for two-pole machines. Note that the generator electric torque output ΔT_e and the exciter electric torque output ΔT_{ex} are negative inputs, and (5-3) is a set of linearized equations. For eigenvalue analysis and for LOEC design, the nonstate variables ΔT_e and ΔT_{ex} must be eliminated.

Turbine Torque and Governor System

The transfer functions of steam turbines are shown in Fig. 5-6 [15]. There are four turbine torques with a total output of ΔT_m,

$$\Delta T_H + \Delta T_I + \Delta T_A + \Delta T_B = \Delta T_m \tag{5-4}$$

All turbine torques are proportional, with each turbine contributing a fraction, and the sum of the fractions is

$$F_H + F_I + F_A + F_B = 1 \tag{5-5}$$

There are also three time constants due to the steam flow, T_{CH} in the chamber in front of the high pressure turbine, T_{RH} in the reheater between the high- and medium-pressure turbines, and T_{CO} in the crossover connection between the medium- and low-pressure turbines.

A two-time-constant governor is assumed in Fig. 5-7 where a denotes the speed relay position and g the governor opening.

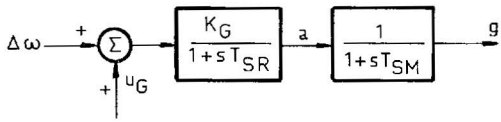

Fig. 5-7 A two-time-constant governor.

Therefore, three differential equations can be written for the turbine torques

$$\begin{aligned}(1 + sT_{CH})\,\Delta T_H &= F_H g \\ (1 + sT_{RH})\,\Delta T_I &= (F_I/F_H)\,\Delta T_H \\ (1 + sT_{CO})\,\Delta T_A &= (F_A/F_I)\,\Delta T_I \\ \Delta T_B &= (F_B/F_A)\,\Delta T_A\end{aligned} \tag{5-6}$$

and two for the governor

$$\begin{aligned}(1 - sT_{SR})a &= K_G(\Delta\omega + u_G), \qquad \Delta\omega \triangleq \omega_{REF} - \omega_m \\ (1 + sT_{SM})g &= a\end{aligned} \tag{5-7}$$

where a supplementary governor control is included in (5-7) as u_G. Both (5-6) and (5-7) can be written in the time domain in the standard state variable form. Note also that the governor gain K_G in (5-7) is the reciprocal of speed regulation which is usually set at 4 to 5% for a full-load to no-load variation.

The Capacitor-Compensated Transmission Line

A series capacitor-compensated transmission line may be represented by an RLC circuit as in Fig. 5-8. Let the total resistance and total reactance, respectively, of the line and transformer be R and L, the series capacitance be C, the voltage across the capacitor be e_C, the voltage per phase at the generator terminal be v_t, that in front the capacitance be v_C, and that at the infinite bus be v_0. The basic equations are

$$\begin{aligned}[i]_{abc} &= p[C][e_C]_{abc} \\ [v_t]_{abc} &= [R + pL][i]_{abc} + [e_C]_{abc} + [v_0]_{abc}\end{aligned} \tag{5-8}$$

where

$$\begin{aligned}[i]_{abc} &= [i_a, i_b, i_c]^T, \qquad [e_C]_{abc} = [e_a, e_b, e_c]^T \\ [v_t]_{abc} &= [v_a, v_b, v_c]^T, \qquad [v_0]_{abc} = [v_{0a}, v_{0b}, v_{0c}]^T \\ [R] &= R[U], \qquad [L] = L[U], \qquad [C] = C[U],\end{aligned} \tag{5-9}$$

where R, L, and C are scalars and $[U]$ is a unit matrix.

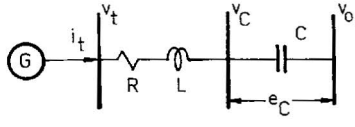

Fig. 5-8 A capacitor-compensated transmission line.

Since the line and transformer are connected in series with the generator, the line current and voltage also must be transformed into d-q components, resulting in

$$\begin{bmatrix}\Delta i_d\\ \Delta i_q\end{bmatrix}=\frac{1}{\omega_b X_C}\begin{bmatrix}\Delta \dot{e}_{cd}\\ \Delta \dot{e}_{cq}\end{bmatrix}+\frac{1}{X_C}\begin{bmatrix}0 & -1\\ 1 & 0\end{bmatrix}\begin{bmatrix}\Delta e_{cd}\\ \Delta e_{cq}\end{bmatrix} \tag{5-10}$$

and

$$\begin{bmatrix}\Delta v_d\\ \Delta v_q\end{bmatrix}=\begin{bmatrix}R & -X\\ X & R\end{bmatrix}\begin{bmatrix}\Delta i_d\\ \Delta i_q\end{bmatrix}+\frac{X}{\omega_b}\begin{bmatrix}\Delta \dot{i}_d\\ \Delta \dot{i}_q\end{bmatrix}+\begin{bmatrix}\Delta e_{cd}\\ \Delta e_{cq}\end{bmatrix}+\begin{bmatrix}\Delta v_{0d}\\ \Delta v_{0q}\end{bmatrix} \tag{5-11}$$

In the foregoing equations, Δe_{cd} and Δe_{cq} of (5-10) are chosen as the state variables, and Δv_d and Δv_q of (5-11) are used to eliminate Δv_t. The coordinate transformation of the capacitor current will be shown in Example 5-1, and that of the voltage will be left as an exercise.

Example 5-1. Transform $[i]_{abc}$ of (5-8) into d-q components.

Solution: Let the transformation matrices be

$$[T]=\begin{array}{c}\\ a\\ b\\ c\end{array}\begin{array}{c}\begin{array}{ccc}0 & d & q\end{array}\\ \begin{bmatrix}1 & C' & -S'\\ 1 & C'' & -S''\\ 1 & C''' & -S'''\end{bmatrix}\end{array},\qquad [T]^{-1}=\frac{2}{3}\begin{array}{c}\\ 0\\ d\\ q\end{array}\begin{array}{c}\begin{array}{ccc}a & b & c\end{array}\\ \begin{bmatrix}\frac{1}{2} & \frac{1}{2} & \frac{1}{2}\\ C' & C'' & C'''\\ -S' & -S'' & -S'''\end{bmatrix}\end{array} \tag{5-12}$$

where

$$\begin{aligned} C' &\triangleq \cos\theta, & C'' &\triangleq \cos(\theta-120^\circ), & C''' &\triangleq \cos(\theta-240^\circ)\\ S' &\triangleq \sin\theta, & S'' &\triangleq \sin(\theta-120^\circ), & S''' &\triangleq \sin(\theta-240^\circ)\end{aligned} \tag{5-12a}$$

Here Park's original transformation matrix is denoted by $[T]$, abbreviations C', C'', etc., are introduced for conciseness, and C' is used to distinguish it from the series capacitance C. Since

$$\begin{aligned}[T]^{-1}[T] &= [U]\\ [T]^{-1}[C][T] &= [T]^{-1}C[U][T]=[C]\end{aligned} \tag{5-13}$$

the capacitor current components of (5-8) in d-q coordinates become

$$\begin{aligned}[i]_{0dq} &= [T]^{-1}[i]_{abc}=[T]^{-1}p[C][T][e_C]_{0dq}\\ &= [T]^{-1}[C][T]p[e_C]_{0dq}+[T]^{-1}\frac{\partial}{\partial\theta}[[C][T]]\cdot p\theta\cdot[e_C]_{0dq}\\ &= [C]p[e_C]_{0dq}\end{aligned}$$

$$+\tfrac{2}{3}C\begin{bmatrix}\frac{1}{2} & \frac{1}{2} & \frac{1}{2}\\ C' & C'' & C'''\\ -S' & -S'' & -S'''\end{bmatrix}\begin{bmatrix}0 & -S' & -C'\\ 0 & -S'' & -C''\\ 0 & -S''' & -C'''\end{bmatrix}\cdot p\theta\cdot[e_C]_{0dq}$$

$$=[C]p[e_C]_{0dq}+C\begin{bmatrix}0 & 0 & 0\\ 0 & 0 & -1\\ 0 & 1 & 0\end{bmatrix}\cdot p\theta\cdot[e_C]_{0dq} \tag{5-14}$$

When the synchronous machine equations are written in per unit value, and $2\pi f$ is chosen as the base speed, then

$$p\theta=\omega \tag{5-15}$$

which is approximately 1 per unit of value. In other words, when p is in per $2\pi f$ second instead of per second, we shall have

$$p\triangleq\frac{1}{\omega_b}\frac{d}{dt},\qquad px=\frac{1}{\omega_b}\dot{x} \tag{5-15a}$$

where t is in seconds. Finally, since C in per unit value is the reciprocal of X_C in per unit value, we shall have

$$\begin{bmatrix}\Delta i_d\\ \Delta i_q\end{bmatrix}=\frac{1}{\omega_b X_C}\begin{bmatrix}\Delta\dot{e}_{cd}\\ \Delta\dot{e}_{cq}\end{bmatrix}+\frac{1}{X_C}\begin{bmatrix}0 & -1\\ 1 & 0\end{bmatrix}\begin{bmatrix}\Delta e_{cd}\\ \Delta e_{cq}\end{bmatrix} \tag{5-10}$$

and there will be no zero-axis component for balanced three-phase operation.

The Synchronous Generator

Assume that there is a second damper winding S on the q axis, with a voltage equation

$$p\psi_S=\dot{\psi}_S/\omega_b=-r_S i_S \tag{5-16}$$

in addition to Eqs. (2-4). We have now two rotor windings per axis; D and F on the d axis and Q and S on the q axis. For the SSR study, however, it is more convenient to choose the generator currents, instead of the flux linkages, as the state variables. Therefore, the synchronous generator voltage

equations in linear form become

$$\frac{1}{\omega_b}(-x_d\,\Delta\dot{i}_d + x_{md}\,\Delta\dot{i}_F + x_{md}\,\Delta\dot{i}_D)$$
$$= (-x_q\,\Delta i_q + x_{mq}\,\Delta i_Q + x_{mq}\,\Delta i_S) + \psi_{q0}\,\Delta\omega + r_a\,\Delta i_d + \Delta v_d$$
$$\frac{1}{\omega_b}(-x_q\,\Delta\dot{i}_q + x_{mq}\,\Delta\dot{i}_Q + x_{mq}\,\Delta\dot{i}_S)$$
$$= -(-x_d\,\Delta i_d + x_{md}\,\Delta i_F + x_{md}\,\Delta i_D) - \psi_{d0}\,\Delta\omega + r_a\,\Delta i_q + \Delta v_q$$
$$\frac{1}{\omega_b}(-x_{md}\,\Delta\dot{i}_d + x_F\,\Delta\dot{i}_F + x_{md}\,\Delta\dot{i}_D) = -r_F\,\Delta i_F + \Delta v_F \tag{5-17}$$
$$\frac{1}{\omega_b}(-x_{md}\,\Delta\dot{i}_d + x_{md}\,\Delta\dot{i}_F + x_D\,\Delta\dot{i}_D) = -r_D\,\Delta i_D$$
$$\frac{1}{\omega_b}(-x_{mq}\,\Delta\dot{i}_q + x_Q\,\Delta\dot{i}_Q + x_{mq}\,\Delta\dot{i}_S) = -r_Q\,\Delta i_Q$$
$$\frac{1}{\omega_b}(-x_{mq}\,\Delta\dot{i}_q + x_{mq}\,\Delta\dot{i}_Q + x_S\,\Delta\dot{i}_S) = -r_S\,\Delta i_S$$

The initial flux linkages from the steady state are

$$\psi_{d0} = (x_{md}i_{F0} - x_d i_{d0})/\omega_0 = (E - x_d i_{d0})/\omega_0$$
$$\psi_{d0} = x_q i_{q0}/\omega_0, \qquad \omega_0 = 1 \tag{5-18}$$

The Excitation System

A two-time-constant excitation system is assumed in Fig. 5-9. The system equations may be written

$$(1 + sT_A)\,\Delta v_R = K_A(\Delta v_t + u_E)$$
$$(1 + sT_E)\,\Delta E_{FD} = \Delta v_R \tag{5-19}$$

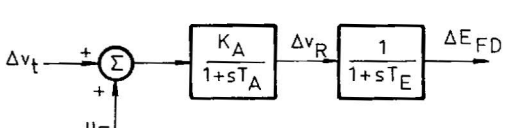

Fig. 5-9 A two-time-constant excitation system.

where

$$E_{FD} \triangleq x_{md} v_F / r_F, \qquad \Delta v_t \triangleq v_{REF} - v_t \tag{5-19a}$$

State Variable Equations and Nonstate Variables

The complete system equations for SSR study will be written in the standard state variable form

$$[\dot{x}] = [A][x] + [B][u] \tag{4-5}$$

which can be partitioned into the mechanical and electrical parts as

$$\begin{bmatrix} \dot{x}_M \\ \dot{x}_E \end{bmatrix} = \begin{bmatrix} A_{MM} & A_{ME} \\ A_{EM} & A_{EE} \end{bmatrix} \begin{bmatrix} x_M \\ x_E \end{bmatrix} + [B] \begin{bmatrix} u_G \\ u_E \end{bmatrix} \tag{5-20}$$

where

$$[x] = [x_M, x_E]^T, \qquad [u] = [u_G, u_E]^T \tag{5-20a}$$

u_G vanishes if only the excitation loop is used for control.

There are 17 mechanical system equations, 12 of (5-3), 3 of (5-6), and 2 of (5-7); and the state variables are

$$\begin{aligned} [x_M] = [&\Delta\omega_H, \Delta\theta_H, \Delta\omega_I, \Delta\theta_I, \Delta\omega_A, \Delta\theta_A, \Delta\omega_B, \Delta\theta_B, \\ &\Delta\omega, \Delta\delta, \Delta\omega_X, \Delta\theta_X; \Delta T_H, \Delta T_I, \Delta T_A; a, g]^T \end{aligned} \tag{5-21}$$

Equations of (5-3) are already in the standard state variable form and Eqs. (5-6) and (5-7) can be readily written in such a form. There are, however, two nonstate variables ΔT_e and ΔT_{ex} that must be eliminated The exciter torque ΔT_{ex} is very difficult to calculate, but relatively small, and may be neglected. The general electric torque ΔT_e can be calculated as follows. Since

$$\begin{aligned} T_e &= i_q \psi_d - i_d \psi_q \\ &= (1/\omega_0)[i_q(-x_d i_d + x_{md} i_F + x_{md} i_D) - i_d(-x_q i_q + x_{mq} i_Q + x_{mq} i_S)] \end{aligned} \tag{5-22}$$

we have

$$\begin{aligned} \Delta T_e = (1/\omega_0)[&-(x_d - x_q) i_{q0}\, \Delta i_d + (x_{md} i_{F0} - (x_d - x_q) i_{d0})\, \Delta i_q \\ &+ x_{md} i_{q0}(\Delta i_F + \Delta i_D) - x_{mq} i_{d0}(\Delta i_Q + \Delta i_S)] \end{aligned} \tag{5-23}$$

There are 12 electrical system equations, 4 of (5-10) and (5-11), 6 of (5-17), and 2 of (5-19), but (5-11) will be used to eliminate Δv_t. The remaining 10 electrical state variables are

$$[x_E] = [\Delta e_{cd}, \Delta e_{cq}; \Delta i_d, \Delta i_q, \Delta i_F, \Delta i_D, \Delta i_Q, \Delta i_S; \Delta v_R, \Delta E_{FD}]^T \tag{5-24}$$

and the nonstate variables Δv_t of (5-19) can be eliminated from

$$\begin{aligned} v_t^2 &= v_d^2 + v_q^2 \\ \Delta v_t &= (v_{d0}/v_{t0})\,\Delta v_d + (v_{q0}/v_{t0})\,\Delta v_q \end{aligned} \tag{5-25}$$

where Δv_d and Δv_q can be found from (5-11),

$$\begin{aligned} \Delta v_d &= R\,\Delta i_d - X\,\Delta i_q + (X/\omega_b)\,\Delta \dot{i}_d + \Delta e_{cd} + \Delta v_{0d} \\ \Delta v_q &= X\,\Delta i_d + R\,\Delta i_q + (X/\omega_b)\,\Delta \dot{i}_q + \Delta e_{cq} + \Delta v_{0q} \end{aligned} \tag{5-26}$$

We shall continue to eliminate Δv_{0d} and Δv_{0q}, the d and q infinite-bus voltages. Let the angle between e_q and v_0 be defined as δ_0 as shown in Fig. 5-10. Then we have

$$\begin{aligned} v_{0d} &= v_0 \sin\delta, & v_{0q} &= v_0 \cos\delta \\ \Delta v_{0d} &= v_0 \cos\delta_0\,\Delta\delta, & \Delta v_{0q} &= -v_0 \sin\delta\,\Delta\delta \end{aligned} \tag{5-27}$$

Finally, the electrical system state equations can be written first in the form of

$$[D_E][\dot{x}_E] = [C_M][x_M] + [C_E][x_E] + [B_E]u_E \tag{5-28a}$$

and then

$$[\dot{x}_E] = [D_E]^{-1}[C_M][x_M] + [D_E]^{-1}[C_E][x_E] + [D_E]^{-1}[B_E]u_E \tag{5-28b}$$

which corresponds to the second row of (5-20).

The complete electrical and mechanical model of a one-machine, infinite-bus system for SSR study is a 27th-order system.

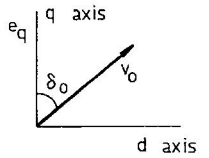

Fig. 5-10 Defining δ_0.

Summary of Section 5-2

In this section a single, unified, and complete electrical and mechanical model of a one-machine, infinite-bus system for SSR study is derived. The effect of the mass-spring system, the turbine torques and governor, the capacitor-compensated transmission line, the generator, the excitation and

control, and the interaction of the electrical and mechanical systems are all included in one model. The model will be used for SSR analysis and control design in subsequent sections.

5-3 FEASIBILITY OF EXCITATION CONTROL AND OTHER STUDIES

The single, unified, and complete electrical and mechanical system model for SSR study is used to investigate (a) the capacitor compensation effect on SSR, (b) the phase-compensation PSS effect on SSR, and (c) the feasibility of linear excitation control of SSR [16]. Important results are presented in this section.

A Functional Block Diagram of the Complete SSR System

A functional block diagram of the complete SSR system may be drawn as in Fig. 5-11. The steam turbine torques, controlled by the governor, are acting on the mass-spring system. The generator receives the mechanical torque from the turbines through the shaft, and also receives the excitation from the excitation system that controls the electric power output of the generator. The generator is connected to the capacitor-compensated transmission line, which corresponds to the First Bench Mark Model of IEEE [17].

The First Bench Mark Model recommended by an IEEE committee for SSR study is shown in Fig. 5-12, which is a one-machine, infinite-bus system. From the generator on the left, there are the transformer, the blocking filter, the line impedance, the series capacitor with dual gap protection, and the infinite bus. Also shown in the figure are two fault reactances x_F at two different locations. A fault may be assumed either at bus A or bus B, but not simultaneously.

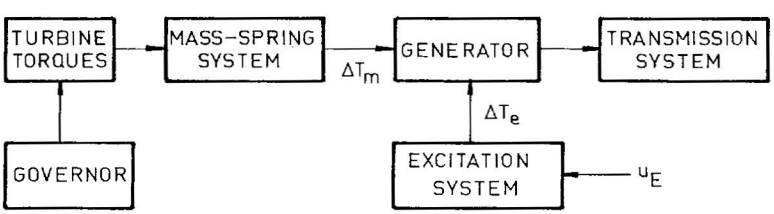

Fig. 5-11 A functional block diagram of the complete SSR system.

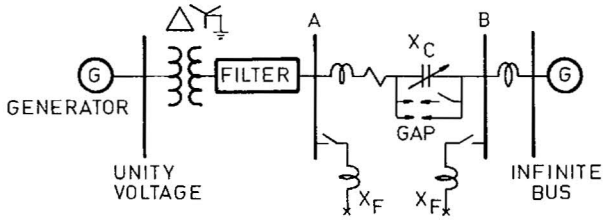

Fig. 5-12 The First Bench Mark Model of IEEE. (From [17], courtesy of IEEE, © 1977.)

System Data

For the SSR studies in the subsequent sections, most data are taken from the First Bench Mark Model and other references.

Inertia and Stiffness Constants. They are given in [17] as

$$\begin{aligned} M_H &= 0.185794 \\ M_I &= 0.311178 \\ M_A &= 1.717340 \\ M_B &= 1.768430 \\ M_G &= 1.736990 \\ M_X &= 0.068433 \end{aligned} \qquad \begin{aligned} K_{HI} &= 19.303 \\ K_{IA} &= 34.929 \\ K_{AB} &= 52.038 \\ K_{BG} &= 70.858 \\ K_{GX} &= 2.822 \end{aligned}$$

Turbine Torques and Governor. Turbine torque and governor parameters are chosen from another IEEE committee report [15] as

$$F_H = 0.3, \quad F_I = 0.26, \quad F_A = 0.22, \quad F_B = 0.22$$
$$T_{CH} = 0.3, \quad T_{RH} = 7.0, \quad T_{CO} = 0.2$$
$$K_G = 25, \quad T_{SR} = 0.2, \quad T_{SM} = 0.3$$

Transformer and Transmission Line. The transformer and transmission line parameters according to [17] are

$$R_T = 0.01, \quad X_T = 0.14, \quad R_L = 0.02, \quad X_L = 0.56$$

The capacitor compensation is expressed in terms of the X_C/X_L ratio, and the following ratios are chosen for various SSR studies:

$$X_C/X_L = 0.1, 0.2, 0.3, \ldots, 0.9$$

The Synchronous Generator. The synchronous generator parameter values in [17] are given in terms of x_d, x'_d, etc., but they can be converted into

the equivalent circuit parameter values according to [18] as

$$x_{md} = 1.660, \quad x_d = 1.790, \quad x_F = 1.700, \quad x_D = 1.666$$
$$x_{mq} = 1.580, \quad x_q = 1.710, \quad x_Q = 1.695, \quad x_S = 1.825$$
$$r_F = 0.001, \quad r_D = 0.0037, \quad r_Q = 0.0053, \quad r_S = 0.0182$$
$$r_a = 0.0015$$

Exciter and Voltage Regulator. A fast-response excitation system is assumed and the following data are chosen from reference [19]:

$$K_E = 50, \quad T_E = 0.002, \quad T_A = 0.01$$

A Power System Stabilizer. A phase-compensation PSS with $\Delta\omega$ as the input is designed and the parameter values are

$K_C = 20$, $T_1 = 0.125$, $T_2 = 0.05$ (comp. block), $T = 3.0$ (reset block)

The Initial Operating Conditions. The initial operating conditions of the synchronous generator in steady state are

$$P_e = 0.9, \quad v_t = 1.05, \quad PF = 0.9 \text{ (lag)}$$

Capacitor Compensation Effect on SSR

Eigenvalue analysis is employed to find the capacitor compensation effect on SSR. Eigenvalue loci of the entire system for $X_C/X_L = 0.1$–0.9 per unit in 0.1 steps are plotted in reference [16], and some results are listed in Table 5-2.

The technique of identifying eigenvalues with system components has been explained in Section 4-7, Chapter 4, in modeling an ac–dc system.

The capacitor compensation effects on an SSR system are as follows:

(a) There is little change in λ_H, the eigenvalue pair corresponding to the high-pressure turbine mass-spring system, and it always has a negative real part.

(b) There are unstable eigenvalue modes of other mass-spring systems, like λ_G at 0.2 per unit compensation, λ_I at 0.3 and 0.5 per unit compensation, etc. The possibility of existence of two unstable eigenvalue modes simultaneously with the mass-spring system increases with an increase of capacitor compensation.

(c) All other eigenvalue modes are stable: the capacitor compensation λ_C, the generator windings λ_{dq}, λ_D, ..., λ_F, the excitation system λ_{VR} and λ_{Efd}, the turbine torque transfer function λ_{CH}, λ_{RH} and λ_{CO}, and the governor λ_{GOVR}.

Table 5-2

Eigenvalues of the 27th-Order System

	X_C/X_L		
	0.2	0.3	0.5
λ_{H1}	$-0.1817 \pm j298.18$	$-0.1818 \pm j298.18$	$-0.1818 \pm j298.18$
λ_1	$-0.2104 \pm j203.20$	$+0.1541 \pm j204.35$	$+0.1560 \pm j202.68$
λ_A	$-0.2266 \pm j160.66$	$-0.2496 \pm j160.72$	$+0.9100 \pm j161.42$
λ_X	$-0.6679 \pm j127.03$	$-0.6706 \pm j127.03$	$-0.6799 \pm j127.08$
λ_B	$-0.2660 \pm j99.13$	$-0.2877 \pm j99.21$	$-0.3545 \pm j99.79$
λ_G	$+0.0415 \pm j8.0234$	$-0.0479 \pm j8.4801$	$-0.2674 \pm j9.5459$
λ_C	$-6.072 \pm j241.01$	$-6.198 \pm j209.20$	$-6.839 \pm j161.47$
$\lambda_{d,q}$	$-6.980 \pm j512.30$	$-7.022 \pm j542.80$	$-7.080 \pm j591.15$
λ_D	-2.020	-1.983	-1.907
λ_Q	-25.40	-25.41	-25.42
λ_S	-32.58	-31.92	-32.81
λ_F	-8.568	-8.440	-8.128
λ_{VR}	-102.0	-101.9	-101.8
λ_{Efd}	-500.0	-500.0	-500.0
λ_{CH}	-2.927	-3.034	-3.334
λ_{RH}	-0.1416	-0.1417	-0.1418
λ_{CO}	-4.668	-4.616	-4.050
λ_{GOVR}	$-4.704 \pm j0.7567$	$-4.673 \pm j0.6269$	$-4.794 \pm j0.3198$

(d) Other findings are that the oscillating frequency of $\lambda_{d,q}$ increases with the degree of capacitor compensation, but is usually above the synchronous frequency; whereas the frequency of λ_C decreases with the increase of compensation, which is below the synchronous frequency and hence may excite the torsional oscillation modes.

PSS Effect on SSR

The PSS adds another eigenvalue pair to the system. The PSS effect on λ_G of the mass-spring system is significant. The λ_G eigenvalue pair that has the lowest oscillating frequency of about 9 rad/s or 1.5 Hz is pushed far into the left region on the complex plane by the PSS, greatly enhancing the positive damping. But in the meantime it also pushes λ_A and λ_B more to the right, and they are already close to the imaginary axis or even on the RHS

of the complex plane, manifesting a detrimental effect of PSS on other modes vulnerable to SSR.

Feasibility of Linear Excitation Control with a Multiple Feedback

In reference [16], the feasibility of linear excitation control with a multiple feedback was investigated. The turbine torque and governor state equations, although included in the initial eigenvalue analysis and final computer simulation test, were neglected in the control design. For further order reduction of the system for the control design, the damper winding equations were also neglected, but their effect was compensated for in the design process.

The basic idea of the new control design is to relocate the unstable eigenvalue modes of the mass-spring system in the stable region. From the eigenvalue analysis of the original high-order system without control over a wide range of capacitor compensation, it is found partly from Table 5-2 that, for this particular system, λ_I, λ_A, and λ_G need relocation badly. We shall also give more left-shift to λ_G to compensate for the damper winding effect, which is omitted in the model for control design.

Some techniques of the eigenvalue-assignment LOC design developed in Section 4-6, Chapter 4, are applied here for the new control design, but it is not yet optimal. Three sets of state equations similar to (4-5), (4-60), and (4-62) are required:

$$\begin{aligned} \dot{x} &= Ax + Bu \\ \dot{z} &= Fz + Gu \\ \dot{y} &= F_0 y + G_0 u \end{aligned} \tag{5-29}$$

The x-state equations are those in the general form, the z-state equations are those with all measurable variables, and the y-state matrix equation is in the canonical form. Since the eigenvalues of the system matrices F and F_0 are identical for a linear transformation, the determinants of the characteristic equations of the system without control are

$$\begin{aligned} |\lambda I - F| &= (\lambda - \lambda_1)(\lambda - \lambda_2)\cdots(\lambda - \lambda_n) \\ |\lambda I - F_0| &= \lambda^n + \alpha_n\lambda^{n-1} + \alpha_{n-1}\lambda^{n-2} + \cdots + \alpha_1 \end{aligned} \tag{5-30}$$

and those of the system matrix in canonical form and with control are

$$\begin{aligned} |\lambda I - (F_0 - G_0 S_0)| &= (\lambda - \hat{\lambda}_1)(\lambda - \hat{\lambda}_2)\cdots(\lambda - \hat{\lambda}_n) \\ |\lambda I - (F_0 - G_0 S_0)| &= \lambda^n + \hat{\alpha}_n\lambda^{n-1} + \hat{\alpha}_{n-1}\lambda^{n-2} + \cdots + \hat{\alpha}_1 \end{aligned} \tag{5-31}$$

Therefore, the new eigenvalues of the system matrix in canonical form and with control $\hat{\lambda}_i$ can be related with the eigenvalues of the system without

control λ_i by the desired eigenvalue shift β_i as follows

$$\hat{\lambda}_i = \lambda_i + \beta_i, \qquad i = i,2, \ldots, n \tag{5-32}$$

Note that the solution of the Riccati matrix equation is not involved in this design process.

Finally, the new control G_0u of (5-29) is written as $-G_0S_0y$. In the characteristic equation of (5-31), however, y is deleted. Therefore S_0 of (5-31) constitutes the desired shift of (5-32), and

$$G_0u = -G_0S_0y \tag{5-33}$$

$$S_0 = [\beta_1, \beta_2, \ldots, \beta_n] \tag{5-34}$$

In z state with all measurable state variables,

$$G_0u = -G_0S_0y = -G_0S_0T^{-1}z \tag{5-35}$$

where

$$z = Ty \tag{5-36}$$

Note that each term of (5-35) is a column matrix, and the coefficients of u, y, and z should be read as diagonal matrices.

With the three turbine torque equations, two governor equations, and three damper winding equations neglected, λ_I, λ_A, and λ_G of the reduced 19th-order system and the desired new eigenvalues $\hat{\lambda}_I$, $\hat{\lambda}_A$, and $\hat{\lambda}_A$ as assumed are as follows:

Modes	λ	$\hat{\lambda}$
I	$-0.2290 \pm j203.22$	$-3.5 \pm j203.22$
A	$-0.2273 \pm j160.66$	$-3.5 \pm j160.66$
G	$-0.2266 \pm j7.9054$	$-11.0 \pm j7.9054$

After the control design, the eigenvalues of the original 27th-order system with and without the new control are given in Table 5-3. Also listed are the eigenvalues of the reduced 19th-order system with control for comparison. The dampings of $\hat{\lambda}_I$, $\hat{\lambda}_A$, and $\hat{\lambda}_G$ are not as large as assumed in the design mainly due to the omission of damper windings. Although the control is designed for a 30% compensation, both eigenvalue analysis and computer

Table 5-3

Eigenvalues of the 27th- and Reduced-Order Models

	Model		
	19th with control	27th no control	27th with control
λ_H	$-0.1818 \pm j298.18$	$-0.1818 \pm j298.18$	$-0.1817 \pm j298.18$
λ_I	$-0.2290 \pm j203.22$	$+0.1541 \pm j204.35$	$-0.4879 \pm j202.65$
λ_A	$-0.2273 \pm j160.66$	$-0.2496 \pm j160.72$	$-0.2555 \pm j160.31$
λ_X	$-0.6677 \pm j127.03$	$-0.6707 \pm j127.03$	$-0.6695 \pm j127.04$
λ_B	$-0.2627 \pm j99.14$	$-0.2827 \pm j99.21$	$-0.2759 \pm j99.22$
λ_G	$-0.2266 \pm j7.9054$	$-0.0479 \pm j8.4801$	$-0.1758 \pm j9.0741$
λ_C	$-3.658 \pm j238.75$	$-6.198 \pm j209.40$	$-6.235 \pm j209.64$
$\lambda_{d,q}$	$-4.821 \pm j514.02$	$-7.022 \pm j542.80$	$-7.055 \pm j542.71$
λ_D		-1.983	$-2.907 \pm j0.2930$
λ_Q		-25.40	
λ_S		-31.92	-25.40
λ_F	-8.006	-8.440	
			$-12.78 \pm j283.06$
λ_{VR}	-93.68	-101.9	
λ_{Efd}	-499.5	-500.0	-684.2
λ_{CH}		-3.034	-0.4650
λ_{RH}		-0.1417	-0.1410
λ_{CO}		-4.616	-4.560
λ_{GOVR}		$-4.673 \pm j0.6269$	$-4.783 \pm j0.8535$

nonlinear simulation test indicate that the control thus designed can effectively stabilize the SSR system up to 70% compensation.

Summary of Section 5-3

Using the unified electrical and mechanical model developed in the last section, and also the reduced-order model, several SSR studies are carried out in this section. It is found that more than one torsional mode of oscillation may exist for a system with high capacitor compensation; that although a conventional phase-compensation PSS increases the damping of λ_G mode significantly, it also has a detrimental effect on other torsional modes; and that the linear excitation control of multimode SSR for system with a wide range of capacitor compensation is feasible.

5-4 LINEAR OPTIMAL EXCITATION CONTROL OF SSR

Several aspects of the linear excitation control of SSR presented in the last section can be improved (a) to find a still lower order model for the design (b) to apply the principle of LOC, and (c) to make all control feedback signals measurable [20].

Before improving the control design technique, we shall identify first the torsional modes and the mode shapes of the six-mass-spring system.

Torsional Oscillation Modes and Mode Shapes

The six torsional oscillation modes of the six-mass-spring system will be identified as mode 0, 1, 2, 3, 4, and 5. Mode 0 signifies that the six masses oscillate in unison without a shaft twist (oscillating in the opposite direction). Mode 1 has one shaft twist, mode 2 has two twists, and so on.

The mode shapes are found from the eigenvectors, which are found from the eigenvalues of the mass-spring system. For the system shown in Fig. 5-4, using the inertia and stiffness constants given in Section 5-3 and neglecting the damping, the oscillating frequencies from the imaginary part of various eigenvalues of the mass-spring system are as follows:

	GEN	LPA	EX	LPB	IP	HP
Frequency (rad/s)	9.469	99.35	127.1	161.4	202.9	298.2
(Hz)	1.51	15.7	20.2	25.7	32.3	47.5

For each eigenvalue, there is an eigenvector that has six components. When the six components of each eigenvector are normalized with respect to the largest component, the six mode shapes of torsional oscillations of all eigenvectors emerge as Table 5-4. While the eigenvector components are arranged in the same order as the mass-spring system, the torsional modes are arranged according to the increasing number of twists. Therefore, the mode shapes can be plotted as in Fig. 5-13.

Order Reduction of the Unified SSR Model for LOEC Design

To find the lowest unified electrical and mechanical SSR model for the LOEC (linear optimal excitation control) design, we can no longer neglect the damper windings in the SSR model. However, we may combine the two damper windings on the q axis, Q and S, into one, as it does not make any appreciable difference in the overall performance of the SSR system [21].

Table 5-4

Normalized Eigenvectors of the Six-Mass-Spring System

	Mode					
	0	1	2	3	4	5
HP	1	−0.777	0.1099	1	0.864	−0.781
IP	1	−0.584	0.065	0.342	−0.044	1
LPA	1	−0.342	0.015	−0.229	−0.503	−0.113
LPB	1	0.112	−0.040	−0.095	1	0.021
GEN	1	0.373	−0.037	0.166	−0.621	−0.0045
EX	1	1	1	−0.253	0.377	0.009

Similar to the approach in the last section, the smallest time constant of the fast excitation system and all five time constants of the turbine torques and governor system can be neglected for the LOEC design.

So far, the 27th-order unified electrical and mechanical SSR model developed in Section 5-2 has been reduced to the 20th order; it is still too high for a LOEC design with all measurable feedback signals.

The Equivalent Mass-Spring System

We shall give a hard, close look into the mass-spring system. From the eigenvalue analysis of the original high-order SSR system for a wide range of capacitor compensation ($X_C/X_L = 0$–0.9), it is found that for the First Bench Mark Model only modes 1, 3, and 4 are vulnerable to torsional oscillations as shown in Table 5-5. Typical eigenvalues of the mass-spring system are given in Table 5-6.

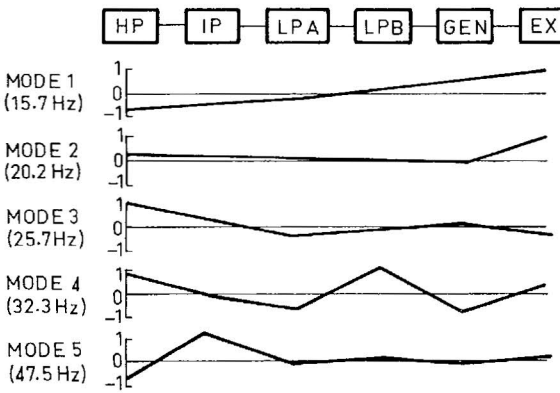

Fig. 5-13 Torsional mode shapes of mode 1, 2, . . . , 5.

Table 5-5

Possible Unstable Modes

Mode	Frequency (Hz)	Compensation
0	1–2	Under 30%
1	15.7 (102 rad/s)	Over 70%
3	25.7 (161 rad/s)	At 50%, 60%
4	32.3 (203 rad/s)	At 40%, 50%, 60%, 70%

Therefore, a low-order equivalent mass-spring system can be derived by retaining the vulnerable mode frequencies only, by adding M_X to M_G, M_H to M_I, and M_B to M_A and by adjusting the stiffness constants of the remaining shaft.

Consider the mass-spring system of Fig. 5-4 as described by (5-3). Neglecting the damping D's and eliminating $\Delta\theta$'s, the characteristic equation of the system may be written in matrix form as

$$\left|\lambda[I] - [M]^{-1}\omega_b[K]\right| = 0 \tag{5-36}$$

where each solution of λ gives one eigenvalue pair since each $\Delta\dot{\omega}$ equation of (5-3) corresponds to a second-order differential equation after eliminating $\Delta\theta$.

After six eigenvalue pairs are found from (5-36) for the data given in Section 5-3, the same equation (5-36) is applied repeatedly for the successive order reduction of the mass-spring system as follows:

(a) Add M_X to M_G to eliminate mode 2, which corresponds to λ_X, substitute the known frequencies to be retained into (5-36) of the reduced order $(12-2)$, one at a time, to find a new K_{BG}, which, and only which, is treated as the unknown, and adjust the average values of K_{BG} to the least-

Table 5-6

Typical Eigenvalues of the Mass-Spring System

	Compensation		
	30%	50%	80%
λ_H	$-0.1818 \pm j298.18$	$-0.1818 \pm j298.18$	$-0.1818 \pm j298.18$
λ_I	$-0.4938 \pm j203.60$	$+0.1237 \pm j202.87$	$+0.0134 \pm j202.89$
λ_A	$-0.2513 \pm j160.64$	$+0.2603 \pm j161.38$	$-0.0967 \pm j160.52$
λ_X	$-0.6705 \pm j127.02$	$-0.6828 \pm j127.05$	$-0.5998 \pm j126.94$
λ_B	$-0.2811 \pm j99.136$	$-0.3528 \pm j99.345$	$+1.7178 \pm j102.17$
λ_G	$-0.0031 \pm j8.4105$	$-0.2327 \pm j9.4692$	$-0.7619 \pm j11.662$

Table 5-7

Mass-Spring Eigenvalues of Various SSR Models

	Order		
	26th	16th	14th
λ_H	$-0.1818 \pm j298.18$		
λ_I	$+0.1237 \pm j202.87$	$+0.1033 \pm j204.01$	$+0.0167 \pm j200.32$
λ_A	$+0.2603 \pm j161.38$	$+0.2341 \pm j161.72$	$+1.0147 \pm j160.11$
λ_X	$-0.6828 \pm j127.05$		
λ_B	$-0.3528 \pm j99.345$	$-0.3053 \pm j100.05$	
λ_G	$-0.2327 \pm j9.4692$	$-0.2566 \pm j9.4905$	$-0.2408 \pm j9.5172$

squares error of all remaining frequencies. For the adjustment, the sensitivity of the frequencies with respect to the new K_{BG} may be utilized.

(b) Add M_H to M_I to eliminate mode 5, which corresponds to λ_H, and repeat the process similar to (a) using an eighth order of (5-36) to find a new K_{IA}.

(c) Add M_B to M_A to eliminate mode 1, which corresponds to λ_B, and repeat the process similar to (a) using a sixth order of (5-36) but this time to find still newer K_{IA} and K_{BG}, one at a time. Note that this reduced-order model is good only for the capacitor compensation up to 70%.

In the order reduction process, attention should be paid only to the eigenvalue frequencies of the vulnerable modes to be retained, and not to the damping.

The mass-spring eigenvalues of the 26th-order SSR system (with only one damper winding on the q axis) are shown in Table 5-7. Also shown are those of the reduced 16th-order model with the omission of turbine and governor time constants, etc., with M_X combined with M_G, and with M_H combined with M_I; and those of the 14th-order model with M_B further combined with M_A.

The mode shapes of the original six-mass-spring system are shown in Fig. 5-14 as (a), those of the five-mass-spring system as (b), and those of the four-mass-spring system as (c). They are very close.

Both the 16th and the 14th reduced SSR order models can be used for the LOEC design.

Procedure of LOEC Design

The general procedure of LOC design developed in Chapter 4 may be summarized as follows:

State equations

$$\dot{x} = Ax + Bu \tag{4-5}$$

Performance index

$$J = \int_0^\infty \left[x^{\mathrm{T}}Qx + u^{\mathrm{T}}Ru\right] dt \tag{4-6}$$

State and co-state system matrix

$$M = \begin{bmatrix} A & -S \\ -Q & -A^{\mathrm{T}} \end{bmatrix}, \qquad S = BR^{-1}B^{\mathrm{T}} \tag{4-31}$$
$$\tag{4-18}$$

Eigenvector matrix

$$X = \begin{bmatrix} X_{\mathrm{I}} & X_{\mathrm{III}} \\ X_{\mathrm{II}} & X_{\mathrm{IV}} \end{bmatrix} \tag{4-35}$$

Riccati matrix

$$K = X_{\mathrm{II}}X_{\mathrm{I}}^{-1} \tag{4-40}$$

Control

$$Bu = -SKx \tag{4-41}$$

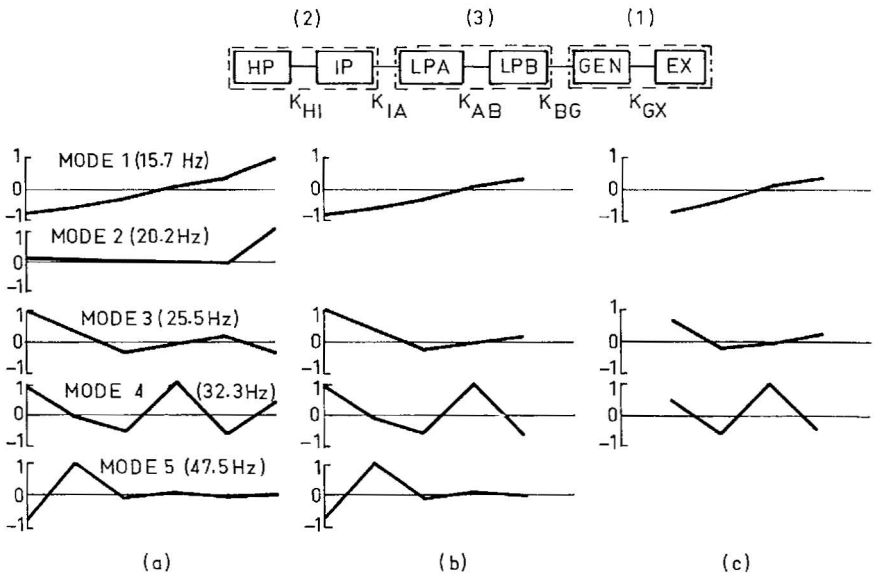

Fig. 5-14 Mode shapes of the original and equivalent mass-spring systems.

Therefore, the matrix state equation of the controlled system may be written

$$\dot{x} = [A - SK]x \tag{4-5a}$$

Let the system matrix with a LOEC be

$$A_c \triangleq A - SK \triangleq A - F \tag{5-37}$$

and let the last state variable be Δv_R of the voltage regulator of an nth-order system F becomes

$$[F] = \begin{bmatrix} & [0] & \\ f_{n1} & \cdots f_{nk} \cdots & f_{nn} \end{bmatrix} \tag{5-37a}$$

Although there are generally n feedback gains, $f_{n1}, f_{n2}, \ldots,$ f_{nn}, of (5-37a), some of them are not as sensitive to the system eigenvalues as others. Therefore, eigenvalue sensitivity may be utilized to simplify the excitation feedback control signals.

Example 5-2. Find the system eigenvalue sensitivity with respect to the LOEC feedback gains.

Solution: The sensitivity coefficient may be calculated as follows. Let

$$A_c x_i = \lambda_i x_i \tag{5-38a}$$

$$A_c^T v_i = \lambda_i v_i \tag{5-38b}$$

The variation of (5-38a) becomes

$$\Delta A_c x_i + A_c \Delta x_i = \Delta\lambda_i x_i + \lambda_i \Delta x_i \tag{5-39}$$

Premultiplying both sides of (5-39) by v_i^T, the last terms of both sides of (5-39) will cancel each other according to (5-38b), resulting in

$$\Delta\lambda_i = \frac{v_i^T \Delta A_c x_i}{v_i^T x_i} \tag{5-40}$$

For the sensitivity study, ΔA_c becomes $-\Delta F$, the variation of A being zero. Since the effect of deleting the kth feedback element on the ith eigenvalue is

$$\Delta\lambda_i = \frac{v_i(n)x_i(k)}{v_i^T x_i}(-f_{nk}) \tag{5-41}$$

the total effect of deleting (d) feedback elements becomes

$$\Delta\lambda_{i(d)} = -\sum_{(d)} \frac{v_i(n)x_i(d)}{v_i^T x_i} f_{nd} \tag{5-42}$$

The LOEC Design and Test Results

For the LOEC design, the state variables of the 14th-order system are

$$[x]_{14} = [\Delta\omega_I, \Delta\theta_I, \Delta\omega_B, \Delta\theta_B, \Delta\omega, \Delta\delta; \Delta i_d, \Delta i_q, \Delta i_F, \Delta i_D, \Delta i_Q, \Delta e_{cd}, \Delta e_{cq}, \Delta v_R]^T \quad (5\text{-}43)$$

and the following weighting matrices are chosen

$$[Q]_{14} = \text{DIAG}\,[5000, 50, 55000, 50, 3000, 25; 1000, 1000, 0, 5, 5, 1, 1, 0]$$
$$[R] = 1 \quad (5\text{-}44)$$

A linear optimal excitation control is then designed and the control is tested on the original 26th-order system with the following state variables,

$$[x]_{26} = [\Delta\omega_H, \Delta\theta_H, \Delta\omega_I, \Delta\theta_I, \Delta\omega_A, \Delta\theta_A, \Delta\omega_B, \Delta\theta_B, \Delta\omega, \Delta\delta, \Delta\omega_X, \Delta\theta_X; \Delta T_H, \Delta T_I, \Delta T_A, a, g; \Delta i_d, \Delta i_q, \Delta i_F, \Delta i_D, \Delta i_Q, \Delta e_{cd}, \Delta e_{cq}, \Delta v_R, \Delta E_{FD}]^T \quad (5\text{-}45)$$

The sensitivity of the control gains on the eigenvalues are examined. It is found that only the gains of the following seven variables

$$[x]_7 = [\Delta\omega_B, \Delta\delta, \Delta i_d, \Delta i_q, \Delta i_F, \Delta i_D, \Delta v_R]^T \quad (5\text{-}46)$$

have substantial effects on the eigenvalue shift of the controlled system, and the gains of the other seven

$$[x]_7' = [\Delta\omega_I, \Delta\theta_I, \Delta\theta_B, \Delta\omega, \Delta i_Q, \Delta e_{cd}, \Delta e_{cq}]^T \quad (5\text{-}47)$$

may be neglected.

Since the seven control signals of (5-46) are not all measurable, they may be replaced by

$$[x]_c = [\Delta\omega_B, \Delta\delta, \Delta P_e, \Delta Q_e, \Delta i_t, \Delta i_F, \Delta v_R]^T \quad (5\text{-}48)$$

To find ΔP_e, ΔQ_e, and Δi_t, the following equations in per unit value are useful,

$$P_e = \psi_d i_q - \psi_q i_d$$
$$Q_e = \psi_d i_d + \psi_q i_q \quad (5\text{-}49)$$
$$i_t^2 = i_d^2 + i_q^2$$

Note also that as $\Delta\dot{\psi}_Q$ is relatively small,

$$\Delta\dot{\psi}_Q \simeq 0$$

Table 5-8

Eigenvalues of the Original System with Low-Order LOC

	Compensation		
	30%	50%	80%
λ_H	$-0.1818 \pm j298.18$	$-0.1818 \pm j298.18$	$-0.1818 \pm j298.18$
λ_I	$-0.8842 \pm j201.52$	$-0.4554 \pm j203.44$	$-0.4788 \pm j203.09$
λ_A	$-0.2672 \pm j160.45$	$-0.4192 \pm j160.36$	$-0.2693 \pm j160.58$
λ_X	$-0.6927 \pm j127.09$	$-0.7322 \pm j127.16$	$-0.2864 \pm j127.16$
λ_B	$-0.4608 \pm j99.295$	$-0.5894 \pm j99.490$	$-0.6186 \pm j100.85$
λ_G	$-1.3517 \pm j6.3035$	$-1.6931 \pm j7.1144$	$-2.5196 \pm j8.2862$

then

$$\Delta i_Q \simeq \Delta i_q \tag{5-50}$$

Eigenvalue analyses are repeated with the 26th-order system for various degrees of compensation with the LOEC designed for the reduced 14th-order model and neglecting the less-sensitive feedback signals. Typical results are given in Table 5-8. The system is stable for up to 80% capacitor compensation.

The LOEC is further given a computer simulation test using a nonlinear 26th-order model. A 20% pulsed torque ΔT_e is applied to the system for 0.2 s. A typical dynamic response of the shaft between the two low-pressure turbines is shown in Fig. 5-15. It clearly indicates the existence of two torsional oscillation modes, one low frequency and one high frequency, and they all attenuate in about 5 s.

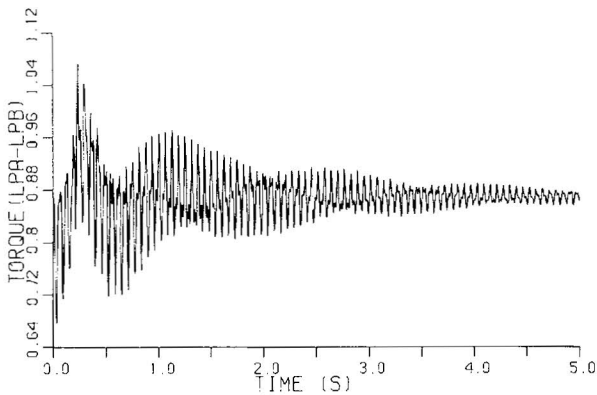

Fig. 5-15 Typical torsional oscillations of the system with LOEC.

Summary of Section 5-4

In this section a linear optimal excitation control (LOEC) is designed to stabilize the torsional oscillations of a one-machine, infinite-bus system. To save computation of the design, the order of the system is reduced. Only one damper winding is assumed per axis, one time constant is assumed for the excitation system, and five time constants of turbine torque and governor system are neglected. Equivalent mass-spring systems are further derived by combining some masses together yet retaining all vulnerable torsional oscillation frequencies found from eigenvalue analysis of the original high-order system over a wide range of capacitor compensation, resulting in 16th- and 14th-reduced-order systems.

The 14th-order model is used for the LOEC design, and the feedback signals of the designed control are further examined and the less sensitive ones rejected, resulting in a feedback of only seven measurable signals.

Both linear test (eigenvalue analysis) and nonlinear simulation test (using a nonlinear model) indicate that the LOEC can effectively stabilize the SSR system over a wide range of capacitor compensation up to 80%.

The LOEC design technique is being extended to multimachine SSR stabilization.

5-5 SUMMARY

In this chapter a relatively new power system dynamic problem, the torsional oscillations of the steam turbine generator shaft due to the electrical resonance of the capacitor compensated transmission system, or the SSR problem, is investigated.

Following a brief presentation of the SSR problem and the countermeasures in practice or being proposed to date in Section 5-1, emphasis is placed on excitation control of SSR in the subsequent sections. A single unified and complete electrical and mechanical model of a one-machine, infinite-bus system for SSR studies is developed in Section 5-2, and the effect of capacitor compensation on SSR and the feasibility of excitation control of SSR is investigated in Section 5-3.

Convinced of the feasibility of excitation control of SSR, Section 5-4 improves the design technique by reducing the order of the system model from the 27th to the 16th or 14th for the LOEC design in order to save computation. An equivalent mass-spring technique is developed. Linear optimal control design techniques are also applied, the designed LOEC is further examined, and some of the less-sensitive control signals are rejected, resulting in a LOEC with only seven measurable feedback signals. Both eigenvalue

analysis and nonlinear simulation test of the original high-order system confirm that the LOEC thus designed is highly effective in stabilizing the system vulnerable to SSR over a wide range of capacitor compensation.

Problems

5-1 Find the equivalent resistance and reactance of Fig. 5-1. Under what conditions will SSR occur to a one-machine, infinite-bus system if the synchronous generator can be represented by Fig. 5-1, the total resistance of transformer and transmission line is R_L, the total reactance X_L, and the line compensation capacitive reactance X_C?

5-2 Derive (5-11) from $[v_t]_{abc}$ of (5-8) through coordinate transformation. Assume a balanced three-phase voltage.

5-3 (a) Find the eigenvalues and eigenvectors of the mass-spring system of Fig. 5-4 alone, using the data for the First Bench Mark Model of Fig. 5-12 and neglecting all damping and mechanical input torques.

(b) What are the mechanical mode frequencies in hertz?

5-4 In the final design of LOC of SSR, part of the state variable vector $[\Delta i_d, \Delta i_q, \Delta i_F, \Delta i_D]^T$ of (5-46) is replaced by $[\Delta P_e, \Delta Q_e, \Delta i_t, \Delta i_F]^T$ of (5-48). Find the linear transformation relation.

References

[1] IEEE PES Symposium, "Analysis and Control of Subsynchronous Resonance," IEEE Publ. 76 CH1066-0-PWR. IEEE, New York, 1976.

[2] M. C. Hall and D. A. Hodges, "Experience with 500 kV Subsynchronous Resonance and Resulting Turbine Generator Shaft Damage at Mohave Generating Station," IEEE Publ. 76 CH1066-0-PWR, pp. 22–29. IEEE, New York, 1976.

[3] R. G. Farmer, A. L. Schwalb, and E. Katz, Navajo project report on subsynchronous resonance analysis and solutions. *IEEE Trans. Power Appar. Syst.* 1226–1232, July/Aug. (1977).

[4] D. N. Walker and A. L. Schwalb, "Results of Subsynchronous Resonance Test at Navajo," IEEE Publ. 76 CH1066-0-PWR, pp. 37–45. IEEE, New York, 1976.

[5] D. N. Walker, C. E. J. Bowler, R. L. Jackson, and D. A. Hodges, Results of subsynchronous resonance test at Mohave. *IEEE Trans. Power Appar. Syst.* 1878–1889, Sept./Oct. (1975).

[6] L. A. Kilgore, D. G. Ramay, and M. C. Hall, Simplified transmission and generation system analysis procedures for subsynchronous resonance problems. *IEEE Trans. Power Appar. Syst.* 1840–1846, Nov./Dec. (1977).

[7] C. E. J. Bowler, D. H. Baker, N. A. Mincer, and P. R. Vandiveer, Operation and test of the Navajo SSR protective equipment. *IEEE Trans. Power Appar. Syst.* 1030–1035, July/Aug. (1978).

[8] O. Saito, H. Mukae, and K. Murotani, Suppression of self-excited oscillations in series compensated transmission lines by excitation control of synchronous machines. *IEEE Trans. Power Appar. Syst.* 1777–1788, Sept./Oct. (1975).

[9] A. A. Fouad and K. T. Khu, Damping of torsional oscillations in power system with series-compensated lines. *IEEE Trans. Power Appar. Syst.* 744–753, May/June (1978).

[10] A. M. El-Serafi and A. A. Ahaltout, Control of subsynchronous resonance oscillations by multi-loop excitation controller. *IEEE PES Winter Meet., 1979* IEEE Paper A79 076-1 (1979).

[11] L. A. Kilgore, D. G. Ramey, and W. H. South, Dynamic filter and other solutions to the subsynchronous resonance problem. *Proc. Am. Power Conf.* **37,** 923–929 (1975).

[12] O. Wasynczuk, Damping of synchronous resonance using reactive power control. *IEEE PES Summ. Meet., 1980* IEEE Paper 80 SM 600-7 (1980).

[13] S. Stevenson and K. Mortensen, Damping of subsynchronous oscillation by an HVDC link—an HVDC simulation study. *IEEE PES Summ. Meet., 1980* IEEE Paper 80 SM 668-4 (1980).

[14] N. G. Hingorani *et al.*, A new scheme for subsynchronous resonance damping of torsional oscillations and transient torque. *IEEE PES Summ. Meet., 1980* Pt. I, IEEE Paper 80 SM 687-4; Pt. II, IEEE Paper 80 SM 688-2 (1980).

[15] IEEE Committee, Dynamic models for steam and hydro turbines in power systems. *IEEE Trans. Power Appar. Syst.* 1904–1915, Nov./Dec. (1973).

[16] Yao-nan Yu, M. D. Wvong, and K. K. Tse, Multi-mode wide range subsynchronous resonance stabilization. *IEEE PES Summ. Meet., 1978* IEEE Paper A78 554–8 (1978).

[17] IEEE Committee, First benchmark model for computer simulation of subsynchronous resonance. *IEEE Trans. Power Appar. Syst.* 1565–1572, Sept./Oct. (1977).

[18] Yao-nan Yu and H. A. M. Moussa, Experimental determination of exact equivalent circuit parameters of synchronous machines. *IEEE Trans. Power Appar. Syst.* 2555–2560, Nov./Dec. (1971).

[19] IEEE Committee, Computer representation of excitation system. *IEEE Trans. Power Appar. Syst.* 1460–1464, June (1968).

[20] A. Yan and Yao-nan Yu, Multi-mode stabilization of torsional oscillations using output feedback excitation control. *IEEE Trans. Power Appar. Syst.* 1245–1253, May (1982).

[21] A. Yan, M. D. Wvong, and Yao-nan Yu, Excitation control of torsional oscillations. *IEEE PES Summ. Meet. 1979* IEEE Paper A79 505-9 (1979).

Chapter 6 Dynamic Equivalents of External Electric Power Systems

Most power system dynamic studies were originally based on one-machine, infinite-bus models and were found satisfactory. With the increasing interconnection of power plants in modern large electric power systems, power system dynamic studies become much more complex. There are, for instance, about 300 machines in the WSCC system and also about 300 machines in the Northeastern and Michigan system, considering major machines alone [1].

Although computer programs have the capability of handling a great number of machines and buses, difficulties still remain. In addition to the large amount of computation, full information on the entire system is required. Some of this may be difficult, if not impossible, to obtain. Moreover, results of hundreds of swing curves can hardly be given meaningful interpretations because they are so involved.

A sensible thing to do is to consider only the local system under study in detail, and to represent the external systems by equivalents. Static equivalents for load flow studies are fairly well developed, and the development of the dynamic equivalents for dynamic studies is is progress. This chapter deals with the dynamic equivalents of the external system. Our primary concern is the dynamic interacting effect of the external system on the local system under investigation. As long as the interacting effect of the external system on the study system can be faithfully represented, the behavior of the various machines within the external system are of secondary interest.

Dynamic equivalents are used for stability analysis, stabilizer design, and investigation of the electric power transfer limits among areas. Much thought has been given in this regard. One idea is to distribute the inertia of the machine to be eliminated to other interconnected machines in proportion to

their transfer admittances [2, 3]. Another is to draw boundaries for areas that are severely affected, less affected, and least affected by a fault, in accordance with a distance factor of swing angle approximated by $(\frac{1}{2})at^2$ where t is the duration of fault and a the acceleration calculated from the steady-state transfer power divided by the machine inertia [4]. Still another suggests that three machine models of different degree of detail be used, a nonlinear full model, a linear model, and a constant voltage behind reactance, decided by a factor of $\Delta\delta_i[Y_{fi}/Y_{ii}]$ where $\Delta\delta_i$ is the rotor angle deviation from the steady state based on an initial stability analysis, and Y_{ii} and Y_{fi} are the self and transfer admittances, respectively [5].

The major approaches of dynamic equivalencing for stability studies are three: the modal approach, which keeps the main eigenvalues of the external system [6–9]; the coherency approach, which separates machines in groups and combines machines within each group closely swinging together into one equivalent [1, 10–13]; and the estimation approach, which derives the equivalents for the external system through estimation [14–18]. These three techniques will be introduced in this chapter, with emphasis on the estimation; it is the only technique that does not require any information of the external system.

Some references on estimating static equivalents and machine parameters are also given at the end of this chapter [19–30].

6-1 EIGENVALUE-BASED DYNAMIC EQUIVALENTS

In the first two papers on modal dynamic equivalents, which were called electromechanical equivalents [6, 7], a large electric power system was divided into three parts, the study system, the surrounding external system, and the remainder beyond the surrounding system. Terminals between the study system and the external system were retained. The original picture is schematically redrawn as Fig. 6-1.

Since the data for the remaining portion of an extensive large system were difficult to obtain, and the remainder's effect on the study system was

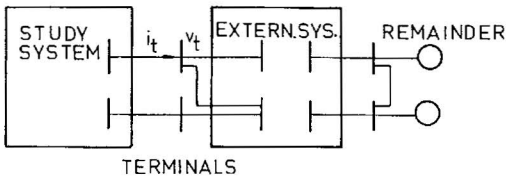

Fig. 6-1 Study and external systems.

secondary, it was suggested that it be represented by a few equivalent generators with highly simplified models.

The main problem was the simplification of the external system which was considered sufficiently remote from the site of disturbance, yet had significant influence on the study system. The idea was to derive relatively simple dynamic equivalents for the external system through eigenvalue analysis. This approach of deriving dynamic equivalents will be referred to hereafter as the modal approach.

Equivalencing Technique

The general procedures for deriving the dynamic equivalents of the external system by the modal approach are as follows [6, 7]:

(1) The external system state equations are first described by the nonlinear differential equations,

$$\dot{x} = F(x, v_t) \tag{6-1}$$

where x is the state variable vector, and v_t the terminal voltage as shown in Fig. 6-1.

(2) Equations (6-1) are linearized on the assumption that the disturbance propagated from the study system to the external system is sufficiently small. Including a set of current deviation equations at the terminals, the complete external system equations may be written as

$$\dot{y} = Ay + B\,\Delta v_t \tag{6-2a}$$

$$\Delta i_t = Cy' + D\,\Delta v_t \tag{6-2b}$$

where y is the deviation of x, Δv_t that of v_t, y' a subset of y, Δi_t that of the terminal currents, and A, B, C, and D are the matrix coefficients. The dynamic behavior of the external system is now described by matrix equation (6-2a), while the current deviations are described by matrix equation of (6-2b), which can be found from a load flow study.

(3) The system matrix A of (6-2) is diagonalized using the eigenvector matrix of A for the transformation, resulting in

$$\begin{aligned} \dot{z} &= \Lambda z + E\,\Delta v_t \\ z &= Ty \end{aligned} \tag{6-3}$$

where z is the new state variable vector, Λ the system eigenvalue matrix in diagonal form, E a new coefficient of Δv_t, and T the transformation matrix that constitutes the eigenvectors of A.

(4) Neglect the eigenvalues of fast decay and those of high frequencies, and keep only the main eigenvalues, resulting in a lower-order external system.

To validate the method, a power system was computer simulated with the study system chosen in two different ways and a fault assumed at different locations [6, 7]. In one case the voltage regulator gains were increased to ten times the ordinary values to bring the system to the verge of dynamic instability. In another case the duration of a three-phase fault was increased to bring the system to the verge of transient instability. The dynamic responses of the system with reduced-order external equivalents were compared with those of the original system for an intentional disturbance. Results were in good agreement. It was observed that the system with equivalents was slightly less stable than the original system, and there were some discrepancies in eigenvalues for different choices of the reference machine in the external system for the linerization. There were interesting discussions of the paper, and one of them pointed out that some thought should be given to the modal interaction of the machines of the study system and those of the external system [6, 7].

The NPCC System Test

The dynamic equivalencing technique of the modal approach was further tested on the vast NPCC (Northeast Power Coordinating Council) system [8]. The test system constitutes five areas: (1) New England, (2) upper New York State, (3) southeast New York State, (4) Ontario Hydro, and (5) Michigan and PJM (Pennsylvania–New Jersey–Maryland), and the entire system was represented by 48 machines and 136 buses. A three-phase fault for six cycles was assumed on two different buses of area 1. In one study area 1 alone was considered as the study system and the other areas were considered as the external system. In another study all areas except area 5 were considered as the study system and only area 5 was considered as the external system. In all studies, constant impedance loads were considered, and each machine of area 5 was represented by a voltage-behind-reactance.

The computer time saving in stability analysis was about 24% with respect to a reference run when area 1 only was considered as the study system, but there was not much saving when area 5 was considered as the external system. The overall computer time saving by this method is not much because of the heavy computation of diagonalization of a large system matrix by eigenvectors. It was also noted in reference [8] that the reference machine in the external system for the linearization process must be properly chosen.

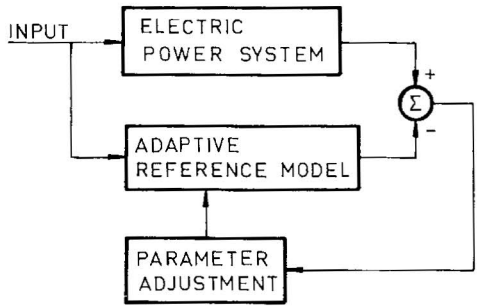

Fig. 6-2 System mode identification. (From [9] courtesy of IEEE, © 1978.)

System Mode Identification

Also based on the modal concept, but without going through the equivalencing process, a technique of identifying the major modes of a power system was proposed [9]. It was advocated that the swings of a local system in a large electric power system can be approximated by a few major modes, one local mode and one or two interarea modes. For instance, the response of a power system was approximated by

$$\delta(t) = \sum_{i=1}^{2} A_i e^{-\alpha_i t} \sin(\omega_i t + \phi_i) \tag{6-4}$$

and the damping factors and the oscillating frequencies were identified with an adaptive reference model as shown in Fig. 6-2.

In the process, the reference model response is compared with the system response, and the model parameters are repeatedly adjusted until the response error reaches the minimum.

Summary of Section 6-1

In this section the dynamic equivalencing techniques of the modal approach are presented. A large electric power system is divided into three parts, the study system, the external system, and the remainder. The external system, which includes a large number of machines, is represented by equivalents. The procedures are as follows: (1) Describe the external system by high-order nonlinear differential equations, (2) linearize the equations, (3) diagonalize the system matrix, and (4) neglect the fast decaying and high frequency eigenvalues. The diagonalization of a large system matrix using eigenvectors is time-consuming, and a proper choice of a reference machine

in the external system for the linearization is important. Also based on the modal concept, but assuming that there are only a few major modes of a local system in a large electric power system, an identification technique is also introduced. All these techniques are useful, and we shall present other dynamic equivalencing techniques in the subsequent sections.

6-2 COHERENCY-BASED DYNAMIC EQUIVALENTS

Another prevailing dynamic equivalencing technique is based on the concept of coherency of swinging machines [1, 10–12]. From a transient stability analysis of a large electric power system, a number of groups of generating units, swinging coherently together at the same frequency and at close angles, are identified; and all units of each group are combined into one or two dynamic equivalents, e.g., one thermal unit and one hydro unit. Since the equivalents are expressed in terms of machine and control parameters, the basic system structures are retained. For a very large electric power system, however, heavy computations are involved because of the transient stability analyses of the system for various contingencies. Examples of coherent groups can be found in reference [1].

Dynamic Aggregation

The equivalencing process of the coherency approach is called dynamic aggregation [11], which may be summarized as follows.

Equivalent Bus. All generators belonging to the same coherent group are connected to an equivalent bus through ideal transformers, each with a complex ratio, to match their terminal voltages and phase angles with those of the equivalent bus. The complex ratios are calculated from

$$a_j = v_j/v_t, \qquad j = 1, \ldots, n \tag{6-5}$$

where v_j and v_t, respectively, are the terminal voltage phasor of the individual machine and the voltage phasor of the equivalent bus. The equivalent bus voltage may be chosen from the voltage of any individual bus or the average values of the coherent group.

Rotor Dynamics. The mechanical equations of individual machines of a coherent group may be written

$$2H_j(d\omega_j/dt) = P_{mj} - P_{ej} - D_j\omega_j, \qquad j = 1, \ldots, n \tag{6-6}$$

Since the speeds of all machines in a coherent group are the same, the aggregated mechanical equations may be written

$$(\sum_j 2H)(d\omega/dt) = \sum_j P_{mj} - \sum_j P_{ej} - (\sum_j D_j)\omega, \qquad j = 1, \ldots, n \tag{6-7}$$

Note that all equations of (6-6) must be written on the same MVA and the same kV bases for the entire electric power system.

Turbines and Governors. The basic equations of the turbines and the governors of a coherent group may be written

$$P_{mj}(s) = G_j(s)\,\Delta\omega(s), \qquad j = 1, \ldots, n \tag{6-8}$$

Therefore

$$\sum_j P_{mj}(s) = [\sum_j G_j(s)]\,\Delta\omega(s), \qquad j = 1, \ldots, n \tag{6-9}$$

For the aggregation of the transfer functions, Bode plots may be used. For unknown transfer functions of machines in the group, standard parameter values may be assigned. To approximate the aggregated results, the least-squares-error curve-fitting technique can be applied. An example of Bode plots of the aggregated phase angles and magnitudes of a coherent group of machines are shown in Fig. 6-3 in dotted lines, and the curve fitting results in solid lines.

Excitation System. Similar techniques can be applied to derive the equivalent transfer function for the excitation systems. The basic equations

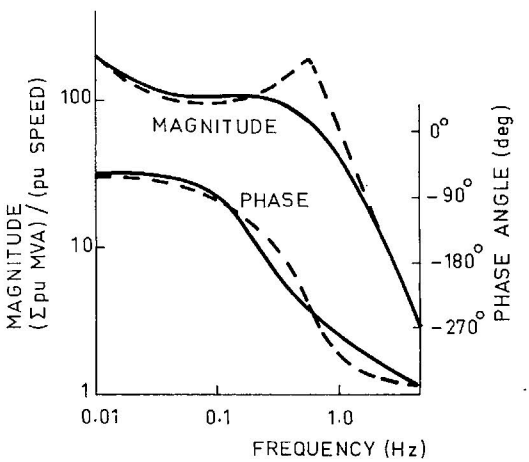

Fig. 6-3 Bode plots of aggregated and equivalent transfer functions. (From [11] courtesy of IEEE, © 1978.)

of the excitation systems may be written

$$e_{\mathrm{FD}j}(s) = G_{\mathrm{E}j}(s)\Delta v_{\mathrm{t}}(s), \qquad j = 1, \ldots, n \tag{6-10}$$

and the equivalent transfer function

$$G_{\mathrm{E}}(s) = \frac{e_{\mathrm{FD}}}{\Delta v_{\mathrm{t}}} = \sum_{j} W_j(s) G_{\mathrm{E}j}(s), \qquad j = 1, \ldots, n \tag{6-11}$$

where $G_{\mathrm{E}j}(s)$ represents the transfer function of individual excitation, $G_{\mathrm{E}}(s)$ the equivalent, $e_{\mathrm{FD}j}(s)$ the individual field voltage, $e_{\mathrm{FD}}(s)$ the equivalent, Δv_{t} the equivalent terminal voltage, and $W_j(s)$ a weighting factor. For details, see reference [11].

Power System Stabilizers. The transfer functions of power system stabilizers may be written

$$\frac{e_{\mathrm{FD}}(s)}{u(s)} = \sum_{j} W_j(s) G_{\mathrm{E}j}(s) G_{\mathrm{S}j}(s), \qquad j = 1, \ldots, n \tag{6-12}$$

and the equivalent

$$\frac{e_{\mathrm{FD}}(s)}{u(s)} = G_{\mathrm{E}}(s) G_{\mathrm{S}}(s) \tag{6-13}$$

where $G_{\mathrm{E}}(s)$ was determined from (6-11), and $G_{\mathrm{S}}(s)$ may be determined from the least-squares fitting.

Most notation used in this section follows reference [11].

Coherent Equivalents with Simplified Power System Model

Since the most time-consuming part of computation in dynamic equivalencing of a large electric power system by the coherent approach is the transient analysis of the system, Podmore suggested that the synchronous generators be modeled by constant voltages behind reactances, and that the excitation, governor, and turbine systems be neglected in the model [12]. In his formulation, the machine equations are written

$$\begin{aligned} M_j \frac{d\,\Delta\omega_j}{dt} &= \Delta P_{\mathrm{m}j} - \Delta P_{\mathrm{e}j} - D_j \Delta\omega_j \\ \frac{d\,\Delta\delta_j}{dt} &= (2\pi f)\,\Delta\omega_j \end{aligned} \tag{6-14}$$

and the power equation

$$\begin{bmatrix} \Delta P_G \\ \Delta P_L \\ \Delta Q_G \\ \Delta Q_L \end{bmatrix} = \begin{bmatrix} & & & \\ & J & & \\ & & & \\ & & & \end{bmatrix} \begin{bmatrix} \Delta\delta \\ \Delta\theta \\ \Delta E \\ \Delta v \end{bmatrix} \tag{6-15}$$

which is approximated by

$$\begin{bmatrix} \Delta P_G \\ \Delta P_L \end{bmatrix} = \begin{bmatrix} \partial P_G/\Delta\delta & \partial P_G/\partial\theta \\ \partial P_L/\Delta\delta & \partial P_L/\partial\theta \end{bmatrix} \begin{bmatrix} \Delta\delta \\ \Delta\theta \end{bmatrix} \tag{6-16}$$

based on the assumption that the power and reactive power flows can be decoupled, and that

$$\Delta E \simeq 0, \quad \partial P_G/\partial v \simeq 0, \quad \partial P_L/\partial v \simeq 0 \tag{6-17}$$

In these equations, P_G, Q_G, E, and δ are the power, reactive power, voltage, and angle of the generator internal buses, and P_L, Q_L, v, and θ those of the load buses, respectively.

Based on the simplified linear model and with a trapezoidal integration algorithm [31], the computer time required for the coherency equivalencing is drastically reduced. It was observed that although the system damping was affected by the simplified modeling, the oscillating frequency was not.

Figure 6-4 compares swing curves of two machines (1 and 2) of the original system (solid lines) with those of the two machines of the equivalent system (broken lines). They are close. Discussions on the paper suggest that (1) a second-order equivalent may not be satisfactory for generators close to the

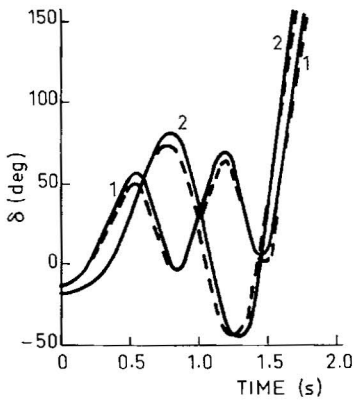

Fig. 6-4 Swing curves of original and equivalent systems. (From [12] courtesy of IEEE, © 1978.)

fault, (2) the coherent groups before and after a switching may change, and (3) dissimilar generators in a given power plant may not swing coherently.

Power Transfer Limits of Coherent Groups

The coherency concept has also been developed at CEGB (Central Electricity Generating Board), England, to study the power transfer limits among machine groups [13]. A criterion based on the rotor angle deviations of individual machines is used to separate the machines into coherent groups. A group leader, usually the largest machine of the group, is chosen, the capacity of the group leader is modified to represent the total MVA of the entire group, and the inertia is adapted to $[\sum(\text{MVA}_i\text{H}_i)/\text{MVA}_i]$, $i = 1, \ldots, n$, for a group with n machines. The resistance and reactance of a machine group are also adapted to $(r \cdot \text{MVA})_{\text{leader}}/(\text{new MVA})$ and $(x \cdot \text{MVA})_{\text{leader}}/(\text{new MVA})$, respectively. Power transfer limits are determined from load flow and transient stability studies with these group equivalents. For details, see reference [13].

Summary of Section 6-2

In this section, the dynamic equivalencing techniques based on the coherency concept are presented. From a transient stability analysis of an electric power system, the generating units are separated into a number of coherent groups. Each group of machines, swinging together at the same frequency and at close angles, are combined into one equivalent. The speed deviations being the same, the torque equations of the machines in one group can be added together on the same MVA and the same kV bases to find the equivalent damping and inertia constant. For the excitation and governor loop transfer functions, Bode plots are used for the aggregation, and the equivalent transfer functions are obtained from the least-squares fitting.

Since the most computer-time-consuming part of the process is the transient stability analysis of a large electric power system, it is suggested that the synchronous machines of the system be modeled by voltages behind reactances and the control loop transfer functions be neglected in the equivalencing process. This simplification is found to perform satisfactorily.

The coherency concept is also developed for the study of the power transfer limits among groups of machines. A leader machine is chosen for each group to represent all machines of the group, with modified inertia, resistance, and reactance. The technique was reported by CEGB engineers.

6-3 ESTIMATED DYNAMIC EQUIVALENTS

The third approach for obtaining external dynamic equivalents is deriving the equivalents through estimation using information only from the study system [14–16]. In such a case, unlike the modal approach or coherency approach, no information about the external system is required. This is very desirable since so many machines, loads, and lines of the external system are involved, and the data are very difficult to obtain and some of them are not even available. Moreover, sooner or later, we may have to face the problem of deriving the external dynamic equivalent with on-line computation for security assessment of stable system operation. In such a case, we do not have any other choice but to estimate the external dynamic equivalent on line.

Pioneer work of dynamic equivalent estimation has been done, which will be presented in this section; other techniques are being developed, which will be presented in subsequent sections.

Maximum Likelihood Identification

Identification of external dynamic equivalent of a power system using a stochastic process was reported in references [14, 15]. A maximum likelihood function and a Kalman filter were used. For the on-line measurements, random load fluctuations normally appearing in the system recording at the power system boundary are processed by a low-pass filter, and the undesirable noises are removed. The general procedures are shown in Fig. 6-5.

In the figure, a likelihood function of the residual δz is constructed, which is the difference between the on-line measurement z and the predicted mea-

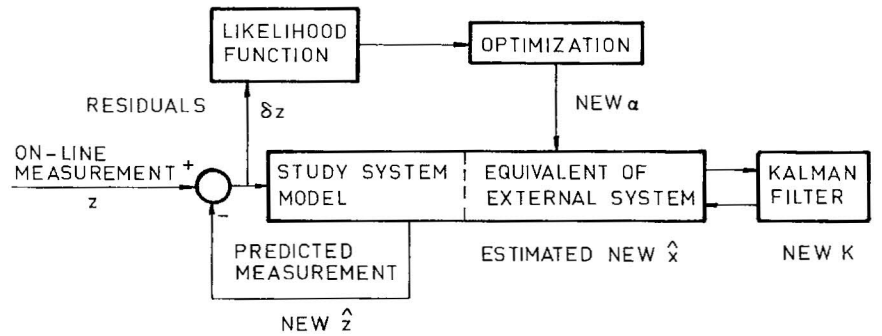

Fig. 6-5 Maximum likelihood identification. (From [15] courtesy of IEEE, © 1975.)

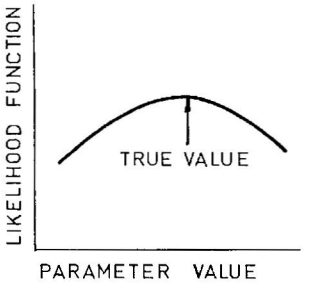

Fig. 6-6 Likelihood function of one parameter.

surement $\hat{z}$. The function is then optimized and a new parameter vector α of the system is found to estimate a new system state $\hat{x}$. The Kalman filter gain K is calculated at each step, which itself involves many iterations. A new measurement $\hat{z}$ is predicted and compared with the on-line measurement z at that instant to give a new residual δz. The process is repeated until the likelihood function reaches maximum, which gives the best estimated parameter values. A typical likelihood function versus one parameter is shown in Fig. 6-6. The mathematics of the process are rather involved and some details are given in reference [14].

The identification technique was applied to a three-machine electric power system with two machines in the study system and one in the external system. Each machine of the study system was represented by two state variables, δ and ω, and a voltage behind reactance; and the external system by two state variables P_L and Q_L, the power and reactive power, respectively. Test results have shown that the technique is feasible and that further development is required [15].

Discussion of the papers pointed out that the noises due to load fluctuations may have a significant single-phase component, and that the model identified may depend on the magnitude of the measurement signals.

Least-Squares-Error Identification

The least-squares-error technique was applied to identify both static and dynamic equivalents of an external electric power system, and the static equivalent was estimated first [16]. A stochastic process was used. It was assumed that the impact of disturbance of the study system on the external system was small, that the external system can be represented by a stochastic process, that the unknown disturbance due to momentary imbalance of the

external generation and load was small, and that the power and reactive power inputs to the external system at the boundary were observable.

The process is represented by a linear difference equation of the form

$$y(k) = \sum_{j=1}^{n} a_j y(k-j) + \sum_{j=1}^{m} a_{n+j} w(k-j) + \sum_{j=1}^{n} \sum_{i=1}^{l} b_{ji} u_i(k-j) + w(k) \quad (6\text{-}18)$$

where $y(k)$ are the state variables of the external equivalent, e.g., the changes in its internal voltage $\Delta E_i'$ and its phase angle $\Delta\delta_i'$, at time k of the process; $y(k-j), j = 1, \ldots, n$, are a series of values of $y(k)$ of order n of an autoregressive process and a_j the corresponding coefficients; $w(k-j), j = 1, \ldots, m$, are the residual errors of $y(k-j)$ of order m and a_{n+j} the corresponding coefficients; $u_i(k-j), j = 1, \ldots, n$, are a series of the ith observable input variables, e.g., the tie-line power $\Delta P_i'$ or the reactive power $\Delta Q_i'$, and b_{ij}, $i = 1, \ldots, n, j = 1, \ldots, n$, are the corresponding coefficients; and $w(k)$ is the error of $y(k)$ at time k.

Since $u_i(k-j), i = 1, \ldots, l$, are deterministic, the first three terms on the RHS of (6-18) can be combined, resulting in

$$y(k) = a^{\mathrm{T}} z(k-s) + w(k) \quad (6\text{-}19)$$

where

$$a^{\mathrm{T}} = [a_1 \cdots a_{n+m}, b_{11} \cdots b_{1l} \cdots b_{nl}]$$

$$z^{\mathrm{T}}(k-s) = [y(k-1) \cdots y(k-n), w(k-1) \cdots w(k-m), \quad (6\text{-}19a)$$

$$u_1(k-1) \cdots u_1(k-n), u_2(k-1) \cdots u_2(k-n) \cdots u_n(k-n)]$$

Let the estimate a be $\hat{a}$, and the residual error be

$$\hat{w}(k, \hat{a}) = y(k) - \hat{a}^{\mathrm{T}} z(k-s) \quad (6\text{-}20)$$

and let a square error function of size N be

$$J_N \triangleq \sum_{k=1}^{N} \hat{w}^2(k, \hat{a}) \quad (6\text{-}21)$$

Recursive formulas for the parameter identification can be found from the minimization of J_N with respect to $\hat{a}$. When the internal voltages $\Delta E_i'$ and angles $\Delta\delta_i'$ are chosen for the external equivalent, as the state variables, and the tie-line power $\Delta P_i'$ and reactive power $\Delta Q_i'$ as the input variables, the

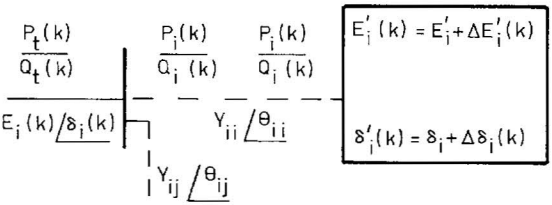

Fig. 6-7 Equivalent of the least-squares identification. (From [16] courtesy of IEEE, © 1976.)

recursive formulas become

$$\Delta E'_i(k) = \sum_{j=1}^{n} \left[a_j \Delta E'_i(k-j) + b_{1j} \Delta P'_i(k-j) + b_{2j} \Delta Q'_i(k-j)\right] + \sum_{j=1}^{m} a_{n+j} w_E(k-j) \tag{6-22}$$

$$\Delta \delta'_i(k) = \sum_{j=1}^{n} \left[c_j \Delta \delta'_i(k-j) + d_{1j} \Delta P'_i(k-j) + d_{2j} \Delta Q'_i(k-j)\right] + \sum_{j=1}^{m} a_{n+j} w_\delta(k-j) \tag{6-23}$$

and the equivalent system may be drawn as Fig. 6-7.

In the process the static equivalent must be estimated first. Several equivalent models were proposed. For details, see reference [16].

Discussions of the paper pointed out that information on the external system was required for the static equivalent estimation and that validity of the models for identification may depend on the nature and location of the disturbance within the study system.

Summary of Section 6-3

In this section two external dynamic equivalent estimation techniques are introduced. By the maximum likelihood technique, the likelihood function of the residual error of the on-line measurement minus the predicted measurement is repeatedly minimized until it reaches an optimum. A new state is estimated in each iteration using the Kalman filter. The best estimation of equivalent parameters corresponds to the maximum of the likelihood function.

A least-squares technique using a stochastic process for the external dynamic equivalent estimation is also introduced. But the external static

equivalent must be estimated first, which requires full information on the external system.

Using a deterministic process for the external dynamic equivalent estimation without the need for any external information, a much simpler least-squares technique with less computation will be derived in the subsequent sections.

6-4 ESTIMATION WITH AN INTENTIONAL DISTURBANCE

One difficulty of all the foregoing dynamic equivalencing techniques of the external system is the heavy computational requirement: the diagonalization of a very large system matrix using eigenvectors of the modal approach, the transient stability analysis of a large electric power system and the dynamic aggregation of the coherency approach, and the iterative stochastic process of the estimation approach.

Another difficulty with these techniques is the requirement for full system data on the external system except in the maximum likelihood approach, which is almost impossible for large electric power systems. As for low-pass filtered tie-line recording for the stochastic process, it is time consuming to compute and there might be a single-phase dc component.

An Intentional Disturbance

To overcome these difficulties, a deterministic process with an intentional disturbance for the estimation of external dynamic equivalent is proposed [17, 18, 32]. The disturbance is so chosen that the system response to the disturbance is much larger than the load fluctuations observed on the tie line, so that the recording noises will not have any significant effect on the estimated results. The system voltage regulation due to the intentional disturbance, of course, must be kept within the safety limits.

There are many ways to generate such a disturbance: a pulsed excitation, a ramp torque, or a temporary switching off of one line section. The last approach is the least desirable since it does alter the structure of the study system. The first is the simplest to apply as it changes the system operating condition only temporarily.

Figure 6-8 shows the response of a machine due to a disturbance in a study system. A 5% pulsed excitation is applied to the machine for one second, and the terminal voltage Δv_t, the electric power ΔP_e, and the speed $\Delta\omega$ of the machine are recorded for four seconds from computer simulation for the dynamic equivalent estimation. The voltage regulation is well within

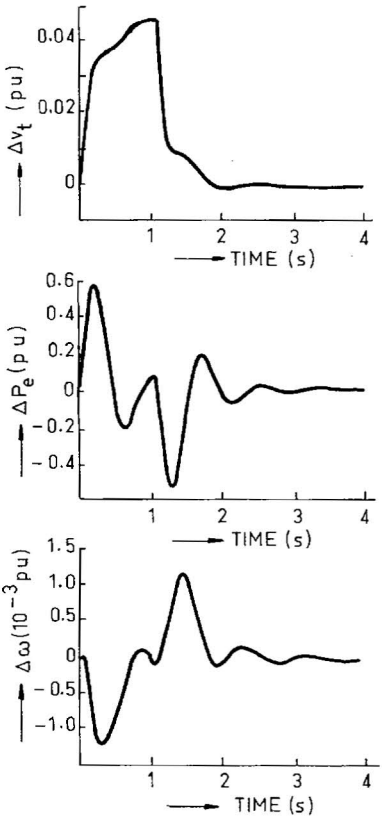

Fig. 6-8 System responses to a pulsed change of excitation.

the safety limit, and the power variation is much larger than the load fluctuations usually found from tie-line recording. There is, of course, no single-phase component. Therefore, these recordings can be used for the deterministic estimation process. In examples to be presented in later sections, it is found that actually only two seconds of Fig. 6-8 recordings are sufficient for the equivalent estimation.

In practice, it is recommended that the pulsed excitation be carefully tried in the beginning, gradually increased, and finally increased to the desired level good enough for the equivalent estimation.

Equivalent Models and the Least-Squares Error

The objective of deriving an external dynamic equivalent is to find a simple representation of the dynamic interacting effect of the external sys-

tem on the study system. For that, many models with various degrees of details could be chosen. But some criteria must be derived for the choices of the model.

The choices of a model for any power system dynamic studies, of course, cannot be dissociated from the problem itself. One has to know whether it is for the low-frequency oscillation study, or for the subsynchronous resonance and torsional oscillation study, or for the transient stability study. Therefore, the external dynamic equivalent should be represented by an equivalent machine instead of a static electrical circuit.

To describe both study system and external system, it is also desirable to have a model in common, and the model can be adapted to describe the individual machines as well as the equivalents. This suggests that the fourth-order model of Fig. 3-1 of Chapter 3 might be a good start, although the model must be extended to describe a multimachine system. The derivation of such a model will be presented in Section 6-4.

The next question is, in how much detail should the external system be represented? Shall we use a full model similar to Fig. 3-1, or omit the T_A block, or even the T'_{d0} block? On the other hand, can we add an extra section of transmission line between the study system and the external system, and some local load for the external equivalent? In any case, the external system should be neither overrepresented nor underrepresented.

To find the most adequate model for the external equivalents of a power system, the following guidelines are proposed:

(1) The error of the predicted and observed measurements must be minimum.

(2) The estimated equivalent parameter values must be unique for any initial guess.

Let a least-squares-error function be chosen as

$$J = \int_{t_0}^{t_\infty} \left[y(t) - \tilde{y}(t, \alpha)\right]^{\mathrm{T}} R \left[y(t) - \tilde{y}(t, \alpha)\right] dt \tag{6-24}$$

While the measurement vector y is a function of time only, the predicted measurement $\tilde{y}$ is a function of both time and the unknown equivalent parameter vector α being estimated at each step. R of (6-24) is a diagonal weighting matrix for the error function $\left[y_i - y_i(\alpha)\right]$, and should be so chosen that a variable with a large unit and hence a small numerical value, like $\Delta\omega$ in per unit value instead in radians per second, be given a large weighting factor, and a variable with a small unit be given a small weighting factor.

After the J function is chosen, the next step is to ensure that J is sensitive with respect to all parameters of the equivalent model chosen, like Fig. 6-9a.

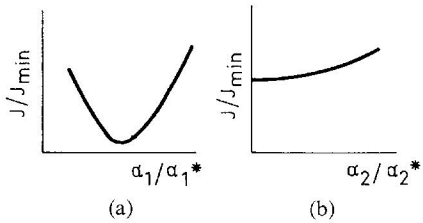

Fig. 6-9 J is sensitive to α_1 but not α_2 (*: optimum values).

The lack of sensitivity, as demonstrated by Fig. 6-9b, implies that the equivalent is overrepresented, and a model of reduced order and/or less parameters should be sought for the equivalent.

Although the sensitivity test is necessary, it may not be sufficient. The ultimate guidelines are still that the estimation error J be minimum and the estimated parameter values be unique. Of course, we may start from a low-order model with least parameters and increase the order and/or the number of parameters whenever warranted.

System Equations and Estimation Algorithm

The system equations including both study system and external system are written in the linear form of

$$\begin{aligned} \dot{x} &= Ax + d \\ y &= Hx \end{aligned} \tag{6-25}$$

where x is the system state variable vector, y the output or measurement vector, d the intentional disturbance, A the system matrix, and H the output matrix. Equation (6-25) can be used also to describe the study system plus the equivalents or the equivalent system, but the system order and number of variables will be reduced owing to the equivalents.

Prior to estimation, the initial steady state of the system must be known, which can be found from a load flow study; and the y measurements must be prerecorded for off-line estimation, although on-line estimation is also conceivable if a fast computer is available.

For the estimation, however, most terms of (6-25) should be explicitly expressed as functions of α, the unknown parameters to be estimated,

$$\begin{aligned} \dot{\tilde{x}}(\alpha) &= \tilde{A}(\alpha)\tilde{x}(\alpha) + d \\ \tilde{y}(\alpha) &= \tilde{H}(\alpha)\tilde{x}(\alpha) \end{aligned} \tag{6-26}$$

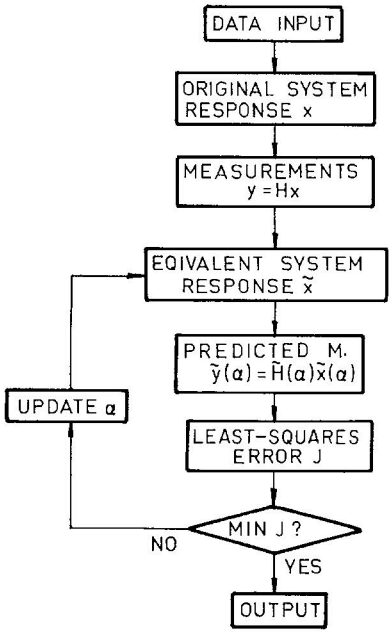

Fig. 6-10 A deterministic estimation algorithm.

The error function J of (6-24) is calculated from (6-25) and (6-26). Note that the independent variable t is omitted from (6-25) and (6-26) for conciseness. All predicted values are shown with a $\sim$, e.g., $\tilde{x}$.

Figure 6-10 illustrates the deterministic estimation algorithm, including the following steps:

(1) Find the initial steady state of the system.

(2) Find the system response x or $\int \dot{x}\, dt$ and the measurement y of the original system to an intentional disturbance d at instant t beginning at t_0.

(3) Compute the equivalent system response $\tilde{x}$ or $\int \dot{\tilde{x}}\, dt$ and the predicted measurement $\tilde{y}$ of the equivalent system, which are functions of both t and α, for the same intentional disturbance at the same instant.

(4) Compute the least-squares-error J and adapt the equivalent parameters α until J reaches the minimum.

Note that for the development of the estimation technique, both x and y are computed in step 2, but y is prerecorded for off-line estimation or recorded on-line for on-line estimation.

There are also two problems associated with the algorithm of Fig. 6-10:

(a) to find an adequate model for the external equivalent;

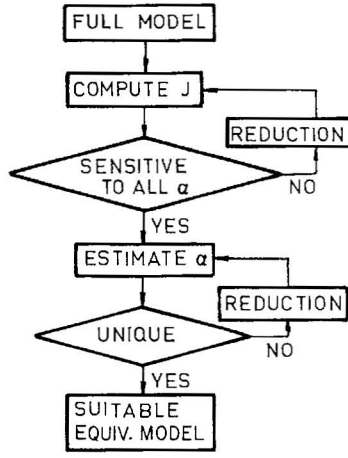

Fig. 6-11 Algorithm to find an adequate model for the equivalent.

(b) to adapt the step size of α at each iteration to ensure fast convergence of the computation.

An algorithm to find an adequate model is given in Fig. 6-11. For this, a large step size may be used.

A Self-Adaptive Step Size

To ensure fast convergence of the iterative scheme as shown in Fig. 6-10, the steepest descent method is adopted, but the step sizes of the equivalent parameters are adapted at each step as follows. Let

$$\alpha_{\text{new}} = \alpha_{\text{old}} - \delta\alpha \tag{6-27}$$

and

$$\delta\alpha = KJ_\alpha \tag{6-28}$$

J_α or $\partial J/\partial\alpha$ is the sensitivity vector of J with respect to α, and K is a diagonal matrix to be decided. As is well known in computation, when J approaches a minimum, the convergence is very slow for a small K, but may overshoot or even diverge for a large K. Therefore, K must be automatically adapted.

Let the step size be constrained by

$$(\delta\alpha)^{\mathrm{T}} G(\delta\alpha) = C^2 \tag{6-29}$$

where G is a positive definite diagonal weighting matrix and C a constant. G can be properly chosen for various estimated parameters with different

units, and C can be adjusted in the process. Let the optimum J be $J^*(\alpha)$, and

$$J^*(\alpha) = J(\alpha) + \lambda g \tag{6-30}$$

where

$$g = (\delta\alpha)^{\mathrm{T}} G(\delta\alpha) - C^2 \tag{6-31}$$

and λ is a Lagrange multiplier. Since for an optimum J^*,

$$J^*_\alpha = J_\alpha + \lambda g_\alpha = 0 \tag{6-32}$$

$$J_\alpha = -2\lambda G(\delta\alpha) \tag{6-33}$$

Substituting $\delta\alpha$ of (6-28) into (6-33) and solving for K gives

$$K = -\frac{1}{2\lambda} G^{-1} \tag{6-34}$$

Substituting K back into (6-28) gives

$$\delta\alpha = \left(-\frac{1}{2\lambda}\right) G^{-1} J_\alpha \tag{6-35}$$

Substituting $\delta\alpha$ of (6-35) into (6-29) and solving for $-1/2\lambda$ yields

$$-\frac{1}{2\lambda} = C\left[J_\alpha^{\mathrm{T}} G^{-1} J_\alpha\right]^{-1/2} \tag{6-36}$$

Therefore, K of (6-34) becomes

$$K = C\left[J_\alpha^{\mathrm{T}} G^{-1} J_\alpha\right]^{-1/2} G^{-1} \tag{6-37}$$

The step size of Fig. 6-10 will now be adapted according to (6-27).

The advantages of this scheme are:

(1) J_α can be calculated numerically and it does not require the computation of $J_{\alpha\alpha}$ and $J_{\alpha\alpha}^{-1}$ as required by other schemes, which is very time-consuming.

(2) The step size is automatically adjusted at each iteration to ensure fast convergence.

(3) By selecting proper values for the diagonal elements of the weighting matrix G, different step sizes can be chosen for different parameters, which usually have different units and ranges of values.

(4) C also can be adjusted: it can be decreased when J tends to diverge and increased if the convergence is too slow.

Summary of Section 6-4

In this section estimation techniques for dynamic equivalents of a power system with an intentional disturbance in the study system are presented. The objective of an intentional disturbance is to intensify the interacting effect of the external system on the study system so that the load fluctuation noises normally observed on the tie-line recordings become insignificant. Then a deterministic process can be used for the estimation, which is much less time-consuming than a stochastic process. On the other hand, the intentional disturbance must be kept within the safe voltage regulation limit of the power system.

The concepts of least-squares error and sensitivity are applied to develop the estimation algorithm and to select the equivalent model. To ensure fast convergence in computation, the steepest descent with automatically self-adaptive step sizes is adopted.

We shall continue to develop a multimachine power system model in the next section, and use the model and apply the dynamic equivalent estimation techniques developed in this section to estimate dynamic equivalents of a large electric power system in Section 6-6.

6-5 A MULTIMACHINE ELECTRIC POWER SYSTEM MODEL

In this section, Fig. 3-1 of Chapter 3 will be extended to describe a multimachine electric power system [17, 33]. Figure 3-1 [34] is chosen as the basis because this is a model familiar to most power engineers. It can be used to describe large and small machines in a system, or adapted for the external equivalent representation by omission of, for instance, the T_A block or even the T'_{d0} block, and/or by approximation, for instance, $x_d = x_q$.

When Fig. 3-1 is extended to describe a multimachine system, a typical block diagram of the ith machine can be represented by Fig. 6-12. Because of the interaction among machines, the branches and loops become multiplied; for instance, K_1 becomes K_{1ij}, $i = 1, \ldots, n$, $j = 1, \ldots, n$, T_A becomes T_{Ai}, $i = 1, \ldots, n$, etc. The state variables also become multiplied; for instance, $\Delta\delta$ becomes $\Delta\delta_i$, $i = 1, \ldots, n$.

Phasor Diagram of the ith Machine

The phasor diagram of the ith machine of a multimachine system may be shown as in Fig. 6-13. While d_i and q_i are the coordinates for the ith

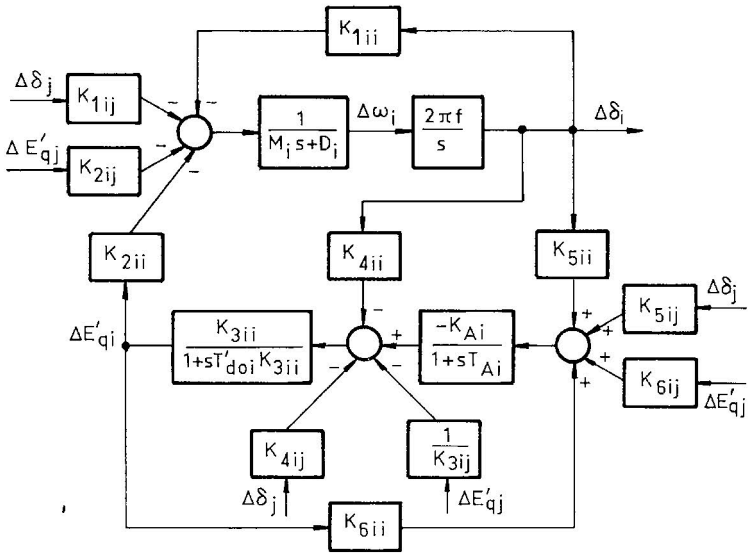

Fig. 6-12 Basic model for a multimachine system.

machine alone, D and Q are the coordinates for all machines of the entire system. The phase angle difference between d_i and D, or q_i and Q, is denoted by δ_i, which is constantly changing and could be positive or negative.

In Fig. 6-13, the phasors of voltages and currents are shown with a bar, like $\bar{E}_{qi}$, $\bar{V}_i$, or $\bar{I}_i$. But the bar will be removed when the magnitude is considered, like E_{qi}, I_{qi}, etc. This convention will be followed throughout the derivation of the multimachine model in this section. Therefore, the terminal voltage $\bar{V}_i$ of the ith machine of the system in common coordinates becomes

$$\bar{V}_i = E'_{qi}e^{j(90-\delta_i)} - jx'_{di}\bar{I}_i + (x_{qi} - x'_{di})I_{qi}e^{-j\delta_i} \tag{6-38}$$

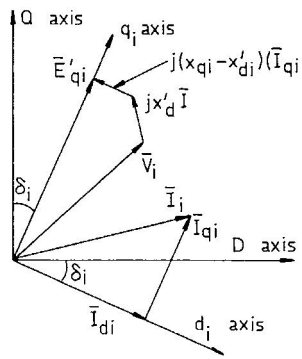

Fig. 6-13 A phasor diagram of the ith machine.

Note that

$$\bar{E}_{qi} = E'_{qi}e^{j(90-\delta_i)}, \qquad \bar{I}_{qi} = jI_{qi}e^{-j\delta_i} \tag{6-38a}$$

For n machines of an n-machine system, (6-38) may be written in matrix form

$$[\bar{V}] = [e^{j(90-\delta)}][E'_q] - j[x'_d][\bar{I}] + [x_q - x'_d][e^{-j\delta}][I_q] \tag{6-39}$$

Since each term of (6-39) is a column matrix, the coefficients $[e^{j(90-\delta)}]$, $[e^{-j\delta}]$, $[x'_d]$, and $[x_q - x'_d]$ should all be read as diagonal matrices.

Current Components

To find $K_{1ii}, K_{1ij}, \ldots, K_{6ij}$ of Fig. 6-12, the current components must be found first, a process similar to the derivation of Fig. 3-1. After a load flow study of a power system, the load buses can be eliminated. Note that the algebraic sum of currents of a load bus is zero. Let the generator current matrix equation be

$$[\bar{I}] = [\bar{Y}_t][\bar{V}] \tag{6-40}$$

where $[\bar{V}]$ is the generator terminal voltage vector and $[\bar{Y}_t]$ the transmission admittance matrix. Substituting the solution of $[\bar{V}]$ of (6-40) into (6-39) and solving for $[\bar{I}]$ gives

$$[\bar{I}] = [\bar{Y}][[e^{j(90-\delta)}][E'_q] + [x_q - x'_d][e^{-j\delta}][I_q]] \tag{6-41}$$

where

$$[\bar{Y}] \triangleq [[\bar{Y}_t]^{-1} + j[x'_d]]^{-1} \tag{6-41a}$$

For the ith machine of an n-machine system in D-Q coordinates, the current has n terms

$$\bar{I}_i = \sum_{j=1}^{n} \bar{Y}_{ij}[e^{j(90-\delta_j)}E'_{qj} + (x_{qj} - x'_{dj})e^{-j\delta_j}I_{qj}] \tag{6-42}$$

including the term of $j = i$.

In $d_i - q_i$ coordinates,

$$\begin{aligned} \bar{i}_i &= \bar{I}_i e^{j\delta_i} \\ &= \sum_{j=1}^{n} Y_{ij}[e^{j(\beta_{ij}+\delta_{ij}+90)}E'_{qj} + (x_{qj} - x'_{dj})e^{j(\beta_{ij}+\delta_{ij})}I_{qj}] \end{aligned} \tag{6-43}$$

where

$$\bar{Y}_{ij} \triangleq Y_{ij}e^{j\beta_{ij}}, \qquad \delta_{ij} \triangleq \delta_i - \delta_j \tag{6-43a}$$

Therefore

$$\begin{aligned} i_{di} &= \mathrm{Re}(\bar{i}_i) = \sum_{j=1}^{n} Y_{ij}\left[-S_{ij}E'_{qj} + (x_{qi} - x'_{di})C_{ij}I_{qj}\right] \\ i_{qi} &= \mathrm{Im}(\bar{i}_i) = \sum_{j=1}^{n} Y_{ij}\left[C_{ij}E'_{qj} + (x_{qi} - x'_{di})S_{ij}I_{qj}\right] \end{aligned} \tag{6-44}$$

where

$$C_{ij} \triangleq \cos(\beta_{ij} + \delta_{ij}), \qquad S_{ij} \triangleq \sin(\beta_{ij} + \delta_{ij})$$

Let the deviation of i_i be defined by

$$\Delta(i_{di} + ji_{qi}) = \Delta I_{di} + j\,\Delta I_{qi} \tag{6-45}$$

From (6-44) and for n machines, we will have

$$\begin{aligned} [\Delta I_d] &= [P_d][\Delta\delta] + [Q_d][\Delta E'_q] + [M_d][\Delta I_q] \\ [L_q][\Delta I_q] &= [P_q][\Delta\delta] + [Q_q][\Delta E'_q] \end{aligned} \tag{6-45a}$$

where

$$\begin{aligned} P_{dij} &= -Y_{ij}\left[C_{ij}E'_{qj} + (x_{qj} - x'_{dj})S_{ij}I_{qj}\right] \qquad j \neq i \\ P_{qij} &= -Y_{ij}\left[S_{ij}E'_{qj} - (x_{qj} - x'_{qj})C_{ij}I_{qj}\right] \qquad j \neq i \\ P_{dii} &= -\sum_{j\neq i} P_{dij}, \qquad P_{qii} = -\sum_{j\neq i} P_{qij} \\ Q_{dij} &= -Y_{ij}S_{ij}, \qquad Q_{qij} = Y_{ij}C_{ij}, \qquad j = 1, \ldots, n \\ L_{qij} &= -Y_{ij}(x_{qj} - x'_{dj})S_{ij} \qquad j \neq i \\ L_{qii} &= 1 - Y_{ii}(x_{qi} - x'_{di})S_{ii} \\ M_{dij} &= Y_{ij}(x_{qj} - x'_{qj})C_{ij} \qquad j = 1, \ldots, n \end{aligned} \tag{6-45b}$$

For the calculation of all P, Q, L, and M coefficients of (6-45b), initial values of E'_{qj}, I_{qj}, and δ_j (for C_{ij} and S_{ij}), $j = 1, \ldots, n$, must be used.

The solutions of $[\Delta I_d]$ and $[\Delta I_q]$ of (6-45a) become

$$\begin{aligned} [\Delta I_d] &= [Y_d][\Delta E'_q] + [F_d][\Delta\delta] \\ [\Delta I_q] &= [Y_q][\Delta E'_q] + [F_q][\Delta\delta] \end{aligned} \tag{6-46}$$

where

$$\begin{aligned} [Y_d] &= [Q_d] + [M_d][Y_q], \qquad & [F_d] &= [P_d] + [M_d][F_q] \\ [Y_q] &= [L_q]^{-1}[Q_q], & [F_q] &= [L_q]^{-1}[P_q] \end{aligned} \tag{6-46a}$$

K_{1ii}, K_{1ij}, K_{2ii}, and K_{2ij}

An electric torque approximately equals an electric power when the synchronous speed is chosen as the base speed. For the ith machine,

$$T_{ei} \simeq \mathrm{Re}(\bar{I}_i^* \bar{V}_i) = I_{qi}E'_{qi} + I_{qi}(x_{qi} - x'_{di})I_{di} \tag{6-47}$$

For n machines and in linear form

$$\begin{aligned}[\Delta T_e] = {} & [I_{q0}]^T[\Delta E'_q] + [I_{q0}]^T[x_q - x'_d][\Delta I_d] \\ & + [E'_q]^T[\Delta I_q] + [I_{d0}]^T[x_q - x'_d][\Delta I_q]\end{aligned} \tag{6-48}$$

which can be written

$$[\Delta T_e] = [K_1][\Delta\delta] + [K_2][\Delta E'_q] \tag{6-49}$$

where

$$\begin{aligned}K_{1ii} &= D_t F_{dii} + Q_t F_{qii}, & K_{1ij} &= D_t F_{dij} + Q_t F_{qij} \\ K_{2ii} &= D_t Y_{dii} + Q_t Y_{qii} + I_{qi0}, & K_{2ij} &= D_t Y_{dij} + Q_t Y_{qij}\end{aligned}$$

and

$$D_t = (x_{qi} - x'_{di})I_{qi0}, \qquad Q_t = (x_{qi} - x'_{di})I_{di0} + E'_{qi0} \tag{6-49a}$$

K_{3ii}, K_{3ij}, K_{4ii}, and K_{4ij}

The internal voltage equation for n machines may be written

$$[[1] + s[T'_{d0}]][\Delta E'_q] = [\Delta E_{FD}] - [x_d - x'_d][\Delta I_d] \tag{6-50}$$

where $[1]$ is a unit matrix, and $[T'_{d0}]$ a diagonal matrix. Substituting $[\Delta I_d]$ of (6-46) into (6-50) and shifting terms gives

$$\begin{aligned}&[[1] + [x_d - x'_d][Y_d] + s[T'_{d0}]][\Delta E'_q] \\ &\quad = [\Delta E_{FD}] - [x_d - x'_d][F_d][\Delta\delta]\end{aligned} \tag{6-51}$$

For the ith machine, it may be written

$$[1 + sT'_{d0i}K_{3ii}]\,\Delta E'_{qi} = K_{3ii}\left[\Delta E_{FDi} - \sum_{j\neq i}^{n} \frac{1}{K_{3ij}}\Delta E'_{qj} - \sum_{j=1}^{n} K_{4ij}\,\Delta\delta_j\right] \tag{6-52}$$

where

$$\begin{aligned}K_{3ii} &= [1 + [x_{di} - x'_{di}]Y_{dii}]^{-1} \\ K_{3ij} &= [[x_{di} - x'_{di}]Y_{dij}]^{-1} \\ K_{4ii} &= [x_{di} - x'_{di}][F_{dii}] \\ K_{4ij} &= [x_{di} - x'_{di}][F_{dij}]\end{aligned} \tag{6-52a}$$

K_{5ii}, K_{5ij}, K_{6ii}, and K_{6ij}

Similar to (3-6) but for n machines,

$$\begin{aligned}[\Delta V_d] &= [x_q][\Delta I_q] \\ [\Delta V_q] &= [\Delta E'_q] - [x'_d][\Delta I_d]\end{aligned} \tag{6-53}$$

Furthermore

$$[\Delta V_t] = [V_{t0}]^{-1}[V_{d0}][\Delta V_d] + [V_{t0}]^{-1}[V_{q0}][\Delta V_q] \tag{6-54}$$

We have

$$[\Delta V_t] = [K_5][\Delta\delta] + [K_6][\Delta E'_q] \tag{6-55}$$

where

$$\begin{aligned}[K_5] &= [D_v][x_q][F_q] - [Q_v][x'_d][F_d] \\ [K_6] &= [D_v][x_q][Y_q] - [Q_v][x'_d][Y_d] + [Q_v]\end{aligned} \tag{6-55a}$$

and

$$[D_v] = [V_{t0}]^{-1}[V_{d0}], \qquad [Q_v] = [V_{t0}]^{-1}[V_{q0}]$$

In these equations, V_{t0}, V_{d0}, V_{q0}, D_v, and Q_v should be read as diagonal matrices, and ΔV_d and ΔV_q as vectors. Note that we have used V's and I's instead of v's and i's to denote voltages and currents in individual machine coordinates in this section since Eq. (6-45).

Summary of Section 6-5

In this section, a multimachine electric power system model is developed. It is an extension of Fig. 3-1 of Chapter 3.

The procedure of derivation is similar to that of Fig. 3-1; that is, to find the d and q current components of the ith machine first. It is found from a voltage phasor diagram for the ith machine in both d_i-q_i and D-Q coordinates and the voltage and current relation of the transmission system. Having found the d and q current components including the transmission relation, K_{1ii}, K_{1ij}, K_{2ii}, and K_{2ij} are found from the electric torque expression, K_{3ii}, K_{3ij}, K_{4ii}, and K_{4ij} from the internal voltage equation, and K_{5ii}, K_{5ij}, K_{6ii}, and K_{6ij} from the terminal voltage relation.

The model can be used to describe a multimachine system in general or adapted to represent an external dynamic equivalent in particular.

6-6 DYNAMIC EQUIVALENTS OF A THIRTEEN-MACHINE SYSTEM

The external dynamic equivalent estimation technique with a deterministic process, using an intentional disturbance within the study system, developed in Section 6-4, and the multimachine electric power system model derived in Section 6-5, have been applied to estimate the equivalents of several systems [17, 18, 32]. In this section, the application to a 13-machine system and the estimation and test results will be presented [17].

A 13-Machine Electric Power System

A 13-machine electric power system is shown in Fig. 6-14. There are 13 generating units as indicated by circled numbers, with data shown separately in Table 6-1. There are 22 buses identified by a, b, ..., v with bus load admittance Y_a, Y_b, etc., shown separately in Table 6-2. Transformers are shown with impedances underneath, and transmission lines with impedances in blocks. All reactances and admittances are given on the basis of 100 MVA and 345 kV, and the inertia constants on the basis of 100 MW.

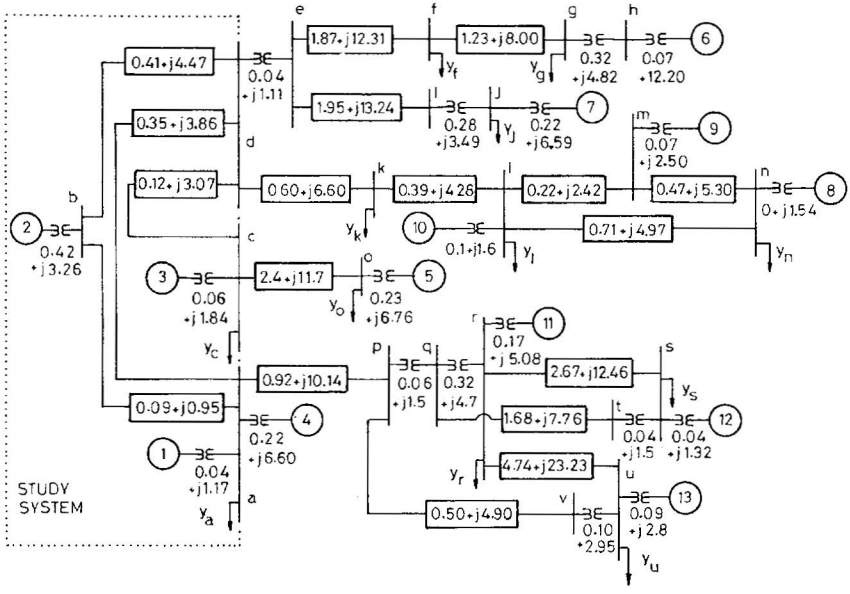

Fig. 6-14 A 13-machine electric power system. (From [17] courtesy of IEEE, © 1981.)

Table 6-1

Generator and Excitation Data[a]

#	MW	M	x'_d	x_d	x_q	T'_{d0}	K_A	T_A
1	960	65.46	0.0208	0.1675	0.1675	6.7	100	0.02
2	600	55.20	0.0560	0.3030	0.2820	5.5	100	0.02
3	660	64.56	0.0440	0.1715	0.1023	6.1	100	0.02
4	100	16.64	0.1269	1.192	1.192	5.6	18.5	0.20
5	135	6.52	0.2467	0.8667	0.5207	3.5	40	0.06
6	390	38.36	0.0386	0.3158	0.2624	4.3	160	0.03
7	184	27.94	0.0789	0.4993	0.4819	3.3	18.5	0.20
8	35,047	3500	0.0010	0.0010	0.0010	(constant E'_q)		
9	600	78.00	0.0179	0.1285	0.1230	4.0	50	0.02
10	800	68.40	0.0579	0.2106	0.2050	4.8	400	0.02
11	140	16.10	0.1060	1.540	1.490	7.9	45	0.06
12	691	70.42	0.0285	0.1801	0.1376	5.5	(no V.R.)	
13	563	56.72	0.0392	0.3366	0.3270	5.5	160	0.02

[a] [17], courtesy of IEEE, © 1981.

The excitation data are also included in Table 6-1. Generating unit 8 itself actually represents an equivalent of a large electric power system. But the data still can be used to test the equivalencing techniques. As for the damping, it is assumed that $\zeta_{ni} = 10\%$ on the individual machine basis.

The Equivalent System and External Equivalent Models

The three generating units 1, 2, and 3 of Fig. 6-14, which are of main concern, constitute the study system, and the rest becomes the external system. Because of the three buses on the boundary, three external dynamic equivalents are assumed as in Fig. 6-15.

Several models with various degrees of detail were considered for the 13-machine and other system external equivalent studies [17, 18, 32]. The most useful ones are

(a) a second-order model with $\Delta\delta$ and $\Delta\omega$ as the state variables and M, ζ_n, and x'_d as the unknown parameters;

Table 6-2

Load Admittances

$Y_a = 5.00 + j2.19$	$Y_c = 3.06 + j1.15$	$Y_f = 2.20 + j0.60$	$Y_g = 3.40 + j0.85$
$Y_j = 3.20 + j1.28$	$Y_k = 2.68 + j1.00$	$Y_l = 7.70 + j1.60$	$Y_n = 358. + j0.90$
$Y_o = 2.00 + j0.53$	$Y_r = 3.97 + j1.25$	$Y_s = 3.33 + j1.14$	$Y_u = 8.45 + j2.16$

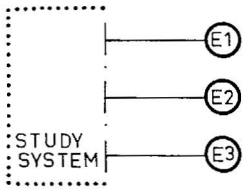

Fig. 6-15 The equivalent system.

(b) a third-order model with $\Delta\delta$, $\Delta\omega$, and $\Delta E'_q$ as the state variables and M, ζ_n, T'_{d0}, x'_d, and x_d as the unknown parameters.

Among those parameters, the damping coefficient of the ith machine is defined by

$$\zeta_{ni} = D_{ei}/(2\omega_{ni}M_i) \tag{6-56}$$

where

$$\omega_{ni} = \sqrt{K_{1ii}\omega_b/M_i}$$

and the damping effect of a PSS or a LOC is included in D_{ei}. The damping coefficient ζ_{ni} is chosen over D_{ei} in the modeling because, similar to (3-39), ζ_{ni} is the damping coefficient of the normalized torque equation, which is more meaningful.

For the estimation of the three dynamic equivalents (E1, E2, and E3) of the 13-machine system, only the second-order model (a) with three unknown parameters gives the minimum error and unique parameter values regardless of the initial guess.

The intentional disturbance described in Section 6-4 can be applied to any one machine of the study system, and the response of any one machine of the study system can be used for the external dynamic equivalent estimation. Examples include response of machine 2 due to a disturbance of machine 1, or response of machine 1 due to a disturbance on machine 1 itself. For the development of the estimation technique, responses due to an initial disturbance are obtained from computer simulation of the full 13-machine system. Typical responses of machine 1 due to a 5% pulsed excitation on machine 1 itself have been recorded in Fig. 6-8.

Theoretically, there is no restriction of the number of responses that must be used for the equivalent estimation. To ensure accuracy of the particular study, however, all three responses, Δv_t, ΔP_e, and $\Delta\omega$ are used.

Many estimations are made based on the techniques developed in Section 6-4 using different sets of responses and various initial guesses. Typical results are shown in Table 6-3.

In the table the last three columns list the estimated parameter values (with initial guesses in parentheses) using responses of machine 1, 2, and 3

Table 6-3

Estimated Parameter Values

	Case I-N	Case I	Case II	Case III
M_{E1}	45.92(80.0)	45.89(30.0)	45.99(40.0)	46.12(40.0)
ζ_{E1}	1.891(3.0)	1.886(0.70)	1.811(1.5)	1.790(1.5)
X'_{dE1}	0.0569(0.50)	0.0570(0.30)	0.0568(0.10)	0.0560(0.10)
M_{E2}	136.9(30.0)	137.0(50.0)	137.7(130)	138.1(130)
ζ_{E2}	2.511(3.0)	2.519(0.80)	2.531(2.0)	2.498(2.0)
X'_{dE2}	0.3421(0.60)	0.3411(0.40)	0.3382(0.30)	0.3321(0.30)
M_{E3}	117.7(30.0)	117.3(70.0)	116.9(110)	118.1(110)
ζ_{E3}	1.995(3.0)	1.989(0.30)	2.011(2.5)	2.105(2.5)
X'_{dE3}	0.4568(0.80)	0.4363(0.50)	0.4410(0.40)	0.4215(0.40)

due to a 5% pulsed excitation applied to the individual machines, respectively. The estimated results are unique and close regardless of the initial guesses and whichever set of responses is used for the estimation. To find the noise effect on the estimation, 10% noise generated by a computer program is arbitrarily added to the responses for estimation, and the estimated results corresponding to case I are listed as case I-N. The addition of 10% noise does not have any effect on the estimated results.

Three-Phase Short-Circuit Test

Having identified the parameter values of the three equivalents, the study system plus the equivalents is given a three-phase short-circuit test. A three phase short-circuit is assumed to occur each time for six cycles on the terminal bus of machine 1, 2, or 3 of the study system, respectively, and all machine responses are recorded. The same short circuit is also assumed on the same bus each time of the original 13-machine system, and again all machine responses are recorded.

Figure 6-16 shows a typical comparison. The short circuit is assumed to occur on the terminal bus of machine 1, and the responses of machine 3 are recorded. The machine responses of the original 13-machine system are shown in solid lines and those of the equivalent system in dashes. The results are very close. More comparisons are recorded in reference [17]. The results show that the equivalents thus obtained faithfully represent the interacting effect of the external system on the study system, which proves that the estimation technique developed in Section 6-4 gives accurate results.

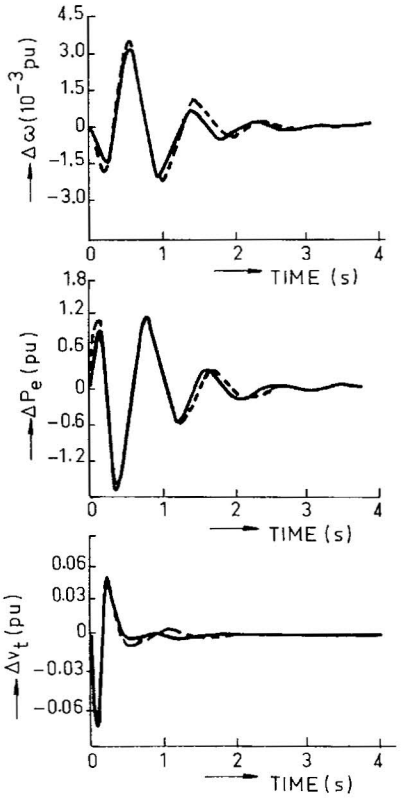

Fig. 6-16 Comparison of three-phase short-circuit tests.

Other Remarks

A Two-Machine Study System. When only machines 1 and 2 of the 13-machine system are considered as the study system, there are only two dynamic equivalents. The second-order three-parameter model is still valid but the new estimated parameter values are

$$M_{E1} = 39.48 \qquad \zeta_{E1} = 1.055 \qquad x'_{dE1} = 0.01352$$
$$M_{E2} = 154.8 \qquad \zeta_{E2} = 2.987 \qquad x'_{dE2} = 0.1868$$

Nonradial System. The 13-machine system shown in Fig. 6-14 happens to be a radial system. To find whether the estimation technique developed in Section 6-4 is also applicable to a nonradial system, two more transmission

lines close to the study system were assumed

$$z_{ko} = 1.0 + j6.0, \qquad z_{op} = 0.5 + j4.0$$

and the unknown parameters of the three external equivalents were re-estimated. It was found that the estimation technique still gave unique and accurate results, but there were changes in the estimated parameter values, especially x'_{dE1}, x'_{dE2}, and x'_{dE3}, which was rather expected. For other details, see reference [17].

On-line Estimation. On-line updating of the off-line estimation is quite conceivable. The CPU time of the three equivalent estimation of the 13-machine system is $\sim$70–80 s. This is based on the assumption that there is no prior knowledge of what range of the estimated parameter values would be. With more information on the system and a better initial guess, the CPU time can be drastically reduced. Therefore, with the known off-line estimated parameter values, on-line updating of the values once a minute, for instance, is readily achievable. One example shows that after doubling the impedance of one transmission line by switching, it takes only six iterations, or less than three seconds, to obtain a new estimation, using the old estimated values for the initial guess. More details are given in reference [17].

Summary of Section 6-6

In this section a 13-machine electric power system is used as an example to test the deterministic estimation procedures developed in Section 6-4. Three generating units are included in the study system and three external dynamic equivalents are assumed. From responses of any machine of the study system due to an intentional pulsed excitation on the said machine or any other machine, the external equivalent parameters can be estimated. The second-order model with three unknown parameters gives minimum error and unique estimated parameter values despite different initial guesses. An addition of 10% noise does not affect the estimated results.

To find whether the estimated external dynamic equivalents are faithfully representing the dynamic interacting effect of the external system on the study system, a three-phase fault is assumed on both the original 13-machine system and its equivalent system. The responses of the original system and the equivalent system agree with each other rather closely, indicating that the external dynamic equivalents obtained by this method are very accurate.

The CPU time of off-line estimation is $\sim$70–80 s. But to update the estimation on-line with prior knowledge of the off-line results takes only a few seconds.

6-7 SUMMARY

For the dynamic stability study of large electric power systems, it is desirable to model the study system in detail and the external system by simple dynamic equivalents. What we want is a faithful representation of the dynamic interacting effect of the external system on the study system, not the dynamic behavior of the external system itself, which usually involves a large number of machines.

Three dynamic equivalencing techniques are introduced: the modal approach in Section 6-1, the coherency approach in Section 6-2, and the estimation approach in Section 6-3. Among them, the estimation approach is the only one that does not require any information on the external system.

The estimation approach with a stochastic process requires heavy computation. This difficulty, however, can be overcome by using a deterministic process with an intentional disturbance as developed in Section 6-4. The disturbance is so controlled that the machine responses of the study system are much larger than the load fluctuations normally observed on the tie line, yet well within the system voltage regulation safety limit. For the description of a multimachine system and equivalents, a multimachine model is developed in Section 6-5. Based on the deterministic estimation technique developed in Section 6-4, dynamic equivalents of a 13-machine system are estimated in Section 6-6, which results in minimum estimation error and unique parameter values. The results are further tested by applying a three-phase short circuit on the original 13-machine system as well as on the equivalent system. Comparison of system responses shows that the dynamic equivalents thus determined are faithfully representing the dynamic interacting effect of the external system on the study system.

Problems

6-1 There are three coherent generating plants. The turbine and governor transfer functions are $G_1(s)$, $G_2(s)$, and $G_3(s)$, and the respective mechanical input powers are P_{m1}, P_{m2}, and P_{m3} per unit on individual 400, 300, and 600-MW bases. Find an equivalent turbine and governor transfer function on a 1000-MW basis.

6-2 Figure 6-12 is a linear model and superposition principle applies. What are the damping and synchronizing torque effects of a supplementary control of the jth machine on the ith machine? Assume that

$$\Delta\delta_j = G_{\delta ij}u_{Ej}, \qquad \Delta E'_{qj} = G_{e'ij}u_{Ej}$$

where u_{E_j} is the supplementary control of the jth machine.

References

[1] R. Podmore and A. Germond, Development of dynamic equivalents for transient stability studies. *Rep. Electr. Power Res. Inst.* **EPRI EL-456** (*Palo Alto, Calif.*) (1977).

[2] W. T. Brown and W. J. Clouses, Combination of load-flow and stability equivalent for power system representation of A-C network analysers. *Trans. AIEE Part 3: Power Appar. Syst.* 782–787, Aug. (1955).

[3] H. E. Brown, R. B. Shipley, D. Coleman, and R. E. Nied, Jr., A study of stability equivalent. *IEEE Trans. Power Appar. Syst.* 200–207, March (1969).

[4] S. T. Y. Lee and F. C. Schweppe, Distance measures and coherency recognition for transient stability equivalents. *IEEE Trans. Power Appar. Syst.* 1550–1557, Sept./Oct. (1973).

[5] A. Ghafurian and B. J. Cory, Improvements in the calculation of transient stability in large interconnected power systems. *Iran. Conf. Electr. Eng., 5th, 1975.*

[6] J. M. Undrill and A. E. Turner, Construction of power system electromechanical equivalents by modal analysis. *IEEE Trans. Power Appar. Syst.* 2049–2059, Sept./Oct. (1971).

[7] J. M. Undrill, J. A. Casazza, E. M. Gulachenski, and L. K. Kirchmayer, Electromechanical equivalents for use in power system stability studies. *IEEE Trans. Power Appar. Syst.* 2060–2071, Sept./Oct. (1971).

[8] W. W. Price, E. M. Gulachenski, P. Kundur, F. J. Lange, G. C. Lochr, R. E. Roth, and R. F. Silvia, Testing of the modal dynamic equivalents technique. *IEEE Trans. Power Appar. Syst.* 1366–1372, July/Aug. (1978).

[9] C. E. Grund, Power system modal identification from large scale simulation using model adaptive reference control. *IEEE Trans. Power Appar. Syst.* 780–788, May/June (1978).

[10] R. W. deMello, R. Podmore, and K. N. Stanton, Coherency-based dynamic equivalents: Applicants in transient stability studies. *PICA Conf. Proc.*, 23–31 (1975).

[11] A. J. Germond and R. Podmore, Dynamic aggregation of generating unit models. *IEEE Trans. Power Appar. Syst.* 1060–1069, July/Aug. (1978).

[12] R. Podmore, Identification of coherent generators for dynamic equivalents. *IEEE Trans. Power Appar. Syst.* 1344–1354, July/Aug. (1978).

[13] P. Humphreys and F. J. Gilchrist, Dynamic equivalents for use in power system stability studies. *IEE Conf. Publ.* **140,** 23 (1976).

[14] W. W. Price, F. C. Schweppe, E. M. Gulanchenski, and R. F. Silva, Maximum likelihood identification of power system dynamic equivalents. *Proc. IEEE Conf. Decision Control, 1974.*

[15] W. W. Price, D. N. Ewart, E. M. Gulanchenski, and R. F. Silva, Dynamic equivalents from on-line measurements. *IEEE Trans. Power Appar. Syst.* 1349–1357, July/Aug. (1975).

[16] M. A. H. Ibrahim, O. M. Mostafa, and A. H. El-Abiad, Dynamic equivalents using operating data and stochastic modelling. *IEEE Trans. Power Appar. Syst.* 1713–1722, Sept./Oct. (1976).

[17] Yao-nan Yu and M. A. El-Sharkawi, Estimation of external dynamic equivalents of a thirteen-machine system. *IEEE Trans. Power Appar. Syst.* 1324–1332, March (1981).

[18] M. A. El-Sharkawi, Estimation of dynamic equivalents of external electric power system. Ph.D. Thesis, Department of Electrical Engineering, University of British Columbia, Vancouver, B.C., Canada (1980).

[19] F. C. Schweppe, "Uncertain Dynamic Systems." Wiley, New York, 1973.

[20] R. D. Masiello and F. C. Schweppe, Multi-machine excitation stabilization via system identification. *IEEE Trans. Power Appar. Syst.* 444–454 March/Apr. (1975).

[21] M. F. Allam and M. A. Laughton, Power system dynamic-state estimation by optimal variable incremental displacements. *Proc. Inst. Electr. Eng.* **123** (5), 433–436 (1976).

[22] J. Giri and A. Bose, Identification of dynamic equivalents for on-line transient security assessment. *IEEE PES Summ. Meet., 1977* IEEE Paper A 77 514-3 (1977).

[23] F. C. Schweppe *et al.*, Power system static-state estimation. Pts. I, II, and III. *IEEE Trans. Power Appar. Syst.* 120–125, 125–130, 130–135. Jan. (1970).

[24] R. E. Larson *et al.*, State estimation in power systems. Pts. I and II. *IEEE Trans. Power Appar. Syst.* 345–352, 353–363, March (1970).

[25] O. J. M. Smith, Power system state estimation. *IEEE Trans. Power Appar. Syst.* 363–379, March (1970).

[26] F. C. Schweppe and E. J. Handschin, Static state estimation in electric power systems. *Proc. IEEE* **62,** 972–982 (1974).

[27] A. S. Debs, Estimation of steady-state power system model parameters. *IEEE Trans. Power Appar. Syst.* 1620–1628, Sept./Oct. (1974).

[28] A. S. Debs, Estimation of external network equivalents from internal system data. *IEEE Trans. Power Appar. Syst.* 273–279, March/Apr. (1975).

[29] C. C. Lee and O. T. Tan, A weighted-least-squares parameter estimator for synchronous machines. *IEEE Trans. Power Appar. Syst.* 97–101, Jan./Feb. (1977).

[30] G. C. Contaxis and A. S. Debs, Identification of external system equivalents for steady-state security assessment. *IEEE Trans. Power Appar. Syst.* 409–414, March/Apr. (1978).

[31] H. W. Dommel and N. Sato, Fast transient solutions. *IEEE Trans. Power Appar. Syst.* 1643–1650, July/Aug. (1972).

[32] Yao-nan Yu, M. A. El-Sharkawi, and M. D. Wvong, Estimation of unknown large power system dynamics. *IEEE Trans. Power Appar. Syst.* 279–289, Jan./Feb. (1979).

[33] Yao-nan Yu and H. A. M. Moussa, Optimal stabilization of a multi-machine system. *IEEE Trans. Power Appar. Syst.* 1174–1182, May/June (1972).

[34] F. P. deMello and C. Concordia, Concepts of synchronous machine stability as affected by excitation control. *IEEE Trans. Power Appar. Syst.* 316–329, April (1969).

Chapter 7 Lyapunov Stability and Transient Stability Controls

In this chapter an introduction will be given to nonlinear stability analysis and transient stability controls. A stability definition adopted previously in Section 1-3, Chapter 1, refers to the transient stability as the power system stability due to a severe disturbance, which exceeds the capability of stability control of the linear type, PSS or LOC. The system stability may be lost at the first swing, and very drastic countermeasures, usually of the discontinuous type, such as dynamic resistance braking, fast valving, generator tripping, or load shedding, may be required to maintain overall system stability. The system using these controls must be described by nonlinear differential equations; its analysis is very involved even for a one-machine system.

One nonlinear stability analytical technique that has fascinated power engineers for years is Lyapunov's direct method. An introduction to the principle and an application of the method will be presented in this chapter. However, the transient stability analysis in general and the transient stability control design in particular will not be addressed in this book. Instead, emphasis will be placed on presenting the main concepts of the nonlinear stability analysis and transient stability controls.

7-1 LYAPUNOV'S DIRECT METHOD AND APPLICATION

The method begins with the choice of a Lyapunov function related to the system state equations [1–11]. By simply examining the nature of the function with certain criteria, the nature of stability of the system can be told without solving the nonlinear differential equations. Both the strength and limits of Lyapunov's direct method will be presented and the best use of the

method will be suggested in this section. Let us define a Lyapunov function first.

Lyapunov Function

If a scalar function V exists in the state space of the system under investigation such that the function is positive definite, and its time derivative $\dot{V}$ is negative definite or negative semidefinite, then the V function is a Lyapunov function of the system.

Examples of positive definite and positive semidefinite functions are the following. First,

$$V_1 = y_1^2 + y_2^2 + y_3^2 \tag{7-1}$$

is a positive definite function because it has a positive value at any point in the space and vanishes only at the origin. Next,

$$V_2 = y_1^2 + (y_2 - 3)^2 + (y_3 + 2)^2 \tag{7-2}$$

is a positive semidefinite function since it does not vanish at the origin; it vanishes at the point $(0, 3, -2)$, although it has positive values at any other points in the space. Note that $-V_1$ is a negative definite function, and $-V_2$ a negative semidefinite function of the foregoing examples.

Let a scalar function of a system under investigation be

$$V = V(y_k), \qquad k = 1, 2, \ldots, n \tag{7-3}$$

where the kth state variable of the system y_k is time dependent. Then

$$V = C, \qquad C = \text{constant} \tag{7-4}$$

represents a hypersurface in the n-dimensional space, corresponding to the system state at some instant; and the time derivative of V

$$\dot{V} = \sum_{k=1}^{n} \frac{\partial V}{\partial y_k} \dot{y}_k, \qquad k = 1, \ldots, n \tag{7-5}$$

is a space vector because $\partial V/\partial y_k$ is the y_k component of the gradient V with respect to y_k, and $\dot{y}_k$ is the time derivative of y_k.

Let the state equations of a system under investigation be

$$\dot{y}_k = Y_k(y_1, y_2, \ldots, y_n), \qquad k = 1, \ldots, n \tag{7-6}$$

and $\partial V/(\partial y_k)$ of (7-5) be expressed by its components in terms of the magnitude of the total gradient and direction cosines. We should have

$$\frac{\partial V}{\partial y_k} = \left[\sum_{k=1}^{n} \left(\frac{\partial V}{\partial y_k} \right)^2 \right]^{1/2} \cdot \cos(\bar{n}, y_k), \qquad k = 1, \ldots, n \tag{7-7}$$

where the square root part is the magnitude and $\cos(\bar{n}, y_k)$ the direction cosine of the gradient $\partial V/\partial y_k$, $\bar{n}$ being a unity normal at the hypersurface $V = C$, $C > 0$. Substituting (7-7) into (7-5) gives

$$\dot{V} = \left[\sum_{k=1}^{n}\left(\frac{\partial V}{\partial y_k}\right)^2\right]^{1/2} \cdot \sum_{k=1}^{n}\left[\cos(\bar{n}, y_k)\cdot Y_k(y_1, y_2, \ldots, y_n)\right]$$

$$= \left[\sum_{k=1}^{n}\left(\frac{\partial V}{\partial y_k}\right)^2\right]^{1/2} \cdot \bar{N} \tag{7-8}$$

where $\bar{N}$ is the normal on the hypersurface. In other words, while the system state corresponds to the hypersurface $V = C$ at some instant, the time derivative of V, or $\dot{V}$, is normal to the hypersurface.

Since a positive $\bar{N}$ points outward from the hypersurface and a negative $\bar{N}$ inward, a negative definite $\dot{V}$ for a positive definite V implies that the hypersurface keeps on shrinking until it is reduced to the origin, which corresponds to a system ultimately returning to the steady state after a disturbance, implying a stable system. On the other hand, if $\dot{V}$ is also positive definite for a positive definite V, the hypersurface will keep on expanding, implying an unstable system. Furthermore, if $\dot{V}$ is negative semidefinite and V is positive definite, the system after disturbance is still stable but will not return to the steady state corresponding to the origin.

Lyapunov's Direct Method

If a Lyapunov function V can be found for a system, which is positive definite, and $\dot{V}$ is negative semidefinite, the system is stable. Furthermore, if $\dot{V}$ is negative definite for a positive definite V, the system is not only stable, but also asymptotically stable.

Figure 7-1 shows regions of stability of a second-order system, where A is the boundary wherein the mathematical solution exists, B the true stability boundary, C the stability region found from a Lyapunov function, and 0 the

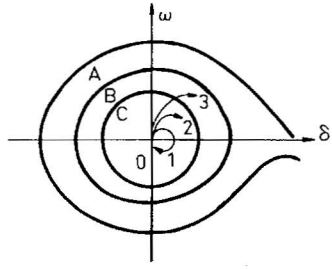

Fig. 7-1 Region of stability of a second-order system.

origin. Mathematically,

$$0 \subset C \subset B \subset A \tag{7-9}$$

which reads that 0 belongs to C, C belongs to B, etc.

Curves 1, 2, and 3 of Fig. 7-1 show three different trajectories on the phase plane, which, in general, would be in an n-dimensional space. Curve 1 shows that after a disturbance, a system not only moves within the stability region of a Lyapunov function, but also ultimately returns to the origin; the system is asymptotically stable. Curve 2 shows that although after a disturbance the system stays within the stability region of Lyapunov function, it does not return to the origin; the system is simply stable. Curve 3 shows that although the system trajectory after a disturbance ultimately stays within the stability region B found from the mathematical solution, it lies outside the region of the Lyapunov function; hence nothing can be told, stable or not, by the Lyapunov direct method.

Attempts are also made to construct a Lyapunov function that will approach the true stability boundary as closely as possible.

Zubov's Method of Constructing a Lyapunov Function

Based on the concept of positive definite V and negative definite or negative semidefinite $\dot{V}$, Zubov suggested that the Lyapunov function be constructed using the following equation [2, 8]

$$\sum_{k=1}^{n} \frac{\partial V}{\partial y_k} \dot{y}_k = -\phi(1 - V) \tag{7-10}$$

The LHS of (7-10) is no more than $\dot{V}$ of (7-5). On the RHS, a positive definite or a positive semidefinite function of the quadratic form may be chosen for ϕ, and V is normalized such that

$$0 < V < 1 \tag{7-11}$$

The direct solution of V from Zubov's equation is possible only for special cases. For high-order nonlinear systems, V may be expressed as a series beginning with the second-degree term,

$$V = V_2 + V_3 + \cdots + V_n \tag{7-12}$$

where V_2 is the second-degree term, V_3 the third-degree term, etc.

To determine various terms of V, the ϕ function must be chosen first and $\dot{y}_k$ must be expanded in a Taylor series,

$$\dot{y}_k = \sum_{k=1}^{n} a_{ik} y_k + \text{(higher degree terms)} \tag{7-13}$$

Substituting the first-degree terms of (7-13) into (7-10) and comparing results on both sides of the same degree, V_2 can be determined. Since the only second-degree terms on the RHS of (7-10) is the function ϕ, the equation to determine V_2 may be written

$$\sum_{i=1}^{n} \frac{\partial V_2}{\partial y_i} \left(\sum_{k=1}^{n} a_{ik} y_k \right) = -\phi \tag{7-14}$$

V_2 thus determined will be homogeneous of the second degree including y_1^2, y_2^2, $y_1 y_2$, $y_2 y_3$, etc.

Next V_3 may be determined from

$$\sum_{i=1}^{n} \frac{\partial V_3}{\partial y_i} \left(\sum_{k=1}^{n} a_{ik} y_k \right) + \sum_{i=1}^{n} \frac{\partial V_2}{\partial y_i} (\text{all 2nd degree terms of } \dot{y}_k) = 0 \tag{7-15}$$

since there are no third-degree terms on the RHS of (7-10).

The higher-degree terms of V generally can be determined from

$$\sum_{i=1}^{n} \frac{\partial V_m}{\partial y_i} \left(\sum_{k=1}^{n} a_{ik} y_k \right) = R_m(y_1, y_2, \ldots, y_n), \; m = 4, 5, 6, \text{ etc.} \tag{7-16}$$

where R_m is a known function of the mth degree determined from ϕ, V_2, $V_3, \ldots, V_{m-2}$ and V_{m-1}.

Example of Constructing a Lyapunov Function by Zubov's Method

An example of constructing the Lyapunov function by Zubov's method with various degrees of truncation, $V(5)$, $V(8)$, $V(10)$, $V(16)$, and $V(26)$, for a power system stability study is given in reference [8]. A one-machine infinite-bus system was modeled by a second-order differential equation

$$M \frac{d^2\delta}{dt^2} + D(\delta) \frac{d\delta}{dt} = P_i - P_e; \qquad M = \frac{H}{\pi f} \tag{7-17}$$

The first term on the LHS is the accelerating torque, the second term the damping torque, P_i on the RHS is the mechanical power input, and P_e the electric power output. For the second-order system, torque and power are approximately equal, if they are in per unit value and $2\pi f$ is chosen as the base speed. For a salient pole machine connected to a transmission line with

a reactance x and a local susceptance B,

$$P_e = P_m \sin \delta + P_s \sin 2\delta \tag{7-17a}$$

where

$$P_m = v_0 E'_q/(x'_d + x - x x'_d B) \tag{7-17b}$$

$$P_s = v_0^2(x'_d - x_q)/[2(x'_d + x - x x'_d B)(x_q + x - x x'_d B)] \tag{7-17c}$$

The damping coefficient $D(\delta)$ derived from Park's equation can be found from reference [8],

$$D(\delta) = \frac{v_0^2(x'_d - x''_d)T''_{d0}}{(x'_d + x)^2} \sin^2 \delta + \frac{v_0^2(x'_q - x''_q)T''_{q0}}{(x'_q + x)^2} \cos^2 \delta \tag{7-17d}$$

The state deviation equation from an initial state may be written in the following normalized form

$$\frac{d^2\delta'}{d\tau^2} + D'(\delta')\frac{d\delta'}{d\tau} + R(\delta') = 0 \tag{7-18}$$

where

$$\tau \triangleq t\sqrt{P_m/M} \tag{7-18a}$$

and δ' is the deviation of δ. $D(\delta')$ and $R(\delta')$ were then expanded in Taylor series to construct a Lyapunov function by Zubov's method. Several positive definite ϕ functions were chosen in the form of

$$\phi = \alpha\delta'^2 + \beta\omega^2 \tag{7-19}$$

and the Lyapunov stability boundaries found from one Lyapunov function for various truncation of the V series of (7-12) are shown in Fig. 7-2.

A three-phase fault for five cycles was assumed on one circuit of a double circuit of the one-machine, infinite-bus system, and the system was restored at the end of the 24th cycle. The phase plane trajectory of the system with the disturbance found from integration is shown in Fig. 7-2. The true stability boundary from mathematical solution is also recorded.

From this study, it is found:

(1) that very heavy computation is required to construct the Lyapunov stability boundaries by Zubov's method even for a second-order system;

(2) that the Lyapunov stability region is not necessarily closer to the true stability boundary by increasing the number of terms of the truncated Taylor series; for instance, the stability region of $V(26)$ is even smaller than that of $V(16)$;

(3) that the system was found stable according to $V(10)$, $V(16)$, and $V(26)$, but unstable according to $V(5)$ and $V(8)$, indicating an uncertainty by the method.

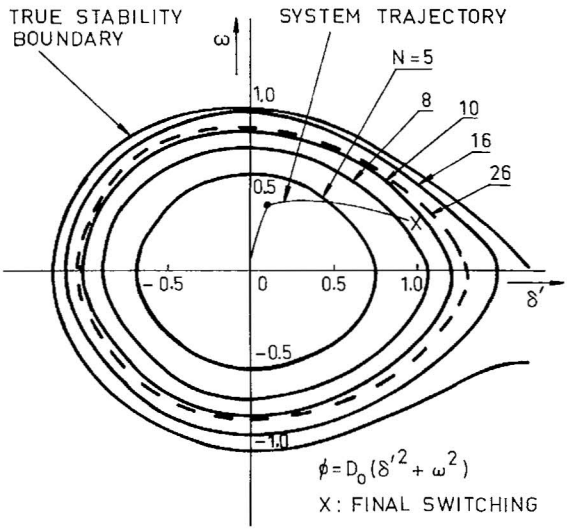

Fig. 7-2 Stability boundaries and phase plane trajectory of a power system.

Optimization of a Lyapunov Function

Another attempt was made to approach the true stability boundary by optimizing a Lyapunov function [10]. The process may be summarized as follows:

(a) Select a positive definite function of the system, say the energy function.

(b) Differentiate it and omit some terms of the result to obtain a negative definite or negative semidefinite $\dot{V}$.

(c) Integrate $\dot{V}$ to find V.

(d) Optimize V.

The method had some success and was applied to a third-order electric power system. But the computation involved remains very heavy.

Comments

From the foregoing results and many other studies, it is suggested that the Lyapunov direct method is not suitable for transient stability study of high-order large electric power systems. However, it can be economically used for power system planning [11], in which a relatively simple Lyapunov function may be chosen, heavy computation is not involved, and an accurate stability boundary is not a problem since power system stabilizers can be

designed later. It would be different in power system operation. By then we must know not only whether the system is stable for certain contingencies, but also how stable the system is and how long it will take for the system to reach stability.

Summary of Section 7-1

The principle of the Lyapunov direct method for nonlinear stability analysis has been presented in this section.

Constructing a Lyapunov function by Zubov's method to approach the true stability boundary is also presented and applied to a second-order electric power system. Extensive computation is involved and there is no guarantee that it would get closer to the true stability boundary by increasing the truncated series terms by Zubov's method.

A process of optimizing a Lyapunov function is also briefly presented. The major steps are: to select a positive definite function for the system, to differentiate it and omit some terms to find $\dot{V}$, to integrate $\dot{V}$ to find V, and to optimize V to obtain a Lyapunov function. Again, computation is extensive.

All studies suggest that the Lyapunov direct method is not suitable for high-order large power system transient stability studies. However, it can be economically used for system planning for which a relatively simple Lyapunov function can be chosen and the true stability boundary is not a problem. Power system stabilizers can be designed at a later stage for the improvement of power system stability.

7-2 PLANT CONTROL OF POWER SYSTEM TRANSIENT STABILITY

Instead of pursuing a rigorous power system transient stability analysis, the main concepts of various types of transient stability controls of power systems will be presented in this and the subsequent sections. Also presented are strategies of coordinating the transient stability control and the dynamic stability control. For convenience, the transient stability controls will be divided into two groups: the plant controls such as fast steam valving, forced excitation, and dynamic resistance braking; and the system controls such as generator tripping, load shedding, and so on.

The most important single concept of power system stability control is the energy balance of the mechanical power input and the electric power output plus various losses of the system at all times.

Small and gradual changes in load or generation concern the steady state stability of a power system and can be taken care of by automatic voltage regulator and governor. Small system swings due to a relatively small disturbance of a system such as a temporary imbalance of the energy input–output of a power plant concern the dynamic stability of a power system and can be taken care of by some supplementary linear excitation and/or governor controls, PSS or LOC. For very large system swings due to severe system disturbances beyond the capability of linear continuous supplementary controls, much more drastic countermeasures, usually of the discrete type [12], must be quickly taken to maintain the overall energy input–output balance of the entire system to maintain system stability.

After the transient stability control is applied to a power system responding to a temporary but severe disturbance, the system swings are usually quickly harnessed and reduced to the extent that the dynamic stability control can take over. This is the essence of coordinating the transient stability control and the dynamic stability control.

Dynamic Resistance Braking

Dynamic resistance braking may be applied to a power plant or a power pool where there is a temporary but very large electric power surplus due to a serious system fault that causes the system to lose its stability quickly. In such a case, the dynamic stability control, PSS or LOC, is no longer effective.

Braking Resistance of B. C. Hydro. Dynamic resistance braking was first developed by B. C. Hydro for the transient stability control of Peace River Hydro plants [13]. The ultimate capacity of the project was 2350 MW, and it was found from computer simulation that a 600-MW braking resistance in 200-MW blocks would give the optimum performance, that the required time of application was about one second, and that the resistance might have to be applied repeatedly. For economic considerations, the three-phase resistance banks were not connected directly to the generating units, but connected to the 500-kV transmission system through a 500/138 kV stepdown transformer.

In the discussion of reference [13] and later in his own paper [14], Park maintained that consideration must be given to the prefault condition, the severity of the fault, and the postfault generator performance. He suggested that the braking resistance be applied momentarily for a severe fault, disconnected shortly after the peak speed, and reapplied if it is warranted.

Braking Resistance of BPA. Dynamic resistance braking also can be applied to a temporarily surplus electric power pool. The WSCC (Western

Systems Coordinating Council) power system along the Pacific coast constitutes mainly hydropower plants of the Northwest Power Pool and thermal power plants of the Southwest Power Pool, and the electric power is normally exported from the north to the south through two 500-kV ac lines from BPA (Bonneville Power Administration) to San Francisco and one ± 400-kV HVDC line from BPA to Los Angeles. One of the transient stability problems is temporary loss of the ± 400-kV HVDC line, which has a transmission capacity of 1400 MW. When that happens, the system will disintegrate if no counter measures are taken.

A braking resistance was designed and installed at the Chief Joseph substation of BPA [15]. It has a capacity of 1400 MW, the same as the capacity of the HVDC line. It is designed as a countermeasure to the temporary loss of the HVDC line. To initiate the braking resistance application, two signals, a sudden power drop of more than 300 MW and a simultaneous decrease in bus voltage greater than 10%, at John Day substation or Chief Joseph substation, must be detected. The duration of application is about one second, which is about one-quarter of the natural oscillating period of the Pacific Northwest power pool.

A photograph of three resistance towers for the three phases are shown in reference [15]; each tower is 90 ft high and supports a $\frac{1}{2}$-inch, 19-strand, stainless-steel resistance wire 14,000 ft long, strung zigzag in 60-ft loops. The braking resistance is connected to a 230-kV bus. Because of the temperature rise, the resistance power may decrease from 1400 MW to 1000 MW in seconds. Multiple applications were not considered [15].

Fast Steam Valving

There are three types of fast steam valving: bypass valving, momentary valving, and sustained valving [12]. Bypass valving, developed in Europe, permits the steam power of both high- and low-pressure turbines to be bypassed for as long as 15 min. Therefore, the generator may remain running after full load rejection, is ready for resynchronization after the system fault clearing, and may quickly return to full load operation. The momentary valving refers to a rapid closure of the intercept valves, immediately followed by full opening at a slower speed. The technique was developed in the USSR. Since the unit returns to full load, a strong postfault transmission tie is necessary. Otherwise, the unit may lose its synchronism at the second positive swing. The sustained valving also refers to a rapid closure of the intercept valves, but both control valves and intercept valves are repositioned for reopening. The advantage of the sustained valving is that with simultaneous valving of several generating units, the output of a power plant can be greatly

reduced without tripping any generating unit, and full load operation can be resumed within minutes after fault clearing.

The idea of fast steam valving is not new. Patents were granted in 1925 and 1928, and tests performed in 1929 and 1930 [16]. Interest diminished because of the development of fast circuit breakers, but has been renewed because of the difficulty of maintaining the stability of large electric power systems; more effective means to maintain stability must be sought. In applying fast valving, the stress of valves and shaft, the effect of safety valves, the change in steam pressure and temperature, the feedwater supply, and so on, must be duly considered in the turbine and boiler design.

Cushing *et al.*'s Paper. In a paper by New England power engineers, the momentary fast valving was viewed as a natural extension of the modern electromechanical governor control to limit the overspeed of steam turbines [17]. Whenever a mismatch of the steam power input and the electric power output exceeds certain limit, the intercept valves are closed in full stroke within 0.1–0.2 s, followed by a slower reopening. The fast closure can quickly reduce the steam power as much as 70% so that the system will not lose its stability at the first swing, which can hardly be achieved by conventional speed governor. The slower reopening allows plenty of time for critical switching. For details, see reference [17].

Park's Paper. Both momentary and sustained valving were discussed at length [16]. For the momentary valving, the rapid closure and slow reopening were emphasized; the application should be held unless and until the delay of fault clearance had been evident; and consideration must be given to the severity of fault, the prefault system condition, and the postfault generator performance. It was also reported that sustained valving has been used in Germany since the late 1960s and there was no problem with the high-pressure safety valves. More details can be found in reference [16].

Other references of fast valving are given at the end of this chapter [18–23].

Forced Excitation

Modern fast-response static exciters also have the capability of reversing the direction of excitation if so designed. Therefore, they can be used not only to control the positive swings of a power system in severe disturbances, but also to control the negative swings.

Forced-Excitation Analysis. Forced excitation to improve the transient stability of a power system was first analyzed by Smith's group [24, 25], which they called "bang-bang" excitation control. Both positive and nega-

tive pulsed excitations were used [24]. Deviations of $\Delta\delta$, $\Delta\omega$ and Δi_F were chosen as the state variables and the control design was formulated as a time minimal problem. In particular, a synchronous machine returning to stability after a load rejection was investigated. Laboratory test results showed that the angle and speed excursions were greatly reduced by the control. Another analysis of the forced excitation control also can be found in reference [26].

Ontario Hydro's Paper. Ontario Hydro engineers found that the transient stability of a power system can be improved substantially by modifying the conventional supplementary excitation control of the phase-compensation type, but applied discretely [27]. A five-area, 94-bus, 44-generator system was investigated, with major generators of two areas and the 230 and 500-kV high-voltage buses represented in details and the rest of the system by equivalents. A three-phase fault was assumed. Simulation testing showed that there were two system oscillating frequencies, a higher frequency of 1.25 Hz and a lower frequency of 0.5 Hz, and the conventional power system stabilizer was not suitable for the low-frequency mode. There were difficulties of introducing another power system stabilizer of the phase-compensation type. As an alternative, a discrete control was introduced using the integral of speed deviation as the control input, and it was applied only when the transient stability of the system was threatened. As a result, the transient stability of the system was considerably improved. For details, see reference [27].

Laboratory Test of Transient Stability Controls

The plant controls of transient stability described in this section were tested in a research laboratory in conjunction with a linear optimal control [28, 29]. The general layout of the test model in a laboratory was shown as Fig. 4-12 in Chapter 4. It has the facility of braking resistance (BR), forced excitation (FE), fast valving (FV), and linear optimal controls.

Figure 7-3 shows the instability of the test model simulated power system due to a severe fault. The system was operating on the verge of transient instability. When a three-phase fault occurred to the system and if there were no transient stability control of the system, the system would lose its stability immediately at the first swing followed by slipping poles. The vertical scale of Fig. 7-3 corresponds to 72° per 10 small divisions, and the horizontal to 10 divisions per second. The lower part of the swing curve is clipped in recording.

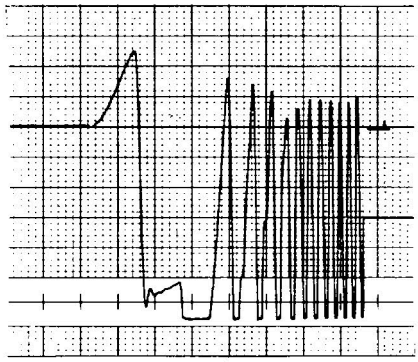

Fig. 7-3 Transient stability of a power system.

Figure 7-4 demonstrates the effect of transient stability controls in conjunction with a linear optimal control (LOC). For the same fault, the swing curve of the system with a resistance braking (BR) is shown on top, that with a forced excitation (FE) in the middle, and that with a momentary intercept valving (FV) at the bottom. For the operating and fault conditions of Fig. 7-3, the system becomes stabilized in less than 8 s with any one of the three transient stability controls, in conjunction with a linear optimal control. Some details are as follows.

Dynamic Resistance Braking. The braking resistance is connected to the generator terminal bus of the test model. It is divided into three banks per phase, automatically selected according to the severity of the fault in terms of ΔP_e or $\Delta\omega$, and can be repeatedly applied up to three times. The

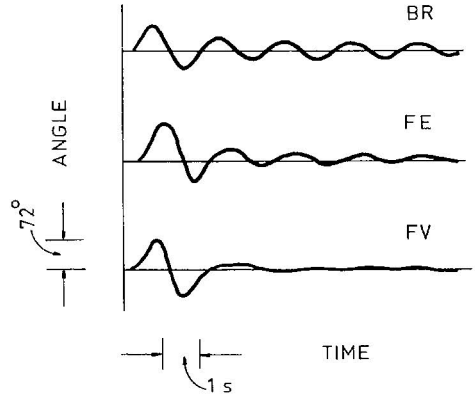

Fig. 7-4 Effect of transient stability controls.

control schemes are

First application: when ΔP_e drops more than 20%
Removal: 0.05 s after peak $\Delta\delta$
Reapplication: when $\Delta\omega > 1.5$ rad/s and $\Delta\dot{\omega} > 0$

The first and the last criteria depend on the capability of the dynamic stability control. For the linear optimal control installed, it has a capability of stabilizing the system even for a ΔP_e change of more than 30%: but it is safe to overlap the transient and dynamic stability controls. The second criterion is to make sure that the swing curve has come down and is not going up, which could happen when the braking resistance is taken off too soon. Of course, the braking resistance is applied only to the positive upswings and is not applied during negative swings or downswings.

Momentary Intercept Valving. The governor-controlled steam turbines and intercept valving are simulated by analog as shown schematically in the lower left corner of Fig. 4-12. There is also a conventional speed governor control. For the momentary intercept valving, logic circuits are designed following control strategies similar to those of the braking resistance control.

Forced Excitation Control. The control is applied to both positive and negative swings. The control strategies for the positive swings are exactly the same as the other two schemes. The "negative" forced excitation is applied only at the peak $\Delta\delta$ and is removed at the minimum $\Delta\omega$ during the negative swing.

Summary of Section 7-2

In this section, concepts of dynamic resistance braking, fast steam valving, and forced excitation control of a system with fault are presented. Several braking resistance schemes are in practice in North America [13, 15]. They are operating with great success. While bypass valving has been developed mainly in Europe [16], momentary intercept valving has been developed in the United States [16, 17]. Sustained valving with repositioned control and intercept valves has great appeal because of the capability of fast reloading without generator tripping. Although forced excitation has the capability of controlling not only the positive swings but also the negative swings of a power system, so far it has not received much attention in the power industry.

Laboratory test results of resistance braking, momentary intercept valving, and forced excitation are also shown, and control strategies are presented. They must be applied and removed at the right moment, and it is desirable to apply them with an overlapping of the dynamic stability

control scheme. Test results of Fig. 7-4 show that all three aforementioned transient stability control schemes are very effective.

7-3 SYSTEM CONTROL OF POWER SYSTEM TRANSIENT STABILITY

An introduction of all other transient stability controls besides resistance braking, fast steam valving, and forced excitation, which may be called the system controls, will be given in this section. For details, see the literature, especially the IEEE committee report [12].

High-speed Reclosing of Circuit Breakers

Since about 80% of line faults are caused by lightning, fast reclosing circuit breakers may be considered as the first-line protection of electric power systems. The deionization time of arc due to fault current is about 200 ms [30, 31], and the breaker should remain open during that time. On the other hand, the circuit breaker must be reclosed before the generator swings over the critical stability limit. Should there be an unsuccessful reclosure, it may cause serious damage to the fault location and also to the shaft [32, 33]. Therefore, the high-speed reclosure of circuit breakers alone may not be sufficient for transient stability control.

Single-Pole Switching

When a single-phase fault occurs in a power system, there is no need to interrupt services in the other two phases. Single-pole switching schemes have been developed, by which the breaker of each phase can be switched on and off independently. The critical fault clearing time can therefore be increased to as long as five cycles, and a mechanical failure of any one pole will not propagate to the other two poles [34, 36]. However, the effect of the unbalanced current and heating of the generator and the transient torque to the shaft must be duly considered in applications.

Series Capacitor Insertion

When a fault occurs in one circuit of a double-circuit transmission system and the faulted section is switched off, temporary insertion of a series capacitance can enhance the power transferability, and the transient stability

of the system can be improved [37]. The idea has been tested in a research laboratory. It is found that a capacitance should be inserted when the generator is over the synchronous speed and should be removed when the generator is under the synchronous speed, and that there is a limit on the capacitance that can be inserted; otherwise it will cause overshoot and negative damping to the generator [38].

Transmission line switching to improve the transient stability of a power system can be formulated as a time minimal problem and solved by a two-point-boundary-value technique of control theory [39].

Power Modulation of HVDC Line

A typical HVDC line has two converters: a rectifier at the sending end and an inverter at the receiving end. Each converter constitutes a set of valves and the power rectified or inverted can be easily controlled by firing angles of the converters in conducting mode. The direction of power flow can also be readily reversed by interchanging the functions of rectifier and inverter.

Because of the capability of fast power modulation of the HVDC line, it can be used for both dynamic and transient stability controls. A power modulation has been implemented on the Pacific ± 400-kV HVDC intertie that is roughly in parallel with the two 500-kV ac lines of the WSCC system. A continuous control proportional to the rate of change of power of the parallel ac interties is used to improve the dynamic stability, and a discrete control at various power levels is used to improve the transient stability of the parallel ac–dc system [40].

Generator Tripping

For a power surplus area with energy imbalance due to a permanent fault, some generating units of the area must be tripped off to maintain the system stability. This has been a practice for many years in the hydroelectric power system. For instance, should the Pacific 1400-MW HVDC intertie be out of service for some time, some hydroelectric generating units of the WSCC system in the north must be taken out of service to avoid overloading the parallel 500-kV ac transmission lines and to maintain system stability [12].

Generator tripping has also been extended to thermal–electric units. In such cases, consideration must be given to the long procedure of plant shut-down, starting up, resynchronization, and reloading. It takes hours to complete the entire process. The simultaneous sustained fast valving of several

generating units described in the last section seems to offer a very attractive alternative to the generator tripping of the thermal–electric unit.

Load Shedding

When the generation of a power area cannot meet the load requirement and there is no assistance available from neighboring areas, the only way to avoid system frequency deterioration and collapse is to shed some area loads.

To develop a load shedding scheme for a power area, consideration must be given to (1) the lowest frequency at which the power house auxiliaries can function, (2) the ability of the spinning reserve to catch up with the frequency deterioration in time, and (3) the time needed to activate the relays and circuit breakers [41]. Further consideration must be given to the following: (1) Is the load interruptable, such as heating, air conditioning, aluminum refinery, etc., (2) have all other control means been applied, and (3) have all reserves been utilized [42]?

One of the earliest load shedding schemes in North America, reported by AEP (American Electric Power Service Corp.) of ECAR (East Control Area Reliability Agreement) and activated by underfrequency relays, is shown in the accompanying tabulation [43, 44]. There is a delay in the first load

Frequency (Hz)	Load shedding (%)
59.5	$3\frac{1}{3}$
59.4	$3\frac{1}{3}$
59.3	$3\frac{1}{3}$
59.1	5
59.0	5
58.9	5

shedding to allow the spinning reserves to catch up with the frequency deterioration. Subsequent load shedding is necessary only when the frequency decline cannot be arrested by the spinning reserves. A smaller shedding of $3\frac{1}{3}\%$ in the first three steps is chosen to avoid shocks to the system, but a larger step of 5% per 0.1 Hz is employed in subsequent sheddings to arrest the fast frequency decline. After a total load shedding of 25% and as soon as the system frequency has deteriorated to 58 Hz, the generating units should be isolated without delay. For details, see references [43, 44].

Controlled System Separation

When a major generation loss or a major transmission line loss occurs in a large electric power system, all available control means have been

applied, and the system still cannot be rescued, there is no other way but to separate the system into several areas or islands to avoid a cascade catastrophic failure of the entire system. However, the separated areas or islands must be definable, and separation schemes must be examined and planned *a priori*, so that not only are the generation and load of each isolated area fairly in balance, but also that there is an appropriate reactive power supply for each area, i.e., not too much to cause an abnormal voltage rise or too little to cause a voltage collapse. It also requires all kinds of protection. It is a very complicated problem. Many valuable lessons have been learned from past power system failures. Should system separation become absolutely necessary, it must be executed in orderly fashion and be well controlled.

Summary of Section 7-3

In this section an introduction has been given to the system control of transient stability of electric power systems, including single-pole switching, series capacitor insertion, HVDC power modulation, generator tripping, under-frequency load shedding, and so on. Experience and analysis have helped us to understand the problem better with time. But it remains a very challenging problem because of the ever-increasing size and complexity of modern electric power systems.

7-4 SUMMARY

In the first section of this chapter, Lyapunov's direct method of nonlinear stability analysis is introduced. The advantage of the method is that the stability of a system can be assessed without solving the nonlinear differential equations. The disadvantages of the method are that nothing can be told beyond the region of the chosen Lyapunov function and that heavy computation is always involved should one attempt to find the true stability boundary by the direct method. Therefore, the best use of the method is probably for power system planning.

In the last two sections of this chapter, transient stability controls of electric power systems are introduced. There are times when system disturbances are so severe that they exceed the corrective capability of linear continuous dynamic stability controls, PSS or LOC, and more drastic countermeasures such as dynamic resistance braking, fast valving, generator tripping, and load shedding must be taken to balance the system energy input–output to maintain the stability. The problem is too complicated to entail a rigorous analysis especially for large electric power systems. This

book takes a moderate approach by presenting the concepts of these controls only. It is hoped that this chapter (and this book in general) will serve as an introduction to the rapidly advancing technology of the dynamic problems of modern electric power systems.

References

[1] J. LaSalle and S. Lefschetz, "Stability by Lyapunov's Direct Method with Applications." Academic Press, New York, 1961.

[2] V. I. Zubov, "Methods of Lyapunov and Their Applications," Transl. AEC-tr-4439, pp. 83–88. U.S. At. Energy Comm., 1961.

[3] A. M. Letov, "Stability in Nonlinear Control Systems." Princeton Univ. Press, Princeton, New Jersey, 1971.

[4] M. Pai, "Power System Stability." North-Holland Publ., Amsterdam, 1981.

[5] G. E. Gless, Direct method of liapunov applied to transient power system stability. *IEEE Trans. Power Appar. Syst.* 159–168, Feb. (1966).

[6] A. H. El-Abiad and K. Nagappan, Transient stability region of multi-machine power systems. *IEEE Trans. Power Appar. Syst.* 169–179, Feb. (1966).

[7] J. M. Undrill, Power system stability studies by the method of Liapunov. Pts. I and II. *IEEE Trans. Power Appar. Syst.* 791–801, 802–811, July (1967).

[8] Yao-nan Yu and K. Vongsuriya, Nonlinear power system stability by Liapunov function and Zubov's method. *IEEE Trans. Power Appar. Syst.* 1480–1485, Dec. (1967).

[9] J. L. Williams, Optimum Lyapunov function and stability regions for multi-machine power systems. *Proc. Inst. Electr. Eng.* **117** (3), 573–577 (1970).

[10] A. A. Metwally and Yao-nan Yu, Optimized Lure type Liapunov function for power system stability studies. *IEEE Winter Power Meet., 1972* IEEE Paper C 72 146-4 (1972).

[11] V. Converti and G. Steinbrenner, Analytical and solution technique for large transient stability program. *Proc. PSCC, 4th, 1972.*

[12] IEEE Committee, A description of discrete supplementary controls for stability. *IEEE Trans. Power Appar. Syst.* 149–165, Jan./Feb. (1978).

[13] H. M. Ellis, J. E. Hardy, A. L. Blythe, and J. W. Skooglund, Dynamic stability of the Peace River transmission system. *IEEE Trans. Power Appar. Syst.* 586–600, June (1966).

[14] R. H. Park, "The Design and Use of Braking Resistors," IEEE Resources Roundup. 69 C12 Ref. 6, pp. 52–61. IEEE, Phoenix, Arizona, 1969.

[15] M. L. Shelton, P. F. Winkelman, W. A. Mittelstadt, and W. J. Bellerby, Bonneville power administration 1400 MW braking resistor. *IEEE Trans. Power Appar. Syst.* 602–611, March/April (1975).

[16] R. H. Park, Fast turbine valving. *IEEE Trans. Power Appar. Syst.* 1065–1073, May/June (1973).

[17] E. W. Cushing, Jr., G. E. Drechsler, W. P. Kilgour, H. G. Marshall, and H. R. Stewart, Fast valving as an aid to power system transient stability and prompt resynchronization and rapid reload after rull load rejection. *IEEE Trans. Power Appar. Syst.* 2517–2527, Nov./Dec. (1971).

[18] W. A. Morgan, H. B. Peck, D. R. Holland, F. A. Cullen, and J. B. Buzek, Modern stability aids for Calvert Cliffs units. *IEEE Trans. Power Appar. Syst.* 1–10, Jan./Feb. (1971).

[19] C. Concordia and P. G. Brown, Effects of trends in large steam turbine driven generator

parameters on power system stability. *IEEE Trans. Power Appar. Syst.* 2211–2218, Sept./Oct. (1971).

[20] A. C. Sullivan and F. J. Evans, Some model experiments to improve transient stability. *IEEE PES Winter Meet., 1972* IEEE PES Paper C72 742-1 (1972).

[21] G. A. Doroshenko, J. N. Luginshi, V. A. Semenov, and S. A. Sovalov, Antidisturbance automation devices for improving power system stability. *USSR CIRGE Int. Conf. High Tension Electr. Syst.*, Aug. (1972).

[22] CIRGE Task Force 34.02.02, The electro-hydraulic governing of large steam turbines. *Electra* **33,** 91–114, March (1974).

[23] P. Kundur and J. P. Bayne, A study of early valve actuation using detailed prime mover and power system simulation. *IEEE Trans. Power Appar. Syst.* 1275–1287, July/Aug. (1975).

[24] G. A. Jones, Transient stability of a synchronous generator under conditions of bang-bang excitation scheduling. *IEEE Trans. Power Appar. Syst.* 114–121, Feb. (1965).

[25] O. J. M. Smith, Optimal transient removal in power systems. *IEEE Trans. Power Appar. Syst.* 361–374, May (1965).

[26] D. H. Kelley and A. H. M. A. Rahim, Closed-loop optimal excitation control for power system stability. *IEEE Trans. Power Appar. Syst.* 2135–2141, Sept./Oct. (1971).

[27] J. P. Bayne, P. Kundur, and W. Watson, Static exciter control to improve transient stability. *IEEE Trans. Power Appar. Syst.* 1141–1146, July/Aug. (1975).

[28] Yao-nan Yu, J. H. Sawada, and M. D. Wvong, A dynamic power system model for teaching and research. *IEEE Trans. Power Appar. Syst.* 1509–1514, July/Aug. (1976).

[29] J. H. Sawada and Yao-nan Yu, Transient power system stability control with braking resistance, forced excitation and/or fast valving. *IEEE PES Summ. Meet., 1975* IEEE PES Paper A 75 584-3 (1975).

[30] I. B. Johnson *et al.*, Fault arc deionization and circuit breaker reclosing on EHV lines—field, laboratory and analytical results. *CIRGE Pap.* No. 307 (1952).

[31] IEEE Committee, Arc deionization time on high speed three pole reclosing. *IEEE Trans. Power Appar. Syst., Spec. Suppl.* 236–253 (1963).

[32] S. S. Cogswell, S. F. Mauser, L. H. Wecks, W. H. Booth, and I. E. Markley, Generator shaft torques resulting from operation of EHV breakers. *IEEE PES Winter Meet., 1974* IEEE PES Paper C 74 087-3 (1974).

[33] A. Abolins, D. Lambrecht, J. S. Joyce, and L. T. Rosenberg, Effect of clearing short circuit and automatic reclosing on torsional stress and life expenditures of turbine-generator shafts. *IEEE Trans. Power Appar. Syst.* 14–25, Jan./Feb. (1976).

[34] C. L. Wagner and H. E. Lokay, Independent pole circuit breakers improve system stability performance. *Westinghouse Eng.*130–137, Sept. (1973).

[35] IEEE Committee, Bibliography on single-pole switching. *IEEE Trans. Power Appar. Syst.* 1072–1078, May/June (1975).

[36] D. R. Holland, G. E. McNair, G. D. Paradis, J. Senuta, and W. H. Van Zee, Conemaugh project—new concepts for 500 kv protection. *IEEE Trans. Power Appar. Syst.* 852–858, March/April (1971).

[37] E. W. Kimbark, Improvement of system stability by switched series capacitors. *IEEE Trans. Power Appar. Syst.* 180–188, February (1966).

[38] R. H. Webster, A. P. Mane, and O. J. M. Smith, Series capacitor switching to quench electromechanical transients in power systems. *IEEE Trans. Power Appar. Syst.* 427–433, March/April (1971).

[39] S. M. Miniesy and E. V. Bohn, Optimum network switching in power systems. *IEEE Trans. Power Appar. Syst.* 2118–2123, Sept./Oct. (1971).

[40] R. L. Cresap and W. A. Mittelstadt, Small signal modulation of the pacific HVDC intertie. *IEEE Trans. Power Appar. Syst.* 536–541, March/April (1976).

[41] H. E. Lokay and V. Burtnyk, Application of underfrequency relays for automatic load shedding. *IEEE Trans. Power Appar. Syst.* 776–783, March (1968).

[42] R. H. Park, Improved reliability of bulk power supply by fast load control. *Proc. Am. Power Conf.* **40,** 1128–1141 (1978).

[43] R. M. Maliszewski, R. D. Dunlop, and G. L. Wilson, Frequency actuated load shedding and restoration. Pt. I. Philosophy. *IEEE Trans. Power Appar. Syst.* 1452–1459, July/Aug. (1971).

[44] S. Horowits, A. Politis, and A. F. Gabrielle, Frequency actuated load shedding and restoration. Pt. II. Implementation. *IEEE Trans. Power Appar. Syst.* 1460–1468, July/Aug. (1971).

Appendix | Computer Programs

For the readers' convenience several computer programs, subprograms, and examples are included in this appendix.

MAIN PROGRAMS*

M1 To find initial state, K constants, system matrix, and eigenvalues for the one-machine infinite-bus system of Fig. 3-1 without u_E control.

PSS To design excitation control from ω_n, the undamped mechanical mode frequency, for the one-machine infinite-bus system of Fig. 3-1.

LOC To design LOC for the one-machine infinite-bus system of Fig. 3-1.

SUBPROGRAMS*

KCONST To find initial state and K constants for the system.
AMEIG To form system matrix A and find its eigenvalues.
EXCTR Excitation control design.
AMCEIG To find eigenvalues of the system with u_E.
AMATRX To form system matrix A for LOC design.
MMATRX To form composite matrix M for LOC design.

* The Computing Centre of the University of British Columbia is gratefully acknowledged for printing the originals of these programs.

EIGNV To find eigenvectors of the matrix M.

XMATRX To separate XII from XI.

RICCT To find Riccati matrix, design LOC, and find eigenvalues of the system with LOC.

WATFIV SUBPROGRAMS

WATFIV library subprograms called by the written main programs or subprograms for the computation are not included in this appendix.

```
      C
      C
      C    M1  A MAIN PROGRAM TO FIND INITIAL STATE, K CONSTANTS,
      C        SYSTEM MATRIX,AND EIGENVALUES ROR THE ONE-MACHINE
      C        INFNITE-BUS SYSTEM OF FIG.3-1 WITHOUT UE CONTROL
      C
      C        PAR1=(P,Q,V,R,X,G,B)
      C        PAR2=(XD,XQ,XDP,M,KA,TA,TDOP)
      C
              IMPLICIT REAL*8 (A-H,O-Z)
              REAL*8 PAR1(7),PAR2(7),K(6),KA,M
              REAL*8 A(20,20),AA(20,20),VECR(20,20),EVR(20),EVI(20)
      C
      C    DATA INPUT
              N=4
              READ(5,51)(PAR1(I),I=1,7)
              READ(5,51)(PAR2(I),I=1,7)
      C
      C    INITIAL STATE AND K CONSTANTS
              CALL  KCONST(PAR1,PAR2,K)
      C
      C    SYSTEM MATRIX A AND EIGENVALUES
              CALL  AMEIG(PAR2,K,A)
      C
       51     FORMAT(7F10.4)
              STOP
              END
      C
      C
      C    KCONST  A SUBPROGRAM TO FIND INITIAL STATE AND
      C            K CONSTANTS FOR THE SYSTEM OF FIG.3-1
      C
      C            PAR1=(P,Q,V,R,X,G,B,)
      C            PAR2=(XD,XQ,XDP,M.KA,TA,TDOP)
      C
              SUBROUTINE KCONST(PAR1,PAR2,K)
              IMPLICIT REAL*8 (A-H,O-Z)
              REAL*8 PAR1(7),PAR2(7),K(6),KA,M
              REAL*8 I,IP,IR,ID,IQ
              COMPLEX*16 CS,CV,CVO,CE,CI,CIL,CIT,CY,CZ,SUM,YMC
              P=PAR1(1)
              Q=PAR1(2)
              V=PAR1(3)
              R=PAR1(4)
              X=PAR1(5)
              G=PAR1(6)
              B=PAR1(7)
              XD=PAR2(1)
              XQ=PAR2(2)
              XDP=PAR2(3)
              M=PAR2(4)
              KA=PAR2(5)
              TA=PAR2(6)
              TDOP=PAR2(7)
      C
      C    INITIAL STATE
              SUM=DCMPLX(P,Q)
              CS=DCONJG(SUM)
      C
      C        PR COMPONENTS,POWER COMPONENT INPHASE WITH V AND
```

```
C          REACTIVE POWER COMPONENT 90 DEG.LEADING
      VR=0.
      CV=DCMPLX(V,VR)
      CI=CS/CV
      YMC=(0.,1.)
      CE=CV+(YMC*XQ)*CI
      EP=DREAL(CE)
      ER=DAIMAG(CE)
      BETA=DATAN2(ER,EP)
      IP=DREAL(CI)
      IR=DAIMAG(CI)
      I=DSQRT(IP**2+IR**2)
      PHI=DATAN2(IR,IP)
      PF=DCOS(PHI)
      CY=DCMPLX(G,B)
      CZ=DCMPLX(R,X)
      CIL=CY*CV
      CIT=CI-CIL
      CVO=CV-CZ*CIT
      VOP=DREAL(CVO)
      VOR=DAIMAG(CVO)
      VO=DSQRT(VOP**2+VOR**2)
      GAMA=DATAN2(VOR,VOP)
      DEL=BETA-GAMA
C
C     DQ COMPONENTS
      VD=V*DSIN(BETA)
      VQ=V*DCOS(BETA)
      VOD=VO*DSIN(DEL)
      VOQ=VO*DCOS(DEL)
      ID=I*DSIN(BETA-PHI)
      IQ=I*DCOS(BETA-PHI)
      EQP=VQ+XDP*ID
      WRITE(6,62)
      WRITE(6,63)
      WRITE(6,61) BETA,GAMA,DEL,PHI,EQP,VO
      WRITE(6,64)
      WRITE(6,61) V,I,P,Q,PF
      WRITE(6,65)
      WRITE(6,61) VD,VQ,ID,IQ
C
C   K CONSTANTS
      SUM=1.+CZ*CY
      C1=DREAL(SUM)
      C2=DAIMAG(SUM)
      R1=R-C2*XDP
      R2=R-C2*XQ
      X1=X+C1*XQ
      X2=X+C1*XDP
      Z2=R1*R2+X1*X2
      YD=(C1*X1-C2*R2)/Z2
      YQ=(C1*R1+C2*X2)/Z2
      CDEL=DCOS(DEL)
      SDEL=DSIN(DEL)
      FD=-VO*(R2*CDEL-X1*SDEL)/Z2
      FQ=VO*(X2*CDEL+R1*SDEL)/Z2
      VDD=(XQ-XDP)*IQ
      VQQ=EQP+(XQ-XDP)*ID
      K(1)=FD*VDD+FQ*VQQ
      K(2)=IQ+YD*VDD+YQ*VQQ
```

```
121             K(3)=1./(1.+(XD-XDP)*YD)
122             K(4)=(XD-XDP)*FD
123             CBETA=DCOS(BETA)
124             SBETA=DSIN(BETA)
125             XDD=-XDP*CBETA
126             XQQ=XQ*SBETA
127             K(5)=FD*XDD+FQ*XQQ
128             K(6)=CBETA+YD*XDD+YQ*XQQ
129             WRITE(6,66)
130             WRITE(6,67)
131             WRITE(6,61) K(1),K(2),K(3),K(4),K(5),K(6)
132     C
133      61     FORMAT(4X,6F10.4)
134      62     FORMAT(//,3X,'INITIAL STATE',/)
135      63     FORMAT(6X,'BETA',6X,'GAMA',6X,'DELTA',5X,'PHI',7X,
136             'EQP',7X,'VO')
137      64     FORMAT(6X,'V',9X,'I',9X,'P',9X,'Q',9X,'PF')
138      65     FORMAT(6X,'VD',8X,'VQ',8X,'ID',8X,'IQ')
139      66     FORMAT(//,3X,'K CONSTANTS',/)
140      67     FORMAT(6X,'K1',8X,'K2',8X,'K3',8X,'K4',8X,'K5',8X,'K6')
141             RETURN
142             END
143     C
144     C
145     C    AMEIG  A SUBROUTINE TO FORM SYSTEM MATRIX A AND FIND
146     C           ITS EIGENVALUES
147     C
148             SUBROUTINE AMEIG(PAR2,K,A)
149             IMPLICIT REAL*8 (A-H,O-Z)
150             REAL*8 PAR2(7),K(6),KA,M
151             REAL*8 A(20,20),AA(20,20),VECR(20,20),EVR(20),EVI(20)
152     C
153             M=PAR2(4)
154             KA=PAR2(5)
155             TA=PAR2(6)
156             TDOP=PAR2(7)
157     C
158             N=4
159             DO 1 I=1,N
160             DO 1 J=1,N
161       1     A(I,J)=0.
162             A(1,2)=-K(1)/M
163             A(2,1)=377.
164             A(1,3)=-K(2)/M
165             A(3,2)=-K(4)/TDOP
166             A(3,3)=-1.0/(TDOP*K(3))
167             A(3,4)=1.0/TDOP
168             A(4,2)=-KA*K(5)/TA
169             A(4,3)=-KA*K(6)/TA
170             A(4,4)=-1.0/TA
171             WRITE(6,62)
172     C    KEEP A AND FIND EIGENVALUES
173     C       DPRMAT AND DGCOPY ARE WATFIV LIBRARY SUBPROGRAMS
174             CALL  DPRMAT(A,N,N,N,N,1,1,20,1)
175             CALL  DGCOPY(A,AA,N,N,20,20)
176             WRITE(6,63)
177             CALL  DREIGN(AA,N,20,EVR,EVI,VECR,IERR,0,0)
178             DO 2 I=1,N
179             WRITE(6,64) EVR(I),EVI(I)
180       2     CONTINUE
```

```
181       C
182        62     FORMAT(//,3X,'A MATRIX')
183        63     FORMAT(//,3X,'SYSTEM EIGENVALUES',/)
184        64     FORMAT(6X,E12.5,'+J(',E12.5,')')
185               RETURN
186               END
  1
  2
  3          DATA INPUT
  4
  5         1.0        0.015      1.05       -.034       .997       .249       .262
  6         0.973      0.55       0.19       9.26      50.         0.05       7.76
  1
  2
  3
  4          INITIAL STATE
  5
  6             BETA       GAMA       DELTA      PHI        EQP        VO
  7               0.4598    -0.7273     1.1871    -0.0150     1.0237     1.0509
  8             V          I          P          Q          PF
  9               1.0500     0.9525     1.0000     0.0150     0.9999
 10             VD         VQ         ID         IQ
 11               0.4659     0.9410     0.4354     0.8471
 12
 13
 14          K CONSTANTS
 15             K1         K2         K3         K4         K5         K6
 16               0.5441     1.2067     0.6584     0.6981    -0.0955     0.8159
 17
 18
 19          A MATRIX
 20
 21                        1                  2                  3                  4
 22           1  0.0              -0.5876299E-01-0.1303181          0.0
 23           2   377.0000         0.0           0.0                0.0
 24           3  0.0              -0.8996615E-01-0.1957125          0.1288660
 25           4  0.0                95.53201     -815.9298         -20.00000
 26
 27          SYSTEM EIGENVALUES
 28
 29              0.29510E+00+J( 0.49596E+01)
 30              0.29510E+00+J(-0.49596E+01)
 31             -0.10393E+02+J( 0.32837E+01)
 32             -0.10393E+02+J(-0.32837E+01)
End of file
```

```
1      C
2      C
3      C   PSS  A MAIN PROGRAM TO DESIGN EXCITATION CONTROL FROM WN,
4      C        THE UNDAMPED MECHANICAL MODE FREQUENCY,FOR THE
5      C        ONE-MACHINE INFINITE-BUS SYSTEM OF FIG.3-1
6      C
7      C        K(I),I=1,6
8      C        PAR=(M,KA,TA,TDOP,ZETA,TR)
9      C        IB   NO.OF COMPENSATION BLOCKS
10     C
11     C        WN      OMEGA N
12     C        GAMA    PHASE ANGLE OF GE
13     C        THETA   PHASE ANGLE OF (1+ST1)
14     C        PHI     PHASE ANGLE OF (1+ST2)
15     C        THETA-PHI+GAMA=0
16     C
17     C
18             IMPLICIT REAL*8 (A-H,O-Z)
19             REAL*8 PAR(6),K(6),M,KA,KC
20             REAL*8 A(20,20)
21     C
22     C   DATA INPUT
23             N=4
24             READ(5,51) (K(I),I=1,6)
25             READ(5,51) (PAR(I),I=1,6)
26             READ(5,50) IB
27     C
28     C   EXCITATION CONTROL DESIGN
29             CALL  EXCTR(PAR,K,IB,KC,T1,T2)
30     C
31     C   SYSTEM MATRIX A AND EIGENVALUES
32             CALL  AMEIG(PAR,K,A)
33     C
34     C   EIGENVALUES OF THE SYSTEM WITH CONTROL
35             CALL  AMCEIG(PAR,K,KC,T1,T2,IB,A)
36     C
37      50     FORMAT(2I5)
38      51     FORMAT(7F10.4)
39             STOP
40             END
41     C
42     C
43     C   EXCTR  A SUBPROGRAM FOR EXCITATION CONTROL DESIGN
44     C
45     C          IB(1)  ONE COMPENSATION BLOCK    T2=0.1
46     C          IB(2)  TWO COMPENSATION BLOCK    T2=0.1
47     C
48             SUBROUTINE EXCTR(PAR,K,IB,KC,T1,T2)
49             IMPLICIT REAL*8 (A-H,O-Z)
50             REAL*8 PAR(6),K(6),M,KA,KC,T1,T2
51     C
52             M=PAR(1)
53             KA=PAR(2)
54             TA=PAR(3)
55             TDOP=PAR(4)
56             ZETA=PAR(5)
57             TR=PAR(6)
58     C
59     C   FIND GE
60             WN=DSQRT(377.*K(1)/M)
```

```
      XX=WN*(TA+TDOP*K(3))
      YY=1.-(WN**2)*TA*TDOP*K(3)+KA*K(3)*K(6)
      ZZ=DSQRT(XX**2+YY**2)
      GE=KA*K(3)/ZZ
      GAMA=-DATAN2(XX,YY)
C
C   CALCULATE T1 OR T2
      GOTO(1,2),IB
    1 T2=0.1
      XX=WN*T2
      YY=1.
      PHI=DATAN2(XX,YY)
      THETA=PHI-GAMA
      ZZ=DTAN(THETA)
      T1=ZZ/WN
      GOTO 3
    2 T2=0.1
      XX=WN*T2
      YY=1.
      PHI=DATAN2(XX,YY)
      THETA=PHI-GAMA/2.
      ZZ=DTAN(THETA)
      T1=ZZ/WN
      GOTO 3
C
C   FIND GC
    3 GC=DSQRT(1.+(WN*T1)**2)/DSQRT(1.+(WN*T2)**2)
C
C   FIND KC
      DE=2*ZETA*WN*M
      KC=DE/(K(2)*GE*GC)
C
C   RESET TIME CONSTANT IS IN DATA INPUT
C
      WRITE(6,62)
      WRITE(6,63)
      WRITE(6,61) GAMA,THETA,PHI,GE,GC
      WRITE(6,64)
      WRITE(6,61) WN,KC,TR,T1,T2
C
   61 FORMAT(4X,7F10.4)
   62 FORMAT(//,3X,'EXCITATION CONTROL')
   63 FORMAT(/,6X,'GAMA',6X,'THETA',5X,'PHI',7X,'GE',8X,'GC')
   64 FORMAT(/,6X,'WN',8X,'KC',8X,'TR',8X,'T1',8X,'T2')
      RETURN
      END
C
C
C   AMEIG  A SUBPROGRAM TO FORM SYSTEM MATRIX A AND FIND ITS
C          EIGENVALUES
C
      SUBROUTINE AMEIG(PAR,K,A)
      IMPLICIT REAL*8 (A-H,O-Z)
      REAL*8 PAR(6),K(6),M,KA,KC
      REAL*8 A(20,20),VECR(20,20),EVR(20),EVI(20),AA(20,20)
C
      M=PAR(1)
      KA=PAR(2)
      TA=PAR(3)
      TDOP=PAR(4)
```

```
      C
            N=4
            DO 1 I=1,N
            DO 1 J=1,N
          1 A(I,J)=0.
            A(1,2)=-K(1)/M
            A(2,1)=377.
            A(1,3)=-K(2)/M
            A(3,2)=-K(4)/TDOP
            A(3,3)=-1.0/(TDOP*K(3))
            A(3,4)=1.0/TDOP
            A(4,2)=-KA*K(5)/TA
            A(4,3)=-KA*K(6)/TA
            A(4,4)=-1.0/TA
            WRITE(6,62)
      C     DPRMAT AND DGCOPY ARE WATFIV LIBRARY SUBPROGRAMS
            CALL  DPRMAT(A,N,N,N,N,1,1,20,1)
            CALL  DGCOPY(A,AA,N,N,20,20)
            WRITE(6,63)
            CALL  DREIGN(AA,N,20,EVR,EVI,VECR,IERR,0,0)
      C     EIGENVECTOE AND SCALING NOT REQUIRED
            DO 2 I=1,N
            WRITE(6,64) EVR(I),EVI(I)
          2 CONTINUE
      C
           62 FORMAT(//,3X,'A MATRIX')
           63 FORMAT(//,3X,'SYSTEM EIGENVALUES',/)
           64 FORMAT(6X,E12.5,'+J(',E12.5,')')
            RETURN
            END
      C
      C
      C   AMCEIG  A SUBPROGRAM TO FIND EIGENVALES OF THE SYSTEM MATRX
      C           WITH UE CONTROL
      C
      C           A   MATRIX OF THE SYSTEM WITH CONTROL
      C           IB  NO.OF COMPENSATION BLOCKS
      C
            SUBROUTINE AMCEIG(PAR,K,KC,T1,T2,IB,A)
            IMPLICIT REAL*8 (A-H,O-Z)
            REAL*8 PAR(6),K(6),M,KA,KC
            REAL*8 A(20,20),VECR(20,20),EVR(20),EVI(20)
      C
            M=PAR(1)
            KA=PAR(2)
            TA=PAR(3)
            TDOP=PAR(4)
            TR=PAR(6)
      C
            N=4
            GOTO(1,2),IB
          1 N=N+2
            GOTO 3
          2 N=N+3
          3 DO 4 I=1,N
            DO 4 J=5,N
            A(J,I)=0.
          4 A(I,J)=0.
            A(4,6)=KA/TA
            A(5,2)=-K(1)/M
```

```
   181              A(5,3)=-K(2)/M
   182              A(5,5)=-1./TR
   183              A(6,2)=A(5,2)*KC*T1/T2
   184              A(6,3)=A(5,3)*KC*T1/T2
   185              A(6,5)=KC*(1.-T1/TR)/T2
   186              A(6,6)=-1./T2
   187              IF(IB.EQ.1) GOTO 5
   188              A(4,6)=0.
   189              A(4,7)=KA/TA
   190              A(7,2)=A(6,2)*T1/T2
   191              A(7,3)=A(6,3)*T1/T2
   192              A(7,5)=A(6,5)*T1/T2
   193              A(7,6)=A(6,6)*T1/T2
   194              A(7,7)=-1./T2
   195        5     WRITE(6,62)
   196      C       DPRMAT AND DREIGN ARE WATFIV LIBRARY SUBPROGRAMS
   197              CALL  DPRMAT(A,N,N,N,N,1,1,20,1)
   198              CALL  DREIGN(A,N,20,EVR,EVI,VECR,IERR,0,0)
   199      C       EIGENVECTORS AND SCALING NOT REQUIRED
   200              WRITE(6,63)
   201              DO 6 I=1,N
   202              WRITE(6,64) EVR(I),EVI(I)
   203        6     CONTINUE
   204       62     FORMAT(//,3X,'SYSTEM WITH CONTROL')
   205       63     FORMAT(//,3X,'SYSTEM EIGENVALUES',/)
   206       64     FORMAT(6X,E12.5,'+J(',E12.5,')')
   207              RETURN
   208              END
End of file
```

```
 1
 2
 3        DATA INPUT
 4
 5        0.5441     1.2067     0.6584  0.6981    -0.0995     0.8159
 6        9.26       50.        0.05    7.76       0.3        5.0
 7         2     1
 1
 2
 3        EXCITATION CONTROL
 4
 5           GAMA       THETA      PHI        GE         GC
 6            -0.8301     1.2700     0.4399     1.0006     3.0543
 7
 8           WN         KC         TR         T1         T2
 9             4.7066     7.0910     5.0000     0.6850     0.1000
10
11        A MATRIX
12
13                     1              2              3              4
14         1  0.0          -0.5875810E-01-0.1303132      0.0
15         2   377.0000     0.0            0.0            0.0
16         3  0.0          -0.8996134E-01-0.1957260      0.1288660
17         4  0.0            99.50000     -815.9000      -20.00000
18
19        SYSTEM EIGENVALUES
20
21            0.30765E+00+J( 0.49713E+01)
22            0.30765E+00+J(-0.49713E+01)
23           -0.10406E+02+J( 0.33060E+01)
24           -0.10406E+02+J(-0.33060E+01)
25
26        SYSTEM WITH CONTROL
27
28
29                1              2              3              4              5
30         1  0.0          -0.5875810E-01-0.1303132      0.0            0.0            0.0
31         2   377.0000     0.0            0.0            0.0            0.0            0.0
32         3  0.0          -0.8996134E-01-0.1957260      0.1288660      0.0            0.0
33         4  0.0            99.50000     -815.9000      -20.00000      0.0             100
34         5  0.0          -0.5875810E-01-0.1303132      0.0           -0.2000000      0.0
35         6  0.0           -2.854217     -6.330057      0.0            61.19449      -10.0
36
37
38        SYSTEM EIGENVALUES
39
40           -0.18677E+02+J( 0.0          )
41           -0.46019E+01+J( 0.74077E+01)
42           -0.46019E+01+J(-0.74077E+01)
43           -0.11568E+01+J( 0.43965E+01)
44           -0.11568E+01+J(-0.43965E+01)
45           -0.20148E+00+J( 0.0          )
End of file
```

```
C
C
C   LOC  A MAIN PROGRAM TO DESIGN LOC FOR THE ONE-MACHINE
C        INFINITE-BUS SYSTEM OF FIG.3-1
C
C        K(I),I=1,6
C        PAR2=(XD,XQ,XDP,M,KA,TA,TDOP)
C        PAR3=(PAR(I),I=1,N)--Q ELEMENTS
C
         IMPLICIT REAL*8 (A-H,O-Z)
         REAL*8 K(6),PAR2(7),PAR3(20)
         REAL*8 A(20,20),B(20),Q(20,20),S(20,20),M(20,20)
         REAL*8 ER(20),EI(20),VR(20,20),RK(20,20),AC(20,20)
         COMPLEX*16 VCM(20,20),AVCM(20,20),XI(20,20),XII(20,20)
C
C   DATA INPUT
         N=4
         READ(5,51) (K(I),I=1,6)
         READ(5,51) (PAR2(I),I=1,7)
         READ(5,51) (PAR3(I),I=1,N)
C
C   A MATRIX
         CALL  AMATRX(PAR2,K,A)
C
C   M MATRIX
         NN=2*N
         CALL  MMATRX(PAR2,PAR3,A,S,M)
C
C   EIGEVECTOR MATRIX OF M MATRIX
         CALL  EIGNV(M,ER,EI,VR,VCM)
C
C   XI AND XII MATRICES
         CALL  XMATRX(ER,EI,VCM,AR,AI,AVCM,XI,XII)
C
C   LOC DESIGN
         CALL  RICCT(A,XI,XII,RK,S,AC)
C
 51      FORMAT(7F10.4)
         STOP
         END
C
C
C   AMATRX  A SUBPROGRAM TO FORM SYSTEM MATRIX A FOR LOC DESIGN
C
         SUBROUTINE AMATRX(PAR2,K,A)
         IMPLICIT REAL*8 (A-H,O-Z)
         REAL*8 PAR2(7),K(6),M,KA
         REAL*8 A(20,20)
C
         N=4
         DO 1 I=1,N
         DO 1 J=1,N
   1     A(I,J)=0.
         M=PAR2(4)
         KA=PAR2(5)
         TA=PAR2(6)
         TDOP=PAR2(7)
         A(1,2)=-K(1)/M
         A(2,1)=377.
         A(1,3)=-K(2)/M
```

```
61              A(3,2)=-K(4)/TDOP
62              A(3,3)=-1.0/(TDOP*K(3))
63              A(3,4)=1.0/TDOP
64              A(4,2)=-KA*K(5)/TA
65              A(4,3)=-KA*K(6)/TA
66              A(4,4)=-1.0/TA
67              WRITE(6,62)
68              CALL  DPRMAT(A,4,4,4,4,1,1,20,1)
69        C     DPRMAT IS A WATFIV LIBRARY SUBPROGRAM
70         62   FORMAT(//,3X,'A MATRIX')
71              RETURN
72              END
73        C
74        C
75        C   MMATRX  A SUBPROGRAM TO FORM COMPOSITE MATRIX M FOR
76        C           LOC DESIGN
77        C
78              SUBROUTINE  MMATRX(PAR2,PAR3,A,S,M)
79              IMPLICIT REAL*8 (A-H,O-Z)
80              REAL*8 PAR2(7),PAR3(20)
81              REAL*8 A(20,20),B(20),Q(20,20),S(20,20),M(20,20)
82              N=4
83              NN=2*N
84        C
85        C   CONTROL MATRIX B
86                 DO 1 I=1,N
87           1     B(I)=0.
88                 B(4)=PAR2(5)/PAR2(6)
89        C
90        C   Q MATRIX
91                 DO 3 I=1,N
92                 DO 2 J=1,N
93           2     Q(I,J)=0.0
94           3     CONTINUE
95                 DO 4 I=1,N
96           4     Q(I,I)=PAR3(I)
97                 WRITE(6,62)
98                 CALL  DPRMAT(Q,N,N,N,N,1,1,20,1)
99        C
100       C   R MATRIX (IT BECOMES A SINGLE ELEMENT FOR THIS DESIGN)
101                R=1.
102       C        DO 5 I=1,N
103       C        DO 5 J=1,N
104       C        R(I,J)=0.0
105       C        IF(I .EQ. J) R(I,J)=1.
106       C 5      CONTINUE
107       C
108       C   S MATRIX
109                DO 7 I=1,N
110                DO 6 J=1,N
111          6     S(I,J)=B(I)*B(J)/R
112          7     CONTINUE
113                WRITE(6,63)
114                CALL  DPRMAT(S,N,N,N,N,1,1,20,1)
115       C        DPRMAT IS A WATFIV LIBRARY SUBPROGRAM
116       C
117       C   M MATRIX
118                DO 9 I=1,NN
119                DO 8 J=1,NN
120          8     M(I,J)=0.0
```

```
      9     CONTINUE
            DO 11 I=1,N
            DO 10 J=1,N
            M(I,J)=A(I,J)
            M(I+N,J+N)=-A(J,I)
            M(I,J+N)=-S(I,J)
     10     M(I+N,J)=-Q(I,J)
     11     CONTINUE
            WRITE(6,64)
            CALL  DPRMAT(M,NN,NN,NN,NN,1,1,20,1)
C
     62     FORMAT(//,3X,'Q MATRIX')
     63     FORMAT(//,3X,'S MATRIX')
     64     FORMAT(//,3X,'M MATRIX')
            RETURN
            END
C
C
C
C   EIGNV  A SUBPROGRAM TO FIND EIGENVECTORS OF THE MATRIX M
C
C           ER=EIGENVALUE(REAL)      EI=EIGENVALUE(IMAGIN)
C           VR=EIGENVECTOR(REAL)     M=EIGENVEC(IMAGIN),AFTER CALL
C           VCM=EIGENVECTOR MATRIX   VCMA=VCM REARRANGED
C
C           NB  NO.OF WRITING BLOCKS
C           IV  THE BEGINNING NO.OF EIGENVALUES OF EACH ROW
C           IE  THE ENDING NUMBER OF EIGENVALUES OF EACH ROW
C
      SUBROUTINE  EIGNV(M,ER,EI,VR,VCM)
      IMPLICIT REAL*8 (A-H,O-Z)
      REAL*8 M(20,20),ER(20),EI(20),VR(20,20)
      COMPLEX*16 VCM(20,20),DCMPLX
      N=4
      NN=2*N
C
      CALL  DREIGN (M,NN,20,ER,EI,VR,IERR,1,1)
C     DREIGN IS A WATFIV LIBRARY SUBPROGRAM
C     EIGENVECTORS AND SCALING ARE REQUIRED
      WRITE(6,62)
      DO 1 I=1,NN
      WRITE(6,63) ER(I),EI(I)
    1 CONTINUE
      WRITE(6,64)
C   NUMBER OF WRITING BLOCKS
      NB=NN/4
      IF(4*NB.LT.NN) NB=NB+1
      DO 5 IB=1,NB
      IF(NN.GT.4) GOTO 2
C   ONLY ONE BLOCK
      IV=1
      IE=NN
      GOTO 3
C   MORE THAN ONE BLOCK
    2 IV=(IB-1)*4+1
      IE=IV+3
      IF(IE.GT.NN) IE=NN
    3 WRITE(6,65)
      WRITE(6,66)(ER(I),EI(I),I=IV,IE)
      WRITE(6,65)
```

```
181             DO 4 I=1,NN
182             WRITE(6,68) I,(VR(I,J),J=IV,IE)
183             WRITE(6,68) I,(M(I,J),J=IV,IE)
184             WRITE(6,65)
185       4     CONTINUE
186             WRITE(6,65)
187       5     CONTINUE
188             DO 7 I=1,NN
189             DO 6 J=1,NN
190       6     VCM(I,J)=DCMPLX(VR(I,J),M(I,J))
191       7     CONTINUE
192       C
193        62   FORMAT(//,3X,'SYSTEM EIGENVALUES')
194        63   FORMAT(6X,E12.5,'+J(',E12.5,')')
195        64   FORMAT('1',//,3X,'EIGENVALUES AND CORRESP.EIGENVECTORS')
196        65   FORMAT(4X,4('-------------------------'))
197        66   FORMAT(3X,'|',4(F10.4,'+J(',F10.4,')|'))
198        68   FORMAT(I2,1X,'|',4(7X,E10.4,7X,'|'))
199             RETURN
200             END
201       C
202       C
203       C    XMATRX  A SUBPROGRAM TO INDENTIFY NEGATIVE EIGENVALUES AND
204       C            CORRESP.EIGENVECTORS, AND TO SEPARATE XII FROM XI
205       C
206             SUBROUTINE  XMATRX(ER,EI,VCM,AR,AI,AVCM,XI,XII)
207             REAL*8 ER(20),EI(20),AR(20),AI(20)
208             COMPLEX*16 VCM(20,20),AVCM(20,20),XI(20,20),XII(20,20)
209             INTEGER MARK(20)
210             N=4
211             NN=2*N
212       C
213       C    SEPARATE GROUP 1(LAMDA-) FROM GROUP 0(LAMDA+)
214             DO 2 I=1,NN
215             IF(ER(I).LT.0.D0) GOTO 1
216             MARK(I)=0
217             GOTO 2
218       1     MARK(I)=1
219       2     CONTINUE
220       C    FIND XI OF (LAMDA-)
221             J=0
222             DO 5 I=1,NN
223             IF(MARK(I).EQ.0) GOTO 4
224             AR(I-J)=ER(I)
225             AI(I-J)=EI(I)
226             DO 3 K=1,NN
227       3     AVCM(K,I-J)=VCM(K,I)
228             GO TO 5
229       4     J=J+1
230       5     CONTINUE
231       C    FIND XII OF (LAMDA-)
232             N=NN/2
233             DO 8 I=1,N
234             DO 7 J=1,NN
235             IF (DABS(ER(J)+AR(I)).GT.1.0D-10) GOTO 7
236             AR(I+N)=ER(J)
237             AI(I+N)=EI(J)
238             DO 6 K=1,NN
239       6     AVCM(K,I+N)=VCM(K,J)
240             ER(J)=0.D0
```

```
241             GO TO 8
242           7 CONTINUE
243           8 CONTINUE
244       C
245             DO 10 I=1,N
246             DO 9 J=1,N
247             XI(I,J)=AVCM(I,J)
248           9 XII(I,J)=AVCM(I+N,J)
249          10 CONTINUE
250             RETURN
251             END
252       C
253       C   RICCT  A SUBPROGRAM TO FIND RICCATI MATRIX,LOC
254       C          AND EIGENVALUES OF THE SYSTEM WITH LOC
255       C
256       C          ER=EVR  EI=EVI  VR=VECR  M=VECI(AFTER THE RECALL)
257       C          VECM=EIGENVECTOR MATRIX  VECMA=VECM REARRANGED
258       C
259             SUBROUTINE  RICCT(A,XI,XII,RK,S,AC)
260             REAL*8 A(20,20),S(20,20),RK(20,20),SK(20,20),AC(20,20
261             REAL*8 VR(20,20),ER(20),EI(20),AR(20),AI(20)
262             COMPLEX*16 VCM(20,20),AVCM(20,20),DET,DCOND
263             COMPLEX*16 XI(20,20),XII(20,20),GAIN(20,20),DCMPLX
264             N=4
265       C
266       C   RICCATI MATRIX
267       C       CDINVT AND CDMULT ARE WATFIV LIBRARY SUBPROGRAMS
268             CALL  CDINVT(XI,N,20,DET,DCOND)
269             CALL  CDMULT(XII,XI,GAIN,N,N,N,20,20,20)
270             DO 6 I=1,N
271             DO 5 J=1,N
272           5 RK(I,J)=DREAL(GAIN(I,J))
273           6 CONTINUE
274             WRITE(6,62)
275             CALL  DPRMAT(RK,N,N,N,N,1,1,20,1)
276       C
277       C   A-SK
278       C       DGMULT IS A WATFIV LIBRARY SUBPROGRAM
279             CALL  DGMULT(S,RK,SK,N,N,N,20,20,20)
280             DO 8 I=1,N
281             DO 7 J=1,N
282           7 AC(I,J)=A(I,J)-SK(I,J)
283           8 CONTINUE
284             WRITE(6,63)
285             CALL  DPRMAT(AC,N,N,N,N,1,1,20,1)
286       C
287       C   EIGENVALUES
288             CALL  DREIGN(AC,N,20,ER,EI,VR,IEER,0,0)
289             WRITE(6,64)
290             DO 9 I=1,N
291             WRITE(6,65) ER(I),EI(I)
292           9 CONTINUE
293       C
294          62 FORMAT('1',//,3X,'RICCATI MATRIX')
295          63 FORMAT(//,3X,'SYSTEM MATRIX WITH LOC')
296          64 FORMAT(//,3X,'EIGENVALUES OF THE SYSTEM WITH LOC')
297          65 FORMAT(6X,E12.5,'+J(',E12.5,')')
298             RETURN
299             END
End of file
```

DATA INPUT

0.5441	1.2067	0.6584	0.6981	-0.0955	0.8159	
0.973	0.55	0.19	9.26	50.	0.05	7.76
10.	2.	1.	1.			

A MATRIX

	1	2	3	4
1	0.0	-0.5875810E-01	-0.1303132	0.0
2	377.0000	0.0	0.0	0.0
3	0.0	-0.8996134E-01	-0.1957260	0.1288660
4	0.0	95.50000	-815.9000	-20.00000

Q MATRIX

	1	2	3	4
1	10.00000	0.0	0.0	0.0
2	0.0	2.000000	0.0	0.0
3	0.0	0.0	1.000000	0.0
4	0.0	0.0	0.0	1.000000

S MATRIX

	1	2	3	4
1	0.0	0.0	0.0	0.0
2	0.0	0.0	0.0	0.0
3	0.0	0.0	0.0	0.0
4	0.0	0.0	0.0	1000000.

M MATRIX

	1	2	3	4
1	0.0	-0.5875810E-01	-0.1303132	0.0
2	377.0000	0.0	0.0	0.0
3	0.0	-0.8996134E-01	-0.1957260	0.1288660
4	0.0	95.50000	-815.9000	-20.00000
5	-10.00000	-0.0	-0.0	-0.0
6	-0.0	-2.000000	-0.0	-0.0
7	-0.0	-0.0	-1.000000	-0.0
8	-0.0	-0.0	-0.0	-1.000000

5	6	7	8
-0.0	-0.0	-0.0	-0.0
-0.0	-0.0	-0.0	-0.0
-0.0	-0.0	-0.0	-0.0
-0.0	-0.0	-0.0	-1000000.
-0.0	-377.0000	-0.0	-0.0
0.5875810E-01	-0.0	0.8996134E-01	-95.50000
0.1303132	-0.0	0.1957260	815.9000
-0.0	-0.0	-0.1288660	20.00000

SYSTEM EIGENVALUES

-0.10001E+04+J(0.0)
0.10001E+04+J(0.0)
-0.22406E+00+J(0.47186E+01)
-0.22406E+00+J(-0.47186E+01)
0.22406E+00+J(0.47186E+01)
0.22406E+00+J(-0.47186E+01)
0.44111E+00+J(0.0)
-0.44111E+00+J(0.0)

EIGENVALUES AND CORRESP.EIGENVECTORS

	-1000.0948+J(0.0)	1000.0948+J(0.0)	-0.2241+J(4.7186)	-0.2241+J(-4.7186)
1	0.3971E-05	0.8607E-05	0.2155E-01	0.2155E-01
1	0.0	0.0	0.9148E-02	-.9148E-02
2	-.1497E-05	0.3245E-05	0.6477E+00	0.6477E+00
2	0.0	0.0	-.1753E+01	0.1753E+01
3	0.3047E-01	-.6606E-01	0.7628E-01	0.7628E-01
3	0.0	0.0	0.2562E-01	-.2562E-01
4	-.2364E+03	-.5128E+03	-.5027E+00	-.5027E+00
4	0.0	0.0	0.1564E+01	-.1564E+01
5	-.8349E-02	0.1882E-01	0.4286E+03	0.4286E+03
5	0.0	0.0	0.1818E+03	-.1818E+03
6	-.2215E-01	-.4991E-01	0.2530E+01	0.2530E+01
6	0.0	0.0	-.5256E+01	0.5256E+01
7	0.1891E+00	0.4269E+00	0.3895E+01	0.3895E+01
7	0.0	0.0	-.1217E+02	0.1217E+02
8	-.2318E+00	0.5231E+00	0.1693E-04	0.1693E-04
8	0.0	0.0	-.2169E-03	0.2169E-03

	0.2241+J(4.7186)	0.2241+J(-4.7186)	0.4411+J(0.0)	-0.4411+J(0.0)
1	-.2621E-01	-.2621E-01	-.3259E-02	0.1230E-01
1	-.1493E-01	0.1493E-01	0.0	0.0
2	-.1290E+01	-.1290E+01	-.2786E+01	-.1051E+02
2	0.2033E+01	-.2033E+01	0.0	0.0
3	0.8584E-01	0.8584E-01	0.1267E+01	0.4782E+01
3	0.5813E-01	-.5813E-01	0.0	0.0
4	-.2749E+01	-.2749E+01	0.4317E+01	-.1645E+02
4	0.4752E+01	-.4752E+01	0.0	0.0
5	0.1341E+04	0.1341E+04	-.4507E+02	-.5547E+03
5	0.7640E+03	-.7640E+03	0.0	0.0
6	0.8766E+01	0.8766E+01	0.5282E-01	-.6494E+00
6	-.1723E+02	0.1723E+02	0.0	0.0
7	0.2132E+02	0.2132E+02	-.3371E+02	0.1269E+03
7	-.3686E+02	0.3686E+02	0.0	0.0
8	-.1152E-03	-.1152E-03	-.1388E-02	-.4584E-02
8	0.6359E-04	-.6359E-04	0.0	0.0

```
RICCATI MATRIX

            1              2              3              4
 1   20458.13      0.5826451      -167.4120    -0.2119704E-01
 2  0.5826451       3.100279       6.681898     0.9548164E-03
 3   -167.4120       6.681898       41.67039     0.4567936E-02
 4 -0.2119704E-01 0.9548164E-03 0.4567936E-02 0.9807881E-03


SYSTEM MATRIX WITH LOC

            1              2              3              4
 1  0.0           -0.5875810E-01-0.1303132      0.0
 2   377.0000      0.0            0.0          0.0
 3  0.0           -0.8996134E-01-0.1957260      0.1288660
 4   21197.04      -859.3164      -5383.836     -1000.788


EIGENVALUES OF THE SYSTEM WITH LOC
   -0.10001E+04+J( 0.0          )
   -0.22406E+00+J( 0.47186E+01)
   -0.22406E+00+J(-0.47186E+01)
   -0.44111E+00+J( 0.0          )
```

Index

T